Chair of Petroleum Geology

Doctoral Thesis

Depositional Environments and Petroleum Potential of Coal in the Miocene Warukin Formation and Eocene Tanjung Formation, South Kalimantan, Indonesia

Hafidz Noor Fikri

April 2023

MONTANUNIVERSITÄT LEOBEN
www.unileoben.ac.at

AFFIDAVIT

I declare on oath that I wrote this thesis independently, did not use other than the specified sources and aids, and did not otherwise use any unauthorized aids.

I declare that I have read, understood, and complied with the guidelines of the senate of the Montanuniversität Leoben for "Good Scientific Practice".

Furthermore, I declare that the electronic and printed version of the submitted thesis are identical, both, formally and with regard to content.

Date 27.04.2023

Signature Author
Hafidz Noor Fikri

Abstract

Indonesia's coal is of foremost significance to the economy of Indonesia, as evidenced by the country´s steam coal exports, which rank fourth in the world. The Barito Basin on the island of Borneo is one of the largest coal-producing basins in Indonesia. Coal seams in the Barito Basin and the adjacent Asem Asem Basin are found in the Eocene Tanjung and the Miocene Warukin formations. Despite of the great economic significance, detailed knowledge of the factors controlling Eocene and Miocene peat-forming depositional environments is not yet available.

Therefore, the main aim of the present thesis is to determine the depositional environment of coal seams in the Tanjung and Warukin formations based on bulk coal data (ash yield, sulphur content) and organic petrological data from a total of 169 samples, and detailed organic geochemical data from sample sub-sets (~80 samples). In addition, the potential of Eocene and Miocene coals to generate liquid hydrocarbons also investigated.

Eocene coals are from the TAJ Pit-1D mine (from base to top: seams D, C, and B), while Miocene coals are from the Tutupan (from base to top: seams T110, T210 and T300) and Jumbang mines (seam BL1). The TAJ Pit-1D and the Tutupan mine are located in the Barito Basin, while the Jumbang mine is located in the Asem Asem Basin.

Based on vitrinite reflectance, the Eocene coals are more mature (~0.56 %Rr) than Miocene coals (Tutupan: ~0.39 %Rr; Jumbang: ~0.34 %Rr).

Ash yields and sulphur contents together with biomarker data show that Eocene coal in the Tanjung Formation accumulated in rheotropic to ombrotrophic mires. Miocene coal from the Warukin Formation at the Tutupan mine accumulated in a kerapah (inland) ombrotrophic mire (seams T110 and T210) or in a rheotropic-ombrotrophic mire (seam T300). Seam BL1 in the Jumbang mine coal in the Asem Asem basin of the Warukin Formation shows an ombrotrophic basinal (coastal) mire. Local brackish influence is indicated by elevated sulphur contents (<1.5 wt.%) in a lower bench of the BL1 seam (BL1L).

While all coals are characterized by high liptinite contents (14.9-49.1 vol.%), petrographic analysis shows remarkable differences in maceral composition between Eocene and Miocene coals. Leaf-derived macerals cutinite and fluorinite are more abundant in Eocene (~6.0 vol.%) than in Miocene coal (~4.5 vol.%), but rootlet-derived suberinite dominantes in Miocene coal (Miocene: ~2.6 vol.%; Eocene: ~0.5 vol.%). The high percentage of funginite reflects high fungal

activity in Miocene and Eocene mires, both in ombrotrophic and rheotropic conditions. Resinite is precent in high amounts in all coal seams.

Organic geochemical parameters (e.g. the terrestrial-aquatic ratio) record a cyclic change of mire environments during deposition of the two lower seams in the Tutupan mine (T110 and T210), which is tentatively related to Milankovich-type cycles (earth's axial precession). The di-/ triperpenoids ratio shows that gymnosperms were largley absent in the Eocene peat-forming vegetation and occurred in very low (BL1 seam) or low amounts in Miocene mires.

Resinite in Miocene coals was produced, at least partly, by dammar resin producing dipterocarpaceae. As dipterocarpaceae were not present in the palm/fern-dominated Eocene vegetation, resinite in Eocene coals must have a different source.

Resinite contents strongly control the Hydrogen Index of the coal samples, which reaches 539 mgHC/gTOC in the BL1 seam. Resins are the primary source of heavy bitumen components with high oxygen content in Miocene and Eocene coals. Pyrolysis-GC data show that the type of oil produced by Miocene and Eocene coals differs in the content of long-chain (waxy) and naphthenic compounds and reflects the differences in resin-forming plants. These data suggest that waxy oil produced from Eocene Tanjung Formation reservoirs in the Barito Basin is derived from Eocene coal, while oil in the Miocene Warukin Formation is generated from Miocene coal.

Kurzfassung

Kohle ist für die indonesische Wirtschaft von größter Bedeutung, wie die Kesselkohleexporte des Landes zeigen, die weltweit an vierter Stelle stehen. Das Barito Becken auf der Insel Borneo (Kalimantan) ist eines der wichtigsten Kohle-Becken in Indonesien. Die Kohleflöze im Barito Becken und im benachbarten Asem Asem Becken befinden sich in der eozänen Tanjung-Formation und der miozänen Warukin-Formation. Trotz der großen wirtschaftlichen Bedeutung liegen keine detaillierten Kenntnisse über die Faktoren vor, die die Torfbildung während des Eozäns und Miozäns steuerten.

Das Hauptziel dieser Arbeit besteht daher darin, das Ablagerungsmilieu der Kohleflöze in der Tanjung- und Warukin-Formation zu rekonstruieren. Dazu wurden Summenparameter (Asche- und Schwefelgehalt) und organisch petrologische Daten von 169 Proben sowie detaillierten organisch-geochemischen Daten von ca. 80 Proben bestimmt. Darüber hinaus wurde das Erdöl-Potenzial eozäner und miozäner Kohlen quantifiziert.

Die eozänen Kohlen stammen aus dem Tagebau TAJ Pit-1D (Flöze D, C und B), während die miozänen Kohlen aus den Tagebauen Tutupan (Flöze T110, T210 und T300) und Jumbang (Flöz BL1) stammen. Die TAJ Pit-1D und Tutupan Tagebaue befinden sich im Barito Becken, während der Jumbang Tagebau im Asem-Asem Becken liegt. Vitrinitreflexionsdaten zeigen, dass die eozänen Kohlen reifer (~0.56 %Rr) sind als die miozänen Kohlen (Tutupan: ~0.39 %Rr; Jumbang: ~0.34 %Rr).

Asche- und Schwefelgehalte sowie Biomarkerdaten belegen, dass die eozäne Kohle in der Tanjung-Formation in rheotrophen bis ombrotrophen Mooren gebildet wurde. Die miozänen Kohlen (Warukin-Formation) im Tutupan Tagebau wurden in einem ombrotrophen Kerapah-Moor (Flöze T110 und T210) oder in einem Moor mit alternierenden rheotrop-ombrotrophen Bedingungen (Flöz T300) gebildet. Das miozäne Flöz BL1 im Jumbang Tagebau im Asem-Asem Becken wurde in einem ombrotrophen küstennahen (Basinal-) Moor gebildet. Ein lokaler brackischer Einfluss wird durch erhöhte Schwefelgehalte (<1,5 Gew.-%) in einer basalen Bank des Flözes BL1 (BL1L) angezeigt.

Während alle Kohlen durch hohe Liptinitgehalte (14.9-49.1 Vol.-%) gekennzeichnet sind, zeigt die petrographische Analyse bemerkenswerte Unterschiede in der Mazeralzusammensetzung zwischen eozänen und miozänen Kohlen. Von Blättern abgeleitete Mazerale der Liptinitgruppe

(Cutinit und Fluorinit) sind in eozänen Kohlen häufiger (~6.0 Vol.-%) als in miozänen Kohlen (~4.5 Vol.-%). Korkstoff, der für feine Wurzelhaare charaktersitisch ist (Suberinit), ist in miozänen Kohlen häufiger (Miozän: ~2.6 Vol.-%) als in eozänen Kohlen (~0.5 Vol.-%). Der hohe Anteil an Funginit spiegelt die hohe Pilzaktivität in miozänen und eozänen Mooren wider, sowohl unter ombrotrophen als auch unter rheotropischen Bedingungen. Fossile Harze (Resinit) ist in allen Kohleflözen in hohen Mengen vorhanden.

Organische geochemische Parameter (z. B. das „terrestrial-aquatic ratio") belegen eine zyklische Veränderung des Moormilieus während der Ablagerung der beiden unteren Flöze im Tutupan Tagebau (T110, T210), die vermutlich mit Milankovic-Zyklen (Achsenpräzession der Erde) zusammenhängt. Das Verhältnis von Di- zu Triperpenoiden zeigt, dass Gymnospermen in der torfbildenden Vegetation des Eozäns weitgehend fehlten und in miozänen Mooren nur in sehr geringen (Flöz BL1) oder geringen Mengen vorkamen.

Resinit in miozänen Kohlen wurde zumindest teilweise von Dammarharz produzierenden Dipterocarpaceaen gebildet. Da Dipterocarpaceaen in der palmen- und farndominierten Vegetation des Eozäns fehlten, muss das Resinit in eozänen Kohlen eine andere Quelle haben.

Der Resinitgehalt kontrolliert den Wasserstoffindex der Kohleproben, der im Flöz BL1 ein Maximum von 539 mgHC/gTOC erreicht. Harze sind die Hauptquelle für schwere Bitumenkomponenten mit hohem Sauerstoffgehalt in miozänen und eozänen Kohlen.

Pyrolyse-GC Daten zeigen, dass sich die Art des von miozänen und eozänen Kohlen produzierten Öls durch den Gehalt an langkettigen (wachsartigen) und naphthenischen Verbindungen unterscheidet, wobei diese Unterschiede die verschiedenen harzbildenden Pflanzen widerspiegelt. Die Pyrolyse-GC Daten bestätigen, dass eozäne Kohlen das wachs-reiche Öl in Reservoir-Horizonten innerhalb der Tanjung-Formation gebildet haben, während miozäne Kohlen das Öl in Reservoir-Horizonten innerhalb der Warukin-Formation gebildet haben.

Acknowledgments

First and above all, I would like to thank God the almighty, for protection and abilility to proceed successfully. The following document summarizes three and half years of effort and achievement. It is a delight to convey my gratitude and thanks to the following individuals for their outstanding support in completing this study.

I'd like to express my sincere gratitude, Univ. Prof. Reinhard Sachsenhofer, for his essential advice, ideas, patience, and support. His insights and expertise have been invaluable in shaping my research.

I am also grateful to my mentor, assoz.Prof. Dr.mont. Doris Groß for her guidance and support throughout my PhD journey. Thank you to Dr. Achim Bechtel for the contributions, ideas and helpful discussions during this research.

I appreciate the great support from Priv.-Doz. Dr.mont. David Misch for the helpful discussion and their interest in this dissertation theme. I thank for great help from Brian Horsfield and Nicolaj Mahlstedt from Geos4 for Pyrolysis-GC analysis and as co-author.

I would like to thank Günter Nobis for the kindness and assistance in biomarker lab, Petra Sleziakova for her help in the biomarker and isotopy lab.

Special thanks go to Alexandra Schellich, the secretary of the Petroleum Geology chair, for her assistance and support throughout my time in the program.

Stephen Ajuaba and Vusala Aghayeva, I am grateful for their unwavering support and encouragement throughout my academic journey since my first year.

All my colleagues in Chair of Petroleum Geology (Montanuniversität Leoben) are recognized for their outstanding friendship and support. During my time at Leoben, I had a lovely environment while working together.

I would like to thank PT. Adaro Indonesia (Pak Fredi and Odont Akhdiannor), PT Tanjung Alam Jaya (Pak Arief), PT Gunung Sambung (Pak Dika), PT. Jhonlin Baratama (Pak Ari), and PT Arutmin Indonesia, for providing access to the mine site, accomodation and allowing to collect samples.

I would also like to acknowledge the financial support provided by ASEA-UNINET-OeAD for providing doctorate scholarship from 2020-2023 (Lisa Genger, Christina Düss, and teams are thanked for their kindness). This doctoral study funded by OeAD Austria’s Agency for Education

and Internationalization for an Ernst Mach Grant, ASEA-UNINET scholarship (Reference number: ICM-2019-13766, MPC-2020-01500, MPC-2021-01331, and MPC-2021-01480)

Thanks to my valuable friends in Austria: Mas Wira Sekeluarga, Bang Andi Wijaya, Mas Fahim and his families, all friends in Leoben, Muslim Grazindo, Wapena, and PPI Austria.

Lecturers and colleagues in the Faculty of Engineering of lambung Mangkurat University are thanked for their encouragement. All my teachers and friends (Arief Al, Reza, and Erwin), who have suppported me and not mentioned here, are gratefully acknowledged.

Much appreciation goes to my families, my mom and my brother family, Papa, Mama, Om Fery and Tante Imah for their pray, support, and love. Finally, a special thank goes to Yuniar, Faris, and Farras, who have been very tolerant over the years and for the endlless support.

Inhaltsverzeichnis

1 Introduction

Coal is still vital as an energy source, although it is well known that coal is the most significant contributor to greenhouse gas emissions in the fossil fuel classification (Steckel, et al., 2015). Southeast (SE) Asia is likely to use 39 % coal by 2040 as a source of electricity generation (WCA, 2022). In order to reduce the resulting environmental impact, technology development needs to continue. One of basic aspects is an improved understanding of the physical and chemical properties of coal (Dai et al., 2020; Littke, 2015; Keller et al., 2016; Dai and Finkelman, 2018). Beside that, the investigation of coal can help improving the understanding of the world's geological history. Using botanical, geochemical, mineralogical, palynological, and petrographic data, paleoenvironmental, paleoclimatic, and geodynamic conditions can be analyzed (Dai et al., 2020).

On the technical and business side, coal is of utmost importance for the economy of Indonesia (Reichl, 2018). Coal exploration and efficient coal mining are based on the knowledge of seam geometries (thickness, lateral continuity, number and position of partings, etc.), whereas coal properties (e.g. rank, ash yield, sulphur contents, maceral composition, etc.) form the base for optimal coal utilization. Seam and coal properties (apart from rank) are mainly determined by the depositional environment of the coal seams (e.g. Diessel, 1992).

The most significant coal deposits of SE Asia are formed in southern Sundaland comprising the islands of Borneo and Sumatra (Friederich, et al., 2016). In Kalimantan (Indonesian part of Borneo) laterally extensive Eocene transgressive coal seams developed in an early post-rift setting and in Miocene to Pliocene time in widespread thick ombrogenous peat mires (Friederich, et al., 2016). South Kalimantan has many coal resources which are suitable for mining activities. Currently coal mining activities take place intensively in South Kalimantan, where 14 large and several small coal mining companies produced 160 million tons of coal in 2014. In this area coal seams occur mainly in the Eocene Tanjung Formation and in the Miocene Warukin Formation (Friederich and Leeuwen, 2017) and often attain the sub-bituminous rank. Coal seams in these formations are often very low in ash and sulphur (Moore and Ferm, 1992;

Demchuk and Moore, 1993). While coal seams in the Tanjung Formation are typically several metres thick, those in the Warukin Formation are partly very thick (e.g., in the Tutupan mine; Demchuk and Moore, 1993). Unfortunately, the knowledge of the depositional environment of coal in these formations is still unsatisfactory.

1.1 Objectives

The main aim of the proposed study is to determine the depositional environment of some world-class coal seams in the Tanjung and Warukin formations. Coal is a not only an important energy source, but also a very sensitive facies indicator reflecting changes in basin evolution, mire types, climate, and vegetation. Thus, both results that are scientifically important and relevant to the technical interests of coal mining activities are expected.

The reconstruction of depositional environments of coal seams in the Tanjung and Warukin formations will provide new insights into the geological evolution of Kalimantan and South East Asia during Cenozoic time. Within this context, it will be especially interesting to see, how a 50-m-thick coal seam with very low ash yield and sulphur content can accumulate (single-stage or multi-stage subsidence, raised mire vs. low-lying mire, etc. (e.g. Gruber and Sachsenhofer, 2001). It is also expected to see changes in vegetation-types between Eocene and Miocene coals (e.g. Moore and Ferm, 1992; Morley, 2013) and changes within single seams (for example: angiosperm vs. gymnosperm dominance), which may be related to climatic changes during the Cenozoic in SE Asia.

Apart from scientific goals, the knowledge of the varying depositional environments will help predicting lateral and vertical variations of coal properties. This will help coal exploration, coal getting, and the optimal usage of the coals. In addition, the potential of coals to generate liquid hydrocarbons will be quantified. This may result in a better understanding of the petroleum potential of sedimentary basins on- and offshore Borneo.

1.2 Type of data used in this thesis

This study is based on two types of data sets from three mine areas in South Kalimantan (TAJ Pit-1D, Tutupan, Jumbang):

- Coal exploration and mine data, which were kindly provided by the mining companies. These data nclude:
  - Borehole data (incl. data from channel samples)
  - Extension and thickness of seams
  - Stratigraphic position of partings
  - Moisture content, ash yield, and sulphur content of coals drilled in exploration wells

- Analytical data obtained within the frame of this thesis along key sections from each of the three mine areas:
  - Moisture content
  - Ash yield
  - Sulphur content
  - Organic and inorganic carbon contents
  - Rock Eval parameters
  - Maceral composition and vitrinite/huminite reflectance
  - Biomarker data
  - Carbon isotope data
  - Pyrolysis gas chromatography

The methodology is described in great detail in the attached publications and is not repeated here. However, some details of biomarker analysis (detected compounds and retention times; Appendices 1-2 ; 4-7), input data and results of the applied probabilistic approach to determine the duration of coal deposition in the tutupan mine (Appendix 3); and the pyrolysis-GC results of five coal samples (Appendix 8) are provided in the Appendix.

1.3 Location of research

Three coal mines were selected for the present study Their location in southern Borneo is shown in Fig. 1:

- TAJ Pit-1D Mine is located in the eastern Barito Basin. Three Eocene coal seam with a total thickness of ~10 m are exploited in this mine.;
- Tutupan coal mine, located in the northern part of the Barito Basin. The Miocene coal seams in this mine are especially thick and have a total net thickness of ~100 m;
- Jumbang Mine, located in the Asem Asem Basin. Miocene coal, about 20 m thick, is produced in this mine.

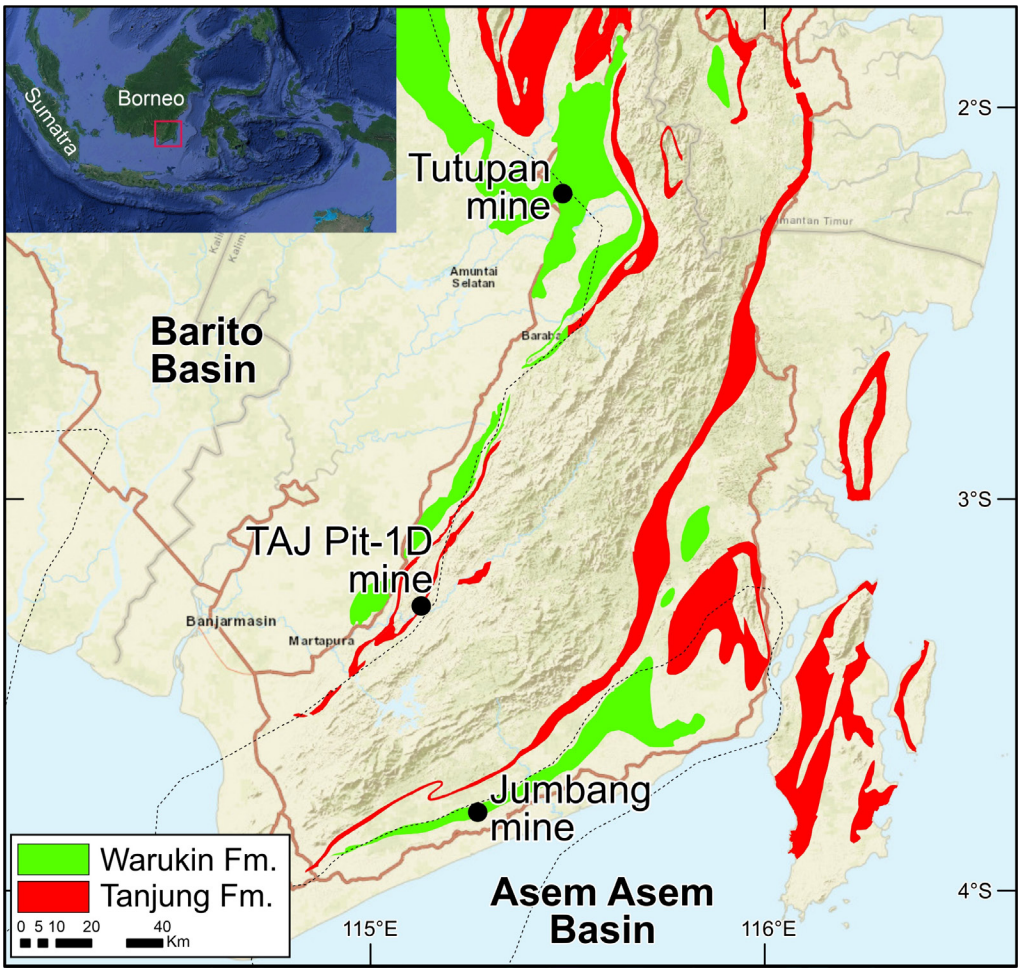

Fig.1. Map showing the distribution of the Tanjung and Warukin formations in southern Borneo (Barito and Asem Asem basins; after Supriatna et al., 1994; Sikumbang and Heryanto, 1994; Heryanto and Sanyoto, 1994) together with location of the three mine sites selected for the present study.

1.3.1 TAJ Pit-1D mine (Eocene coal in Barito Basin)

The TAJ Pit-1D mine is one of the mine sites owned by Tanjung Alam Jaya (TAJ) Company with a total land concession of more than 9500 Ha (TIMAH, 2023). In 2014, TAJ produced 250,000 tons of coal and had reached 950,000 tons in 2010 (ESDM, 2015). There are three economic coal seams in the TAJ Pit-1D mine, namely the D, C and B seams, which are 2.8 m, 3.4 m and 1.4 m thick, respectively (Fig. 2). Layer A is very thin and is often absent because of non-deposition.

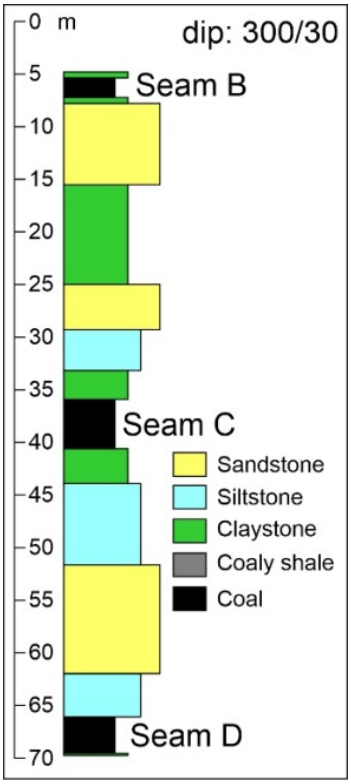

Fig. 2. Simplified drill hole of DHP1D.02 log in TAJ Pit-1D mine

1.3.2 Tutupan mine (Miocene coal in Barito Basin)

The Tutupan Mine is a coal mine licensed by Adaro Indonesia Company. Adaro Indonesia's concessions (Tutupan Mine, Wara Mine, and Paringin Mine) have coal reserves of 731 Mt, with estimated resources of 3.3 Bt (ADARO, 2022). Meanwhile, the Tutupan mine coal production reaches more than 30 million tons per year using the 20 km long open/strip-pit mining method (ADARO, 2008).

The Tutupan Mine is divided into three areas: South Tutupan, Central Tutupan, and North Tutupan. The coal deposits in the Tutupan mine have major coal seams, labelled from base T100, T200, and T300, with various branching and minor coal seams. The dip of the seams ranges from 25° to 75° (Fig. 3). The total thickness of coal in the Tutupan mine reaches more than 100 m. The maximum thickness of seams T100, T200 and T300 reches 60 m, 20 m, and 35 m, respectively.

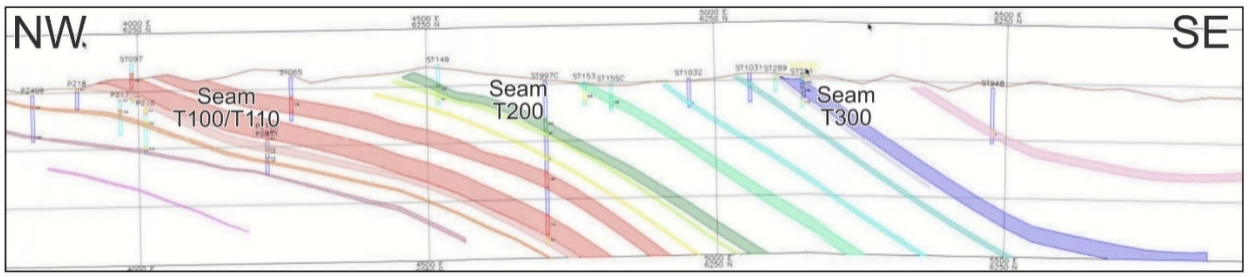

Fig. 3. Cross-section sketch of coal seams at the south Tutupan Mine (modified after ADARO, 2008)

1.3.3 Jumbang mine (Miocene coal in Asem-Asem Basin)

The third location is the Jumbang Pit Mine. This mine is owned by Arutmin Indonesia Company. Arutmin Indonesia has many coal mining concessions in the Asem-Asem Basin, and Pit Jumbang is one of the largest coal production sites. Jumbang mine is an open pit coal mine with coal reserves of 39 million tons and a stripping ratio of 2.5. Using a minimum mine slope safety factor of more than 1.3, with a single slope angle of up to 15 m and a maximum angle of 60°, the Jumbang mine produces up to 6 million tons of coal per year (Arutmin, 2015).

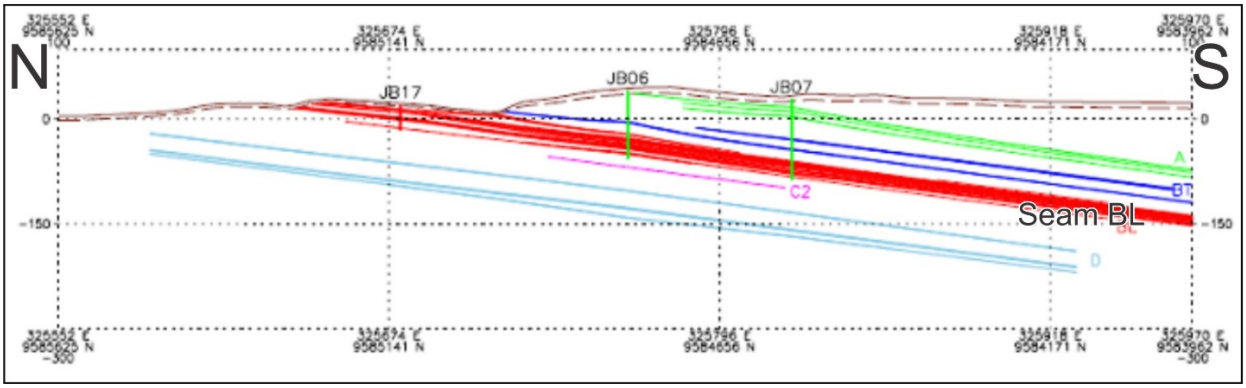

Fig. 4. Schematic cross-section of the Jumbang coal mine (modified after Arutmin, 2015)

Jumbang mine is one of several pits located in the Mulia Mine area. The Jumbang coal seam shows a general strike direction of N 35°E (Fig. 4) with an average dip of 6 – 14°. Coal thickness varies from 0.3 m to 14 m. The main seams in the Jumbang Pit are seams A1 and A2 with an average thickness of 1.6 m, BL1 10 m, and D2 4 m, while Seam C is not well developed (Arutmin, 2015).

2 Coal formation and distribution in Indonesia

2.1 Coal geology

The oldest coal is found in Silurian and Lower Devonian strata, but intensive seams appear only in Carboniferous and Permian units. Later, major coal seams were formed during the Jurassic-Cretaceous and the Paleogene-Neogene (See Walker, 2000; Fig. 5).

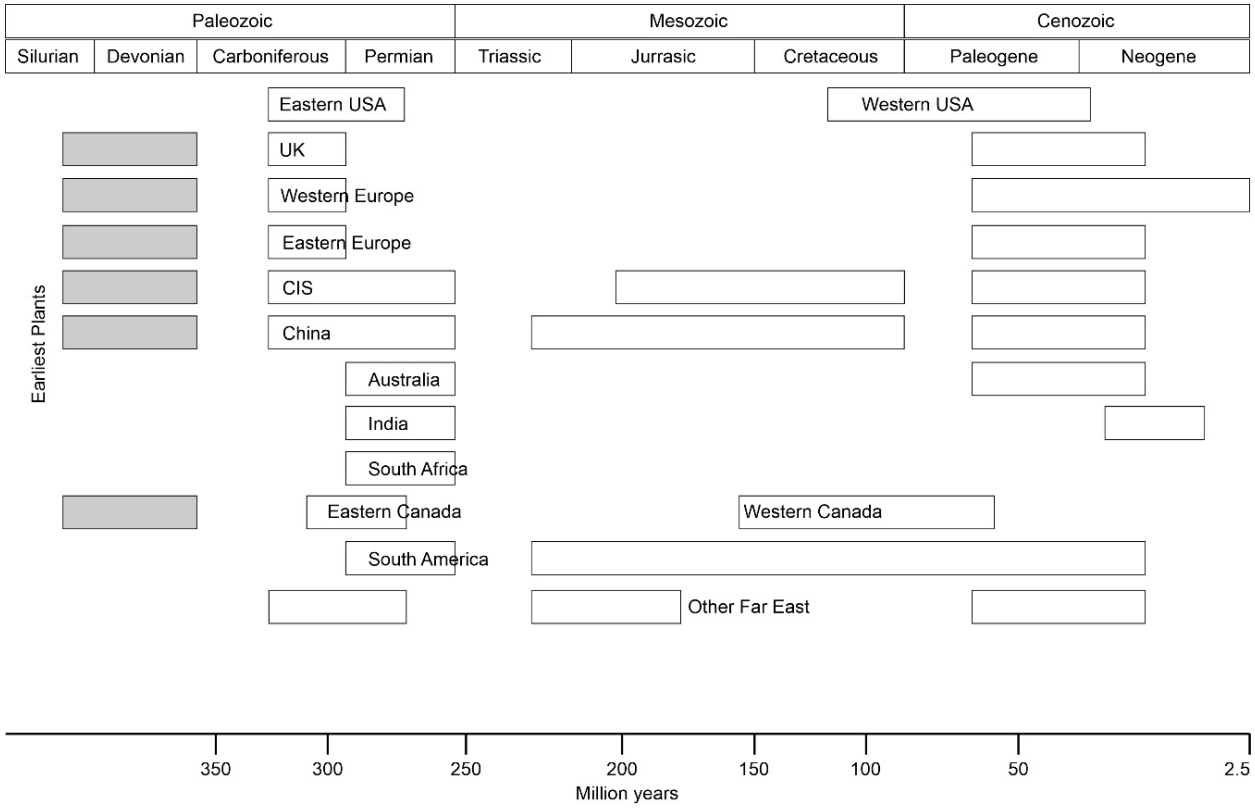

Fig. 5. Distribution of coal deposits based on geological age (after Walker, 2000)

The global distribution of coal is controlled by plate tectonic processes. Before the Early Triassic separation of Laurasia in the northern hemisphere and Gondwana in the southern hemisphere, the world was dominated by a supercontinent, called Pangaea (du Toit, 1937). During the Carboniferous Period, coal was widely formed in Laurasia, covering western and central Europe, eastern USA, and the former Sowjet-Union. Coal deposition in Laurasia ended due to a change towards an arid climate in the Permian Period. At the same time, peatlands formed at cooler and moderate temperatures on the southern side of Pangaea (Gondwanaland), which now includes South America, Africa, India, Australia, and Antarctica (Thomas, 2020).

In SE Asia, Sundaland is the largest contributor to coal-forming regions (Friederich et al., 2016). Classically, Sundaland is considered part of the Eurasian plate (Pubellier and Morley, 2014), but can be treated independently ("Sunda plate"). Friederich et al. (2016) classified the coal basins in SE Asia into five divisions: northern Sundaland, southern Sundaland, the Philippine archipelago, western Myanmar, and eastern Indonesia (Fig. 6). In the southern part of Sundaland on the islands of Sumatra and Borneo, coal was formed intensively in the Eocene and Miocene.

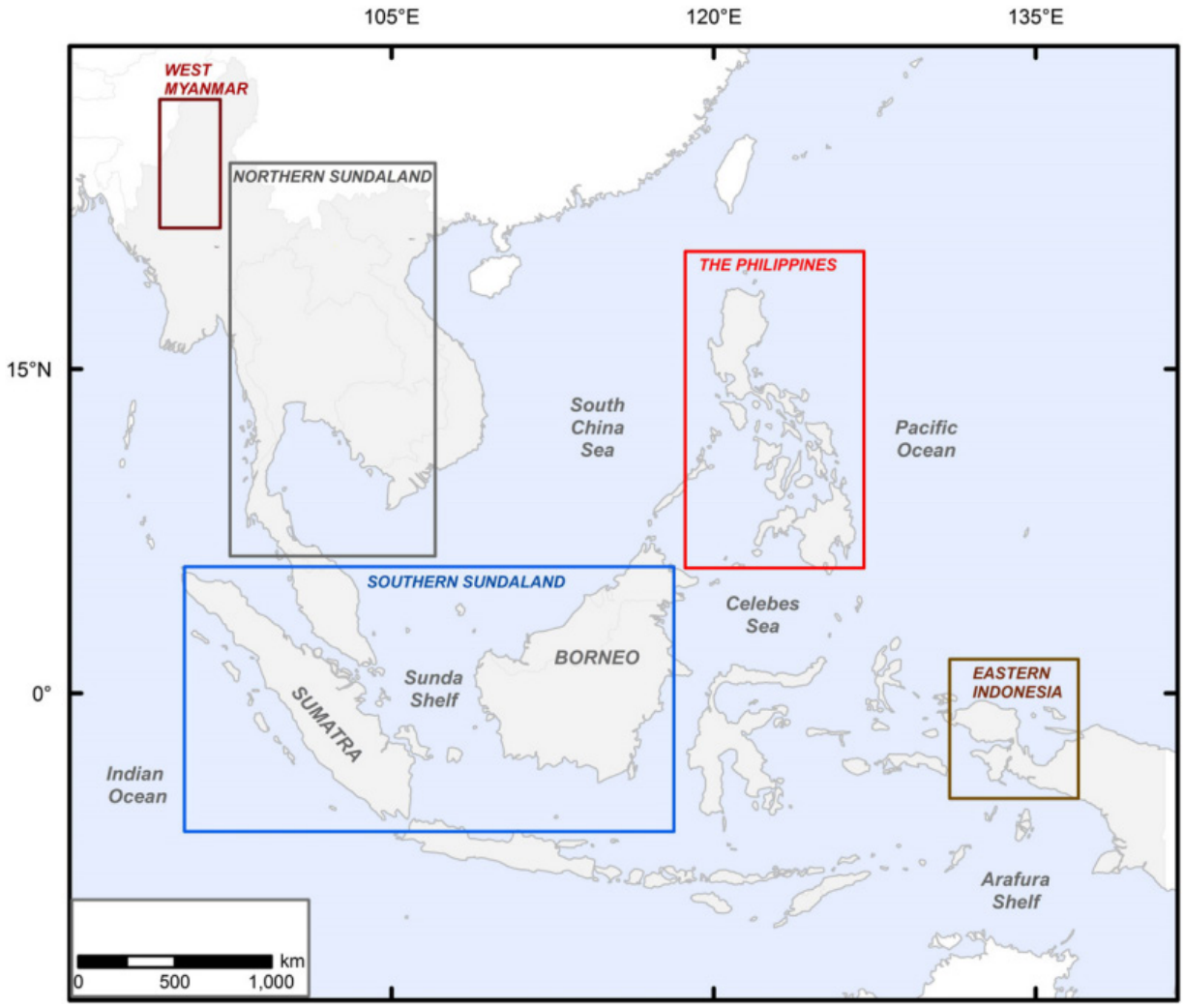

Fig. 6. SE Asian coal-bearing sedimentary basins division (Friederich et al., 2016)

2.2 Coal formation and mire types

Coal is formed in mires from organic deposits that have undergone coalification after sedimentation (Fig. 7a). There are two main types of mires that are mainly controlled by the availability and origin of water: ombrotelmites (also called ombrotrophic or raised mires), which receive water exclusively from excessive rainfall, and topotelmites (also called rhetrophic or low-lying mires), which are associated with a high (ground)water level (Fig. 7b; Diessel, 1992). Ombrotrophic (raised) mires are low in mineral matter (<< 10 % adb) and sulphur (<< 1 % adb) and poor in nutirents. Furthermore, they are characterized by acidic conditions favouring the transformation of ash layers into kaolinite (e.g., Gruber and Sachsenhofer, 2001). In contrast, low-lying mires are rich in mineral matter, often contain high amounts of sulphur (especially in mires influenced by brackish water), and are characterized less acidic conditions, which may result in the transformation of ash layers into montmorillonite (e.g., Gruber and Sachsenhofer, 2001). Pyrite is a common mineral in low-lying mires.

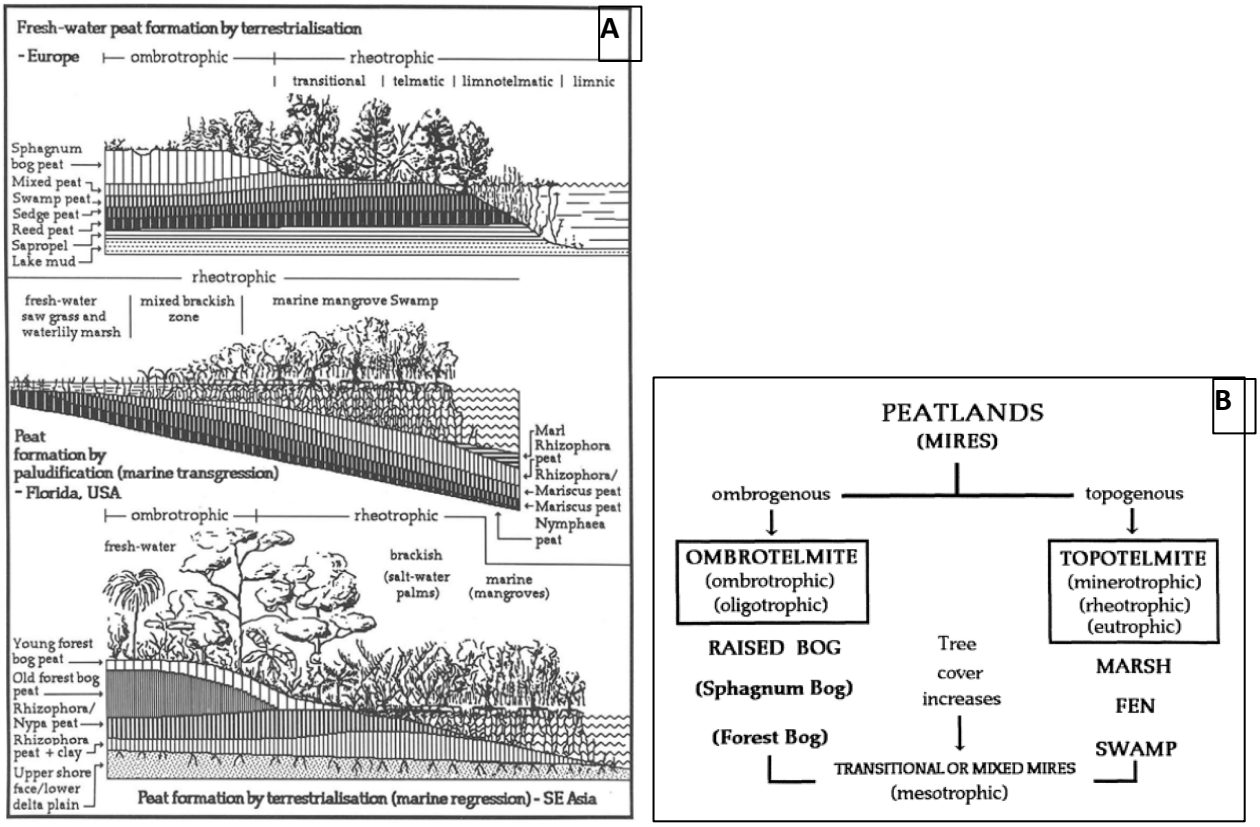

Fig. 7 (A) Three cases of peat formation in different situations. (B) Classification of mires. After Diessel (1992)

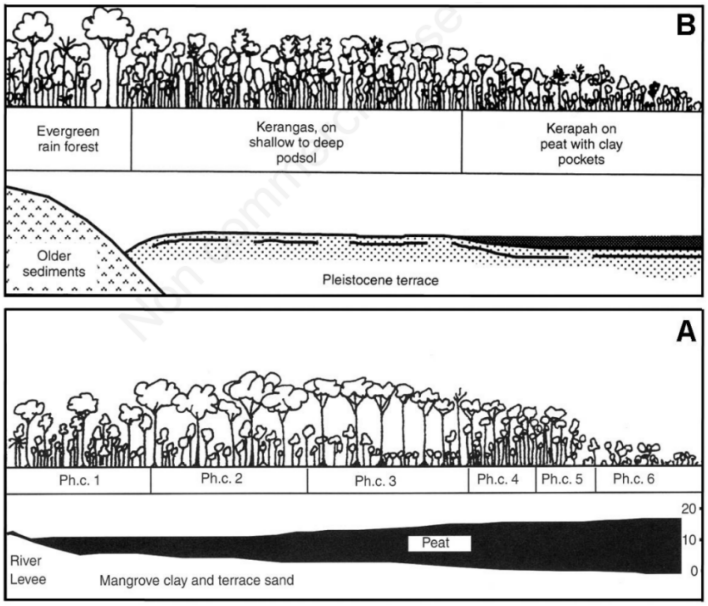

Fig. 8 Sketches of (A) Basinal mire and (B) Kerapah mire. After Morley (2013)

Many coals in SE Asia formed in ombrotrophic (raised) mires, although mixed or rheotrophic mires also contributed to coal formation. There are two types of ombrotrophic mires in SE Asia: basinal mires, which are mires close to the coast, and Kerapah or watershed mires (Fig. 8,a,b; Morley, 2013). The formation of Kerapah mires is mainly influenced by weather conditions and partly by how well water can flow out of them. Unlike basinal mires, they are not influenced by rise or fall of sea level. Moreover, in contrast to basinal mires, gymnosperms are present in significant, but small amounts (Anderson, 1963; 1964; Morley, 2013).

Basinal mires (Fig. 8a) develop along coastlines or lowland river valleys and are characterized by concentrically zoned vegetation. The vegetation in these mires changes along a gradient from the periphery to the center of the mire. The structure of these mires and the representation of phasic communities is strongly influenced by the presence of one dominant species, *Shorea albida* (Morley, 2013). Kerapah mires (Fig. 8b) develop in areas of podsolic soils where drainage is impeded and can occur in coastal regions, inland, or in mountainous regions. Kerapah mires composition has been studied in Sarawak and Brunei and is floristically similar to Kerangas (stunted, notophyllous, open-canopied forests of white podsolic sands). Although structural trends and concentric zoning within kerapah mires bear some similarities with those seen in basinal mires, consistent trends on different mires have not been identified (Morley, 2013).

2.3 Coal geology in Indonesia

Indonesia is an archipelago consisting of five large islands, Sumatra, Java, Kalimantan (= the Indonesian part of Borneo island), Sulawesi (Celebes), and Papua which are integrated with Papua New Guinea. The islands of Sumatra and Kalimantan, contribute the most to coal resources in Indonesia (Figs. 9, 10). Their combined share of world coal production reaches 9% (BP, 2021) (see Fig. 10).

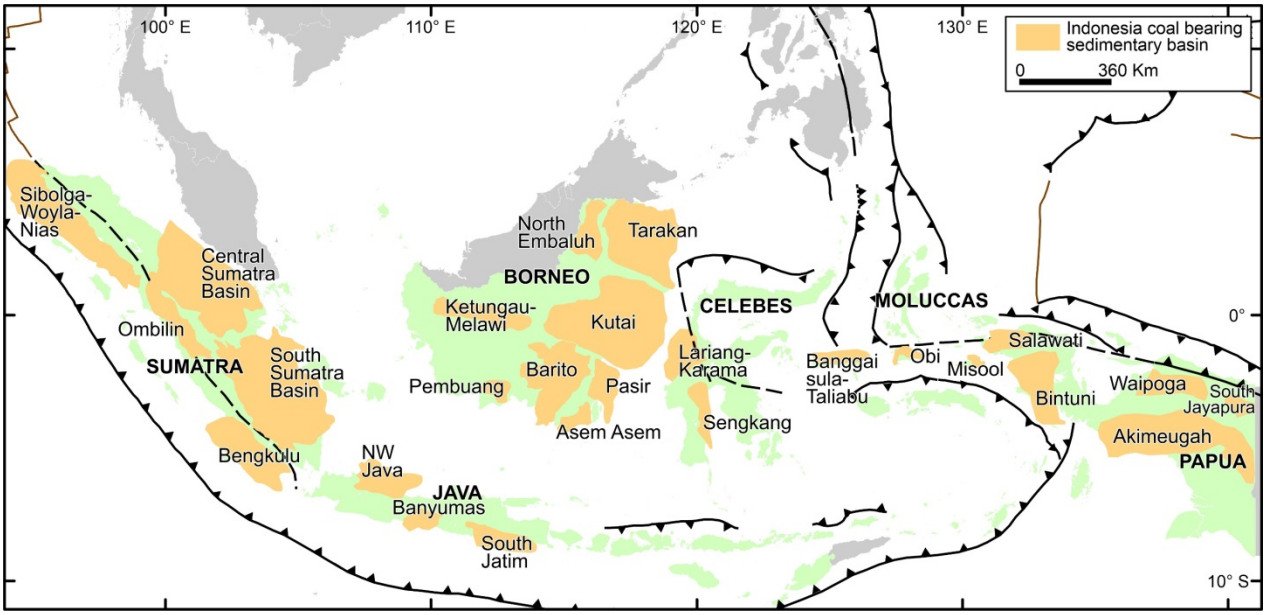

Fig. 9. Indonesia coal bearing sedimentary basin. After ESDM (2023)

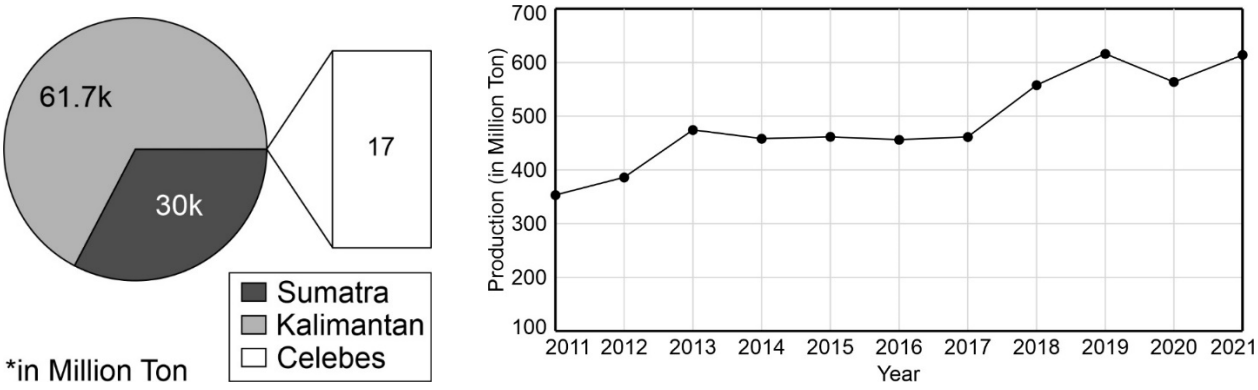

Fig. 10. Indonesia coal resources and coal production. After ESDM (2022)

Pre-Cenozoic coals are rare in Indonesia. Permian coal deposits are present in the Aiduna Formation in the Akimeugah Basin on Papua Island (Panggabean and Pigram, 1989; Fig. 9). Jurassic coals occur in the Bobong Formation, which forms part of the basal (syn-rift?) transgressive series in the Banggai Sula/Taliabu Basin on the Maluku/Moluccas Islands (Kusnama, 2008; Septriandi et al., 2012; Nompo et al., 2021).

In a tectonic-stratigraphic analysis, Koesoemadinata (2000) and Amijaya and Littke (2005) identified three Cenozoic periods of coal deposition in western Indonesia (southern Sundaland):

(1) Syn-rift deposition (Eocene-Oligocene), for example, the Sawahlunto Formation of Central Sumatra Basin.
(2) Oligocene and early Miocene post-transgressive phase deposits are found in the Sihapas Formation (Central Sumatra Basin) and the upper Talang-Akar Formation (South Sumatra Basin). The lower Tanjung Formation in the Barito and Pasir basins in southeast Kalimantan has similar post-transgressive deposits.
(3) The Mio-/Pliocene Muara Enim Formation in the South Sumatra Basin accumulated during a syn-orogenic regressive phase, similar to the Miocene Warukin Formation in the Barito, Asem-Asem and Pasir basins.

Cretaceous flysch on Celebes/Sulawesi Island was unconformably covered by less-deformed Middle Eocene clastic sediments. Minimal coal deposits formed during deposition of early rift sediments (Kalumpang Formation in Lariang-Karama Basin) dominated by platform carbonates (Calvert and Hall, 2003).

Oligocene rift sub-basins with lacustrine sediments and coal layers are present in the South Jabar (NW Java) basin on Java Island. These sediments are considered the source rock for oil and gas in the basin (Doust and Noble, 2008).

Indonesian coals often have very low sulphur contents. However, some high sulphur contents have been recorded for some coals:

- Sulphur contents of coals in the Jurassic Bobong Formation in the Banggai Sula/Taliabu Basin reach 8.0 % adb (Taliabu Island-Moluccas Group Island; Nompo et al., 2021) and even 9.7 % adb (Sehu Island; Kusnama, 2008).
- Middle Eocene coal in the Sembukung/Sembakung Formation (Tarakan Basin, Borneo Island) has a total sulphur value of 14.8 % adb (Yosep et al., 2014).
- Eocene-Oligocene coals in Malawa Formation (Sengkang/Western S. Sulawesi Basin) has sulphur contents of 9.2 % (in Bakeko Block coal) and 23.8 (?) % (in Kandangsapi Block coal) (Kusnama and Mangga, 2007).

2.1.1 Coal geology in Borneo Island

Borneo is surrounded by three marginal basins: the South China Sea, the Sulu Sea, and the Celebes Sea. To the north-northeast are microcontinental fragments of South China origin, such as Dangerous Grounds and Reed Bank. Mainland Southeast Asia (Indochina and Peninsula Malaysia) is located to the west-northwest, and the Javanese volcanic arc is to the south (Wilson and Moss, 1999). The formation of Borneo is the result of Mesozoic accretion, which involved the addition of ophiolitic material, marginal basin fill, island arc material, and microcontinental fragments onto the Palaeozoic continental core of the Schwaner Mountains in the southwest (Hutchison, 1989; Metcalfe, 1996). Borneo was originally a promontory on the southeastern margin of Sundaland. The North and South Makassar Basins (Makassar Straits), lie east of Borneo and separate it from Sulawesi (Situmorang, 1982). These basins were formed by the Middle Eocene and are bounded by two fault zones that run in a northwest-southeast direction to the north and south of the North Makassar Basin (Wilson and Moss, 1999).

There are eight main coal basins in Kalimantan. These are the Barito, Asem-Asem, Pasir, Kutai, Tarakan, North Embaluh, Ketunggau-Melawi, Mandai Keriau, and Pembuang basins (Table 1). Among them, five basins contain many large coal deposits, i.e., Barito, Asem-Asem and Pasir, Kutai, and Tarakan Basin (Figs. 11, 12).

Some authors assumed that all basins in eastern Kalimantan formed due to the Cenozoic spreading center in the Makassar Strait. Hamilton (1979), Katili (1978), and Situmorang (1982)

argued that lateral movements of around 200 km followed the rifting and opening stages of the Makassar Strait, and caused the formation of five Cenozoic sedimentary basins with coal deposits. These are from north to south the Tarakan, Kutai, Barito, Pasir, and Asem-Asem basins (Figs. 11, 12). Hamilton (1979) and Sikumbang (1986) hypothesized that the Cenozoic basins initially formed a single large depocenter that was later disrupted by uplift zones (such as the Mangkalihat Ridge and Meratus Highs) during Late Miocene orogenic activity.

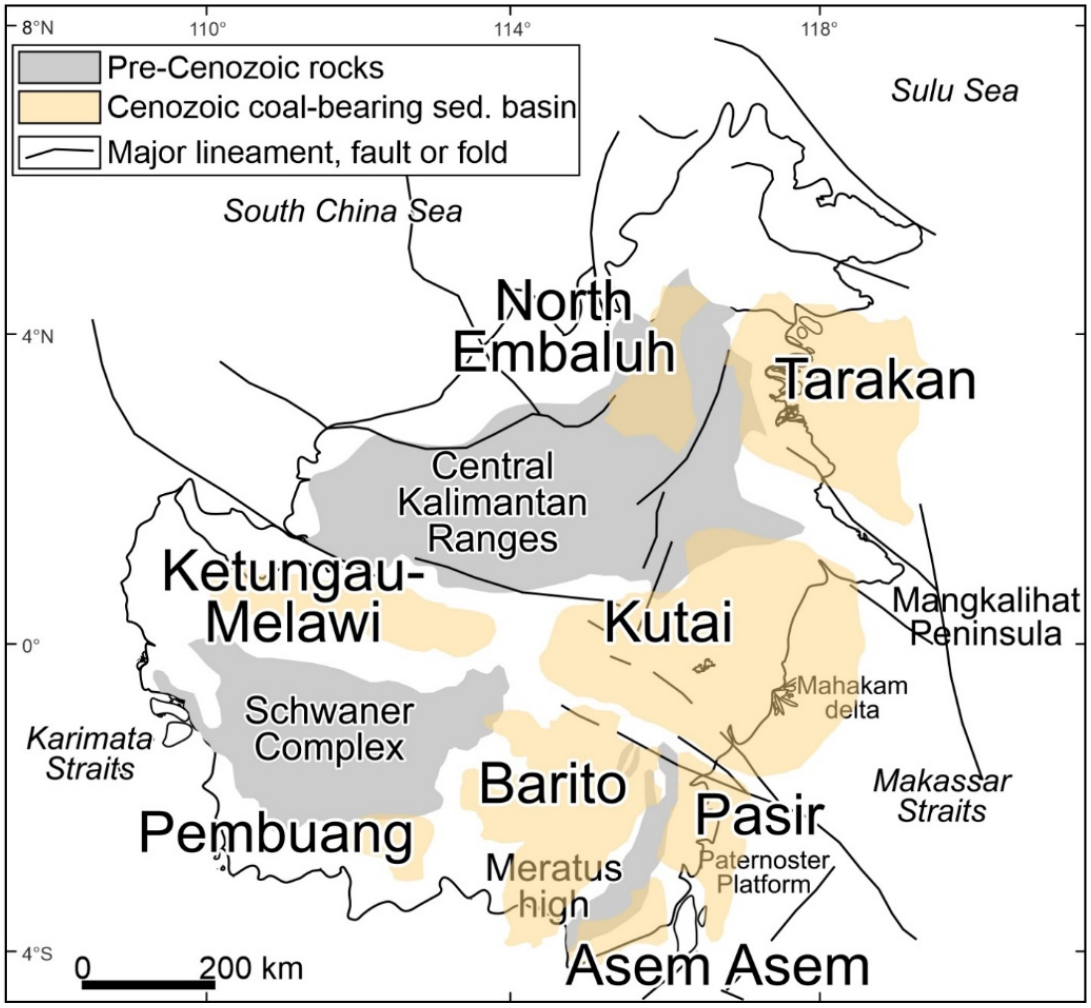

Fig. 11. Main coal bearing sedimentary basin in Borneo Island. Modified from Wilson and Moss (1999)

Table 1. Coal-bearing formations in Borneo Island

Basin	Coal-bearing formation	Geological age	Reference
North Embaluh	Longbawan	Paleocene	Willyam (2013)
	Tebidah	Oligocene	Wilson and Moss (1999)
Ketungau - Melawi	Ketungau	Early Eocene - Oligocene	Santy and Panggabean (2013)
	Kantu	Middle Eocene	Wilson and Moss (1999)
	Kampungbaru	Pliocene	Wilson and Moss (1999)
(NE) Kutai	Balikpapan	Late Miocene	Widodo et al. (2010)
	Pulaubalang	Mid Miocene	Winarno et al. (2017) Widodo et al. (2010)
	Pamaluan	Oligo-Miocene	Wilson and Moss (1999)
	Sujau	Early Eocene	Achmad and Samuel (1984)
Tarakan (Berau)	Sembukung/Sembakung	Middle Eocene	Yosep et al. (2014)
Barito (Asem-Asem, Pasir)	Warukin	Mid Miocene	Novita and Kusumah (2016)
	Tanjung	Eocene	Heryanto (2009)
Pembuang	Dahor (?)	Late Miocene - Pliocene	ESDM (2023)

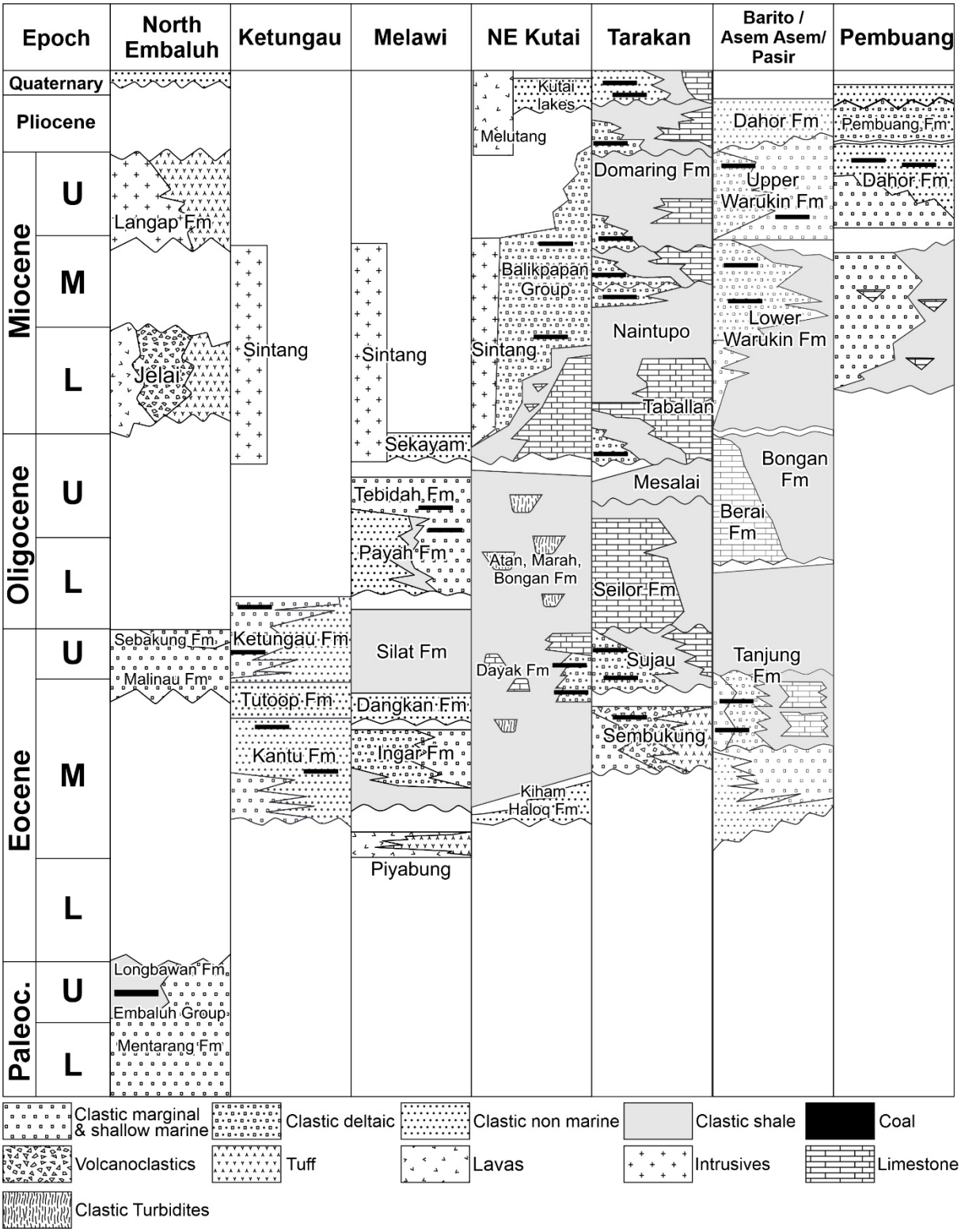

Fig. 12. Simplified stratigraphy of coal-bearing basins on the island of Borneo. Modified from Wilson and Moss (1999); Heryanto et al. (1995); Soetrisno et al. (1995)

A. North Embaluh Basin

The North Embaluh Basin is located in the northern part of Borneo Island and administratively lies between Indonesia and Malaysia, covering Malinau Regency in province of East Kalimantan. The basin is located west of the Tarakan Basin. The Cenozoic succession starts with the Paleocene Embaluh Group, which consists of two main formations: Mentarang Formation and Longbawan Formation (Fig. 12). Above a hiatus, the Upper Eocene marginal and shallow marine clastics of the Malinau Formation and Sebakung Formation follow (Heryanto et al., 1995; Sodiq and Hermiyanto, 2021). The Jelai Group and Langap Formation include volcanic deposits and were deposited during the Miocene.

Coal is found in the Longbawan Formation. According to Willyam (2013), seam B in a Malinau mine has an ash yield of 1.5 % adb and a calorific value of 5911 cal/g, while seam A has an ash yield of 1.6 % and a calorific value of 5941 cal/g, with thickness ranging from 8 to 35 m according to well logs.

B. Ketungau and Melawi Basin

The early development of the Melawi Basin has a similar stratigraphic succession and lithologic distribution to that of the Ketungau Basin. The sedimentary phase of the Ketungau Basin occurred during Eocene until Oligocene (Fig. 12). The Piyabung/Haloq Formation, the oldest sediments deposited in the Melawi Basin, is regarded as an equivalence of Lower Ketungau (Kantu Formation). This formation consists of fluvial quartz sandstone and conglomeratic unit, deposited until Upper Eocene. The Ingar Formation unconformably overlying the Piyabung Formation, consists of alternating mudstone, silt, and fine sandstone of lacustrine deposit. The Dangkan Formation was deposited unconformably over the Ingar Formation. In the Melawi Basin, It is followed by the Silat Formation that was deposited during Upper Eocene – Oligocene, while in the Ketungau Basin, at the same time, the Ketungau Formation was deposited (Santy and Panggabean 2013).

In the early Oligocene, the size of the depocenter in the predominantly fluviatile west Kalimantan Basin (comprising the Ketungau and Melawi basins) began to decrease or had

already been filled. According to fission track dating of apatite grains and seismic data, the Semitau ridge began its uplift during the Oligocene (Moss et al., 1998). This uplift likley caused more erosion than deposition in this region (Wilson and Moss, 1999).

Middle Eocene coal is found in the Kantu Formation, while Eocene-Oligocene coal occurs in the Ketungau and Tebidah formations. Santy and Panggabean (2013) showed that coal in the Ketungau Formation has a TOC value of 50.6 %, an HI of 132 mg HC/g TOC, and a Tmax of 412°C.

C. Kutai Basin

The Kutai Basin lies partly onshore in the eastern part of the island and offshore in the nearby Makassar Strait. Several publications (Gerard and Oesterle, 1973; Samuel and Muchsin, 1975; Rose and Hartono, 1978; Nuay et al., 1985; Carbonel and Moyes, 1987; Ott, 1987; Caratini and Tissot, 1988) in (Daulay, 1994) show the evolution of the Kutai Basin. In particular, the complex nature of the Mahakam River delta, which has been growing into the Makassar Strait since the Early Miocene, has attrated much attention. The Kutai Basin is the widest and deepest Cenozoic basin in eastern Kalimantan and in all of Indonesia.

The Kutai Basin is bounded by the Laut High to the south, the Meratus High to the southwest, the Kuching High to the northwest, and the Mangkalihat Ridge / Suikerbrood High to the northeast. These boundaries have little effect on the depositional pattern, except for transient uplift in the Late Oligocene (Daulay, 1994). The Meratus High and the Laut High are located onshore and received sedimentation of moderate thickness, whereas the Mangkalihat / Suikerbrood High is located near the axis of early Cenozoic subsidence (Daulay, 1994 and references therein). The Kuching Arc was transgressed in the early Cenozoic, and the arc was uplifted in the Oligocene. This is evidenced by the fact that the remaining sediments in the arc have been mapped as early Cenozoic (Daulay, 1994 and references therein).

Coal in the Kutai Basin is found in the Miocene Balikpapan Group (Kampungbaru, Balikpapan, Pulaubalang, and Pamaluan formations). Winarno et al. (2017) reported that coal in the Pulaubalang Formation has a moisture content of 12.7 % adb, an ash yield of 4.6 % adb, a

calorific value of 6099 cal/gr, and a sulphur content of 1.6 % adb. Coal in the Balikpapan Formation has a moisture content of 13.9 % adb, an ash-yield of 3.4 % adb, a calorific value of 6005 cal/gr, and a sulphur content of 1.9 % adb. Based on its calorific value, this coal is categorized as Subbituminous A.

Widodo et al. (2010) showed that coal from the Sebulu and Centra Busang mines has higher sulphur (up to 3.2 wt.%) and pyrite (up to 4.3 vol.%) contents than coal from the Embalut mine in the Mahakam Delata, which is characterized by low sulphur (< 1.0 wt.%) and pyrite (< 0.7 vol.%) contents. Pyrite was found in the coal as framboidal, euhedral, massive, anhedral, and epigenetic pyrite in cleats/fractures. Widodo et al. (2010) related the high ash, sulphur, and pyrite contents of coals in the Kutai Basin to Cenozoic volcanic activity, whereby aeolian material was transported to the mire during peat accumulation. Using biomarker and isotope data, Widodo et al. (2009) showed floral changes during deposition of the Miocene Embalut coal. The aromatic hydrocarbon fractions of all coal samples were dominated by cadalene in the lower boiling point range and picene derivatives in the higher boiling point range. Cadalene was attributed to the contribution of Dipterocarpaceae and various hydrated picenes to the contribution of additional angiosperms to the coal-forming vegetation.

D. Tarakan Basin

The Tarakan Basin is a collective name for four sub-basins located in northeast Kalimantan. It consists of the offshore Tarakan and Muara sub-basins and the onshore Berau and Tidung sub-basins onshore. The Tarakan Basin is bounded to the north by the Semporna Peninsula, to the west by the Sekatak-Berau Ridge (which is part of Kuching High), to the south by the Mangkalihat Peninsula, and to the east by the deepwater area of the Sulawesi/Celebes Sea (Achmad and Samuel, 1984; Husein, 2017).

Achmad and Samuel (1984) divided the Tarakan stratigraphy into five depositional cycles.

- The first cycle comprises from base to top Sembakung/Sembukung Fm, the Sujau clastics, Seilor carbonates, and Mangkabua marls, which represent a Late Eocene to Late Oligocene transgressive event.

- The second cycle datet as latest Oligocene to early Middle Miocene, includes the Tempilan clastics interfingering with Tabalar limestones and overlain by Naintupo shales.
- The third cycle lasted from the Middle to Late Miocene and is marked by a tremendous supply of Meliat deltaic sediments followed by deeper marine Tabul and Santul clastics.
- The fourth cycle was deposited during the Pliocene and includes the Tarakan deltaic sequences.
- The fifth cycle (early to late Pleistocene) is formed by the Bunyu deltaic succession depositing during the ongoing sea-level rise.

Coal was found in the Upper Eocene Sujau Formation (Achmad and Samuel, 1984). Coal outcrops on Tarakan Island may be of Miocene age (Husein, 2017). Based on ESDM (2023), the calorific value of coal found in the northern Tarakan Basin is 6100 - 7100 cal/gr, while its calorific value decreases towards the east (towards the coast), ranging from 6000 to less than 5100 cal/gr. Yosep et al. (2014) reported that middle Eocene coal in Sembukung/Sembakung Formation has a moisture value of 0.7 – 4.5 % adb, ash yield of 18.3 – 25.5 % adb, a total sulphur content of 1.9 – 14.8 % adb and a calorific value of 4193 – 6212 cal/gr adb.

E. Barito (Asem-Asem and Pasir) Basin

The Barito, Asem-Asem, and Pasir basins are located in southeast Kalimantan and are separated by structural features of the Mesozoic. The Sunda Shield (Schwaner Complex) bounds the Barito Basin in the west and the Meratus High, which consists of melange belts and ophiolites, in the east. In the north, these basins are separated from the Kutai Basin by the South Kutai Fault (also called Paternoster High), while to the south the basin joins the East Java offshore Basin.

The Asem-Asem Basin and the Pasir Basin (formerly called the Pasir Sub-Basin of the Kutai Basin and Barito Basin) are separated from the Barito Basin by the Meratus High in the west. The Pasir Basin is bounded by the Makassar Straits in the east, and South Kutai Boundary Fault (the Paternoster High) in the north (Fig. 11).

Bishop (1980) and Siregar and Sunaryo (1980) stated that Cenozoic sedimentation in the Barito Basin and Asem-Asem Basin was completed as a single major transgressive-regressive cycle,

which was only disturbed by slight variations and sub-cycles locally. The transgressive Tanjung Formation (Eocene-Oligocene; Witts et al., 2012), which covers the basement and has relatively low relief, was deposited in shallow marine to deltaic environments and consists of sequences of coarse clastic rocks intercalating with shales and coal beds. The marine influence increased during the Oligocene and continued into the Early Miocene, producing extensive limestone and marl deposits of the Berai Formation (Fig. 12). The Barito and Asem-Asem Basins subsided quickly. At the same time, both continental cores (to the west) and proto-Meratus High (to the east) were uplifted. The Warukin and Dahor formations represent paralic and delta sequences.

Orogenic activity in Plio-Pleistocene times produced a strong westward movement of the Meratus High (tectonic nappes). It folded and thrusted the basin fill into a series of anticlinal structures, partially controlled by basement features (Siregar and Sunaryo, 1980).

Witts et al., (2012) explains in detail about the Tanjung Formation. The Tanjung Formation is the oldest sedimentary unit in the Cenozoic Barito Basin. It was formed from late Middle Eocene to late Early Oligocene, and records the initial rifting and subsidence of the basin, followed by a marine transgression. The formation consists of three members: the Mangkook, the Tambak and the Pagat. The Mangkook Member is composed of alluvial and fluvial deposits that eroded the basement rocks. The Tambak Member is dominated by fluvio-tidal and estuarine deposits that reflect a coastal floodplain environment. The Pagat Member is a thin layer of marginal and shallow marine deposits that marks the final phase of the Tanjung Formation. The formation was mainly sourced from the Schwaner Complex in west Borneo, the Karimunjawa Arch and the southern extension of the Meratus Complex under the Java Sea, as indicated by heavy minerals and zircon geochronology.

The marine Berai Formation follows above the Tanjung Formation. This formation is Oligocene to Early Miocene in age and consists of thick limestone, marl, and fine-grained clastic strata. This formation is coeval with the Pemaluan Formation in the Kutai Basin. The differences between these two formations regard facies and lithology ((Rustandi et al., 1984) [in Daulay, 1994]).

The Mid-Miocene Warukin Formation, deposited during the regressive phase of the Cenozoic transgressive-regressive cycle, overlies the Berai Formation. The Warukin Formation consists of soft, fine-grained clastic rocks with siltstone, sandstones, and coal seams reaching a thickness of 40 meters (Heryanto and Panggabean, 2013).

The Dahor Formation, Pliocene to Pleistocene in age, consists of poorly consolidated sandstones and fine-grained clastic sediments with coal seams. Quaternary deposits in the Dahor Formation include alluvium, estuary mud, and coastal sands.

Novita and Kusumah (2016) reported that coal in the Warukin Formation (Kalumpang district, Binuang, South Kalimantan) has a high vitrinite content (up to 94 %), while liptinite and inertinite contents are up to 4 %. Mineral percentages (dominated by pyrite) are up to 5.5 %. The vitrinite reflectance (%Rr) values range from 0.29 – 0.49 %Rr. Heryanto and Panggabean (2013) reported that the coal in Binuang (Kandangan area, Warukin Formation) is 0.5 to 12 m thick and shows varying vitrinite (59.4 – 86.6 %), liptinite (0.8 – 9.5 %), and inertinite (3.4 – 17.4 %) contents. %Rr values are 0.42 – 0.45 %. Kusnama (2008) explained that the Warukin Formation in the western part of the Barito Basin is 30 to 180 cm thick and that moisture contents range from 12.0 – 22.2 % adb. Ash yields (1.6 – 21.1 % adb) and calorific values (4279 – 5630 cal/g adb) are highly variable, while sulphur contents are generally low (0.2 – 0.3 % adb).

Heryanto (2009) reported that coal in the Tanjung Formation (in the Rantau city area, South Kalimantan) has vitrinite reflectance values ranging from 0.43 – 0.50 %Rr. The percentage of vitrinite reaches 89.4 %Rr, while liptinite (up to 74.0 %?) and inertinite (up to 16 %) are locally very high.

F. Pembuang Basin

Pembuang rock is mainly characterized by notching of structure intracratonic basin while in the north-north east parts it is more oriented to shelf edge (Sunarjanto et al., 2008). The oldest Cenozoic rocks are Early-Middle Miocene clastic sediments (Soetrisno et al., 1995). These sediments resemble the lower part of the Warukin Formation in the Barito Basin. The Upper Miocene succession consists of sandstones, claystones, and coal seams. There are similarities with the Dahor Formation in the Barito Basin. The Pliocene-Pleistocene Pembuang Formation includes carbonaceous sandstone, conglomerate, siltstone, claystone, and peat. This formation probably developed in a deltaic environment. Pangkalanbun coal in this basin has calorific values < 5100 cal/gr (ESDM, 2023).

2.2.2 Coal geology in Sumatra Island

Six coal-bearing basins exist on Sumatra island: North Sumatra, Central Sumatra, South Sumatra, Woyla (Meulaboh)-Sibolga-Nias, Ombilin, and Bengkulu Basins (Figs. 13, 14; Table 2).

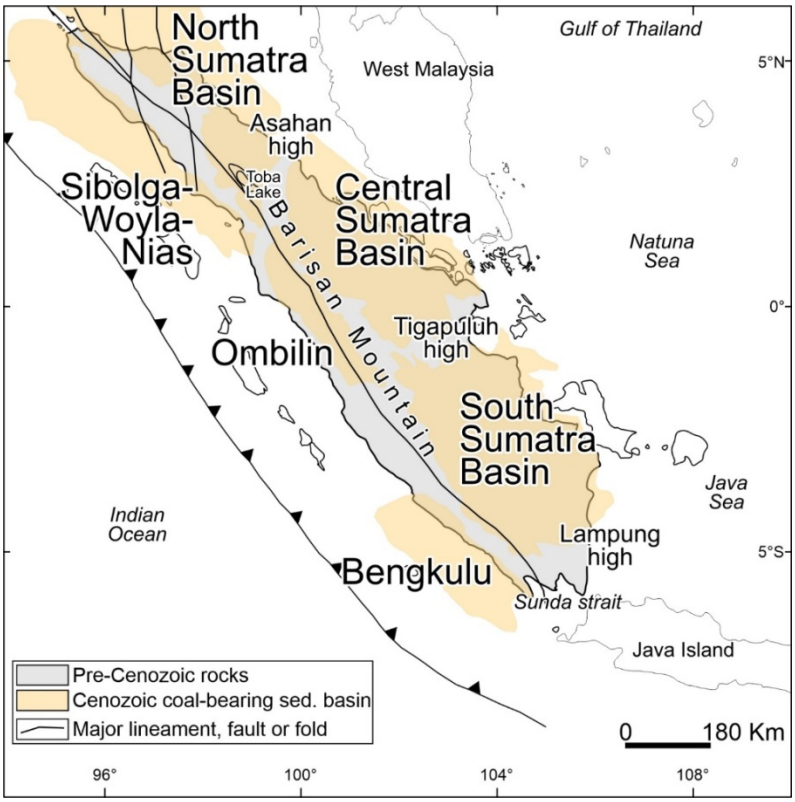

Fig. 13. Simplified map of cenozoic coal bearing sedimentary basin in Sumatra Island. Modified from Barber et al. (2005) and ESDM (2023)

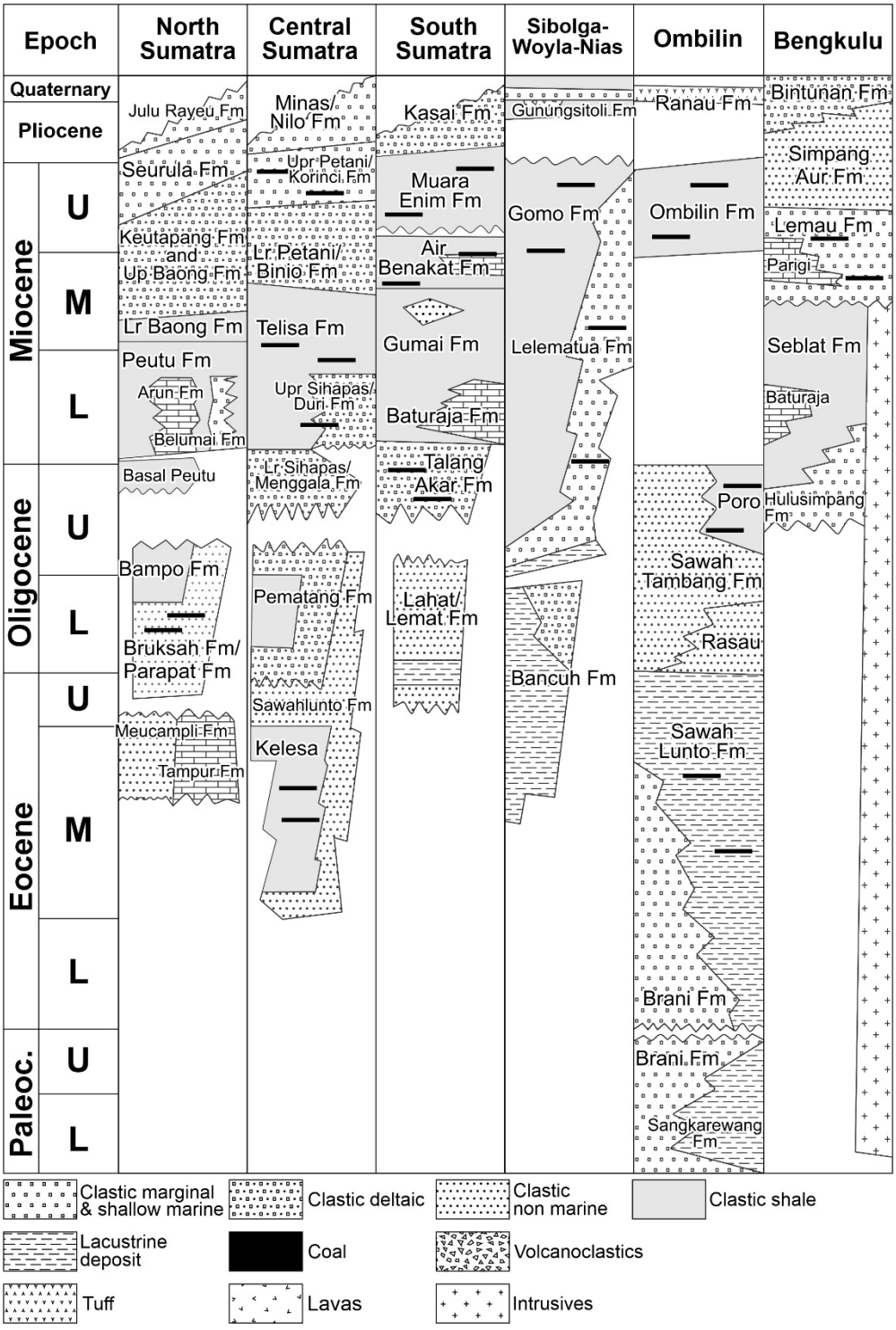

Fig. 14. Simplified map of cenozoic coal bearing sedimentary basin in Sumatra Island. Modified from De Smet and Barber (2005); Hidayatillah et al. (2017)

Table 2. Coal-bearing formation in Sumatra Island, Indonesia

Basin	Coal-bearing formation	Geologic time	Reference
North Sumatra	Bruksah/Parapat	Early Oligocene	Thomas (2005); Kamili et al. (1976)
Central Sumatra	Korinci	Mio-Pliocene	Coster (1974)
	Telisa	Late Miocene	Thomas (2005)
	Sihapas -Lakat	Oligocene-Miocene	Thomas (2005)
	Kelesa	Eocene	Aulia et al. (1990)
South Sumatra	Muaraenim	Mio-Pliocene	Coster (1974); Amijaya and Littke (2005; 2006)
	Airbenakat	Mid Miocene	Thomas (2005)
	Talang Akar	Late Oligocene – Early Miocene	Bishop (2001)
Nias-Woyla-Sibolga	Gomo	Pliocene	Thomas (2005)
	Lelematua	Miocene	De Smet and Barber (2005)
	Bancuh	Oligocene	De Smet and Barber (2005)
Ombilin	Ombilin	Late Miocene	Koesaemadinata and Matasak (1981)
	Poro Member	Late Oligocene	Koesaemadinata and Matasak (1981)
	Sawah Lunto	Eocene	Koesaemadinata and Matasak (1981)
Bengkulu	Lemau	Mio-Pliocene	Heryanto R and Suyoko (2007)

A. North Sumatra

The North Sumatr Basin is separated from the Central Sumatra Basin by the Asahan Basement High (Figs. 13,14). The sediments in the North Sumatra Basin are primarily of Paleogene age.

Cenozoic sedimentation in the North Sumatra Basin (Fig. 13) commenced during a marine transgression from the NW across the surface of eroded Paleozoic and Mesozoic sedimentary rocks and igneous rocks. Along with this transgression, a sequence of (continental and paralic) coarse clastic sediments with coal seams and subordinate limestones was widely deposited from Nias Island (west) to Malacca Straits (east). The age of these sequences ranges from Eocene and Oligocene in the north to Lower Miocene in the south-east. A second marine transgression occurred in Oligocene to Miocene times with deposition of thick marine shales, accompanied by subordinate sandstones and limestones, as evidenced by the Bampo, Bruksah/Parapat formations (Kamili et al., 1976) in the central and northern areas of the basin.

In the foothills west of the Barisan Range (Meulaboh area), coals and carbonaceous shales have been recorded in the Neogene sequence. Five coal seams, 0.4 to 3.0 m thick, have been

observed. The coal intercalates with clay and bituminous shale. In the north of Aceh, to the east of the Barisan Mountains, there is Paleogene basalt and coal with a thickness of less than one meter. Based on Darman et al. (2000) and the interpretation of the Geological Map of Indonesia (Medan Sheet) (Cameron et al., 1982), basalt overlies the coal seam. West of Medan (Bohorok Regency) there is coal in layers, 0.4 – 0.5 m thick, with a dip of 45° and dip direction is N 135° E, and relatively thick coal (six meter) is found in the Kalu River (Bemmelen, 1949 and Robertson Research 1974 in Thomas, 2005). Coal contains significant amounts of pyrite.

The coal in this basin (Indra Makmur coal and Birem Bayeun coal) has a low calorific value (<5100 cal/g; ESDM, 2023), Thomas (2005) also mentioned that in the central part of this basin, the coal seams are low rank coal.

B. Central and South Sumatra

At the end of the Cretaceous period, the Central and South Sumatra regions formed a large landmass. At the beginning of the Cenozoic era, fault-bounded troughs formed within this land. The earliest Cenozoic sediments were deposited in these troughs. Afterward, sedimentation expanded across the margins to form the Central and South Sumatra Basin. Throughout the Cenozoic age, this basin was separated from the North Sumatra Basin by the Asahan Basement High (Fig. 13). The basin is asymmetrically bound to the SW by faults and horst structures formed by pre-Cenozoic rocks along the Barisan Range and towards the NE by pre-Cenozoic rocks on Tigapuluh High near the original Cenozoic era depositional boundary. Cenozoic sediments along the southwest coast of Sumatra near Bengkulu (west of the Barisan Range; Fig. 13) suggest that the South Sumatra Basin extended farther west than the present outcrop boundary.

The Central and South Sumatra Basins include Paleogene and Neogene sediments. Paleogene sediments consist of paralic and tuffaceous non-marine clastic sediments preserved in graben structures (Lahat/Lemat, Pematang, and Kelesa formations) (Thomas, 2005). Neogene sediments, consisting of marine shale, limestone, and shallow water sandstones, represent a transgressive phase of the sea, passing upwards into non-marine shale (Muara Enim Formation)

and Korinci Formation from the late Miocene and Pliocene series and extensive coal formation (Coster, 1974).

Some coal is exposed in Central Sumatra in the Korinci, Telisa, Upper Sihapas, and Kelesa formations (Van-Bemmelen, 1970 in Thomas, 2005). Generally, there are only one or two coal seams at all sites. Most coal seams are thin (<1 m) and of low quality with clay or carbonaceous shale.

Significant Paleogene coal deposits occur in the Painan Regency (Kelesa Formation) on the west coast of Sumatra south of Padang, where six coal seams are up to two meters thick. This coal has been affected by basalt volcanic intrusion and dolerite. There is also coal interbedded with shale, with a total thickness of 10 – 15 m and a dip of up to 45°. The Sungei-Sapuh / Sungei-Turuh District has several coal seams, one of which is 2 – 4 m thick. In the Batang Tui area and many areas on the west and east coast, uneconomical coal is also found (Thomas, 2005).

Other significant coal deposits in central and southern Sumatra originated in the Neogene period. Neogene coal occurs in the Korinci Fm in the Central Sumatra Basin (Fig. 13). This coal occurs in the Pliocene Muaraenim Formation; usually there are two or three seams are interbedded with tuffaceous horizons. The most significant coal development is along the Piladang River. There are three coal seams with a total thickness of around nine meters (Thomas, 2005).

In southern Sumatra, almost all coal is found in the Lahat Formation in Jambi Province. Coal is estimated to have the same age as coal in Ombilin but has a lower thickness. Seam thickness does not exceed 1.5 m and usually is less than 0.5 m. Coal is present in conglomerates, sandstones, and shales, similar to those in Ombilin. Paleogene coal in South Sumatra has yet to be proven to have economic value. On the other hand, Neogene coal in Jambi Province produces economic two- or three-seam lignite, with 5 – 7 m thick and low dip.

In Bukit Asam in the South Sumatera Province, Miocene coal in the Pelambang group has been exploited since 1919. There are three coal groups.

- The lowest group contains the Merapi seam (8-10 m thick) and a few thin coal seams.
- The middle group contains the Mangus seam with 14 to 22 m thick coal and a four-meter-thick clay-tuff band. This layer is separated from the overlying Suban seam by 15 m of barren rocks. The Suban seam has 7-10 m thick coal, containing a 1.5 m clay layer, and about 30 m above, includes 5-8 m of coal (Petai seam).
- The third and top group contains six or seven coal seams, the youngest reaching 30 m. In the Bukit Asam area, coal has been converted by young andesite intrusions from the Serelo Mountains to produce locally altered coal in the form of sub-bituminous, bituminous, and anthracite coal.

Coal-bearing sediments with two lignite seams, 2 and 5 m thick, occur in Sukamarinda, which is directly adjacent to Bukit Asam. These seams have been altered locally by igneous intrusions. In the Ajer Serillo area, the lignite layer is quite thick, while in the Bunian region (SNI, 2011), changes in thickness and continuity of lignite due to thermal influences. In the Kendin-Ringin area, more than twelve seams (5 – 15 m thick) are present. All of these areas have coal similar to those found at Bukit Asam.

Amijaya and Littke (2005) present the results of microfacies analysis and paleoenvironmental reconstruction of Cenozoic Tanjung Enim area (Muara Enim Formation) low-rank coal from the South Sumatra Basin, Indonesia. The research conducted petrographic, mineralogical, and geochemical investigations on 20 coal samples collected from four boreholes. This study classified coal facies into four types: vitrinite-dominated, inertinite-dominated, liptinite-dominated, and mineral-dominated. Based on the relationship between facies and coal quality indicators, the coal depositional setting is inferred with the hypothesis that Tanjung Enim coal was formed in environments with varying degrees of marine influence, peat accumulation, and preservation. Amijaya and Littke (2006) describe the thermally metamorphosed coal from the Muara Enim Formation in the South Sumatra Basin in detail. This coal has a low moisture content (only < 3 wt.%) and volatile matter content (< 24 wt.%, daf), as well as high carbon

content (> 80 wt.%, daf) and vitrinite reflectance (Rr_{max} 1.87 – 6.20 %Rr), which the typical coal have high moisture content (4.1 – 11.3 wt.%) and volatile matter content (> 40 wt.%, daf), and carbon less than 80 wt.% (daf) and low vitrinite reflectance (Rr_{max} 0.52 – 0.76 %Rr). In the coal samples from the Tanjung Enim area in South Sumatra Basin, Indonesia, the maceral percentages vary depending on the rank of the coal. Vitrinite is the most abundant maceral in low-rank coal from Mangus seams, composing 69.6 – 86.2 vol.%, while liptinite and inertinite are minor constituents. In high-rank coal from Suban seams, thermally altered vitrinite contains 82.4 – 93.8 vol.%. The Tmax values increase with maturity, ranging from 420 – 440°C for low-rank coals to 475 – 551 °C for high-rank coals. The Oxygen Index of all studied coals is low (OI < 5 mg CO_2/g TOC), and the high-rank coals have a lower Hydrogen Index (< 130 mg HC/g TOC) than the low-rank coals (about 300 mg HC/g TOC).

C. Sibolga-Woyla-Nias Basin

The Nias Basin is part of the Sumatran Forearc and the Sunda subduction system. The Sumatran arc has a classic morphology of trench, accretionary prism, outer-arc ridge, forearc basins, and a volcanic chain with active andesitic volcanism. The outer-arc ridge along Sumatra comprises the outer part of the forearc rather than forming part of the accretionary prism. The subduction direction varies from nearly orthogonal off Java to oblique west of Sumatra, where the trench strikes N 140° E (Deighton, 2014; Samuel and Harbury, 1996).

In the northeastern part of Nias Island (in West Sumatera province), coal is derived from Paleogene sediments; there are one to two relatively thin coal seams with a dip of 20 – 40° to the west. On the west coast of the island of Sumatra, coal originates from Paleogene Sibolga and Loser formations in the Tapaktuan and Tapanuli Bay areas. In Tapaktuan, two coal seams dip 25 – 45°. The thickness is 0.2 – 0.6 m. The coal is rich in pyrite and clay-rich. In the northern part of Tapanuli Bay, coal has a dip of 8-20° and is relatively thin (0.2 – 0.5 m) (Thomas, 2005).

Coal is found in the Oligocene Bancuh Formation, the Miocene Lelematua Formation, and the Gomo Formation (De Smet and Barber, 2005). In some areas, coal is indicated with a calorific

value of < 5100 cal/g (Woyla coal, Reudeup coal, Sumber Batu coal), and there are many coal deposits with a calorific value of 5100 – 6100 cal/g in this basin (ESDM, 2023).

D. Ombilin Basin

The most important coal deposit in the Central Sumatera province (Ombilin Basin) and the main coal producer is the Ombilin Coalfield, which occurs in the Eocene Sawahlunto Formation (Fig. 8). This coal is located in the Barisan Mountains 90 km inland from Padang (Fig. 7). Coal deposits occur in the intermontane Ombilin Basin, oriented NW-SE, in line with the main structural trends of the Barisan Range. This basin has a block-faulted WNW-ESE direction and an NNE-SSW direction. The coal-bearing sediments are folded and affected locally by normal and reverse faults, making the correlation of coal seams difficult (Koesaemadinata and Matasak, 1981). The Ombilin Coalfield is located in the northwestern part of the Ombilin Basin. The coal mines are geographically divided into the coal mining areas of Sungai-Durian, Tanah Hitam, Sugar, Sigalut, and Parambahan (Thomas, 2005).

The Sawahlunto Formation in the Ombilin Basin consists of conglomerates, sandstones, and shales. In the Tanah Hitam and Sungai Durian areas, the lower part of the sequence contains a thin layer of coal, called layer D. The upper part of the formation comprises three main coal seams, designated as A (average thickness: 2 m), B (0.6 – 1.0 m) and layer C (average thickness: 6 m). These seams occur in depths of 40-80 m and dips 12° to the east. (Thomas, 2005).

East of the Ombilin Basin, Neogene-aged coal was discovered in the Cerenti area near Rengat in Riau in 1988. Here, the Mio-Pliocene Korincio Formation contains six coal seams with thicknesses ranging from 1.6 to 14.0 m. In the Sinamar coal basin, which is further south, on the border between Jambi and West Sumatera provinces, there is Oligocene coal, which has a thickness of 2.0 to 9.0 m. Adjacent to the Sinamar area, in Mampun Pandan, a 5.0 to 11.0-meter-thick coal seam was also observed (Thomas, 2005).

Patria and Anggara (2022) describe coals from the Ombilin Basin are high-volatile bituminous C coals with mean random vitrinite reflectance of 0.58 – 0.66 %Rr. Vitrinite content is the most

dominant maceral (61.1 vo.l% mmf), followed by liptinite (25.0 vol.% mmf), and inertinite (13.8 vol.% mmf). Minerals observed in the coal samples comprised pyrite, quartz, and clay. Pyrite was present as discrete crystals, massive crystals, framboidal pyrite, and cell-filling on other macerals. Both syngenetic and epigenetic pyrite was found in the Ombilin coal.

E. Bengkulu Basin

The Bengkulu Basin, located in the southwestern part of Sumatra Island, is another forearc basin. It contains Oligo-Miocene siliciclastic, coal, and carbonate sediments. Coal is found in the Middle to Upper Miocene Lemau Formation in Ketaun, Bengkulu, and Seluma. The coal seams are 1 – 2 m thick in Ketaun area, 1.0 – 3.5 m thick in Bengkulu, and up to 4.5 m thick in Seluma area (Heryanto and Suyoko, 2007).

Miocene coal also was found in the Bukit Sunur area in Bengkulu Regency (Fig. 7). Coal mining is carried out in three areas. The Bukit Sunur Coalfield is the most important of these deposits and contains three main seams, with a thickness of 1.6 to 3.5 m (maximum 10 m). This coal has been affected by the Sunur andesite intrusion and, in some places, has turned into coke. Susup Leman has two coal seams, more than two meters thick. In Bukit Puding, there are five or six coal seams, with some seams reaching a thickness of more than 1.4 m. In Pilubang, there is coal showing evidence of thermal influence by andesite, resulting in a loss of volatile matter. Due to the effect of contact metamorphism, the quality of coal varies greatly. In all these areas, the deposits are intensely folded (Thomas, 2005).

The mean vitrinite reflectance value (%Rr) of the coal seam in the Ketaun area ranges from 0.41 to 0.49 %Rr, whereas in the Bengkulu and Seluma areas, it varies from 0.44 to 1.12 %Rr. The higher vitrinite reflectance of the Bengkulu and Seluma coals is probably due to the influence of andesitic sill intrusion (Heryanto R and Suyoko, 2007).

2.2.3 Java, Sulawesi (Celebes), Maluku (Mollucas), and Papua Island

The locations of the coal-bearing basins on the islands of Java, Celebes, Moluccas, and parts of Papua (in the territory of Indonesia) are shown in Fig. 15. The stratigraphy of the coal-bearing formations is summarized in Figs. 16, 17, 18 and Table 3.

A. Java Island (Figs. 15a, 16)

The Northwest (NW) Java Basin extends from onshore to offshore. It consists of three main sub-basins: The offshore Ardjuna Sub-basin, rich in hydrocarbons and the onshore Jatibarang (to the west) and Jatibarang sub-basins (to the southeast) (Noble et al., 1997). Based on geochemical data, Oligocene coal in the Talang Akar Formation is the source rock for oil in the Ardjuna Sub-basin (Doust and Noble, 2008). In the Banyumas Basin (Kaliglagah Formation), there is vitrinite-rich coal (up to 97 %), up to 9.5 m thick (Abian et al., 2020). The coal seam in the Campurdarat Formation in the South Jatim Basin was confirmed by coal outcrops and geoelectric data (Muhlisin, 2019). ESDM (2023) named it as Watulimo coal with calorific value < 5100 cal/g.

Table 3. Coal-bearing formation in Java, Sulawesi (celebes), Maluku (Mollucas), and Papua Island

Island	Basin	Coal-bearing formation	Geologic time	Reference
Java	NW Java	Talangakar	Oligocene	Doust and Noble (2008)
	Banyumas	Kaliglagah	Pliocene	Abian et al. (2020)
	South Jatim	Campurdarat	Early Miocene	Samodra and Gafoer (1990); Samodra et al. (1992)
Celebes	Sengkang/Western S. Sulawesi	Malawa/Toraja	Eocene	Hasibuan, (2001)
	Lariang – Karama	Kalumpang	Mid Eocene	Calvert and Hall (2003, 2007)
Molluccas	Banggai Sula / Taliabu	Bobong	Early Jurassic	Kusnama (2008); Septriandi et al. (2012); Nompo et al. (2021)
Papua	Misool	Atkari	Pliocene	Ibrahim (2007)
	Salawati	Kais	Early Miocene	Satyana and Herawati (2011)
		Aifam	Permian	Wisesa, et al. (2017)
	Bintuni	Steenkool/Buru	Pliocene	Fakhruddin (2023)
	Akimeugah/Waghete	Aiduna	Permian	Panggabean and Pigram (1989)
	Waipoga/South Jayapura	Unk	Pliocene	Gafoer and Budhitrisna (1995)

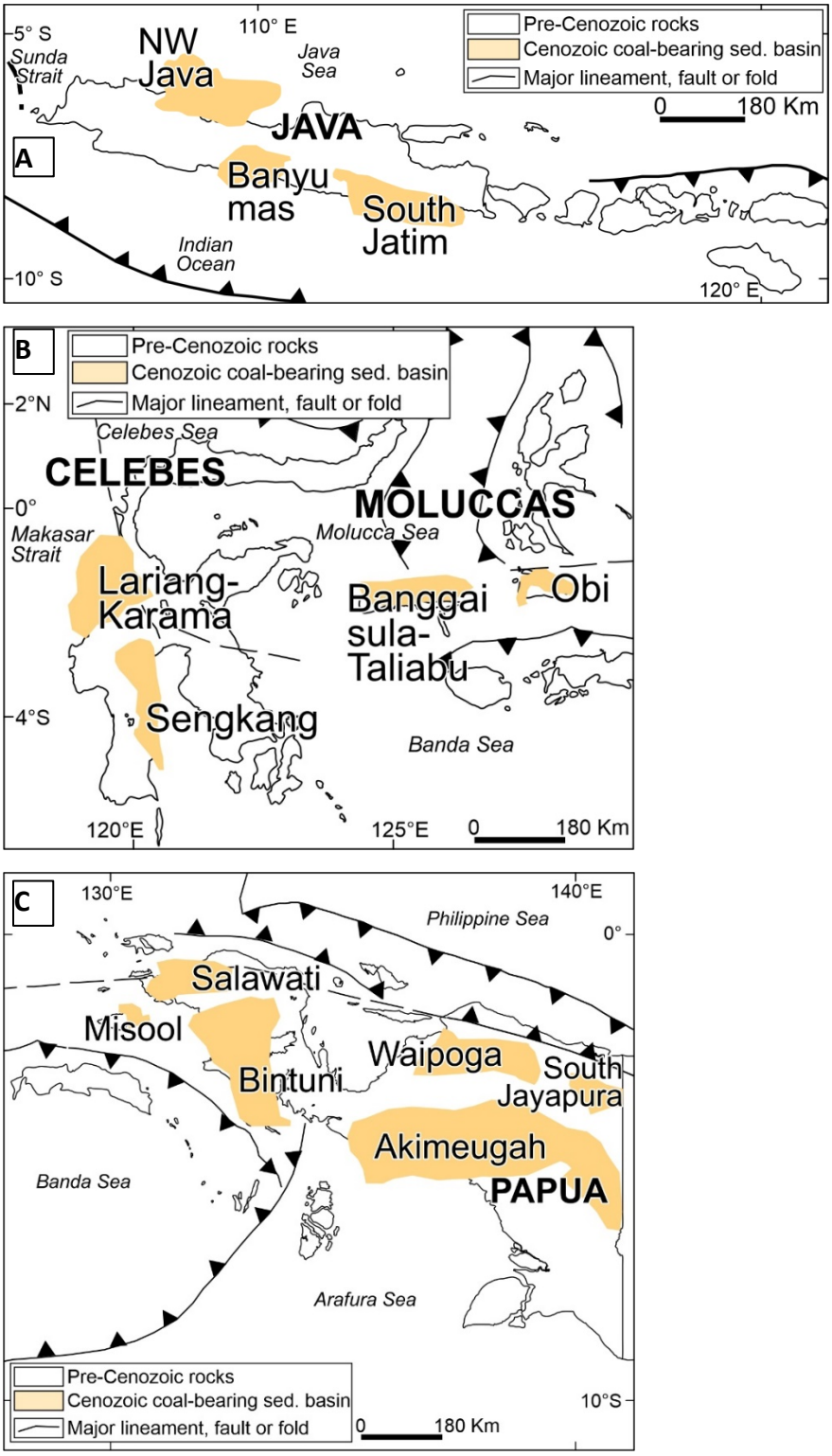

Fig. 15. Coal Basin in (A) Java, (B) Celebes, Moluccas, and (C) Papua Island. Modified from ESDM, (2023)

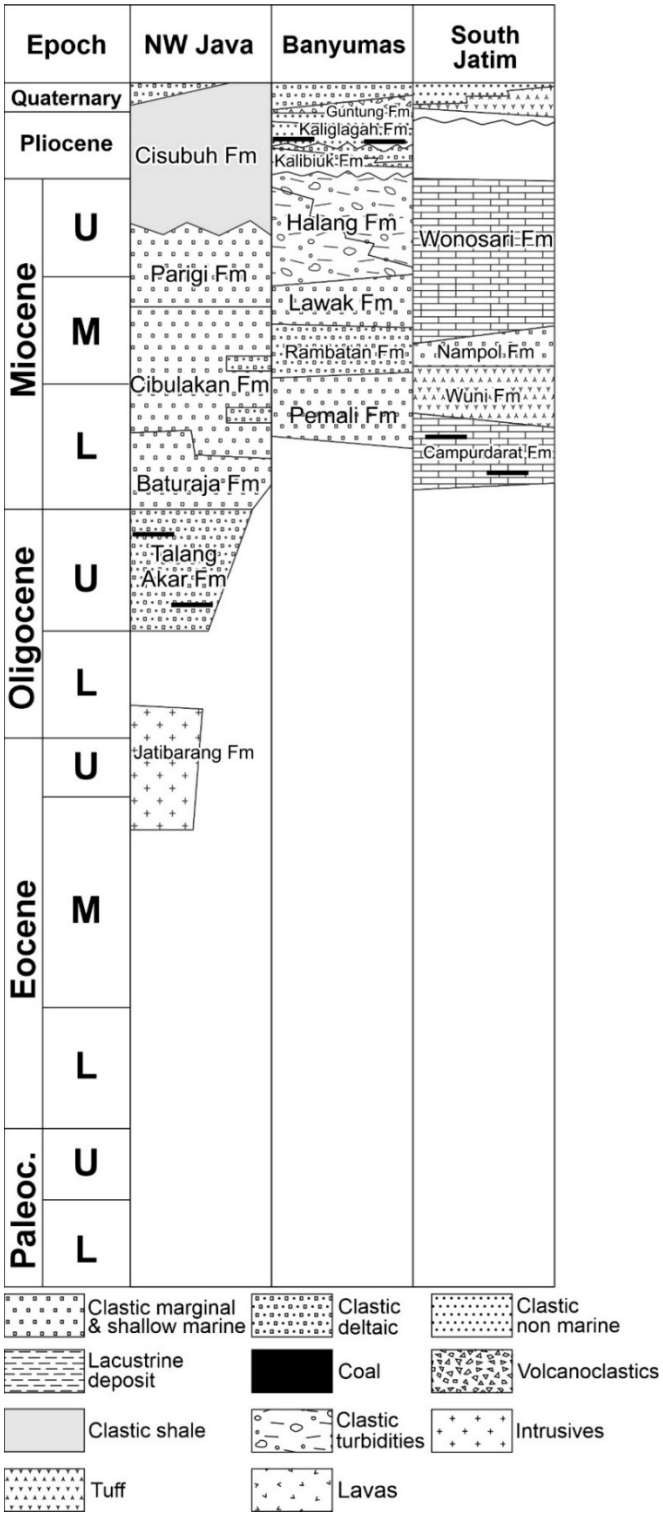

Fig. 16. Stratigraphy of Cenozoic coal-bearing sedimentary basins on Java Island (simplified). Modified from Doust and Noble (2008); Samodra and Gafoer (1990).

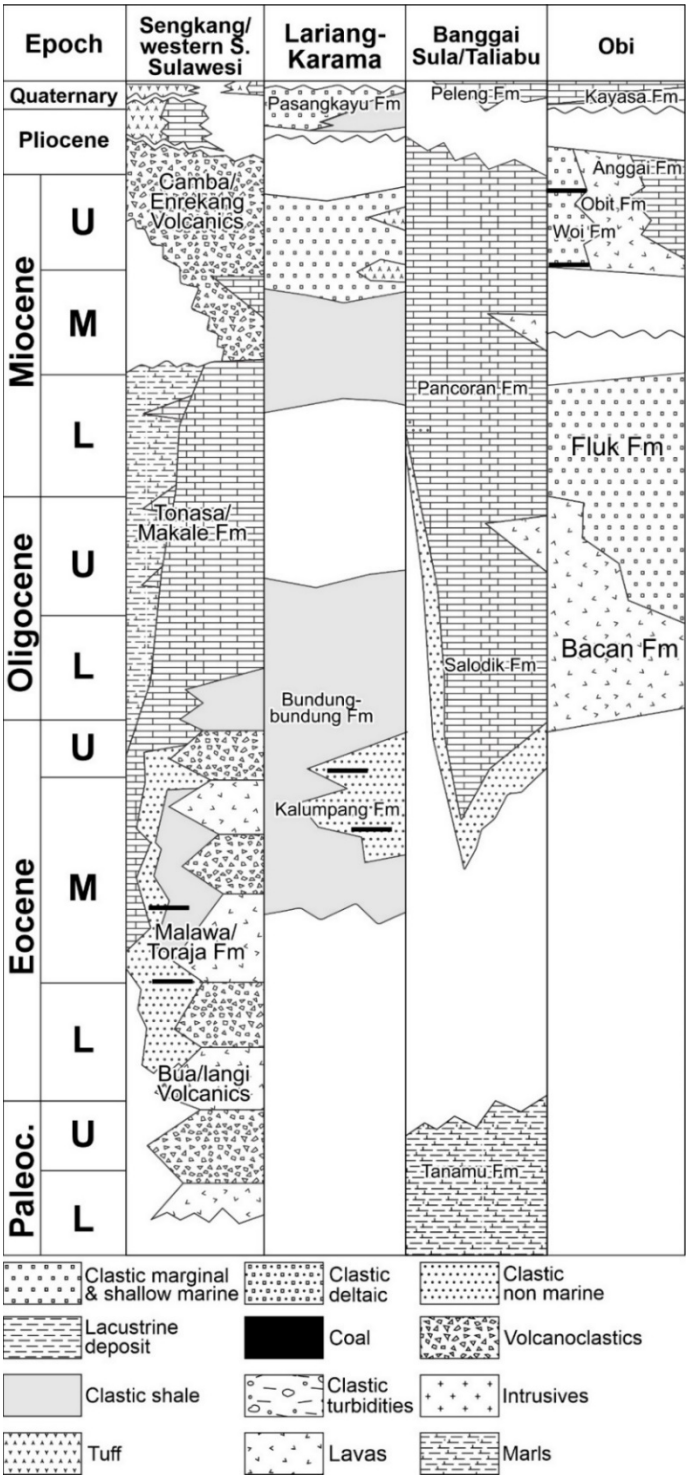

Fig. 17. Stratigraphy of Cenozoic coal-bearing sedimentary basins on Celebes and Moluccas Island. Coal in Banggai Sula/Taliabu Basin (Bobong Fm.) is in Early Jurassic age (not shown). Modified from Hasibuan (2001), Calvert and Hall (2003; 2007), Kusnama (2008), Septriandi et al. (2012), Nompo et al. (2021).

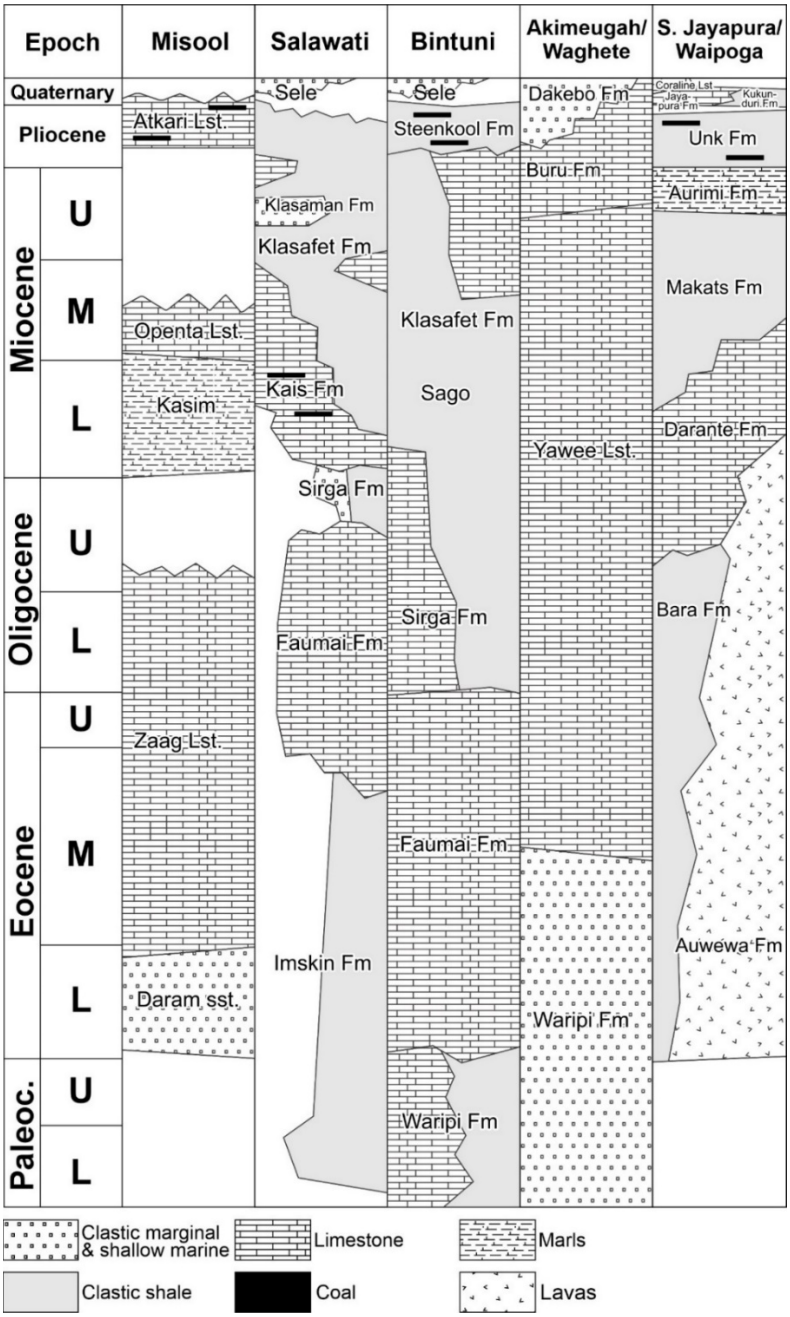

Fig. 18. Stratigraphy of Cenozoic coal-bearing sedimentary basins on Papua Island. Coal in the Akimeugah / Waghete Basin (Aiduna Fm.) and in Bintuni Basin (Aifam Fm.) is Permian in age. Modified from Panggabeanand Pigram (1989), Gafoer and Budhitrisna (1995), Ibrahim (2007), Satyana and Herawati (2011), Fakhruddin (2023), Wisesa, et al. (2017).

B. Celebes and Moluccas Islands (Figs. 15b,17)

The Malawa Formation in the Sengkang/Western S. Sulawesi Basin includes coal of Eocene-Oligocene age with a thickness of up to 1.2 m. Two coal exploration areas (Bakeko block and Kandangsapi block) have been defined. The moisture content of coal in the Bakeko Block is up to 17.3% adb(?) and up to 13.8% adb(?) in the Kandangsapi Block. Ash yields (Bakeko: up to 49.6% adb(?), Kandangsapi: 13.8% adb(?)) and total sulphur contents (Bakeko: 9.23 %, Kandangsapi: 23.76 %) are very high in both blocks (Kusnama and Mangga, 2007).

The Lariang and Karama basins in western Celebes cover an area of approximately 10,000 km^2. Western Celebes was influenced by the development of the Makassar Straits to the west and the collision of continental, ophiolitic, and island-arc fragments to the east. The oldest sediments are non-marine and could be as old as Paleocene. Rifting started in the Middle Eocene and continued into the Late Eocene. Thermal subsidence began by the latest Eocene, and by the end of the Oligocene, most of western Celebes was an area of post-rift shelf carbonate and mudstone deposition. In the Pliocene, sedimentation changed significantly with uplift and erosion, followed by the deposition of coarse clastics derived from an orogenic belt to the east of the study area (Calvert and Hall, 2003, 2007).

The Middle to Upper Eocene Kalumpang Formation (previously: Kalumpang Beds) rests unconformably on Upper Cretaceous rocks and is approximately 3200 m thick (Calvert and Hall, 2003, 2007). The Formation comprises a sequence of shales, coal beds, and meter-thick quartzose sandstones that are exposed in the northern Quarles Mountains.

Taliabu Island is located in the Sanana-Sula Islands (Banggai Sula/Taliabu Basin), which is part of the westernmost region of North Maluku province. The island is believed to have originated from the northern boundary of the Australian Continent, which separated at the end of the Mesozoic or until the Paleogene and was moved along the Sorong Fault System (North and South Sula faults) due to the movement of the Philippine Sea Plate. The shape of Taliabu-Mangole Island characterizes the left-lateral movement of the Sorong Fault. Meanwhile,

Sanana-Sula Island, which runs north-south, cuts perpendicularly across both islands (Kusnama, 2008).

The stratigraphy of Taliabu Island consists of several formations, including the Bobong Formation, a coarse clastic sedimentary rock succession consisting of breccia and conglomerate facies in the lower part, followed by quartz sandstone with intercalations of claystone facies. Upwards, the rock succession gradually changes to alternating shale, claystone, and mudstone. The Formation is Jurassic and was deposited within a fluvial transition to a shallow marine environment. Coal beds are found within quartz sandstone and shale and claystone-mudstone facies occupying the upper part succession of the Bobong Formation (Kusnama, 2008; Septriandi et al., 2012).

The bobong Formation includes three seams (Nompo et al., 2021): seam 1 is 0.5 – 1.0 m thick, seam 2 is 1 m thick, and seam 3 is 0.5 – 0.9 m thick. The coal seams predominantly include bright coal and banded bright coal lithotypes. The coal has a gross calorific value of up to ~8000 cal/g, and a fixed carbon content of 36.1 – 43.9 % (adb). The volatile matter is very high (38.2 – 47.9 % adb), and the moisture content ranges from 6.5 – 12.3% (adb) and ash yield from 64.5 – 21.3 % (adb). The ultimate analysis provided the following values: carbon 64.4 – 74.8 % (daf), hydrogen 6.2 – 7.0 % (daf), nitrogen 0.8 – 0.9 % (daf), sulphur 4.4 – 8.0 % (adb), oxygen 9.4 – 18.1 % (daf). Meanwhile, maceral group percentages (vitrinite 69.7 – 77.6 vol.%; liptinite 17.5– 22.5 vol.%; inertinite 3.6 – 7.8 vol.%) show a very high amount of liptinite.

C. Papua Island (Figs. 15c,18)

The Misool Basin (including Misool Island) is located in the westernmost part of the Raja Ampat Islands, West Papua Province. The Misool Basin comprises several geological formations, including the Yefbie, Demu, and Lelinta formations. The Jurassic Yefbie Formation, about 80 m thick, consists of sandstone, conglomerate, calcareous shale, shale, and limestone. The up to 80 m thick Demu Formation consists of sandy limestone and a middle Callovian-late Oxfordian tuff. The Lelinta Formation, about 100 m thick, overlies the Demu Formation and consists of shale, sandy shale, and limestone of the late Oxfordian-early Berriasian. The Jurassic to Early

Cretaceous succession of the Misool Archipelago was likely deposited on a continental shelf and continental slope of low energy. A Bositra ornati facies indicates restricted anoxic condition for a short period during the Aalenian. Paleogeographically, the Misool Archipelago in Jurassic time was likely located at the northern margin of Gondwana or the southern coast of the Tethys Ocean (Hasibuan, 2010).

The Pliocene-Pleistocene Atkari Formation on Misool Island (Raja Ampat Islands; West Papua Province) is mainly composed of shallow marine limestone. Coal deposits within the Atkari Formation are on average 1.7 m thick. Of the five samples analyzed, the moisture value reached 14.6 % adb, ash yield reached 21 % adb, and the calorific value reached a maximum of 5600 cal/gr adb. The high sulphur content (7.1 % adb; Ibrahim, 2007) agrees with the marine depositional environment.

The Salawati Basin is an east-west trending asymmetric foreland basin on the northern margin of the Indo-Australian Plate. The basin is bounded to the north and west by the deformed zone of the left-lateral Sorong Fault and on the south and east by uplifted Miocene carbonates of the Misool-Onin Anticline and the Ayamaru Platform (Satyana and Herawati, 2011). The basin fill comprises Paleocene to Quaternary deposits. Within this succession, the Miocene Kais Formation comprises thick carbonate rocks that overlie clastic rocks of the Upper Oligocene Sirga Formation. The transgressive Kais carbonates evolved in diverse environments ranging from lagoons to deeper waters and are an important petroleum source rock, but also contain coal (Satyana and Herawati, 2011).

The Bintuni Basin is a Pliocene foreland basin in Papua's Bird's Head area. Coal is present in Permian basement of the Bintuni Basin (Aifam Formation) and in the Pliocene Steenkool Formation (Wisesa et al., 2017). This area contains very high calorific value coal (> 7100 cal/g, named Merdey coal) and high calorific value coal (6100 – 7100 cal/g, named Tuhiba coal and Ransiki coal) (ESDM, 2023).

The Akimeugah Basin is underlain by Paleozoic sediments. The Cenozoic sediments (Paniai Group) include the Waripi Formation (clastic marginal and shallow marine deposit) and the Yawee Limestone (Panggabean and Pigram, 1989). Coal is present in the Permian Aiduna Formation (Panggabean and Pigram, 1989). In addition, ESDM (2023) mentioned Potaway and Umuk coal with low calorific values (<5100 cal/gr adb), but their stratigraphic position is not provided.

The Waipoga/South Jayapura Basin is located in the northern part of Papua Island. It includes extensive Eocene sediments (Bara Formation) and volcanic rocks (Auwewa Formation). Coal is found in the Pliocene Unk Formation (Gafoer and Budhitrisna, 1995). ESDM (2023) reported coal from four outcrops. Two of these outcropds contain low calorific value coal and two contain medium calorific value coal (5100 – 6100 cal/gr adb).

3 Summary of publications

3.1 Publication I

Organic geochemistry and petrography in Miocene coals in the Barito Basin (Tutupan Mine, Indonesia): Evidence for astronomic forcing in kerapah type peats

Fikri, H. N., Sachsenhofer, R. F., Bechtel, A., Gross, D., 2022. Organic geochemistry and petrography in Miocene coals in the Barito Basin (Tutupan Mine, Indonesia): Evidence for astronomic forcing in kerapah type peats. . Int. J. Coal Geol., 256, 103997.
https://doi.org/10.1016/j.coal.2022.103997

The article presents a detailed organic geochemical and organic petrographic study of three Middle Miocene coal seams. The Barito Basin in Borneo contains extensive coal seams in the Miocene Warukin Formation. The net thickness of sub-bituminous C coal exceeds 100 m in the Tutupan mine. This study aims to explore the paleo-peat type and the factors controlling paleo-peat accumulation in three coal seams (T110, T210, T300) based on geochemical and petrographic analyses.

A total of 100 (93 coal and seven non-coal) samples were taken from the open-pit mine, each representing an interval of 1 m. The samples were analyzed for ash yield, moisture content, carbon and sulphur contents, Rock-Eval pyrolysis, maceral composition, vitrinite reflectance, and biomarker analysis.

The low ash and sulphur contents of the studied coals imply that peat formation occurred in an ombrotrophic mire with limited mineral (and sulphate) input.

The geochemical data indicate that angiosperms (including dipterocarps) dominated the forest swamp vegetation. The dominance of angiosperms over gymnosperms reflects Southeast Asia's tropical climate and vegetation during the Miocene. The presence of gymnosperms, however, suggests that the coals formed in Kerapah-type peats, which are located in watersheds and have a higher diversity of plants than other peat types. The cyclic variations in biomarker ratios, such as TAR, Paq, CPI, and ACL, indicate changes in the contribution of grassland vs. forest vegetation and aquatic vs. terrestrial organic matter. These changes could be related to changes in precipitation, water table level, and peat accumulation rate driven by astronomic forcing.

Five cycles were recognized in the T110 seam and three cycles in the T210 seam, each 6 to 13 m thick. The duration of a single cycle was estimated to be 10.8 kyr (P10) to 61.1 kyr (P90), with a 50% probability that the true value is 22.7 kyr. A causal relationship between the climatic variability and the precession index (17–24 kyr) is suspected.

The maceral composition of the Tutupan coals is characterized by moderately high tissue preservation and low gelification, which is typical for tropical ombrotrophic mires. Huminite is the most important maceral group. Liptinite macerals (including resinite, cutinite, fluorinite, and suberinite) are abundant, while inertinite macerals are rare. Exsudatinite is present due to suberinite and resinite, despite the low rank of the coal (lignite to sub-bituminous C). Funginite is one of the main inertinite macerals. The maceral composition of the coals does not show the same cyclicity as the geochemical data. This situation is because the macerals are mainly influenced by the original plant types and the degradation processes that make the plant material more uniform.

This study provides new insights into the organic geochemistry and petrography of Miocene coals in the Barito Basin (Tutupan Mine, Indonesia). The study shows that peat accumulation was controlled by astronomic forcing related to the precession index, resulting in cyclic changes in vegetation. The petrographical results are consistent with ombrotrophic mire conditions with angiosperm-dominated vegetation and low detrital input, as the organic geochemical data suggested.

3.2 Publication II

Coal deposition in the Barito Basin (Southeast Borneo): The Eocene Tanjung Formation compared to the Miocene Warukin Formation

Fikri, H. N., Sachsenhofer, R. F., Bechtel, A., Gross, D., 2022. Coal deposition in the Barito Basin (Southeast Borneo): The Eocene Tanjung Formation compared to the Miocene Warukin Formation. Int. J. Coal Geol., 263, 104117.
https://doi.org/10.1016/j.coal.2022.104117

The Barito Basin in Borneo Island contains two coal-bearing units of Late Eocene (Tanjung Formation) and Middle Miocene (Warukin Formation). Little is known about the peat-forming environments and the differences between Eocene and Miocene coals. This study aims to fill this gap by comparing the geochemical and petrographic characteristics of Eocene coal seams from the TAJ Pit–1D mine with the last result of Miocene coal seams from the Tutupan Mine.

38 coal and six non-coal samples were collected for analysis from three Eocene coal seams (D, C, and B). The samples were taken at 20-cm intervals along the vertical sequence of each seam. The samples were analyzed for various parameters such as ash yield, moisture, carbon, sulphur, maceral composition, vitrinite reflectance, and organic geochemistry.

The aim was to reconstruct the peat-forming environment and compare the characteristics of the Eocene and Miocene coals. The samples were analyzed for ash yield, carbon and sulphur contents, maceral composition, Rock-Eval parameters, vitrinite reflectance, and biomarkers.

The results show that Eocene coals have lower ash yields, lower sulphur contents, lower suberinite and resinite, higher cutinite and fluorinite, and higher n-alkane ratios than Miocene coals. The fungal activity was high in both low-ash ombrotrophic (seam D) and high-ash rheotrophic mires (seam C and B).

Biomarker data indicate that at least part of the resinite in Miocene coals is derived from dammar resin produced by Dipterocarpaceae, which is absent in Eocene coals. Eocene coals were deposited in rheotrophic mires with palm/fern-dominated vegetation, while Miocene coals accumulated in ombrotrophic mires dominated by angiosperm trees.

The comparison reveals significant differences in peat types, flora, and climate between Eocene and Miocene. The Eocene coals reflect a coastal plain setting with frequent flooding events and a relatively low diversity of plants. The Miocene coals reflect a more stable and humid climate with higher plant diversity and more decay-resistant tissues.
The investigation adds to our understanding of the factors that influence coal characteristics by providing a fresh perspective on Borneo Island's coal formation.

3.3 Publication III

Organic geochemistry and petrography of Miocene ombrotrophic coals in the tropical Asem-Asem Basin (Borneo, Indonesia): Comparison to coeval subtropical coals in the Eastern Alps

Fikri, H. N., Sachsenhofer, R. F., Bechtel, A., Gross, D., accepted (in press). Organic geochemistry and petrography of Miocene ombrotrophic coals in the tropical Asem-Asem Basin (Borneo, Indonesia): Comparison to coeval subtropical coals in the Eastern Alps. Austrian J. Earth Sci.

The article presents a comprehensive study of organic geochemistry and petrography of Miocene ombrotrophic coals from three different regions: the Asem-Asem Basin and the Barito Basin in Kalimantan, Indonesia, and the Leoben Basin in the Eastern Alps, Austria.
22 coal and three non-coal samples from a 20-m-thick coal seam (BL1) in the Jumbang mine in the Asem-Asem Basin were be gathered, which is considered a sub-basin of the Barito Basin. The samples were analyzed for ash yield, sulphur content, total organic carbon (TOC), maceral composition, huminite reflectance (%Rr), biomarker composition, Rock-Eval parameters, hydrogen index (HI), and carbon isotope ratios ($\delta^{13}C$). The results were compared with previously published data from coeval coals in the Tutupan mine in the Barito and Leoben Basin.
The main objectives of the article were: (1) to reconstruct the environmental conditions during the accumulation of the BL1 seam; (2) to contrast the peat-forming conditions in the Asem-Asem Basin and the Barito Basin; and (3) to compare the characteristics of Miocene ombrotrophic coals from tropical and subtropical regions to investigate the effects of climate on maceral and biomarker compositions.

The BL1 seam was deposited in an ombrotrophic basinal mire under tropical conditions. The vegetation was dominated by angiosperms, including abundant dammar resin-producing Dipterocarpaceae, while gymnosperms were negligible. The seam has very low ash yields and sulphur contents, indicating a minimal clastic sediments and brackish water influence. The TOC content is high, and the HI values range from 154 to 539 mgHC/gTOC, reflecting a high preservation potential of organic matter. The $\delta^{13}C$ values range from -28.26 ‰ to -27.54 ‰, suggesting a C3 plant origin. The %Rr values are very low indicating a lignite rank.

The result also reveals that the coals from the Tutupan mine in the Barito Basin have similar characteristics to those from the Jumbang mine in terms of ash yield, sulphur content, TOC content, HI values, $\delta^{13}C$ values, and %Rr values, implying similar peat-forming environments and vegetation. However, some minor differences exist in biomarker composition, such as higher amounts of gymnosperm-derived diterpenoids and lower amounts of cadinane-type sesquiterpenoids and resinite in Tutupan coals, indicating less dominance of Dipterocarpaceae in kerapah peats than in basinal peats.

The main differences between the ombrotrophic coals from Kalimantan (Indonesia) and Leoben (Austria) are:

- The Kalimantan coals were formed in a tropical climate, while the Leoben coal was formed in a subtropical/Warm temperate climate.
- Marine influence was detected in the lower coal bench BL1L of the Jumbang mine (Asem-Asem Basin), as indicated by locally increased sulphur contents and a near-shore environment. The other coals from Tutupan mine (Barito Basin) and Leoben Basin did not show evidence of marine influence, suggesting that they were formed in more inland or isolated ombrotrophic mires.
- The Kalimantan coals have higher amounts of resinite and cadinane-type sesquiterpenoids due to the presence of Dipterocarpaceae, a family of tropical angiosperms. The Leoben coal has lower amounts of these compounds due to the absence of Dipterocarpaceae.
- The Kalimantan coals have lower concentrations of gymnosperm-derived diterpenoids than the Leoben coal, reflecting the dominance of angiosperms over gymnosperms in the tropical peatlands.

3.4 Publication IV

Factors controlling oil potential in Eocene and Miocene coals from Borneo: Implications for the petroleum system in the Barito Basin

Fikri, H. N., Sachsenhofer, A., Gross, D., Horsfield B., Mahlstedt N., Misch, D., submitted in Int. J. Coal Geol. Factors controlling oil potential in Eocene and Miocene coals from Borneo: Implications for the petroleum system in the Barito Basin.

The article investigates the factors that control the oil potential and type of Eocene and Miocene coals from Borneo Island, which are important source rocks for oil in several Indonesian sedimentary basins, by using a large data set of organic geochemical and petrographic parameters from over 150 coal samples collected from three mines in the Barito and Asem-Asem Basins in South Kalimantan. New pyrolysis data from solvent-extracted coals, pyrolysis-gas chromatography, and carbon isotope data have been analyzed to determine the amount and origin of resinite, a key component in oil production.

The results show that the oil potential and type of the coals are mainly influenced by the amount and origin of resinite, which reflects the resin-producing vegetation in different depositional environments. The Eocene coals, which were deposited in rheotrophic mires with palm/fern-dominated vegetation, produce a high wax paraffinic oil with an average hydrogen index (HI) of 374 mgHC/gTOC and an average pristane/phytane ratio (Pr/Ph) of 12.3. The Miocene coals, which were deposited in ombrotrophic mires with angiosperm-dominated vegetation (including dammar resin-producing dipterocarps), produce a paraffinic-naphthenic-aromatic mixed oil with an average HI of 203 mgHC/gTOC and an average Pr/Ph of 12.8.

The two oil groups in the Barito Basin, previously distinguished by biomarker ratios and carbon isotope values, are associated with specific coal intervals. Eocene coals source the Tanjung oils, and Miocene coals source the Warukin oils. Nevertheless, the suggestion is that most of the Barito Basin oil belongs to the Tanjung oils, although the Miocene coals have a higher oil potential than Eocene coals. However, the Miocene coals reach the oil window only in the basin's deepest parts with Tmax values above 400 °C.

4 Concluding remarks

In general, the findings of this study highlight the importance of a comprehensive coal analysis, which includes bulk parameters (ash yield, moisture, total organic carbon, total inorganic carbon, total sulphur), Rock-Eval pyrolysis and Pyrolysis-GC, maceral analysis, vitrinite reflectance (%Rr) measurements, and biomarker analysis.

Bulk parameters are able to provide an overview of the coal's depositional environment. Maceral identification shows great differences between coals despite having the same type of depositional environment, as well as petrographic differences between Eocene and Miocene coals in Borneo Basin, and the corresponding %Rr indicating coal type. These results reinforce the importance of maceral analysis in coal investigations. Nonetheless, the weak correlation between maceral percentages and organic geochemistry results should be noted.

The biomarkers well record the plant derivatives, both angiosperms and gymnosperms, that formed the coal. The cycles seen in the coal seam at Tutupan mine are expected to provide useful insights into coal exploration activities, as well as a new perspective on the paleoclimate of Southeast Asia.

Rock-eval pyrolysis and Pyrolysis-GC successfully demonstrated that coal has a very strong correlation with the oil formed in the area. The combination and analysis of all these data provide solid conclusions on coal forming and coal properties in the Barito and Asem-Asem Basins.

Future research on the coal deposits of Indonesia is essential to better understand their formation, composition, and implications. One useful opportunity of research is to apply palynological methods to study the organic matter preserved in the coal seams and their associated rocks. Palynology can provide valuable information on the coal-forming vegetation, paleoclimatic conditions, and paleoenvironmental settings of the peat swamps that gave rise to the coal deposits.

Another possible avenue of research is to conduct more in-depth analysis on the host rocks that under- and overlie the coal seams (roof and floor rocks). These rocks can provide clues on the sedimentary processes, tectonic influences, and sequence stratigraphic framework that controlled coal deposition.

It will also be interesting to compare the characteristics of the Eocene coals in the Asem-Asem Basin, which are relatively close to the coast, with those of other coal deposits in Indonesia that are located in different geographic and geologic settings.

The elements contained in the coal should also be properly investigated as they may have economic and environmental implications for large-scale coal mining. For example, some elements/minerals may have potential value as by-products or indicators of coal quality, while others may pose problems such as ash formation or acid mine drainage.

In addition, considering that Indonesia has many coal deposits distributed across different islands or basins, similar investigations could be conducted in different regions of Indonesia to better understand the variability and diversity of coal deposition in tropical climates. Such investigations could also contribute to the global knowledge of coal geology and its applications.

5 References

Abian, M., Nurdrajat, R. M., Firmansyah, Y., 2020. Karakteristik dan Lingkungan Pengendapan Batubara Formasi Kaliglagah Berdasarkan Analisis Petrogafi di Daerah Bentarsari, Kecamatan Salem, Kabupaten Brebes, Provinsi Jawa Tengah. Padjajaran Geoscience J. 4, 107-116.

Achmad, Z., Samuel, L., 1984. Stratigraphy And Depositional Cycles in the N.E. Kalimantan Basin. Proceedings Indonesian Petroleum Association Second Annual Convention, 109-120.

ADARO, 2008. Feasibility Study for Increasing Production Capacity – 45 Million Tons Per Year. PT Adaro Indonesia.

ADARO, 2022. PT Adaro Energy Tbk's Annual Report 2021 Staying Resilent and Reliable through the Headwinds. Corporate Secretary and Investor Relations Division PT Adaro Energy Tbk., pp 427.

Amijaya, H., Littke, R., 2005. Microfacies and depositional environment of Tertiary Tanjung Enim low rank coal, South Sumatra Basin, Indonesia. Int. J. Coal Geol. 61, 197–221. https://doi.org/10.1016/j.coal.2004.07.004

Amijaya, H., Littke, R., 2006. Properties of thermally metamorphosed coal from Tanjung Enim Area, South Sumatra Basin, Indonesia with special reference to the coalification path of macerals. Int. J. Coal Geol. 66, 271-295. https://doi.org/10.1016/j.coal.2005.07.008

Anderson, J.A.R., 1963. The flora of the peat swamp forests of Sarawak and Brunei, including a catalogue of all recorded species of flowering plants, ferns and fern allies. Botanic Gardens ed., Singapore, 238 pp

Anderson, J.A.R., 1964. The structure and development of the peat swamps of Sarawak and Brunei. J. Trop. Geogr. 18, 7-16.

Arutmin, 2015. Laporan internal pengembangan penambangan batubara PT. Arutmin Indonesia 2015-2020 (Internal report on coal mining development of PT Arutmin Indonesia 2015-2020). pp 441.

Barber, A. J., Crow, M. J., Milsom, J., 2005. Sumatra: Geology, resources and tectonic evolution. Geol. Soc. Lond. Mem. 31.

Bishop, M. G., 2001. South Sumatra Basin Province, Indonesia; the Lahat/Talang Akar-Cenozoic total petroleum system. Denver, Colorado, USA: US Geological Survey. https://doi.org/10.3133/ofr9950S

Bishop, W.F., 1980. Structure, Stratigraphy, and Hydrocarbons Offshore Southern Kalimantan, Indonesia. AAPG Bull. 64, 37-58. https://doi.org/10.1306/2F918923-16CE-11D7-8645000102C1865D

BP, 2022. Statistical Review of World Energy 2021 71th edition. https://www.bp.com/content/dam/bp/business-sites/en/global/corporate/pdfs/energy-economics/statistical-review/bp-stats-review-2022-full-report.pdf

Calvert, S. J., Hall, R., 2003. The Cenozoic geology of the Lariang and Karama regions, Western Sulawesi: new insight into the evolution of the Makassar Straits region. Proceedings Indonesian Petroleum Association 29th Annual Convention and Exhibition, 1-17.

Calvert, S. J., Hall, R., 2007. Cenozoic evolution of the Lariang and Karama regions, North Makassar Basin, western Sulawesi, Indonesia. Pet. Geosci. 13, 353-368. https://doi.org/10.1144/1354-079306-757

Cameron, N. R., Aspden, J. A., Bridge, D. McC., Djunuddin, A., Ghazali, S. A., Harahap, H., Hariwidjaja, S., Johari, Kartawa, W., Keats, W., Ngabito, H., Rock, N. M. S., Whandoyo, R., 1982. Geologic map of the Medan quadrangle, Sumatra. Geological Research and Development Centre. Scale 1:250.000.

Caratini, C., Tissot, C., 1988. Paleogeographical evolution of the Mahakam delta in Kalimantan, Indonesia during the quaternary and late pliocene. Rev. Palaeobot. Palynol. 55, 217-228. https://doi.org/10.1016/0034-6667(88)90087-5

Carbonel, P., Moyes, J., 1987. Late Quaternary paleoenvironments of the Mahakam Delta (Kalimantan, Indonesia). Palaeogeogr. Palaeoclimatol. Palaeoecol. 61, 265-284. https://doi.org/10.1016/0031-0182(87)90054-X

Coster, d. G. L., 1974. The Geology of the Central and South Sumatra Basins. Proceedings Indonesian Petroleum Association Third Annual Convention, 77-110.

Dai, S. and Finkelman, R.B., 2018. Coal as a promising source of critical elements: Progress and future prospects. Int. J. Coal Geol. 186, pp.155-164. https://doi.org/10.1016/j.coal.2017.06.005

Dai, S., Bechtel, A., Eble, C.F., Flores, R.M., French, D., Graham, I.T., Hood, M.M., Hower, J.C., Korasidis, V.A., Moore, T.A. and Püttmann, W., 2020. Recognition of peat depositional environments in coal: A review. Int. J. Coal Geol. 219, p.103383. https://doi.org/10.1016/j.coal.2019.103383

Darman, H., Sidi, F.H., 2000. An outline of the geology of Indonesia. Indonesian Association of Geologists.

Daulay, B., 1994. Tertiary coal belt in eastern Kalimantan, Indonesia: the influence of coal quality on coal utilisation Doctor of Philosophy thesis. Wollongong, Department of Geology University of Wollongong.

Deighton, I., Mukti, M. M. R., Singh, S., Travis, T., Hardwick, A., Hernon, K., 2014. Nias Basin, NW Sumatra–new insights into forearc structure and hydrocarbon prospectivity from long-offset 2D seismic data. Proceedings Indonesian Petroleum Association Thirty-Eight Annual Convention and Exhibition, IPA14-G-299.

Demchuk, T., Moore, T.A., 1993. Palynofloral and organic characteristics of a Miocene bog-forest, Kalimantan, Indonesia. Org. Geochem. 20, 119–134. https://doi.org/ 10.1016/0146-6380(93)90032-7

Diessel, C.F.K., 1992. Coal-Bearing Depositional Systems. Springer, Berlin, Heidelberg. https://doi.org/10.1007/978-3-642-75668-9

Djamal, B., Gunawan W., Simandjuntak, T.O., Ratman, N., 1994. Geologic map of the Nias sheet, Sumatra. Geological Research and Development Centre. Scale 1:250.000.

Doust, H., Noble, R. A., 2008. Petroleum systems of Indonesia. Mar. Pet. Geol. 25, 103-129. https://doi.org/10.1016/j.marpetgeo.2007.05.007

Du Toit, A.L., 1937. Our wandering continents: an hypothesis of continental drifting. Oliver and Boyd.

ESDM, 2015. Indonesia Mineral and Coal Information 2015. Ministry of Energy and Mineral Resources Republic of Indonesia

ESDM, 2022. Handbook of Energy & Economic Statistics of Indonesia. Ministry of Energy and Mineral Resources Republic of Indonesia. 129 p.

ESDM, 2023. Ministry of Energy and Mineral Resources and Coal database. Online access: geoportal.esdm.go.id/minerba

Friederich, M. C., Leeuwen, T. V., 2017. A review of the history of coal exploration, discovery and production in Indonesia: The interplay of legal framework, coal geology and exploration strategy. Int. J. Coal Geol. 178, pp. 56-73. https://doi.org/10.1016/j.coal.2017.04.007

Friederich, M. C., Moore, T. A., M.Flores, R., 2016. A regional review and new insights into SE Asian Cenozoic coal-bearing sediments: Why does Indonesia have such extensive coal deposits? Int. J. Coal Geol. 166, pp. 2-35. https://doi.org/10.1016/j.coal.2016.06.013

Gafoer, S., Budhitrisna, T., 1995. Geological Map of the Sarmi & Bufareh Sheets, Irian Jaya. Geological Research and Development Centre. Scale 1:250.000.

Gerard, J., Oesterle, H., 1973. Facies Study of the Offshore Mahakam Area. Proceedings Indonesian Petroleum Association Second Annual Convention, pp. 187-195.

Ginting, C. S. P., Baok, S. F., 2008. Hydrocarbon Exploration Trend at Akimeugah Basin Based on Structural and Tectonostratigraphic Control. Proceeding 37th IAGI (Indonesian Association of Geologists) Annual Scientific Conference, 463-475.

Gruber, W., Sachsenhofer, R., 2001. Coal deposition in the Noric Depression (Eastern Alps): raised and low-lying mires in Miocene pull-apart basins. Int. J. Coal Geol. 48, pp. 89-114. https://doi.org/10.1016/S0166-5162(01)00049-0

Hamilton, W. B., 1979. Tectonics of the Indonesian region. Professional Paper 1078. US Govt. Print. Off., 345 pp.

Hasibuan, F., 2010. Analisis Lingkungan Pengendapan Batuan Berumur Jura di Kepulauan Misool, Papua Berdasarkan Fosil Makro. J. geol. mineral resources 20, 235-250. https://doi.org/10.33332/jgsm.geologi.v20i5.176

Heryanto, R., 2009. Karakteristik dan Lingkungan Pengendapan Batubara Formasi Tanjung di daerah Binuang dan sekitarnya, Kalimantan Selatan. Indones. J. Geosci 4, 239-252.

Heryanto, R., Panggabean, H., 2013. Lingkungan Pengendapan Formasi Pembawa Batuabara Warukin di Daerah Kandangan dan Sekitarnya, Kalimantan Selatan. J. geol. mineral resources 23, 93-103. https://doi.org/10.33332/jgsm.geologi.v23i2.93

Heryanto, R., Sanyoto P., 1994. Geological map of the Amuntai Quadrangle, Kalimantan. Geological Agency, Bandung Indonesia (1:250,000).

Heryanto, R., Supriatna, S., Abidin, H.Z., 1995. Geological Map of the Malinau Sheet, Kalimantan. Geological Research and Development Centre, Bandung Indonesia (1:250,000).

Heryanto, R., Suyoko, S., 2007. Karakteristik batubara di Cekungan Bengkulu. Indones. J. Geosci. 2, 247-259. https://dx.doi.org/10.17014/ijog.2.4.247-259

Hidayatillah, A. S., Tampubolon, R. A., Ozza, T., Arifin, M. T., Prasetio, R. M. A., Furqan, T. A., Darman, H., 2017. North Sumatra Basin: A New Perspective in Tectonic Settings and Paleogene Sedimentation. Proceeding 41th IAGI (Indonesian Association of Geologists) Annual Scientific Conference, IPA17-719-G.

Husein, S., 2017. Sedimentology and Stratigraphy of Upper Tarakan Formation, Tarakan Island, North Kalimantan, Indonesia. Proceedings International Annual Engineering Seminars Faculty of Engineering Universitas Gadjah Mada Yogyakarta Indonesia.

Hutchison, C. S., 1989. Geological evolution of South-east Asia (Vol. 13). Oxford: Clarendon Press. 368 p.

Ibrahim, D., 2007. Inventarisasi Batubara Marginal Daerah Pulau Misool Provinsi Irian Jaya Barat. Proceeding Pemaparan Hasil Kegiatan Lapangan dan Non Lapangan Tahun 2007 Pusat Sumber Daya Geologi, 1-12.

Kamili, Z. A., Kingston, J., Achmad, Z., Wahab, A., Sosromihardjd, S., Crausaz, C. U., 1976. Contribution to the Pre–Baong Stratigraphy of North Sumatra. Proceedings Indonesian Petroleum Association Fifth Annual Convention and Exhibition, 91-116.

Katili, J.A., 1978. Past and present geotectonic position of Sulawesi, Indonesia. Tectonophysics, 45, 289-322. https://doi.org/10.1016/0040-1951(78)90166-X

Keller, B.D., Ferralis, N. and Grossman, J.C., 2016. Rethinking coal: thin films of solution processed natural carbon nanoparticles for electronic devices. Nano Lett. 16, 2951-2957. https://doi.org/10.1021/acs.nanolett.5b04735

Koesoemadinata, R. P., & Matasak, T., 1981. Stratigraphy and Sedimentation: Ombilin Basin, Central Sumatra (West Sumatra Province). Proceedings Indonesian Petroleum Association Tenth Annual Convention and Exhibition, 217-249

Koesoemadinata, R.P., 2000. Tectono-stratigraphic framework of Tertiary coal deposits of Indonesia. Proceedings of Southheast Asia Coal Geology. Directorate of Mineral Resources, pp.8-16.

Kusnama, 2008. Batubara Formasi Warukin di daerah Sampit dan sekitarnya, Kalimantan Tengah. Indones. J. Geosci. 3, 11-22.

Kusnama, 2008. Fasies dan lingkungan pengendapan Formasi Bobong berumur Jura sebagai pembawa lapisan batubara di Taliabu, Kepulauan Sanana-Sula, Maluku Utara. Indones. J. Geosci. 3, 161-173. https://dx.doi.org/10.17014/ijog.3.3.161-173

Kusnama, Mangga, S. A., 2007. Hubungan Lingkungan Pengendapan Formasi Malawa dan Keterdapatan Batubara di Daerah Soppeng, Sulawesi Selatan. J. geol. mineral resources 17, 218-232. https://doi.org/10.33332/jgsm.geologi.v17i4.291

Metcalfe, I., 1996. Pre-Cretaceous evolution of SE Asian terranes. Geol. Soc. Spec. Publ. 106. 97-122. https://doi.org/10.1144/GSL.SP.1996.106.01.09

Moore, T.A., Ferm, J.C., 1992. Composition and grain size of an eocene coal bed in southeastern Kalimantan, Indonesia. Int. J. Coal Geol. 21, 1–30. https://doi.org/ 10.1016/0166-5162(92)90033-S

Morley, R.J., 2013. Cenozoic ecological history of South East Asian peat mires based on the comparison of coals with present day and Late Quaternary peats. J. Limnol. 72, 36–59. https://doi.org/10.4081/jlimnol.2013.s2.e3

Moss, S.J., 1998. Embaluh Group turbidites in Kalimantan evolution of a remnant oceanic basin in the Late Cretaceous to Palaeogene. J Geol Soc, London 155, 509–524. https://doi.org/10.1144/gsjgs.155.3.0509

Muhlisin, M. Z., 2019. Identifikasi sebaran batubara menggunakan metode geolistrik polarisasi terinduksi (IP): Studi kasus daerah Klatak Kecamatan Besuki Kabupaten Tulungagung. Undergraduate theses, Universitas Islam Negeri Maulana Malik Ibrahim

Noble, R. A., Pratomo, K. H., Nugrahanto, K., Ibrahim, A. M., Prasetya, I., Mujahidin, N., #Wu, C. H., Howes, J. V. C. (1997). Petroleum systems of northwest Java, Indonesia. 1997. Petroleum systems of Northwest Java, Indonesia. In: Howes, J.V.C., Noble, R.A. (Eds.), Proceedings of International Conference on Petroleum Systems of SE Asia and Australasia Indonesian Petroleum Association, pp. 585–600

Nompo, S., Amijaya, D. H., Anggara, F., 2021. Karakteristisasi Petrografi dan Geokimia Batubara Formasi Bobong Daerah Taliabu, Provinsi Maluku Utara. Jurnal Geomine 9, 1-8. https://doi.org/10.33536/jg.v9i1.764

Novita, D., Kusumah, K.D., 2016. Karakteristik dan Lingkungan Pengendapan Batubara Formasi Warukin di Desa Kalumpang, Binuang, Kalimantan Selatan. J. geol. mineral resources 17, 139-152. https://doi.org/10.33332/jgsm.geologi.v17i3.12

Nuay, E.S., Astarita, A.M. and Edwards, K., 1985. Early Middle Miocene Deltaic Progradation in the Southern Kutai Basin. Proceedings Indonesian Petroleum Association Fourteenth Annual Convention, 63-82.

Ott, H.L., 1987. The Kutei Basin – A Unique Structural History. Proceedings Indonesian Petroleum Association Sixteenth Annual Convention, 307-317.

Panggabean H., Pigram, C.J., 1989. Geological Map of the Waghete Sheet, Irian Jaya. Geological Research and Development Centre. Scale 1:250.000.

Patria, A. A., Anggara, F., 2022. Petrological, mineralogical, and geochemical compositions of coal in the Ombilin Basin, West Sumatra, Indonesia. Int. J. Coal Geol. 262, 104099. https://doi.org/10.1016/j.coal.2022.104099

Pubellier, M. and Morley, C.K., 2014. The basins of Sundaland (SE Asia): Evolution and boundary conditions. Mar. Pet. Geol. 58, pp.555-578. https://doi.org/10.1016/j.marpetgeo.2013.11.019

Reichl, M. S. G. Z. C., 2018. World Mining Data 2018 Vol 33. Vienna: Bundesministerium Für Nachhaltigkeit und Tourismus.

Rose, R., Hartono, P., 1978. Geological Evolution of the Tertiary Kutei-Melawi Basin, Kalimantan Indonesia. Proceedings Indonesian Petroleum Association Seventh Annual Convention, 225-252.

Samodra, H., Gafoer, S., 1990. Geological Map of the Pacitan Sheet, Java. Geological Research and Development Centre, Bandung Indonesia (1:100,000).

Samodra, H., Suharsono, Gafoer, S., Suwarti, T., 1992. Geological Map of the Tulungagung Quadrangle, Java. Geological Research and Development Centre, Bandung Indonesia (1:100,000).

Samuel, L., Muchsin, S., 1975. Stratigraphy and Sedimentation in the Kutai Basin, Kalimantan. Proceedings Indonesian Petroleum Association Fourth Annual Convention, 27-40.

Samuel, M.A., Harbury, N.A., 1996. The Mentawai fault zone and deformation of the Sumatran Forearc in the Nias area, in: Hall, R., Blundell, D. (Eds.), Tectonic Evolution of Southeast Asia, Geological Society Special Publication No. 106. Geological Society, pp. 337–351. https://doi.org/10.1144/GSL.SP.1996.106.01.22

Santy, L. D., Panggabean, H., 2013. The Potential of Ketungau and Silat Shales in Ketungau and Melawi Basins, West Kalimantan: For Oil Shale and Shale Gas Exploration. Indones. J. Geosci. 8, 39-53.

Satyana, A. H., Herawati, N., 2012. Sorong fault tectonism and detachment of Salawati island: implications for petroleum generation and migration in Salawati basin, bird's head of Papua. Proceedings Indonesian Petroleum Association Thirty-Fifth Annual Convention and Exhibition 201, 1-22.

Septriandi, Syafri, I., Adriana S, Y., Ferdian, F., 2012. Jurassic Sandstone Characteristic of Bobong Formation in Taliabu Island, Eastern Indonesia: Outcrop and Petrography Observations. Proceedings Indonesian Petroleum Association Thirty-Sixth Annual Convention, IPA12-SG-068.

Sikumbang, N. and Heryanto, R., 1994. Geological map of the Banjarmasin Sheet, Kalimantan. Geological Agency, Bandung, Indonesia (1:250,000)

Sikumbang, N., 1986. Geology and tectonics of pre-tertiary rocks in the Meratus Mountains, south east Kalimantan, Indonesia. Dissertations University of London, Royal Holloway and Bedford New College (United Kingdom).

Siregar, M.S., Sunaryo, R., 1980. Depositional Environment and Hydrocarbon Prospects, Tanjung Formation, Barito Basin, Kalimantan. Proceedings Indonesian Petroleum Association Ninth Annual Convention, 379-400.

Situmorang, B., 1982. The Formation of the Makassar Basin as Determined from Subsidence Curves. Proceedings Indonesian Petroleum Association Eleventh Annual Convention, 83-107.

SNI, 2011. Pedoman pelaporan sumberdaya dan cadangan batubara. Badan Standardisasi Nasional Indonesia.

Sodiq, M. F., Hermiyanto Z, Moh., 2021. Potensi Batuan Induk Hidrokarbon di Cekungan Mesozoikum Embaluh Utara, Daerah Kalimantan Utara dan Kalimantan Timur. J. geol. mineral resources 22, 33-43. https://doi.org/10.33332/jgsm.geologi.v22i1.566

Soetrisno, Jamal, B., Rusmana, E., Koesoemadinata S., 1995. Geological Map of the Kualapembuang Quadrangle, Kalimantan. Geological Research and Development Centre, Bandung Indonesia (1:250,000).

Steckel, J.C., Edenhofer, O. and Jakob, M., 2015. Drivers for the renaissance of coal. PNAS 112, E3775-E3781. https://doi.org/10.1073/pnas.1422722112

Sunarjanto, D., Wijaya, S., Munadi, S., Wiyanto, B., Prasetio, D. F., 2008. Indonesian Tertiary Sedimentary Basin. SCOG 31, 19-27.

Supriatna, S., Djamal, B., Heryanto, R. and Sanyoto, P., 1994. Geological map of Indonesia, Banjarmasin Sheet, Geological Research Centre Bandung, Indonesia.

Thomas L. P., 2005. Chapter 11: Fuel resources: coal. In: Barber, A.J., Crow, M.J. & Mmsom, J.S. (Eds) Sumatra: Geology, Resources and Tectonic Evolution. Geol. Soc. Lond. Mem. 31, 142-146.

Thomas L., 2020. Coal Geology, Third Edition. John Wiley & Sons Ltd. DOI:10.1002/9781119424307

TIMAH, 2023. Company profile of PT Tanjung ALam Jaya (TAJ). https://timah.com/blog/about-us/pt-tanjung-alam-jaya-taj.html Accessed on April 06, 2023

Walker, S., 2000. Major coalfields of the world (Technical Report). IEA Coal Research, London (United Kingdom), 131 pp.

WCA, 2022. Coal & Electricity. World Coal Association. https://www.worldcoal.org/coal-facts/coal-electricity/ access on: 01 September 2022.

Widodo, S., Bechtel, A., Anggayana, K., Püttmann, W., 2009. Reconstruction of floral changes during deposition of the Miocene Embalut coal from Kutai Basin, Mahakam Delta, East Kalimantan, Indonesia by use of aromatic hydrocarbon composition and stable carbon isotope ratios of organic matter. Org. Geochem. 40, 206-218. https://doi.org/10.1016/j.orggeochem.2008.10.008

Widodo, S., Oschmann, W., Bechtel, A., Sachsenhofer, R. F., Anggayana, K., Püttmann, W., 2010. Distribution of sulfur and pyrite in coal seams from Kutai Basin (East Kalimantan, Indonesia): Implications for paleoenvironmental conditions. Int. J. Coal Geol. 81, 151-162. https://doi.org/10.1016/j.coal.2009.12.003

Willyam J., 2013. analysis langap formation formation as carrier of coal and coal quality assessment based on observations geophysical well logging in langap area, kecamatan

south malinau, kabupaten malinau, east kalimantan province (theses abstract) UPN "Veteran" Yogyakarta.

Wilson, M. E., & Moss, S. J., 1999. Cenozoic palaeogeographic evolution of Sulawesi and Borneo. Palaeogeogr. Palaeoclimatol. Palaeoecol. 145, 303-337. https://doi.org/10.1016/S0031-0182(98)00127-8

Winarno, A., Amijaya, D. H., Harijoko, A., 2019. Mineral and Geochemistry Study of Lower Kutai Basin Coal East Kalimantan. In IOP Conference Series: Earth and Environmental Science 375, 012009.

Wisesa, K. D., Mangala, A., Arbi, H., Adlan, Q., Gani, R. M. G., 2017. Distribution of Permian Source Rocks Maturation Related to Lengguru Fold-Thrust Belt Position in Bintuni Basin. Proceedings, Indonesian Petroleum Association Forty-First Annual Convention and Exhibition 201, IPA17-405-SG.

Witts, D., Hall, R., Nichols, G., Morley, R., 2012. A new depositional and provenance model for the Tanjung Formation, Barito Basin, SE Kalimantan, Indonesia. J. Asian Earth Sci. 56, 77–104. https://doi.org/10.1016/j.jseaes.2012.04.022

Yosep, R., Sugiarto, W., Suhada, D. I., 2014. Karakteristik Batubara Pada Formasi Sembakung di Daerah Segah, Kabupaten Berau, Provinsi Kalimantan Timur. Bul. sumber daya geol. 9, 56-63.

6 Publication I:

Organic geochemistry and petrography in Miocene coals in the Barito Basin (Tutupan Mine, Indonesia): Evidence for astronomic forcing in kerapah type peats

Chapter 6 was published by the author of this thesis in “International Journal of Coal Geology”. (https://doi.org/10.1016/j.coal.2022.103997)

Author contribution: Conceptualization, methodology, investigation, writing – original draft, and visualization

International Journal of Coal Geology 256 (2022) 103997

Contents lists available at ScienceDirect

International Journal of Coal Geology

journal homepage: www.elsevier.com/locate/coal

Organic geochemistry and petrography in Miocene coals in the Barito Basin (Tutupan Mine, Indonesia): Evidence for astronomic forcing in kerapah type peats

Hafidz Noor Fikri [a,b], Reinhard F. Sachsenhofer [a,*], Achim Bechtel [a], Doris Gross [a]

[a] Department Applied Geosciences and Geophysics, Montanuniversitaet Leoben, Austria
[b] Department of Mining Engineering, Lambung Mangkurat University, Banjarmasin, South Kalimantan, Indonesia

ARTICLE INFO

Keywords:
Sulphur
Ash yield
Ombrotrophic peat
Kalimantan
Climate
Milankovich cycle

ABSTRACT

In the Barito Basin of Borneo, there are extensive coal seams in the Miocene Warukin Formation. The net thickness of subbituminous C coal exceeds 100 m in the Tutupan mine. Three coal seams (from bottom to top: T110, T210, T300) were studied to explore the paleo-peat type and the factors controlling paleo-peat accumulation. The study is based on 93 coal and 7 non-coal samples, each representing a stratigraphic interval of 1 m. The samples were analyzed for ash yield, moisture, carbon and sulphur contents. All samples were analyzed using the Rock-Eval method and maceral analysis. Every second coal sample was used for detailed organic geochemical analysis.

The coal in the T110 (46 m thick) and T210 (24 m) seams are very low in ash and sulphur, suggesting peat formation in an ombrotrophic mire. Accumulation of seam T300 (24 m), which contains a higher amount of detrital minerals, is interpreted to have occurred in rheotrophic and ombrotrophic settings. *n*-Alkane and biomarker ratios indicate that accumulation of seam T110 began in a mire with a relatively high contribution of grassland vegetation. Apart from this early stage, angiosperms (including dipterocarps) dominated the forest swamp vegetation. The presence of gymnosperms, albeit at lesser extent, indicates that coal formation occurred in a kerapah (watershed) type peat. The geochemical data reveal a cyclic structure in the T110 and T210 seams, possibly controlled by climatic fluctuations. Five cycles were recognized in the T110 seam and three cycles in the T210 seam, each 6 to 13 m thick. Using accumulation rates of tropical peat in SE Asia and the compaction of low-rank coal, the duration of a single cycle was estimated to be 10.8 kyr (P10) to 61.1 kyr (P90), with a 50% probability that the true value is 22.7 kyr. A causal relationship between the climatic variability and the precession index (17–24 kyr) is suspected.

The maceral composition of the Tutupan coals is characterized by moderately high tissue preservation and low gelification, which is typical for tropical ombrotrophic mires. Huminite is the most important maceral group. Liptinite macerals (including resinite, cutinite, fluorinite and suberinite) are abundant, while inertinite macerals are rare. Funginite is one of the main inertinite macerals.

1. Introduction

Indonesia's steam coal production in 2020 was 562 million tons. This production places Indonesia as the third-largest coal-producing country in the world (BP, 2021). Nearly 10% of Indonesia's coal production was from the Tutupan mine in the Barito Basin, located in the southern part of the island of Borneo (Figs. 1, 2). This mine has 468.2 million tons of coal reserves and produced 54.5 million tons of coal in 2020 (ADARO, 2021) from three seams within the middle to late Miocene Warukin Formation (Fig. 3). Each of the three main seams can be up to 50 m thick (Friederich and Van Leeuwen, 2017). The quality of the coal in the Tutupan mine has been described as excellent with very low ash yield (<3 wt% air dried basis [adb]), low sulphur content (0.12 wt%adb), and relatively high calorific value (4848 Kcal/kg; Friederich and Van Leeuwen, 2017) characterizing the coal as sub-bituminous C.

Despite its great economic significance, the structure of coal seams in the Barito Basin is poorly investigated. This refers especially to vertical variation of basic coal properties like ash yield, sulphur content, and

* Corresponding author.
E-mail address: reinhard.sachsenhofer@unileoben.ac.at (R.F. Sachsenhofer).

https://doi.org/10.1016/j.coal.2022.103997
Received 10 February 2022; Received in revised form 11 April 2022; Accepted 11 April 2022
Available online 16 April 2022

maceral composition. Apart from the economic significance, coal seams may also provide important information on Miocene environments in the Barito Basin and in Southeast Asia in general.

One of the objectives of the present study is to reconstruct the conditions that favored the accumulation of three seams of great thickness. Important aspects in this context comprise the prevailing mire type (ombrotrophic [raised or domed] mire vs. rheotrophic [low-lying or topogenous] mire, e.g. Gruber and Sachsenhofer, 2001), changes in vegetation (e.g., angiosperm vs. gymnosperm dominance; Bechtel et al., 2001, 2003, 2007b; Gross et al., 2015), and tectonic controls on peat accumulation (e.g. single- vs. multi-stage subsidence; e.g. Lambiase, 1990; Markic and Sachsenhofer, 1997). To achieve the objectives of the study, a total of 100 samples were taken from the open-pit mine, each representing an interval of 1 m. The coal samples were analyzed for ash yield, moisture content, biomarker data and maceral composition.

2. Geological setting

The continental core of Southeast Asia is collectively referred to as "Sundaland" (Fig. 1), the southeastern promontory of Eurasia (Hall and Morley, 2004; Pubellier and Morley, 2014). It is composed of continental blocks separated by suture zones assembled during the Triassic Indonesian orogeny (Hutchison, 1973, 1989, 2014; Hall and Morley, 2004). During the Cenozoic, Sundaland was affected by several tectonic events, including (i) the collision of the Indian plate with Asia east of Sundaland, which began during Eocene time, (ii) rapid Eocene northward movement of the Australian plate, which triggered subduction along the southwestern margin of Sundaland, (iii) an extensional regime during the Eocene and Oligocene that initiated basin subsidence, and (iv) a compressional event that began in the Miocene (~20 Ma) and continued into the Pliocene, reflecting collision and rotation of adjacent plates (e.g. Philippine archipelago; assembly of Sulawesi; Friederich et al., 2016).

Within this setting, the most significant Cenozoic coal-bearing sedimentary basins formed in southern Sundaland, which includes the South Sumatera Basin as well as the Barito and Kutai Basins in the southern part of Indonesian Borneo (Kalimantan; Friederich et al., 2016; Fig. 1). The South Sumatera Basin formed in a back-arc setting associated with Eocene to Oligocene rifting (Friederich et al., 2016). Around the same time, coal measures in Kalimantan accumulated in transgressive post-rift settings (e.g. Eocene Tanjung Formation in the Barito Basin [Fig. 3] and equivalents; Witts et al., 2012; Friederich et al., 2016). In contrast to the Paleogene coals, the Neogene coals in southern Sundaland formed over extensive coastal plains in a regressive setting. Whereas the Neogene coals in southern Sundaland are laterally extensive, the Neogene coals in northern Sundaland formed in disconnected continental (half-)grabens

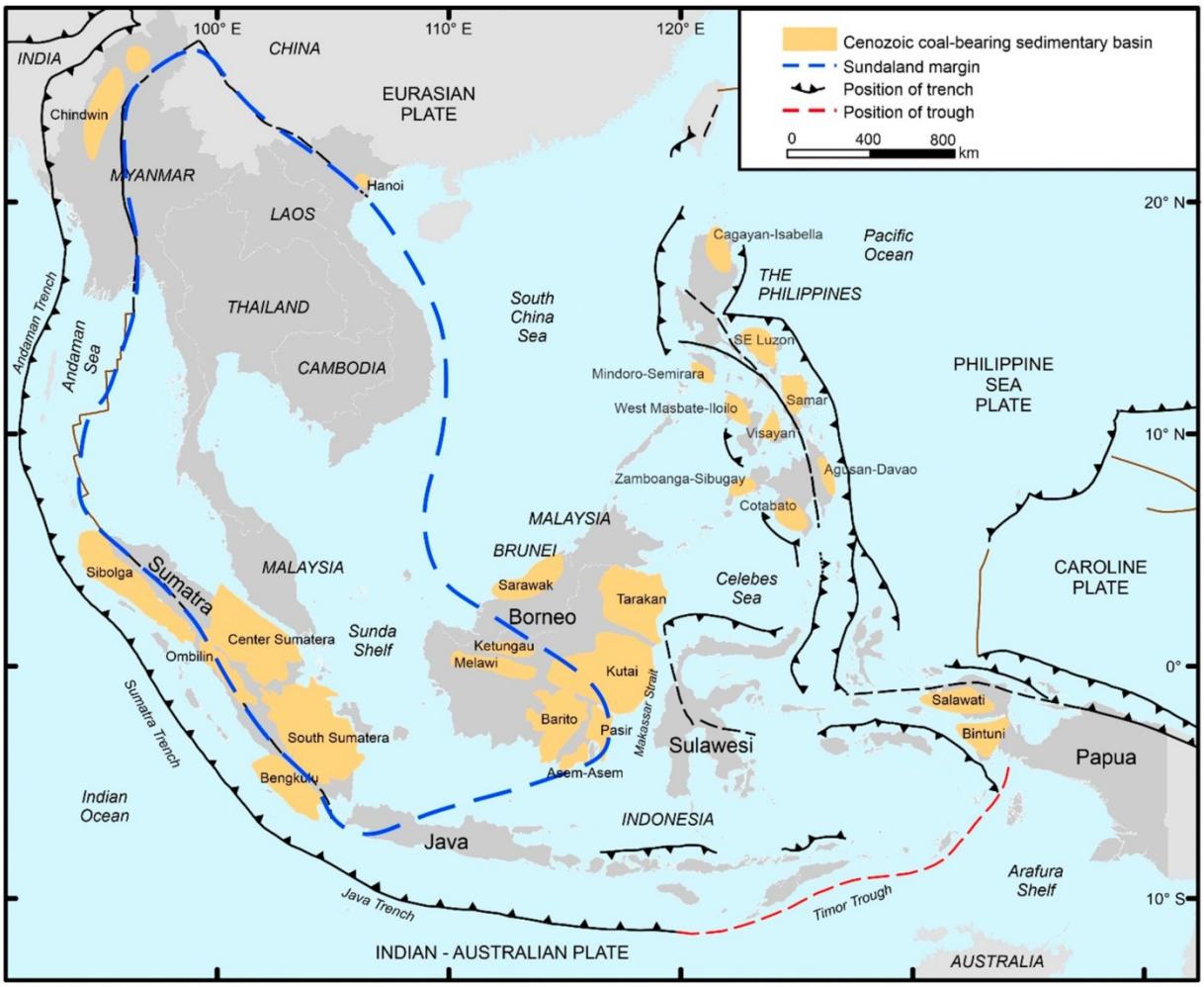

Fig. 1. The main on-shore Cenozoic coal-bearing sedimentary basins in SE Asia (from Friederich et al., 2016).

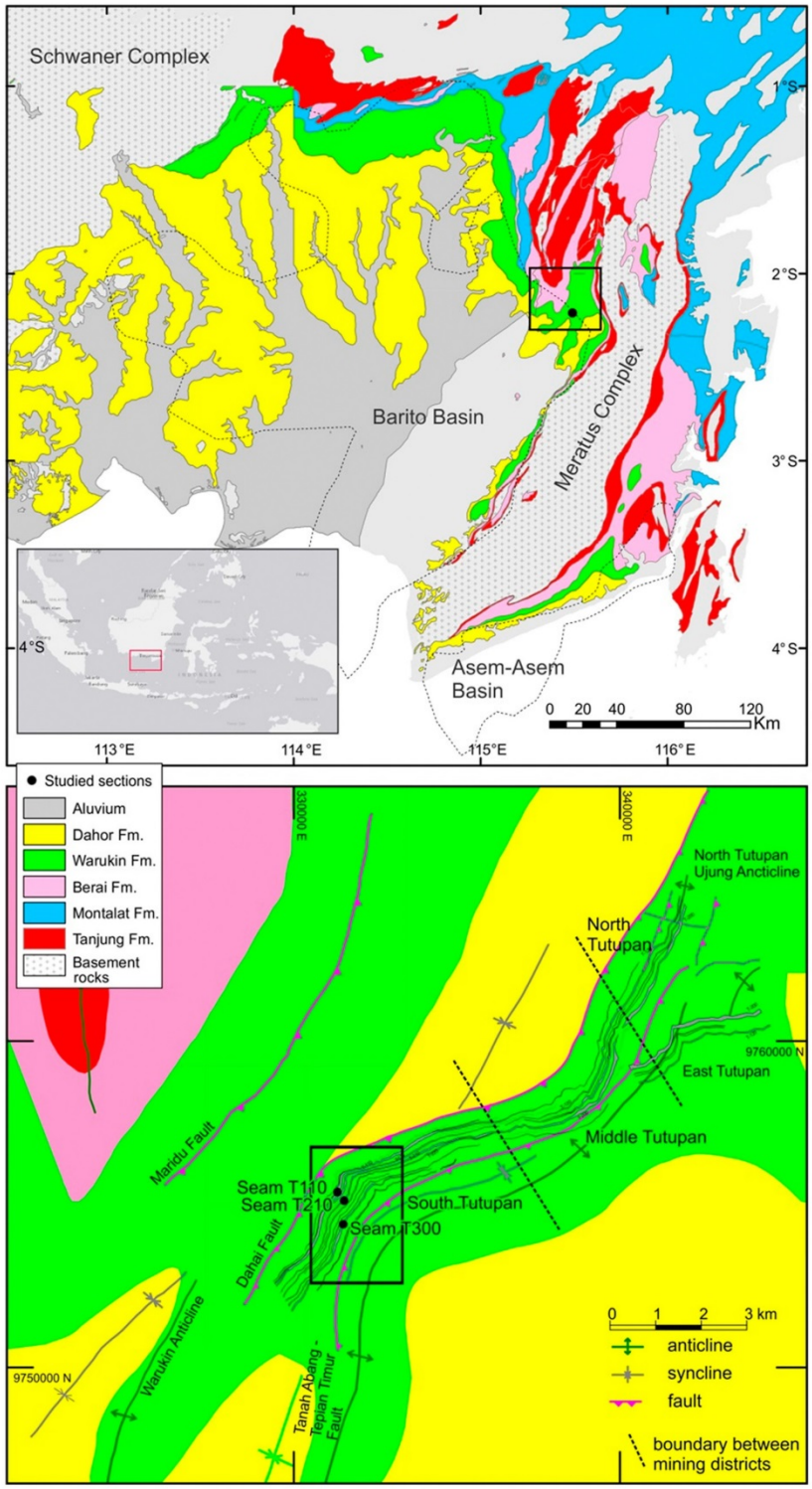

Fig. 2. a) Geological map of the Barito Basin. b) Geological map of the surrounding of the Tutupan Mine (after Supriatna et al., 1994, Sikumbang and Heryanto, 1994 and Heryanto and Sanyoto, 1994). Dots show the sample locations. The rectangle corresponds to the area of the inset in Fig. 12.

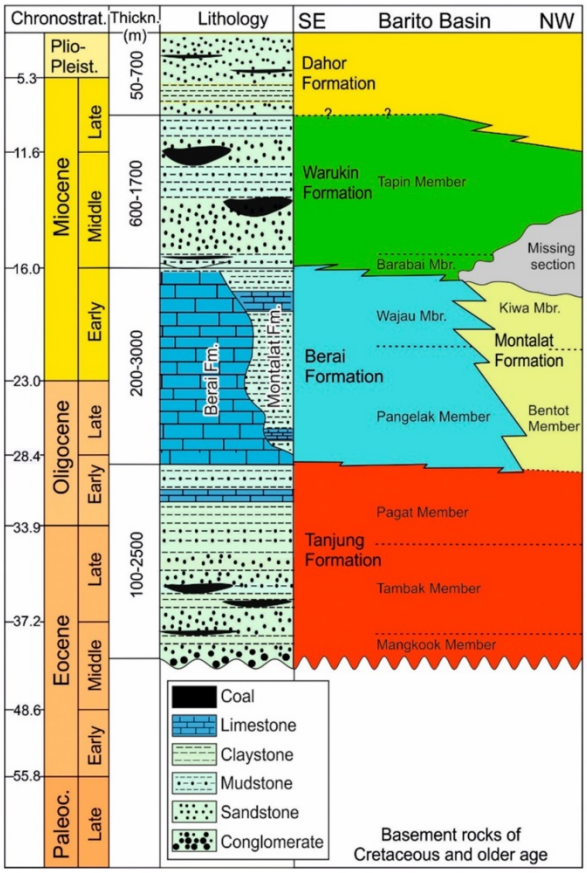

Fig. 3. Stratigraphy and lithology of the basin fill in the Barito Basin (modified after Witts et al., 2012, 2014).

related to the India-Asia collision. As a result, coal seams in northern Sumatra are often associated with *syn*-rift deposits, less extensive, but thicker than in southern Sundaland (Friederich et al., 2016).

The coal seams studied have accumulated in the Barito Basin, which is located on the southeastern margin of Sundaland in south Kalimantan. It is bounded on the west by the continental Schwaner Complex and on the east by the accreted Meratus Complex (Satyana et al., 1999; Fig. 2a). To the north, a flexure separates the Barito Basin from the Kutai Basin, while to the south the basin continues into the Java Sea (Figs. 1, 2a).

The thickness of the Cenozoic basin fill (Fig. 3) increases in an easterly direction towards the Meratus Mountains. This gives the Barito Basin an asymmetrical shape (Satyana et al., 1999). Structurally, the Barito Basin is a platform near the Schwaner Complex and a foredeep near the thrusted front of the Meratus Complex (Satyana et al., 1999). Similar to the Tarakan and Kutai basins, the development of the Barito Basin was initiated by the rifting of the Makassar Strait in the Eocene (Daly et al., 1991; Pubellier and Morley, 2014; Zahirovic et al., 2014; for location see Fig. 1). This extensional event led to the formation of NW-SE oriented horst and graben structures along a succession of NW-SE trending strike-slip faults (Satyana et al., 1999). Rifting in the Barito Basin ended towards the end of the Early Oligocene (Pubellier and Morley, 2014). Basin inversion commenced in the middle Miocene, around the time of the uplift of the Meratus Mountains (Satyana et al., 1999; Witts et al., 2014).

The Cenozoic fill of the Barito Basin overlies Cretaceous and older basement rocks unconformably and comprises, from base to top, the Middle Eocene to Lower Oligocene Tanjung Formation, the Upper Oligocene to lower Miocene Berai and Montalat Formations, the middle to upper Miocene Warukin Formation, and the upper Miocene to Pleistocene Dahor Formation (Witts et al., 2012, 2014; Fig. 3). Coal seams occur in the Tanjung Formation and the Warukin Formation (Friederich et al., 2016).

The Tanjung Formation represents a transgressive succession. It starts with alluvial and fluvial plain deposits filling a pre-existing relief (Mangkook Member) and continues with fluvio-tidal and estuarine deposits containing thick and laterally extensive coal seams (Tambak Member). The upper part of the Tanjung Formation consists of marginal to shallow marine rocks dominated by calcareous mudstones (Pagat Member; Witts et al., 2012). In the south, the Tanjung Formation is overlain with a sharp boundary by shallow marine carbonates (Berai Formation) and in the north by intertidal and fluviodeltaic strata (Montalat Formation; e.g. Supriatna et al., 1994).

The regressive Warukin Formation comprises marginal marine rocks with thin coal seams (typically <2 m; Sapiie and Rifiyanto, 2017) in its lower part (Barabai Member of Witts et al., 2012). The overlying Tapin Member (Witts et al., 2012) represents eastward prograding fluviodeltaic sedimentary rocks with thick coal seams in its lower part (Satyana et al., 1999; Witts et al., 2012). A change in paleocurrent directions during the deposition of the uppermost part of the Tapin Member indicates the onset of uplift of the Meratus Complex (Witts et al., 2014).

Regression and basin inversion continued during the deposition of the Dahor Formation, which forms the *syn*-inversion sequence of the basin (Witts et al., 2014). The Dahor Formation consists mainly of alluvial to shallow marine reddish sandstone, polymict conglomerate and siltstone (Sapiie and Rifiyanto, 2017). The thickness of the Dahor Formation near the Meratus Complex can exceed 3000 m (Kusuma and Darin, 1989).

The Tutupan mine (Fig. 2b), located within the study area, is the most important mining site for coal from the Warukin Formation. The mining area, about 15 km long (Waterhouse et al., 2008), is located between two NE-SW trending reverse faults: the Dahai Fault in the northwest and the Tanah Abang - Tepian Timur Fault in the southeast. The coal seams dip towards the southeast with variable gradients (20–60°) and are intercalated with fine-grained sandstone, mudstone and carbonaceous mudstones (Waterhouse et al., 2008).

Exploration drilling in the Tutupan area led to the discovery of three main and five secondary seams. The main coal seams are labelled T100, T200 and T300 from bottom to top. Thus, T300 is the youngest seam, although an internal report discussed the possible presence of an overturned succession (ADARO, 2008). Seam T100 is up to 60 m thick, while seams T200 (up to 25 m) and T300 (up to 35 m) are thinner. The thickness of the lower split coal (T110, T210) is similar to that of the unsplit coal, but the upper split coal (T120, T220) is generally thinner (e.g. 15 m for T220). The T120 seam is separated from the T110 seam by sandstone, which is up to 100 m thick (ADARO, 2008).

3. Samples

Coal samples were collected from the southern sector of the Tutupan Mine (Tutupan Selatan) with seams T110, T210, and T300 being the most economically important. Sampling focused on sites with freshly exposed coal in order to exclude any weathering effect. The coal at the studied sites is very thick (T110: 46 m; T210: 24 m; T300: 24 m). For this reason, and because the coal appears largely homogenous macroscopically, vertically-continuous one meter segments of the coal were collected, which cover each seam completely. Additional samples represent the floor and roof rocks of each seam. Thus, the sample set comprises 93 coal and 7 non-coal samples (including one non-coal sample representing a parting in seam T300), which were wrapped in gas-tight plastic immediately after collection to prevent loss of moisture content.

4. Methods

With the exception of the determination of ash yield and moisture content, all analytical data were obtained at the Montanuniversitaet Leoben.

Ash yield and moisture content were determined for all samples to obtain information on the peat type (e.g. Moore and Shearer, 1997) and the degree of coal compaction. Sample preparation was carried out at the Mineral and Coal Laboratory at the Mining Engineering Department, Faculty of Engineering, Lambung Mangkurat University. Analyses were performed at Coal Laboratory PT Geoservices, Banjarbaru, South Kalimantan following standard procedures (ASTM, 2012, 2017). During sample handling, care was taken to ensure that the moisture content was not affected.

Total organic carbon (TOC) contents are needed for the normalization of biomarker data, total inorganic carbon (TIC) contents provide information on the amount of carbonate minerals and the total sulphur (S) content is an important peat-facies indicator (e.g. Dai et al., 2020). Total carbon (TC), TOC and S contents were determined in duplicate using an Eltra Helios C/S analyzer on all samples. The TIC content was calculated as the difference between TC and TOC.

Rock-Eval pyrolysis provides information on the type and maturity of organic matter (Espitalie et al., 1977). It was performed in duplicate using a Vinci Rock-Eval 6 instrument. The amount of free hydrocarbons (S1) and the amount of hydrocarbons generated during thermal cracking (S2 in mg HC/g rock) were recorded together with the temperature of maximum hydrocarbon generation (Tmax, °C).

Maceral analysis was performed to characterize the petrography of the coal samples. For microscopic analyses, the samples were crushed to a maximum size of 1 mm. Maceral analysis was performed using a single-scan method (Taylor et al., 1998) with Leica MPV microscope using reflected white and fluorescent light and was used under oil immersion with 50 × magnification. At least 500 points were counted in every sample. Due to the low rank of coals, the nomenclature of huminite macerals (Sýkorová et al., 2005) is used in this paper. The nomenclature of liptinite and inertinite macerals follows Pickel et al. (2017) and ICCP (2001).

Vitrinite reflectance, an important maturity parameter, was determined for different huminite macerals (ulminite, densinite, phlobaphinite) using 10 coal samples. Random vitrinite reflectance (%Rr) was measured in non-polarized light at a wavelength of 546 nm with a magnification of 50 × using standard techniques (Taylor et al., 1998). On phlobaphinite macerals, at least 50 points were assessed for each sample.

Biomarker analysis was performed to obtain information on the peat-forming vegetation. Approximately every second coal sample was selected for organic geochemical analysis. Samples were extracted for 1 h using dichloromethane in a Dionex ASE 350 accelerated solvent extractor at 75 °C and 100 bar. After evaporation of the solvent to a total volume of 0.5 ml total solution in a Zymark TurboVap 500 closed cell concentrator, asphaltenes were precipitated from a hexane-dichloromethane solution (80:1) and separated by centrifugation. The hexane-soluble fractions were separated into NSO compounds, saturated hydrocarbons and aromatic hydrocarbons using a Köhnen-Willsch medium-pressure liquid chromatography (MPLC) instrument (Radke et al., 1980).

n-Alkanes and isoprenoids within the saturated hydrocarbon fractions were analyzed using a gas chromatograph (Trace GC-Ultra) with a flame ionization detector (GC-FID). The gas chromatograph was equipped with a 50 m HP-PONA capillary column (inner diameter [i.d.] 0.20 mm, 0.50 μm film thickness). After sample injection (2 μl at 270 °C), the oven temperature was increased from 70 °C to 310 °C and held constant for 35 min.

The hydrocarbon fractions were analyzed by a gas chromatograph equipped with a 60 m TG-5MS fused silica capillary column (i.e. 0.25 mm; 0.25 μm film thickness) coupled to a ThermoFisher ISQ mass spectrometer. The oven temperature was programmed from 40 °C to 310 °C at 4 °C/min, followed by an isothermal period of 30 min. Helium was used as the carrier gas. The sample was injected in a split mode (split ratio 20) at an injector temperature of 260 °C. The spectrometer was operated in the EI (electron ionization) mode over a scan range from mass-to-charge ratio (*m/z*) 50 to m/z 650 (0.7 s total scan time). Data were processed with the Xcalibur data system. Individual compounds were identified based on retention time in the total ion current (TIC) chromatogram and by comparison of the mass spectra with published reference data. Relative percentages and absolute concentrations of different compound groups in the saturated and aromatic hydrocarbon fractions were calculated using peak areas in the TIC chromatograms relative to that of internal standards (squalane and 1,1′-binaphthyl, respectively), or by integration of peak areas in appropriate mass chromatograms using response factors to correct for the intensities of the fragment ion used for quantification of the total ion abundance. The concentrations were normalized to TOC.

5. Results

5.1. Bulk parameters

The bulk parameters of Tutupan coals are listed in Table 1. Their vertical variation is shown in Fig. 4.

The ash yields are generally low, but differences within and between the seams are observed. Seam T110 contains coal with very low ash yield (average 2.2 wt%). In the lower part of the seam (1–23 m) the ash yield is slightly higher (av.: 2.9 wt%) than in the upper part (23–47 m; av.: 1.4 wt%). Within the upper part, the ash yield exceeds 5 wt% in the sample from 38 to 39 m and in the uppermost sample (46–47 m).

Very low ash yields (0.9–1.7 wt%) are also characteristic of the T210 seam. Higher ash yields (7–14 wt%) occurred only at the base of the seam (1–2 m) and at its top (23–25 m).

Although low-ash intervals occur in seam T300 (e.g. 1–8 m; 17–21 m; 23–25 m), the average ash yields (4.4 wt%) in this seam are relatively high. In addition, seam splitting occurs near the top of the seam (22–23 m).

As expected, the TOC contents are negatively correlated with ash yields. The TOC contents of samples with ash yields below 2 wt% are about 60 wt%. Floor and roof rocks from seam T110 contain very low TOC contents (0.59 and 0.69 wt%, respectively). In contrast, the TOC contents in the floor and roof rocks of seams T210 (1.17 and 1.21 wt%) and seam T300 (2.34 and 1.54 wt%) are somewhat higher. A mudstone parting near the top of seam T300 contains 1.36 wt% TOC. The samples examined are largely free of carbonate minerals, with the exception of the roof of seam T300 (2.6 wt%).

The sulphur contents in the T110 seam are very low (0.08–0.16 wt %). Only the topmost sample contains 2.0 wt% sulphur. In seam T210, sulphur contents tend to be even lower (0.06–0.17 wt%), contents above 0.1 wt% being restricted to the lowest and uppermost 2 m of the seam. Seam T300 also contains low-sulphur coal (0.07–0.12 wt%), but sulphur contents in three samples with moderately high ash yields range from 0.2 to 0.3 wt%. Sulphur contents in floor and roof rocks are generally very low (0.01–0.04 wt%). Only the roof of seam T300 contains 0.33 wt % sulphur.

The average moisture content increases from seam T110 (18.8 wt%) to seams T210 (20.6 wt%) and T300 (26.3 wt%).

The HI values of the coal samples in seam T110 range from 115 to 310 mgHC/gTOC. With one exception, all samples with HI values >200 mgHC/gTOC occur in the upper part of the seam. Similar HI values are found in seam T210 (136–331 mgHC/gTOC) and seam T300 (133–349 mgHC/gTOC). The HI values of non-coal samples are generally lower (51–131 mgHC/gTOC).

The Tmax values of coal samples range from 371 to 411 °C and show a negative correlation with HI values ($r^2 = 0.54$). This indicates that hydrogen-rich samples are characterized by low Tmax values and that

Table 1
Bulk parameters of Tutupan coals.

Sample	Lithology	Position	Ash	Moisture	TOC	Sulphur	HI	Tmax	EOM	NSO	Sat.HC	Arom.HC
		(m above base)	(wt.% adb)		(wt.% db)		(mgHC/gTOC)	(°C)	(mg/g TOC)			
T300-roof	mudstone	25	88.03	5.2	1.51	0.33	51	425				
T300-1	coal	24	1.54	30.6	51.6	0.09	201	383				
T300-2	coal	23	1.54	31.4	50.8	0.09	167	402	122.4	52.2	1.3	1.9
T300-3	mudstone	22	88.25	4.8	1.36	0.06	82	422				
T300-4	coal	21	5.03	28.6	51.3	0.10	275	372	235.4	90.4	1.6	3.6
T300-5	coal	20	1.20	27.6	52.8	0.07	315	374				
T300-6	coal	19	1.12	27.9	53.6	0.07	349	373	316.1	119.7	1.6	4.0
T300-7	coal	18	2.09	31.1	50.0	0.10	200	375				
T300-8	coal	17	1.64	32.3	48.8	0.10	133	403	75.8	16.6	0.9	1.6
T300-9	coal	16	13.88	19.9	34.4	0.12	189	403	159.4	73.9	1.4	2.8
T300-10	coal	15	3.69	20.5	51.8	0.11	240	375				
T300-11	coal	14	7.39	24.9	45.9	0.11	158	405	89.4	45.1	1.2	2.0
T300-12	coal	13	6.74	26.7	49.1	0.26	194	372				
T300-13	coal	12	1.73	27.4	54.6	0.11	244	373	162.2	42.3	1.5	2.2
T300-14	coal	11	12.85	25.9	41.7	0.09	201	373	120.7	40.3	1.4	3.0
T300-15	coal	10	15.61	23.1	43.1	0.30	241	378				
T300-16	coal	9	7.69	24.1	49.9	0.21	286	372				
T300-17	coal	8	3.96	23.6	53.6	0.10	143	371	99.8	25.1	0.8	1.7
T300-18	coal	7	1.76	23.3	54.6	0.09	257	375				
T300-19	coal	6	3.69	30.2	49.2	0.09	190	382				
T300-20	coal	5	1.49	30.0	49.6	0.09	187	399	96.9	24.5	1.2	2.1
T300-21	coal	4	1.86	22.7	56.1	0.09	291	374				
T300-22	coal	3	1.68	22.9	56.1	0.11	226	376	105.2	15.5	0.7	1.1
T300-23	coal	2	1.19	21.5	60.0	0.08	269	375				
T300-24	coal	1	1.94	28.5	52.5	0.09	232	378	122.6	33.7	1.2	2.1
T300-floor	mudstone	0	85.46	5.5	2.34	0.04	119	416				
T210-roof	mudstone	25	89.47	3.0	1.21	0.03	68	423				
T210-1	coal	24	13.55	18.9	36.7	0.11	213	377	254.4	152.5	1.4	1.6
T210-2	coal	23	7.16	21.1	49.2	0.10	156	407				
T210-3	coal	22	1.60	24.0	56.8	0.10	136	403	93.7	33.7	0.7	1.3
T210-4	coal	21	1.21	17.7	60.9	0.07	331	377	179.3	73.7	0.9	1.3
T210-5	coal	20	1.31	21.4	56.4	0.08	202	379				
T210-6	coal	19	1.14	23.1	55.7	0.07	165	387				
T210-7	coal	18	1.14	21.2	58.3	0.07	209	375	180.3	86.8	1.1	2.0
T210-8	coal	17	1.24	17.0	63.1	0.07	301	377	219.5	84.5	1.1	2.6
T210-9	coal	16	1.26	20.3	58.2	0.08	159	405				
T210-10	coal	15	1.26	19.5	61.1	0.06	197	378				
T210-11	coal	14	1.70	20.3	58.9	0.08	186	376	126.8	16.1	0.8	0.8
T210-12	coal	13	1.22	19.4	59.3	0.08	176	403				
T210-13	coal	12	1.34	19.7	60.5	0.08	197	375	164.1	68.6	1.3	2.1
T210-14	coal	11	1.22	19.5	61.1	0.08	253	374				
T210-15	coal	10	1.24	21.5	59.3	0.08	185	376	129.1	53.5	1.0	1.7
T210-16	coal	9	1.32	18.9	60.6	0.08	268	372				
T210-17	coal	8	1.28	19.8	59.8	0.08	249	374	186.4	63.5	1.2	2.1
T210-18	coal	7	1.26	20.8	59.6	0.08	157	397				
T210-19	coal	6	0.98	22.8	59.0	0.07	188	399	77.0	10.1	0.7	0.9
T210-20	coal	5	1.05	21.9	59.6	0.07	193	392				
T210-21	coal	4	1.19	20.2	61.2	0.09	252	374	216.9	94.8	1.8	3.6
T210-22	coal	3	1.08	21.0	60.8	0.08	179	378				
T210-23	coal	2	1.30	26.9	54.2	0.11	172	397				
T210-24	coal	1	14.15	18.0	40.7	0.17	191	403	110.3	27.6	1.3	2.3
T210-floor	mudstone	0	88.90	4.4	1.17	0.02	131	364				
T110-roof	mudstone	47	91.13	3.5	0.69	0.04	89	372				
T110-1	coal	46	5.19	17.1	53.5	2.03	269	375	214.7	92.7	1.7	1.7
T110-2	coal	45	1.44	18.3	62.8	0.12	295	378	139.2	83.9	0.8	1.0
T110-3	coal	44	1.12	19.7	63.8	0.10	273	376				
T110-4	coal	43	1.12	20.3	62.7	0.09	230	377	133.0	62.0	1.0	1.3
T110-5	coal	42	1.18	20.7	59.7	0.12	262	376				
T110-6	coal	41	1.12	18.9	62.7	0.10	208	392	182.4	99.0	1.4	1.8
T110-7	coal	40	1.08	19.2	61.9	0.09	170	399				
T110-8	coal	39	1.16	21.6	60.7	0.09	140	401	108.5	42.6	0.9	1.2
T110-9	coal	38	5.87	18.4	55.3	0.13	222	377				
T110-10	coal	37	1.18	20.6	60.8	0.10	202	403	110.2	26.1	1.5	1.6
T110-11	coal	36	1.33	21.9	58.1	0.09	156	384				
T110-12	coal	35	0.98	19.5	62.5	0.10	161	404	172.6	107.8	2.0	2.0
T110-13	coal	34	0.98	19.2	62.5	0.11	242	382				
T110-14	coal	33	0.96	19.7	60.8	0.09	174	401	99.0	2.0	0.8	1.1
T110-15	coal	32	1.04	18.8	60.5	0.10	189	399				
T110-16	coal	31	0.92	17.5	63.1	0.08	310	376	260.6	140.1	2.9	3.0
T110-17	coal	30	1.02	19.7	60.7	0.08	228	379				
T110-18	coal	29	1.02	19.9	59.0	0.09	169	405	65.2	11.6	0.9	0.9

(*continued on next page*)

Table 1 (*continued*)

Sample	Lithology	Position	Ash	Moisture	TOC	Sulphur	HI	Tmax	EOM	NSO	Sat.HC	Arom.HC
		(m above base)	(wt.% adb)		(wt.% db)		(mgHC/gTOC)	(°C)	(mg/g TOC)			
T110-19	coal	28	1.05	19.2	60.4	0.10	209	383				
T110-20	coal	27	1.10	19.1	60.5	0.09	229	377	254.1	113.0	2.7	2.7
T110-21	coal	26	1.37	18.1	58.8	0.09	179	403				
T110-22	coal	25	0.64	18.6	59.5	0.08	181	401	157.5	79.0	1.7	1.7
T110-23	coal	24	0.60	19.5	58.9	0.08	187	405				
T110-24	coal	23	0.61	18.7	61.5	0.09	174	404	106.8	28.1	0.8	1.1
T110-25	coal	22	4.27	16.8	51.7	0.08	169	399				
T110-26	coal	21	2.78	16.6	53.3	0.08	199	398	116.1	11.9	1.2	1.3
T110-27	coal	20	1.58	15.7	60.4	0.09	226	384				
T110-28	coal	19	2.08	18.1	57.2	0.10	189	404	92.6	21.3	1.6	1.5
T110-29	coal	18	2.56	17.6	54.2	0.10	185	402				
T110-30	coal	17	1.17	18.4	59.1	0.09	193	401	126.0	40.8	1.1	1.1
T110-31	coal	16	1.73	16.7	58.4	0.09	143	400				
T110-32	coal	15	1.10	18.3	59.4	0.08	193	401	116.8	37.9	1.2	1.5
T110-33	coal	14	1.18	19.5	59.3	0.09	154	405				
T110-34	coal	13	2.08	18.9	54.2	0.10	123	408	117.0	54.1	1.4	2.1
T110-35	coal	12	1.28	19.0	58.2	0.10	127	406				
T110-36	coal	11	1.32	18.3	59.2	0.10	168	406	76.4	11.3	1.2	2.4
T110-37	coal	10	3.03	18.6	51.7	0.09	177	404				
T110-38	coal	9	1.69	19.2	53.0	0.10	160	405	125.4	58.5	2.1	3.7
T110-39	coal	8	2.35	18.3	54.5	0.10	178	406				
T110-40	coal	7	2.24	17.9	56.6	0.10	197	405	98.6	25.9	2.0	2.0
T110-41	coal	6	2.81	18.5	55.4	0.12	160	404				
T110-42	coal	5	2.37	19.2	56.4	0.13	144	408	69.6	21.2	1.3	1.9
T110-43	coal	4	6.04	20.2	47.8	0.16	115	411				
T110-44	coal	3	15.91	16.1	38.7	0.14	154	408	71.7	16.6	1.2	1.6
T110-45	coal	2	3.22	18.4	54.5	0.13	182	405				
T110-46	coal	1	1.16	18.5	59.3	0.10	171	403	78.6	19.9	1.8	2.5
T110-floor	mudstone	0	92.78	1.1	0.59	0.01	55	421				

TOC – total organic carbon, HI – hydrogen index, EOM – extractable organic matter, NSO – hetero-compounds, Sat.HC – saturated hydrocarbons, Arom.HC – aromatic hydrocarbon.

the wide variation is at least partly controlled by the coal facies. Average Tmax values for coal in seams T110, T210, and T300 are 396 °C, 385 °C, and 381 °C, respectively. The Tmax of the non-coal samples is in the order of 420 °C, but roof rocks from seam T110 (364 °C) and floor rocks from seam T210 (372 °C) have very low Tmax values.

5.2. Biomarkers

Forty-eight samples were selected for biomarker analysis. The amount of extractable organic matter (EOM; Table 1) correlates positively with the HI values ($r^2 = 0.56$). The extracts are dominated by asphaltenes and NSO compounds. Aliphatic and aromatic hydrocarbons occur in very low amounts (Fig. 5; Table 1), which is consistent with the low rank of the samples. GC traces of selected samples from different seams are shown in Figs. 6 and 7. The *n*-alkane distributions show significant differences, although all samples are dominated by long-chain *n*-alkanes (n-$C_{25–33}$) (Figs. 6, 7). To highlight these differences, different ratios were calculated based on *n*-alkane and isoalkane distributions, listed in Table 2 and plotted in Fig. 5 as a function of stratigraphic position.

- The terrestrial/aquatic ratio (TAR; Bourbonniere and Meyers, 1996) is the ratio of long to short chain *n*-alkanes (n-$C_{27+29+31}$/n-$C_{15+17+19}$). It shows stratigraphic trends with upward increasing values in seams T110 and T210. These trends are labelled from base to top cycles 110–1 to 110–5 and 210–1 to 210–3 in Fig. 5. The highest ratios (max. 38.4), but no clear depth trend are observed in seam T300.
- The P-aqueous (Paq) ratio (Ficken et al., 2000) compares the abundance of medium chain to the sum of medium and long chain *n*-alkanes (($C_{23} + C_{25}$)/($C_{23} + C_{25} + C_{29} + C_{31}$)). The ratio increases upwards in seam T110 from 0.05 to 0.25. Intermediate values (0.05–0.19) are observed in seam T210 and low values (0.05–0.11) occur in seam T300. The stratigraphic trends reflect the subdivision into distinct cycles, although Paq ratios suggest a slightly deeper position of the boundary between cycles 110–4 and 110–5. Two cycles (330–1 and 300–2) are recognized in seam T300.
- The carbon preference index (CPI; Bray and Evans, 1961) is very high (2.2–6.2) and shows stratigraphic trends, similar to those of Paq.
- The average chain length (ACL = $27 \times C_{27} + 29 \times C_{29} + 31 \times C_{31}$)/($C_{27} + C_{29} + C_{31}$)) of long chain *n*-alkanes was calculated according to Poynter and Eglinton (1990). The ratios vary between 28.2 and 30.2 and displays rather irregular trends in seam T110. In seams T210 and T300 they reflect the subdivision into distinct cycles.
- The n-C_{29}/n-C_{27} ratio (Buggle et al., 2010) varies strongly in the lower part of seam T110 (cycles 100–1 to 100–4) and is about 1.0 in its upper part (100–5). It increases gradually from 1.0 to 2.2 upwards in seam T210 and is relatively high in seam T300 (2.1–4.8).
- The ratio of (n-C_{31+33})/(n-C_{27+29}) (Zech et al., 2009) decreases from 2.2 to 0.2 in the lower part of seam T110 (cycle 100–1) and remains low in the rest of the seam. Higher ratios (0.8–2.2) are observed in seam T210 and form two upward increasing trends. In contrast, the ratios are rather uniform (0.5–0.9) in seam T300.
- Pristane/phytane ratios are very high (3.9–23.6). Average values decrease from the lower seam T110 to the upper seam T300. A moderate positive correlation ($r^2 = 0.45$) exists with CPI.

Steranes occur in very low amounts and were not quantified, but tetracyclic and pentacyclic terpenoids are present in all samples in significant amounts (Table 2; Figs. 6, 7, 8).

- Saturated, unsaturated and aromatic sesquiterpenoids of the cadinane (0.2–40.0 µg/gTOC) and drimane type (0.3–25.5 µg/gTOC) are observed in low, but varying quantities. Aromatic sesquiterpenoids are typically slightly more abundant than saturated ones.
- Diterpenoids are generally rare (3.1–28.0 µg/gTOC) and dominated by aromatic compounds. Pimarane occurs in all seams (up to 3.1 µg/

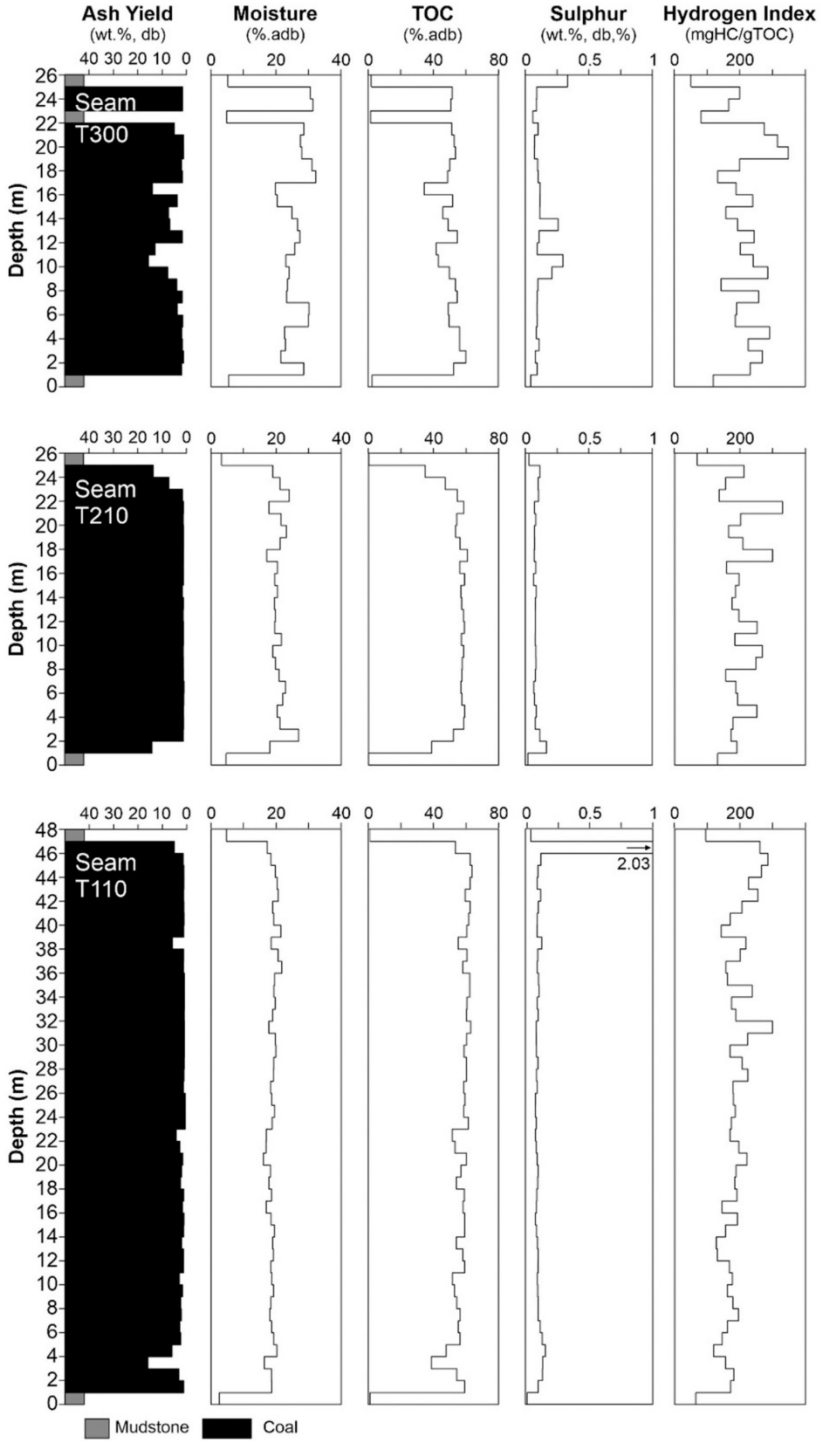

Fig. 4. Variations of ash yield, moisture content, total organic carbon (TOC) content, sulphur content and hydrogen index in seams T110, T210 and T300 in the southern part of the Tutupan mine. The stratigraphic distance between seams T110 and T210 and between seams T210 and T300 is approximately 250 and 350 m, respectively.

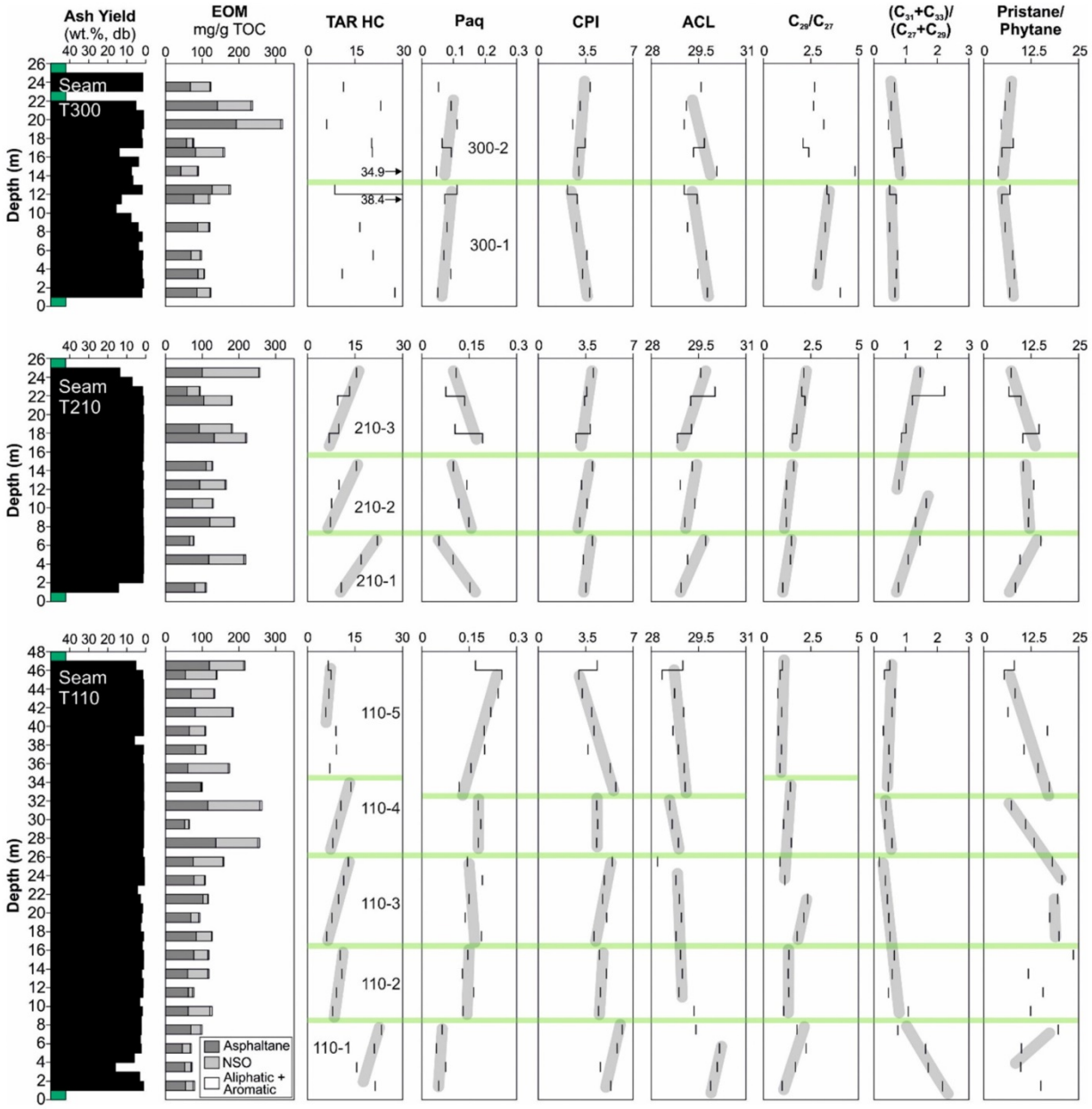

Fig. 5. Variations of EOM, *n*- and isoalkane ratios in seams T110, T210 and T300. Selected trends are highlighted by grey lines. Cycles 110–1 to 300–2 have been defined based on geochemical parameters (primarily TAR). Boundaries between cycles are shown by green lines. See text for details. EOM – extractable organic matter; TAR – terrestrial/aquatic ratio (Bourbonniere and Meyers, 1996); Paq - P-aqueous (Ficken et al., 2000); CPI – carbon preference index (Bray and Evans, 1961); ACL – average chain length (Poynter and Eglinton, 1990). (For interpretation of the references to colour in this figure legend, the reader is referred to the web version of this article.)

gTOC), while phyllocladane is observed only in the T110 seam (up to 0.1 μg/gTOC).

- Angiosperm-derived triterpenoids (107–718 μg/gTOC) are much more abundant than diterpenoids. Representatives of the ursane (11–156 μg/gTOC), oleanane (20–137 μg/gTOC) and lupane types (7–88 μg/gTOC) were identified in decreasing concentrations. The concentrations of lupane decrease upwards in seam T210 and increase upwards in seam T300.

Because of the dominance of angiosperm-derived triterpenoids, the obtained di−/(di − + triterpenoids) ratios (Bechtel et al., 2003) are low (0.01–0.12) in all samples (Table 2; Fig. 8). Average ratios are slightly lower (0.02) in the lower part of seam T110 (cycles 110–1 to 110–3) than in its upper part (110–4 to 110–5) (0.05). A relatively high average value is found in seam T210 (0.07), whereas the average value for seam T300 is 0.02.

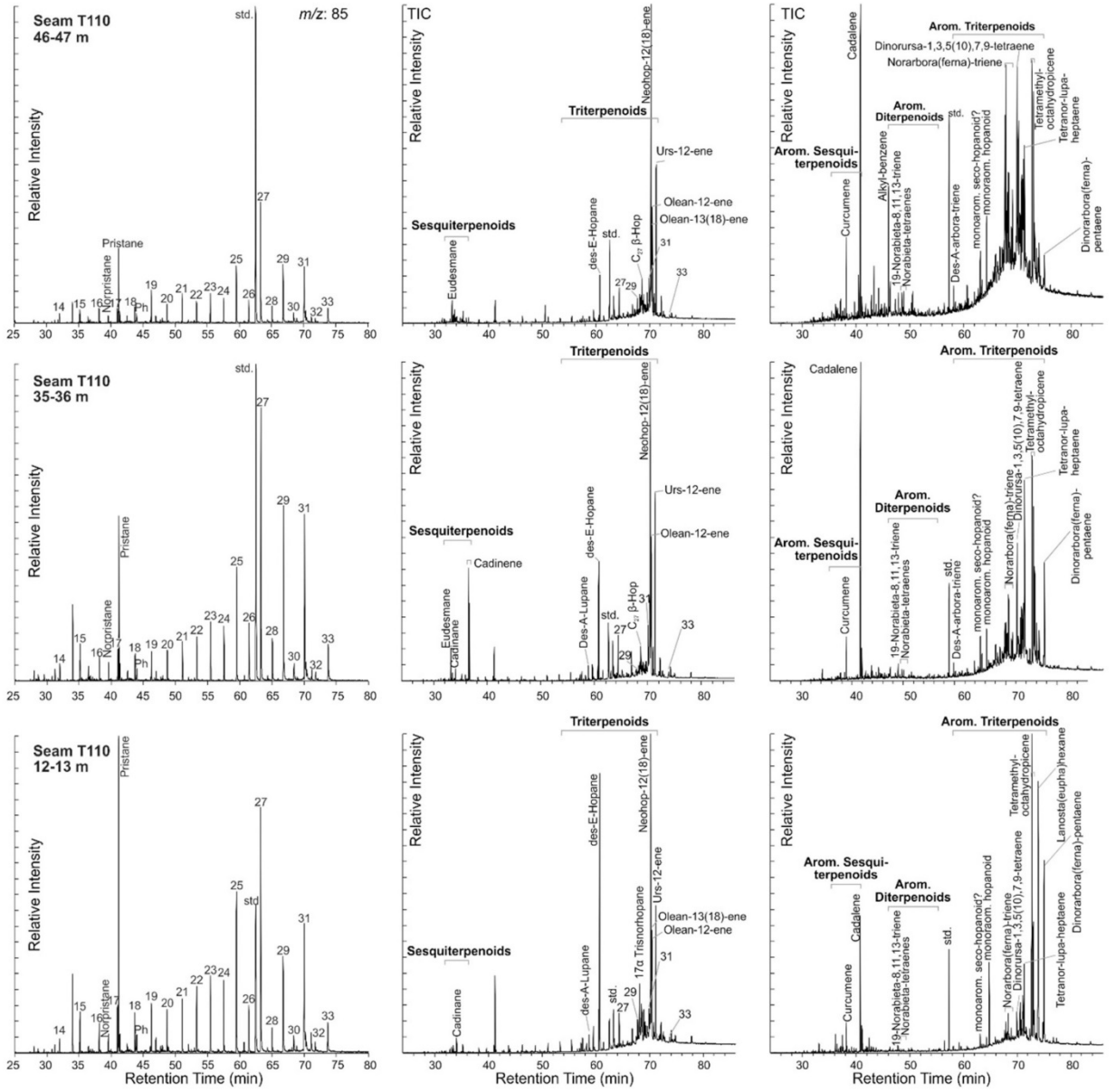

Fig. 6. *M/z* 85 and total ion current (TIC) chromatograms of the saturated and aromatic hydrocarbon fractions of selected samples from seam T110. The *m/z* 85 chromatogram shows the distribution of *n*-alkanes and isoprenoids. Std. standard.

- Aromatic triterpenoids of the arborane−/fernane-type (e.g., des-A-arbora(ferna)-triene, norabrora(ferna)-triene, dinorarbora(ferna)-pentaene) are identified in high concentrations in the samples (9–116 μg/gTOC).
- C_{29} neohop-13(18)-ene is dominating within the hopanoid hydrocarbons (0.2–174 μg/g TOC). Samples from seams T110 and T300 show strongly varying amounts, whereas samples from seam T210 exhibit lower values and hardly variations. 17α-trisnorhopane (TM), 17β,21β(H)-C_{29} hopane and 17β,21β(H)-C_{30} hopane occur in small amounts. Aromatic hopanoids are represented by benzohopanes and monoaromatic hopanoids (3.5–21.8 μg/gTOC).

PAHs (fluoranthene, [methyl]pyrene) are generally rare, but relatively high concentrations are observed in the upper part of seam T300 (Fig. 8).

5.3. Organic petrography

5.3.1. Maceral composition

Photomicrographs of macerals from seams T110, T210 and T300 are shown in Figs. 9 and 10. Maceral percentages and derived petrography-based facies indicators are listed in Table 3 and plotted versus depth in Fig. 11. Huminite is the dominant maceral group in all seams (52–82 vol %), followed by substantial amounts of liptinite (15–45 vol%) and rare inertinite (1–7 vol%).

Telohuminite is the most abundant maceral subgroup. High

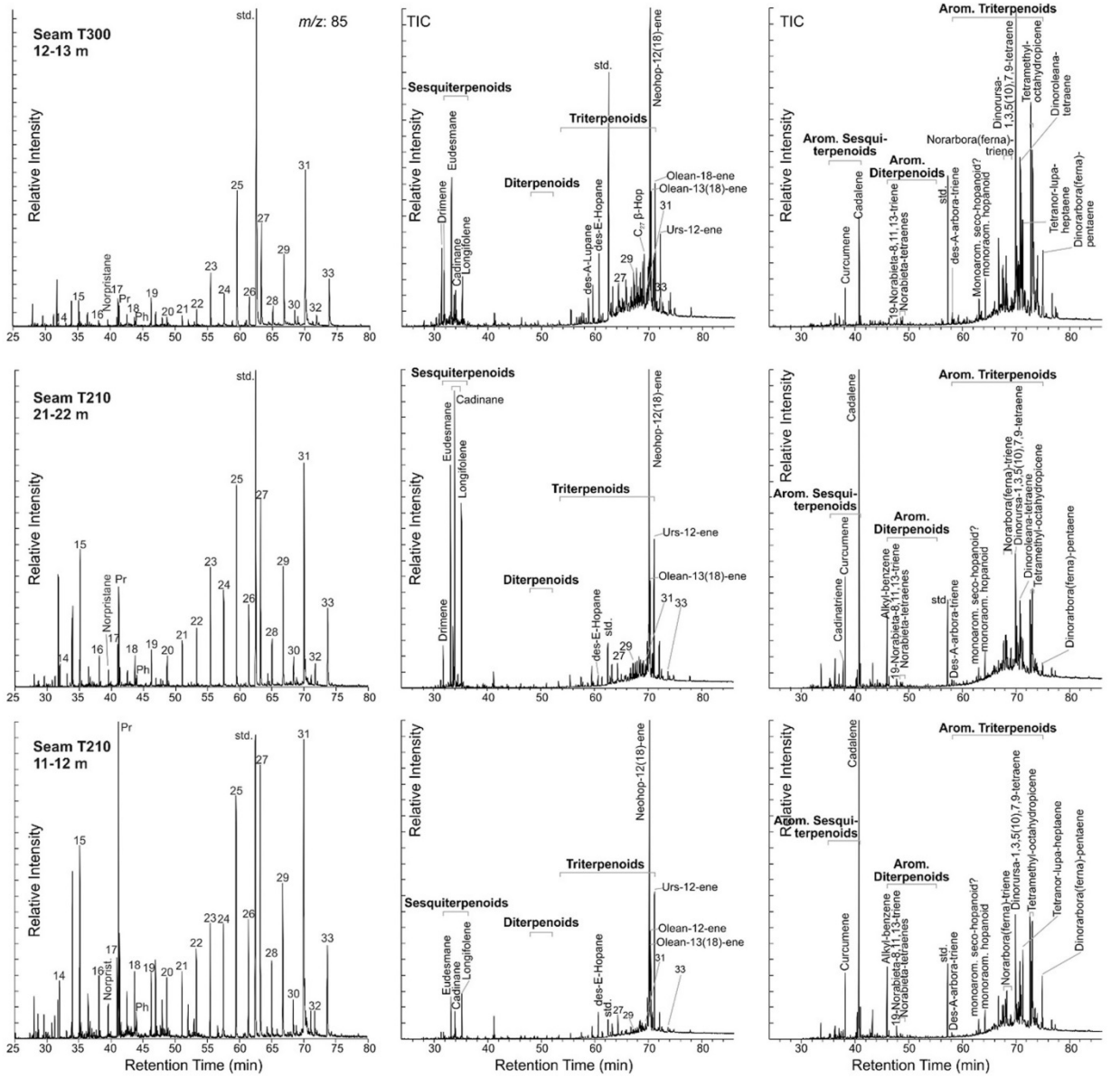

Fig. 7. *M/z* 85 and total ion current (TIC) chromatograms of the saturated and aromatic hydrocarbon fractions of selected samples from seams T210 and T300. The *m/z* 85 chromatogram shows the distribution of *n*-alkanes and isoprenoids. Std. standard.

percentages of ungelified textinite (e.g. Fig. 9a,b) are observed in seam T110, whereas texto-ulminite and gelified ulminite are typically rare. Increased contents of ulminite occur only in the middle part of seam T110 (21–30 m), which is also characterized by abundant phlobaphinite (Fig. 11). Textinite also prevails in seams T210 and T300, but percentages of texto-ulminite are higher in these seams. Ulminite is rare in seam T210. Detrohuminite is less abundant than telohuminite. Within the detrohuminite subgroup, ungelified attrinite (e.g. Fig. 10c) is more common than gelified densinite. Densinite percentages in seam T210 are especially low (Fig. 11).

Liptinite macerals in Tutupan coals are dominated by liptodetrinite (9–26 vol%), but resinite is also abundant (2–19 vol%). Three different varieties of resinite have been distinguished: in-situ resinite (Fig. 9b), detrital resinite (Fig. 9c,d), and fluorinite (Fig. 9g,h) (cf. Pickel et al., 2017). All resinite varieties are more abundant in the upper part of the seam T110 (23–47 m) than in the lower part (1–23 m). This is particularly evident for fluorinite, which is remarkably abundant between 23 and 38 m (3–9 vol%). The relative contribution of detrital and in-situ resinite is similar in the lower and upper parts of seam T110. In seam T210 percentages of in-situ resinite (2–4 vol%), detrital resinite (<3 vol %), and fluorinite (<3 vol%) are relatively low, but a single sample in the upper part of the seam (21–22 m) contains high amounts of both, in-situ and detrital resinite (10 and 9 vol%, respectively). Seam T300 is characterized by strongly varying resinite percentages (2–13 vol%), which show positive relations with HI ($r^2 = 0.60$) and cadinane type sesquiterpenoids ($r^2 = 0.85$). In contrast to other seams, in-situ resinite is more abundant than detrital resinite.

Leaf-derived cutinite (<1–5 vol%) is often associated with fluorinite

Table 2
Organic geochemical parameters.

Sample	TAR HC	Paq	CPI	ACL	nC_{29}/nC_{27}	$(C_{31}+C_{33})/(C_{27}+C_{29})$	Pr/Ph	Sesqui-	Di-	Tri-	Cadi	Drim	Phyl clad	Pim	Abiet	Lup	Olean	Urs	Arbor	Di−/(Di− + Tri-) terpenoids	Hop	Neo-hop	PAH
								terpenopids															
								(μg/g TOC)			(μg/g TOC)										(μg/g TOC)		
T300–2	11.4	0.05	3.8	29.6	2.7	0.6	6.8	45.9	11.6	486,4	1.1	5.9	n.d.	2.05	3.4	48.7	38.1	70.6	115.9	0.02	11.6	2.2	9.6
T300–4	23.1	0.09	3.1	29.1	2.6	0.5	5.6	191.2	15.1	610,9	5.4	23.7	n.d.	3.10	2.5	88.0	57.0	136.2	72.4	0.02	18.2	8.9	4.4
T300–6	6.0	0.11	2.5	29.0	3.2	0.5	4.6	100.7	9.2	565,2	6.2	12.4	n.d.	1.20	2.7	72.1	73.6	155.9	60.5	0.02	17.0	32.0	10.6
T300–8	20.3	0.06	3.5	29.7	2.1	0.9	7.8	15.2	4.8	378,8	0.6	1.6	n.d.	0.37	2.5	39.4	38.1	54.1	52.9	0.01	17.2	35.7	8.2
T300–9	20.5	0.09	2.9	29.3	2.4	0.6	4.8	51.6	6.1	501,7	2.5	10.9	n.d.	0.55	2.6	61.5	66.2	107.5	57.3	0.01	35.4	52.2	3.2
T300–11	34.9	0.05	3.0	30.1	4.8	0.9	3.9	19.3	4.4	456,8	1.0	4.7	n.d.	0.31	2.5	44.9	71.1	75.8	38.7	0.01	44.9	75.0	2.4
T300–13	8.6	0.11	2.2	29.0	3.3	0.5	6.9	49.5	4.9	259,3	2.0	15.6	n.d.	0.32	2.7	29.1	35.6	70.4	21.8	0.02	14.4	22.1	2.1
T300–14	38.4	0.07	2.9	29.5	3.4	0.7	4.8	54.5	4.0	460,3	2.2	18.1	n.d.	0.50	1.8	42.0	68.3	79.0	26.2	0.01	35.0	74.3	3.1
T300–17	16.5	0.08	2.8	29.2	3.3	0.5	5.6	82.6	9.6	263,1	4.1	5.1	n.d.	0.21	2.8	25.2	22.7	54.0	34.2	0.03	6.7	15.5	3.0
T300–20	20.7	0.07	3.6	29.7	3.0	0.7	7.6	31.2	6.5	288,6	1.3	7.3	n.d.	1.81	1.6	26.8	50.9	56.2	46.4	0.02	34.0	57.0	2.7
T300–22	10.9	0.09	3.3	29.5	2.8	0.7	8.1	45.3	5.3	211,6	1.3	3.4	n.d.	0.56	1.5	23.2	24.7	40.0	36.3	0.02	9.6	19.0	3.3
T300–24	27.6	0.05	3.8	29.8	4.0	0.7	6.9	34.4	6.3	253,1	1.9	10.0	n.d.	3.13	1.3	20.0	50.3	64.5	32.2	0.02	38.8	57.2	1.7
T210–1	15.5	0.11	4.1	29.6	2.1	1.5	7.2	77.5	21.2	160,2	3.6	8.2	n.d.	0.13	2.6	8.2	29.4	61.4	20.8	0.11	22.5	29.7	1.7
T210–3	13.3	0.08	3.6	30.0	2.0	2.2	6.7	52.2	8.0	197,0	8.8	6.6	n.d.	0.16	2.2	15.9	28.5	37.4	9.4	0.04	10.8	17.8	1.2
T210–4	9.5	0.14	3.4	29.2	2.2	1.2	9.9	150.2	16.6	113,2	40.0	25.5	n.d.	0.06	2.3	7.5	21.5	36.8	13.0	0.12	12.2	13.8	0.6
T210–7	9.9	0.11	3.8	29.3	1.8	1.0	14.6	116.6	26.9	252,8	4.9	8.9	n.d.	0.08	5.6	32.9	33.9	54.6	31.5	0.09	17.3	22.8	2.3
T210–8	6.8	0.19	2.8	28.8	1.5	0.9	10.3	139.6	23.5	173,4	4.5	9.9	n.d.	0.12	3.0	35.4	27.2	35.6	20.1	0.11	17.9	14.8	0.7
T210–11	15.4	0.10	4.0	29.3	1.6	0.9	10.4	28.1	7.8	169,3	1.2	3.2	n.d.	0.35	2.0	17.9	27.5	41.3	12.6	0.04	13.5	24.7	0.8
T210–13	9.9	0.14	3.2	28.9	1.2	0.8	13.2	99.4	30.1	288,8	2.7	9.7	n.d.	0.27	5.4	48.8	44.3	60.9	32.8	0.09	23.2	30.4	0.9
T210–15	7.6	0.12	3.6	29.4	1.2	1.7	11.9	117.0	23.0	233,5	9.7	18.7	n.d.	0.61	3.5	28.1	41.6	69.5	22.3	0.08	14.6	33.5	1.0
T210–17	7.2	0.15	3.1	29.1	1.2	1.3	11.8	65.5	22.8	322,5	3.0	9.7	n.d.	0.25	5.3	58.0	52.2	74.2	37.3	0.06	21.5	31.2	0.9
T210–19	22.1	0.05	4.0	29.7	1.5	1.5	15.1	8.7	5.3	155,0	0.6	1.3	n.d.	0.03	3.1	21.1	22.7	35.0	15.3	0.03	11.5	16.3	0.7
T210–21	16.9	0.10	3.3	29.2	1.4	1.1	9.6	60.0	18.2	469,6	3.8	8.4	n.d.	0.28	5.8	87.2	72.1	104.4	50.3	0.04	24.3	38.9	1.2
T210–24	10.6	0.15	3.5	28.9	1.0	0.8	8.4	57.6	13.1	282,6	2.4	7.3	n.d.	0.12	2.8	40.5	36.2	58.7	37.4	0.04	21.8	27.6	1.1
T110–1	6.5	0.17	4.3	29.0	1.0	0.5	8.1	43.0	16.8	235,5	1.9	5.7	n.d.	0.16	4.6	13.9	52.1	60.4	38.2	0.06	14.6	80.7	1.4
T110–2	7.4	0.25	3.0	28.3	0.9	0.3	5.4	30.5	8.2	107,8	1.9	3.3	n.d.	0.12	2.1	11.2	20.3	11.7	29.3	0.07	8.6	23.6	0.7
T110–4	6.7	0.24	3.3	28.7	0.8	0.7	8.3	21.9	8.8	161,1	1.3	3.1	n.d.	0.03	3.5	23.4	39.9	33.3	16.6	0.05	10.1	42.7	1.0
T110–6	5.8	0.22	3.9	29.0	1.0	0.6	6.4	23.8	13.2	401,9	0.8	3.4	n.d.	0.06	6.0	42.0	52.5	48.1	28.2	0.03	14.5	60.9	1.1
T110–8	9.0	0.20	4.1	28.7	0.8	0.3	16.8	17.1	8.5	188,0	0.8	1.3	n.d.	n.d.	3.9	20.1	23.6	26.3	19.6	0.04	8.0	28.9	1.2
T110–10	9.1	0.20	3.7	28.9	0.9	0.5	10.6	60.4	9.2	306,2	1.6	3.2	0.13	0.05	4.3	38.2	55.0	56.1	36.9	0.03	15.7	69.0	1.3
T110–12	7.0	0.16	5.3	29.0	0.9	0.5	14.3	81.6	14.9	384,8	33.3	1.8	n.d.	n.d.	6.3	24.0	67.1	56.4	15.2	0.04	11.7	75.3	6.8
T110–14	13.7	0.12	5.7	29.1	1.4	0.5	17.3	10.0	4.4	181,0	0.4	1.1	0.05	0.04	1.8	15.6	29.7	27.9	14.6	0.02	6.2	40.7	1.9
T110–16	10.5	0.18	4.3	28.6	1.3	0.4	7.3	94.0	27.1	414,8	3.9	7.0	n.d.	0.61	5.7	79.9	59.2	88.8	45.8	0.06	11.3	52.9	2.0
T110–18	9.1	0.19	4.4	28.7	1.1	0.3	11.0	42.4	10.3	162,1	0.8	1.3	n.d.	0.03	2.7	14.7	33.7	34.2	21.2	0.06	6.4	45.3	1.1
T110–20	8.0	0.18	4.3	28.9	1.5	0.6	13.3	151.2	27.6	481,8	4.6	8.4	n.d.	0.21	6.2	31.6	137.0	139.3	35.5	0.05	23.7	174.3	2.6
T110–22	12.9	0.14	5.5	28.2	0.9	0.2	18.1	51.6	7.9	396,7	1.5	2.3	n.d.	0.02	3.0	32.1	75.3	50.1	30.1	0.02	10.5	57.2	13.3
T110–24	11.4	0.19	4.9	28.8	1.1	0.4	20.6	7.0	3.8	223,4	0.2	0.3	n.d.	0.03	1.6	21.1	41.9	33.0	2.9	0.01	5.0	32.0	3.7
T110–26	9.8	0.15	4.7	28.9	2.3	0.4	19.5	35.8	10.1	241,5	1.0	2.6	n.d.	n.d.	2.5	21.3	56.3	64.5	14.7	0.04	14.2	94.0	1.0
T110–28	7.7	0.14	5.0	29.0	2.1	0.5	17.4	44.1	9.0	320,3	0.8	3.1	n.d.	n.d.	3.9	16.8	91.7	76.2	16.2	0.02	16.6	118.4	1.7
T110–30	6.0	0.19	4.1	28.8	1.8	0.5	19.8	51.4	8.1	228,5	0.9	3.0	n.d.	n.d.	2.2	15.0	66.9	59.3	13.7	0.03	13.3	92.5	0.9
T110–32	10.3	0.15	4.5	28.9	1.3	0.6	23.6	58.3	6.8	306,3	1.3	2.6	n.d.	n.d.	2.3	24.3	61.0	48.9	10.9	0.02	13.0	69.0	2.2
T110–34	10.8	0.13	5.0	29.0	1.3	0.6	11.8	39.6	6.1	310,6	1.2	3.0	0.05	n.d.	2.0	17.6	70.5	49.6	18.4	0.01	19.6	89.1	1.5
T110–36	9.1	0.16	4.6	28.9	1.3	0.5	15.6	35.9	6.5	512,9	0.6	1.7	0.10	n.d.	2.4	31.0	63.5	35.0	69.7	0.01	18.1	59.8	2.3
T110–38	7.9	0.13	4.4	29.4	1.1	1.1	12.4	81.8	17.5	718,3	1.6	3.3	0.05	0.05	6.0	35.3	67.1	56.6	24.6	0.02	12.3	97.7	1.7
T110–40	23.4	0.06	6.2	29.4	1.8	0.8	19.6	40.8	8.9	342,3	1.1	2.1	n.d.	0.04	3.4	25.0	52.1	67.3	27.3	0.02	21.1	120.1	2.7
T110–42	21.1	0.05	5.8	30.2	2.2	1.6	9.9	13.4	15.2	345,6	1.3	2.9	0.04	0.05	4.8	23.5	79.4	63.5	31.5	0.04	17.7	112.2	2.9
T110–44	15.5	0.08	4.6	30.1	1.7	1.7	9.7	13.5	7.8	201,0	1.1	2.6	0.08	0.05	2.0	12.9	56.4	48.4	12.6	0.04	14.8	81.3	1.9
T110–46	21.3	0.05	5.4	29.9	1.0	2.2	15.0	19.7	12.5	379,7	0.7	1.5	0.03	0.04	5.4	26.3	46.9	44.9	42.8	0.03	13.6	75.2	4.1

TAR - terrestrial/aquatic ratio (Bourbonniere and Meyers, 1996), Paq - P-aqueous ratio (Ficken et al., 2000), CPI - carbon preference index (Bray and Evans, 1961), ACL - average chain length (Poynter and Eglinton (1990), Pr/Ph – pristane/phytane ratio, Cadi – cadinane-type, Drim – drimane-type, Pim – pimarane-type, Abiet – abietane-type, Lup – lupane derivatives, Olean – oleanane derivatives, Urs – ursane derivatives, Arbor – arborane-type, Hop – hopanes, Neohop - Neohop-13(18)-ene, PAH – polycyclic aromatic hydrocarbons, n.d. – not detected.

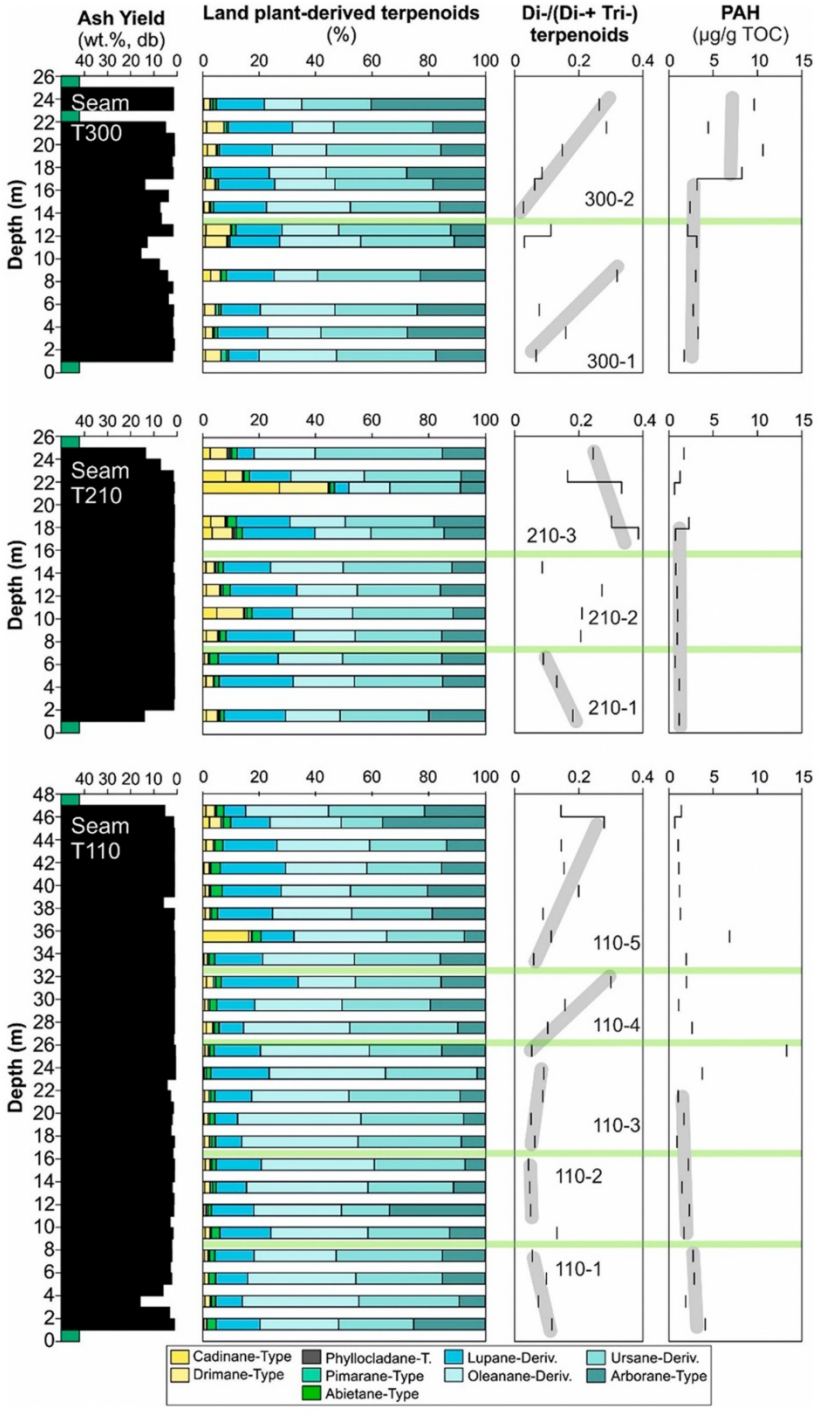

Fig. 8. Variations of land plant-derived terpenoids and PAHs in seams T110, T210 and T300. Selected trends are highlighted by grey lines. Cycles defined by *n*-alkane ratios (see Fig. 5) are labelled 110–1 to 300–2 (see right column). Cycle boundaries are shown by green lines. PAH – polyaromatic hydrocarbons. (For interpretation of the references to colour in this figure legend, the reader is referred to the web version of this article.)

(Fig. 9g,h). Clear depth trends in cutinite percentages cannot be observed, although they decrease upwards in the upper parts of the T110 (31–46 m) and T210 (12–24 m) seams and in two section within the T300 seam (1–14 m; 14–22 m; Fig. 9). The ratio between fluorinite and cutinite varies considerably between and within seams. Therefore, positive correlations with high correlation coefficients are observed only for certain sections. For example, in the interval from 8 to 16 m in the lower part of T110, the correlation coefficient (r^2) is 0.86 and the

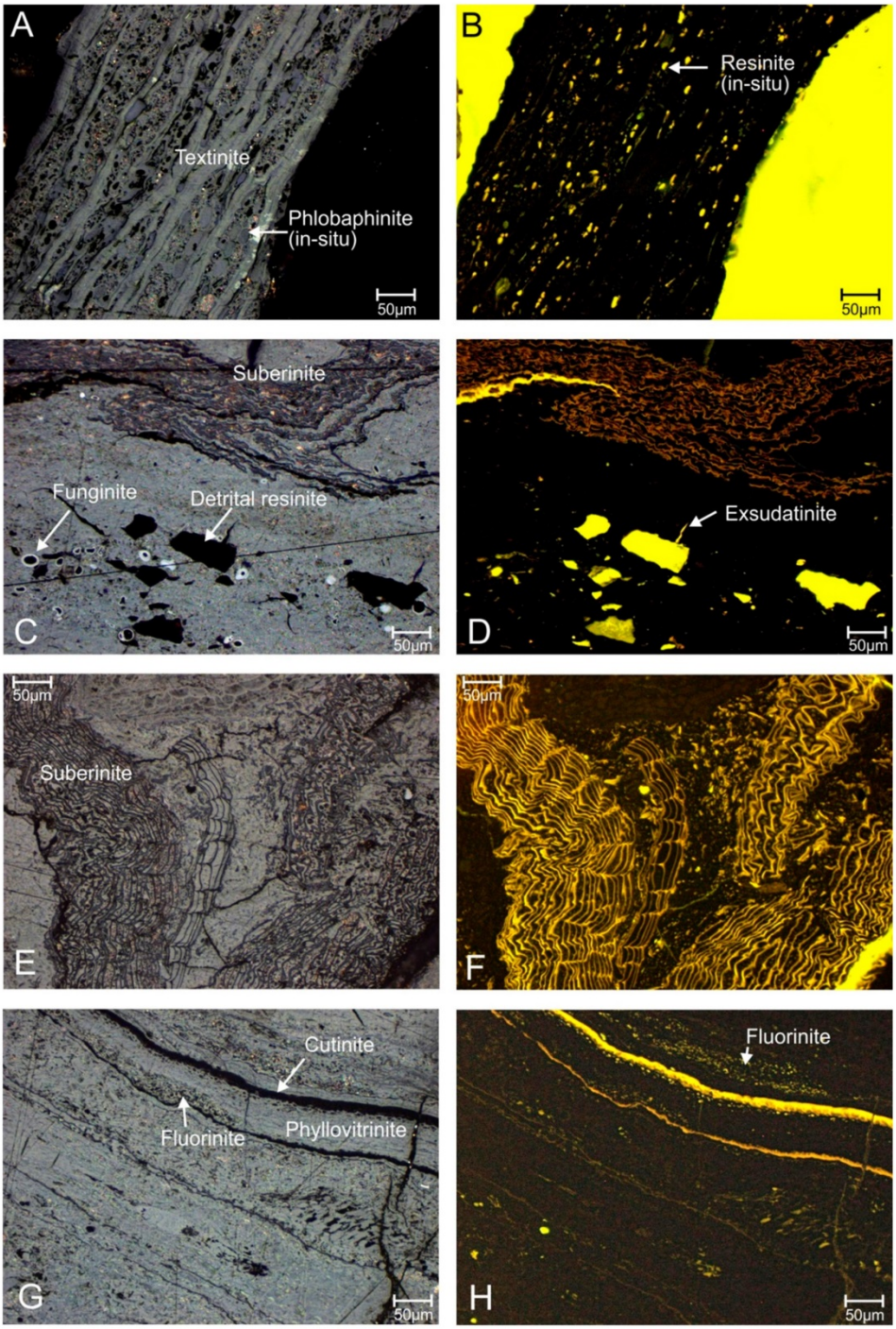

Fig. 9. Representative photomicrographs of coal samples. Left: white light; right blue light. (For interpretation of the references to colour in this figure legend, the reader is referred to the web version of this article.)
a,b) Seam T300 (2–3 m); textinite fragment with in-situ phlobaphinite and resinite;
c,d) Seam T210 (10–11 m); detrital coal with abundant funginite, resinite and suberinite.
e,f) Seam T110 (31–32 m); suberinite in liptinite-rich coal with high HI (310 mgHC/gTOC).
g,h) Seam T110 (11–12 m); cutinite, fluorinite and phyllovitrinite representing fossil leaves.

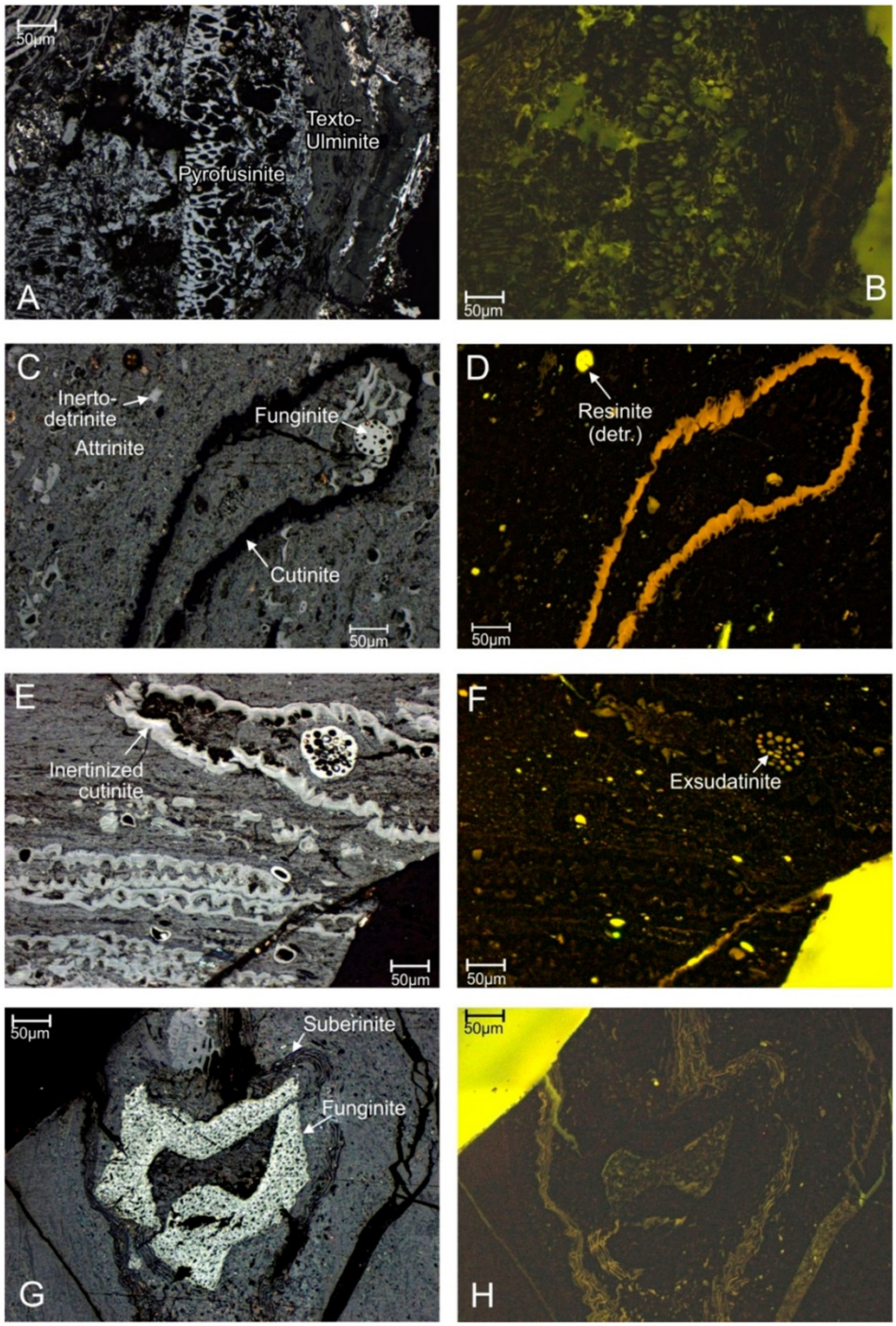

Fig. 10. Representative photomicrographs of coal samples. Left: white light; right blue light. (For interpretation of the references to colour in this figure legend, the reader is referred to the web version of this article.)
a,b) Seam T210 (22–23 m); pyrofusinite.
c,d) Seam T210 (1–2 m); high-ash coal (~14 wt%) from the base of the seam with detrital resinite and funginite inside cutinite (HI: 191).
e,f) Seam T110 (45–46 m); ash: 1.44 wt%; HI: 295; inertinized cutinite(?) with funginite; inertinization of cutinite may have been caused pathogenic fungi (cf. Arya et al., 2021). Similar oxidized macerals in peat and coal have been interpreted as altered epidermal layers of roots (Moore and Swanson, 1993; Moore et al., 1996).
g,h) Seam T110 (11–12 m); ash: 1.32 wt%; HI: 168; suberinite with funginite suggesting fungal attack on rootlets.

Table 3
Maceral percentages (in vol.%) and facies indicators (seam T110).

Sample	Text	Texto-Ulm	Ulm	Attr	Dens	Phlobaphinite		Cutin	Suber	Resinite		Fluor	Liptodet	Pyrofusinite	Degradofusinite	Fung	Inertodetr	TPI	GI	GWI
						in situ	detr.			in situ	detr.									
T300-roof	1.6	12.7	0.0	12.7	0.0	0.0	0.0	0.0	0.0	0.0	0.0	0.0	0.0	0.0	0.0	0.0	3.2	1.1	0.0	1.5
T300-1	25.6	12.3	4.4	16.1	2.8	5.0	6.1	3.4	3.0	1.0	0.6	1.0	13.1	0.2	1.4	1.4	1.0	2.0	0.2	0.1
T300-2	22.3	7.2	3.4	14.1	6.0	4.4	10.9	4.8	4.6	1.0	0.8	3.2	11.5	2.0	1.6	1.0	0.6	1.3	0.2	0.2
T300-3	6.9	6.9	5.5	9.7	6.9	1.4	0.0	0.0	0.0	0.0	0.0	0.0	0.0	0.0	0.0	0.0	0.0	1.3	0.6	2.3
T300-4	20.8	11.8	5.9	14.4	3.9	2.4	8.5	1.0	0.8	3.3	2.4	0.8	19.7	0.4	0.4	1.4	1.2	1.6	0.2	0.3
T300-5	25.0	10.6	5.2	12.2	1.0	4.2	12.2	0.8	1.0	8.0	1.4	0.8	11.8	0.0	1.6	2.0	0.8	1.8	0.2	0.1
T300-6	24.7	8.0	9.2	10.0	2.2	4.8	9.8	1.6	2.0	6.0	3.0	3.2	12.2	0.2	0.6	0.6	0.6	2.2	0.3	0.3
T300-7	24.9	15.8	6.1	10.7	4.0	4.3	10.5	2.8	2.4	1.2	1.4	1.2	9.1	0.6	0.8	2.0	1.2	2.1	0.2	0.2
T300-8	21.5	17.1	7.4	7.4	1.2	4.2	8.5	3.8	0.4	0.4	1.4	4.6	14.7	1.6	1.6	1.2	1.8	3.1	0.2	0.2
T300-9	19.1	14.7	6.4	13.7	2.6	4.4	9.8	2.2	0.8	4.0	1.4	0.8	15.3	0.0	0.8	1.0	1.0	1.7	0.2	0.3
T300-10	28.1	15.5	4.0	9.2	5.0	3.2	3.8	3.6	1.0	4.0	1.0	2.8	13.9	0.6	0.8	1.6	0.4	2.9	0.2	0.2
T300-11	26.5	14.4	7.5	7.5	1.4	6.1	4.4	4.0	2.8	0.6	0.2	3.2	16.8	1.2	0.2	1.2	0.8	4.2	0.3	0.3
T300-12	21.8	11.9	5.5	15.8	2.4	7.7	13.1	0.4	1.2	1.8	0.2	0.2	11.7	0.8	1.2	0.6	1.4	1.6	0.2	0.2
T300-13	24.1	13.4	12.0	10.6	3.8	6.6	8.6	0.8	1.8	3.4	0.6	2.0	8.6	0.0	0.6	1.4	0.4	2.5	0.4	0.3
T300-14	26.2	15.4	4.8	9.2	5.2	5.4	5.6	2.6	3.4	2.2	0.6	1.4	14.8	0.2	0.4	0.6	0.4	2.6	0.3	0.3
T300-15	13.7	13.3	3.4	21.5	5.8	5.2	5.2	0.4	1.6	4.0	0.8	0.2	18.3	1.2	0.6	2.0	1.2	1.2	0.3	0.3
T300-16	21.8	15.3	3.6	9.9	4.2	5.6	10.9	0.8	1.4	4.0	1.8	0.0	13.7	0.8	1.4	2.6	0.4	1.9	0.2	0.2
T300-17	15.9	15.5	7.1	4.0	3.0	11.5	11.3	1.6	1.4	4.6	1.2	1.2	14.1	2.2	1.4	1.6	1.4	2.9	0.4	0.3
T300-18	22.5	15.1	8.2	9.0	2.9	5.5	11.0	1.6	1.6	3.1	0.4	1.4	15.3	0.4	0.0	0.8	0.6	2.3	0.3	0.3
T300-19	27.2	17.8	1.6	8.2	2.7	6.5	8.2	2.4	2.0	2.4	0.8	1.0	13.5	0.2	0.8	2.0	1.4	2.8	0.2	0.1
T300-20	28.9	16.1	1.2	13.3	4.4	5.8	10.8	1.4	0.8	0.8	0.8	0.4	12.1	0.0	0.2	1.2	0.8	1.8	0.2	0.1
T300-21	22.5	13.7	9.4	9.4	5.0	5.2	8.6	1.6	1.0	5.2	1.6	1.4	11.0	0.0	0.0	2.8	0.6	2.2	0.4	0.3
T300-22	24.9	16.7	3.2	7.2	5.2	4.4	8.0	2.4	3.8	1.8	1.2	2.6	14.5	0.2	0.4	1.4	1.4	2.4	0.2	0.2
T300-23	19.2	7.9	1.6	14.6	4.0	8.7	12.1	1.8	4.2	2.4	0.4	1.2	18.2	0.0	0.6	2.0	0.6	1.2	0.3	0.1
T300-24	20.7	19.5	3.3	7.7	1.6	5.7	11.8	2.8	2.4	1.2	1.8	2.6	14.2	0.2	0.6	2.2	0.6	2.4	0.2	0.1
T300-floor	4.2	4.2	0.0	18.4	0.0	0.0	1.4	0.0	0.0	2.8	0.0	0.0	7.1	0.0	0.0	0.0	1.4	0.4	0.0	1.5
T210-roof	0.0	0.0	0.0	15.9	1.8	3.5	0.0	0.0	0.0	0.0	0.0	0.0	0.0	0.0	0.0	0.0	0.0	0.2	0.3	2.7
T210-1	18.0	10.3	5.7	19.8	1.8	7.7	5.3	0.6	3.2	2.6	0.8	1.4	16.0	0.0	1.4	1.4	1.8	1.6	0.3	0.3
T210-2	23.6	9.9	6.3	14.3	1.8	10.9	12.7	1.8	1.2	0.8	1.4	0.8	9.3	0.4	1.2	1.6	0.8	1.8	0.3	0.2
T210-3	24.0	7.8	2.8	14.6	1.8	14.2	8.6	2.4	1.6	3.4	1.6	1.8	10.4	0.0	0.4	2.2	2.0	2.0	0.3	0.1
T210-4	14.5	1.6	0.4	13.9	1.0	10.5	10.5	0.2	2.6	10.5	8.7	0.2	20.3	0.0	1.0	1.6	2.2	1.1	0.3	0.1
T210-5	20.8	7.3	3.4	18.0	0.4	10.7	7.5	1.6	2.0	2.4	1.4	1.4	17.8	0.0	1.6	1.4	1.6	1.7	0.3	0.1
T210-6	16.3	20.0	3.3	17.9	2.0	7.9	9.2	0.8	3.3	2.2	2.0	0.2	12.0	0.0	0.0	1.0	1.4	1.6	0.2	0.1
T210-7	17.1	9.4	1.2	17.3	1.0	5.4	5.4	2.4	6.4	1.6	2.6	1.2	25.7	0.0	0.6	1.2	0.8	1.4	0.2	0.1
T210-8	23.9	8.5	2.2	17.0	2.8	9.3	6.7	1.8	1.2	3.6	2.0	2.0	12.4	0.0	1.6	2.0	1.8	1.7	0.2	0.1
T210-9	27.2	17.8	2.0	20.2	0.8	4.3	6.5	2.0	2.5	0.2	0.8	1.6	10.8	0.2	0.6	1.6	0.4	1.9	0.1	0.1
T210-10	26.8	17.3	3.1	17.5	2.3	7.2	7.6	1.0	1.7	0.6	0.6	0.6	10.3	0.2	0.0	1.4	1.2	2.0	0.2	0.1
T210-11	22.6	6.7	1.8	23.8	1.2	8.5	4.2	1.8	3.8	1.6	2.0	0.8	17.1	0.0	0.8	1.0	1.4	1.4	0.2	0.1
T210-12	17.1	16.9	1.2	16.7	0.6	6.6	5.0	2.2	5.0	1.4	2.2	2.4	18.7	0.0	0.2	1.6	2.0	1.9	0.1	0.0
T210-13	18.0	8.1	2.4	19.6	0.4	9.1	1.8	3.2	3.8	1.8	2.0	3.0	20.8	0.0	0.8	2.8	1.8	1.8	0.2	0.1
T210-14	26.5	14.6	3.4	20.6	1.6	7.7	3.2	0.8	1.6	1.2	0.8	1.4	14.6	0.0	0.0	1.4	0.0	2.0	0.2	0.1
T210-15	16.1	18.4	3.4	18.0	0.8	4.0	5.9	2.6	4.4	0.8	1.6	1.0	16.3	0.4	3.2	1.2	0.2	1.9	0.1	0.1
T210-16	18.8	9.8	0.4	17.8	0.2	5.3	4.9	3.5	5.7	3.7	1.2	1.4	23.9	0.2	0.0	1.2	1.0	1.5	0.1	0.0
T210-17	21.0	13.1	0.8	15.3	1.2	9.1	8.5	2.4	2.2	1.8	1.0	3.0	16.5	0.2	0.2	1.6	1.4	1.8	0.2	0.1
T210-18	24.3	10.9	0.6	20.8	1.4	6.1	9.9	3.0	3.8	1.0	1.0	0.8	12.3	0.0	0.8	1.2	1.0	1.3	0.1	0.0
T210-19	23.4	13.3	2.2	15.7	2.2	6.6	7.3	1.4	5.4	1.2	1.0	1.2	13.9	0.0	0.2	3.2	1.2	1.8	0.2	0.1
T210-20	17.9	7.6	0.4	15.8	3.2	5.6	9.2	4.4	7.0	1.4	1.2	1.6	20.7	0.0	0.2	1.4	1.2	1.1	0.2	0.1
T210-21	18.3	10.6	1.4	18.5	5.6	8.0	9.6	2.0	1.0	3.0	0.8	0.4	16.0	0.0	0.8	2.4	1.0	1.2	0.3	0.2
T210-22	15.0	8.8	2.2	22.2	3.0	7.6	10.8	2.6	4.8	1.0	0.6	1.8	14.0	0.4	0.2	2.4	1.8	1.0	0.2	0.1
T210-23	26.3	16.5	3.2	12.7	3.6	6.0	7.6	2.8	2.6	2.0	0.4	0.2	11.9	0.2	0.8	1.6	0.4	2.2	0.2	0.1
T210-24	19.2	9.7	3.2	17.9	5.2	8.9	4.6	2.0	2.4	2.6	0.4	0.6	17.3	0.4	0.4	1.2	1.2	1.5	0.3	0.3

(*continued on next page*)

Table 3 (*continued*)

Sample	Text	Texto-Ulm	Ulm	Attr	Dens	Phlobaphinite		Cutin	Suber	Resinite		Fluor	Liptodet	Pyrofusinite	Degradofusinite	Fung	Inertodetr	TPI	GI	GWI
						in situ	detr.			in situ	detr.									
T210-floor	3.7	1.8	0.0	5.5	3.7	1.8	0.0	0.0	0.0	0.0	1.8	0.0	0.0	0.0	0.0	0.0	0.0	0.8	0.5	4.1
T110-roof	2.0	2.0	0.0	2.0	2.0	0.0	0.0	0.0	0.0	2.0	0.0	0.0	0.0	0.0	0.0	0.0	0.0	1.0	0.3	7.4
T110-1	35.9	10.4	6.7	12.6	7.9	4.7	1.6	0.8	0.8	2.6	1.0	0.2	11.4	0.0	0.8	0.0	1.0	2.6	0.3	0.3
T110-2	39.1	11.9	1.4	12.3	8.5	2.8	3.8	0.8	0.2	1.8	1.4	1.8	9.3	0.2	0.4	1.2	2.0	2.3	0.2	0.2
T110-3	38.1	9.0	8.6	9.8	8.2	2.9	0.6	1.0	0.6	3.5	2.0	2.5	8.6	0.4	1.0	0.2	0.0	3.2	0.3	0.3
T110-4	38.9	6.2	2.9	12.8	1.4	2.1	1.2	2.3	1.6	2.5	2.1	3.5	18.3	0.0	0.2	0.4	2.3	3.3	0.1	0.1
T110-5	33.0	6.5	6.9	8.3	8.1	6.3	1.6	1.2	2.4	3.6	3.2	1.8	13.2	0.2	0.4	0.4	1.8	3.0	0.4	0.3
T110-6	40.2	8.9	6.1	9.9	2.4	4.3	2.0	1.2	1.6	1.6	2.6	2.0	14.0	0.2	0.6	0.4	1.2	4.2	0.2	0.2
T110-7	25.1	3.3	7.0	11.7	2.9	10.9	2.9	2.1	2.9	2.5	3.1	2.7	17.7	0.2	0.6	0.4	2.5	2.7	0.4	0.3
T110-8	26.5	3.1	7.0	10.9	2.5	8.8	6.0	3.3	3.1	4.7	2.1	2.3	16.2	0.0	0.4	0.8	1.8	2.4	0.4	0.2
T110-9	37.7	9.1	3.4	9.3	3.4	8.3	0.8	1.6	0.8	2.6	3.0	2.0	13.6	0.0	0.6	0.2	1.4	4.4	0.3	0.2
T110-10	34.6	5.6	5.4	5.1	2.3	12.4	0.4	1.9	1.2	1.6	3.9	6.2	14.8	0.8	0.2	1.2	1.6	7.5	0.4	0.2
T110-11	20.5	3.5	7.3	13.4	1.6	15.3	2.4	1.6	0.8	4.1	2.8	3.1	18.5	0.0	0.0	1.0	2.8	2.7	0.6	0.3
T110-12	36.3	4.1	2.5	12.9	3.9	10.7	2.9	1.8	2.1	1.0	2.1	5.1	11.1	0.0	0.0	0.0	1.6	2.7	0.3	0.1
T110-13	37.0	2.9	5.0	8.5	3.3	11.0	1.4	3.3	2.9	1.7	2.9	6.4	9.1	0.0	0.0	0.2	3.1	4.2	0.4	0.2
T110-14	32.9	4.1	3.5	9.3	2.3	18.1	2.5	1.6	3.1	2.3	4.1	4.5	9.3	0.0	0.0	0.4	1.4	4.2	0.5	0.1
T110-15	32.9	4.7	1.6	16.2	3.9	12.5	1.4	2.7	3.7	1.6	1.6	7.6	6.2	0.2	0.0	0.8	1.4	2.4	0.3	0.1
T110-16	24.6	1.0	3.3	5.9	1.4	13.3	2.3	3.9	2.7	3.9	2.9	9.2	22.4	0.0	0.0	0.6	1.8	4.4	0.5	0.2
T110-17	40.7	2.7	2.9	7.0	1.2	10.8	1.0	1.4	1.4	2.9	3.3	4.7	16.2	0.2	0.0	1.2	1.2	6.2	0.3	0.1
T110-18	34.9	3.3	11.9	8.6	2.7	8.0	0.8	1.6	1.0	1.6	3.1	4.9	13.9	0.4	0.0	1.2	1.2	4.8	0.5	0.3
T110-19	22.5	5.8	8.6	5.8	2.4	10.6	0.4	0.6	1.5	4.8	3.2	3.5	25.3	0.6	0.4	0.4	2.6	5.6	0.6	0.3
T110-20	21.0	2.2	8.8	14.1	4.3	7.4	1.6	0.2	4.3	4.3	3.3	1.0	24.5	0.0	0.0	0.0	1.0	2.0	0.5	0.4
T110-21	20.2	2.2	6.9	10.4	2.9	10.8	0.2	1.4	2.0	5.5	2.2	7.4	24.7	1.0	0.2	0.0	0.8	3.1	0.6	0.3
T110-22	18.5	5.8	11.2	7.3	4.2	18.7	2.1	3.1	2.1	2.9	1.7	6.4	11.2	0.0	0.2	0.0	2.7	4.0	0.9	0.5
T110-23	17.9	2.8	16.1	9.2	5.1	15.9	3.3	2.0	2.0	3.9	2.2	4.3	12.4	0.0	0.2	0.0	1.6	3.0	1.1	0.7
T110-24	20.8	4.9	13.0	9.5	2.5	22.5	0.4	2.7	2.1	1.2	1.2	8.0	8.7	0.0	0.0	0.0	1.2	5.0	1.0	0.4
T110-25	24.7	6.0	11.3	7.8	2.3	17.7	0.8	0.6	3.1	1.2	0.6	1.2	20.4	0.2	0.0	0.0	0.4	5.5	0.8	0.4
T110-26	34.5	2.7	11.6	7.8	2.2	10.4	1.4	0.2	1.4	2.0	1.6	0.6	19.8	0.0	0.0	1.4	1.4	5.2	0.5	0.3
T110-27	35.2	8.1	6.1	7.1	2.2	8.7	0.8	3.8	3.0	2.8	2.4	4.2	11.9	0.0	0.4	1.4	0.8	5.8	0.3	0.2
T110-28	36.2	9.5	1.0	11.9	1.4	4.9	1.2	2.2	4.9	2.0	1.8	1.8	17.6	0.2	0.2	1.6	0.8	3.6	0.1	0.1
T110-29	33.9	11.2	4.8	5.8	1.0	7.2	1.8	2.6	3.0	2.4	0.4	4.2	14.9	0.2	0.4	1.4	3.4	6.7	0.2	0.1
T110-30	36.0	14.5	5.2	5.4	0.2	10.9	0.4	2.4	1.8	1.4	1.6	0.8	15.9	0.0	0.2	0.4	2.0	11.1	0.3	0.1
T110-31	35.0	11.7	4.8	12.1	1.0	9.5	1.2	0.6	3.2	1.4	1.6	0.6	13.5	0.0	0.6	1.4	0.6	4.3	0.3	0.1
T110-32	31.2	11.8	5.4	7.8	0.2	13.4	1.6	2.2	1.8	2.0	2.4	2.2	14.8	0.0	0.0	0.8	1.2	6.4	0.4	0.1
T110-33	32.3	16.5	1.8	6.1	0.6	6.7	1.4	4.1	3.3	1.0	2.0	3.7	13.4	0.0	0.6	1.8	1.8	7.1	0.2	0.1
T110-34	34.0	17.5	4.2	9.1	3.2	8.0	0.8	3.4	1.6	0.8	1.2	2.0	10.7	0.0	0.2	0.6	1.4	4.9	0.2	0.1
T110-35	31.2	15.8	0.6	10.7	4.1	8.5	5.5	2.0	1.0	0.8	2.0	2.2	9.1	0.0	1.2	1.0	2.4	2.8	0.2	0.1
T110-36	24.8	7.6	1.0	12.7	2.3	13.5	5.7	5.5	1.8	1.6	1.6	6.2	10.9	0.0	0.6	1.4	2.1	2.3	0.3	0.1
T110-37	26.7	10.8	2.2	7.0	3.6	10.6	4.8	2.4	3.6	2.0	2.6	2.0	14.8	0.2	0.8	1.4	2.8	3.3	0.3	0.2
T110-38	27.6	11.6	1.0	9.0	2.6	9.0	9.6	3.0	3.6	2.0	1.4	2.6	13.6	0.0	0.4	0.6	1.0	2.3	0.2	0.1
T110-39	24.8	10.2	3.0	13.2	2.2	6.0	8.4	2.8	1.6	0.6	0.8	3.6	20.4	0.0	0.4	0.8	0.4	1.9	0.2	0.1
T110-40	31.2	13.6	1.0	8.4	2.2	5.4	7.0	2.6	3.2	1.0	1.2	1.6	18.6	0.0	0.6	0.8	0.6	2.9	0.1	0.1
T110-41	24.1	13.1	2.6	11.7	1.8	4.6	8.4	5.0	1.0	0.6	0.8	4.6	16.3	0.2	2.4	0.4	1.0	2.1	0.1	0.1
T110-42	28.8	15.3	1.8	14.1	2.7	5.5	7.0	2.7	0.6	1.6	1.2	3.1	10.8	0.0	0.8	0.8	2.5	2.2	0.1	0.1
T110-43	39.5	7.9	2.2	13.1	1.2	3.6	6.5	1.2	2.2	0.6	0.6	2.4	16.1	0.0	0.2	0.2	0.8	2.6	0.1	0.1
T110-44	18.1	13.7	2.0	17.3	1.2	6.3	8.9	2.8	0.2	0.4	2.0	3.4	20.2	0.0	0.2	0.2	1.4	1.5	0.2	0.2
T110-45	24.3	14.0	2.2	15.4	1.2	5.1	7.3	3.6	4.0	1.4	1.2	1.0	14.8	0.0	1.6	0.4	1.6	2.0	0.1	0.1
T110-46	22.3	12.4	2.2	16.6	0.8	10.8	5.6	1.6	5.8	2.4	1.2	1.4	14.0	0.0	0.6	1.0	0.6	2.1	0.2	0.1
T110-floor	0.0	1.9	0.0	5.7	3.8	0.0	0.0	0.0	0.0	0.0	0.0	0.0	0.0	0.0	0.0	0.0	0.0	0.2	0.5	6.1

Text – textinte, Ulm – ulminite, Attr – attrinite, Dens – densinite, Cutin – cutinite, Suber – suberinite, Fluor – fluorinite, Liptodet. – liptodetrinite, Fung – funginite, Inertodetr – inertodetrinite, TPI – tissue preservation index, GI – gelinifaction index, GWI – groundwater index.

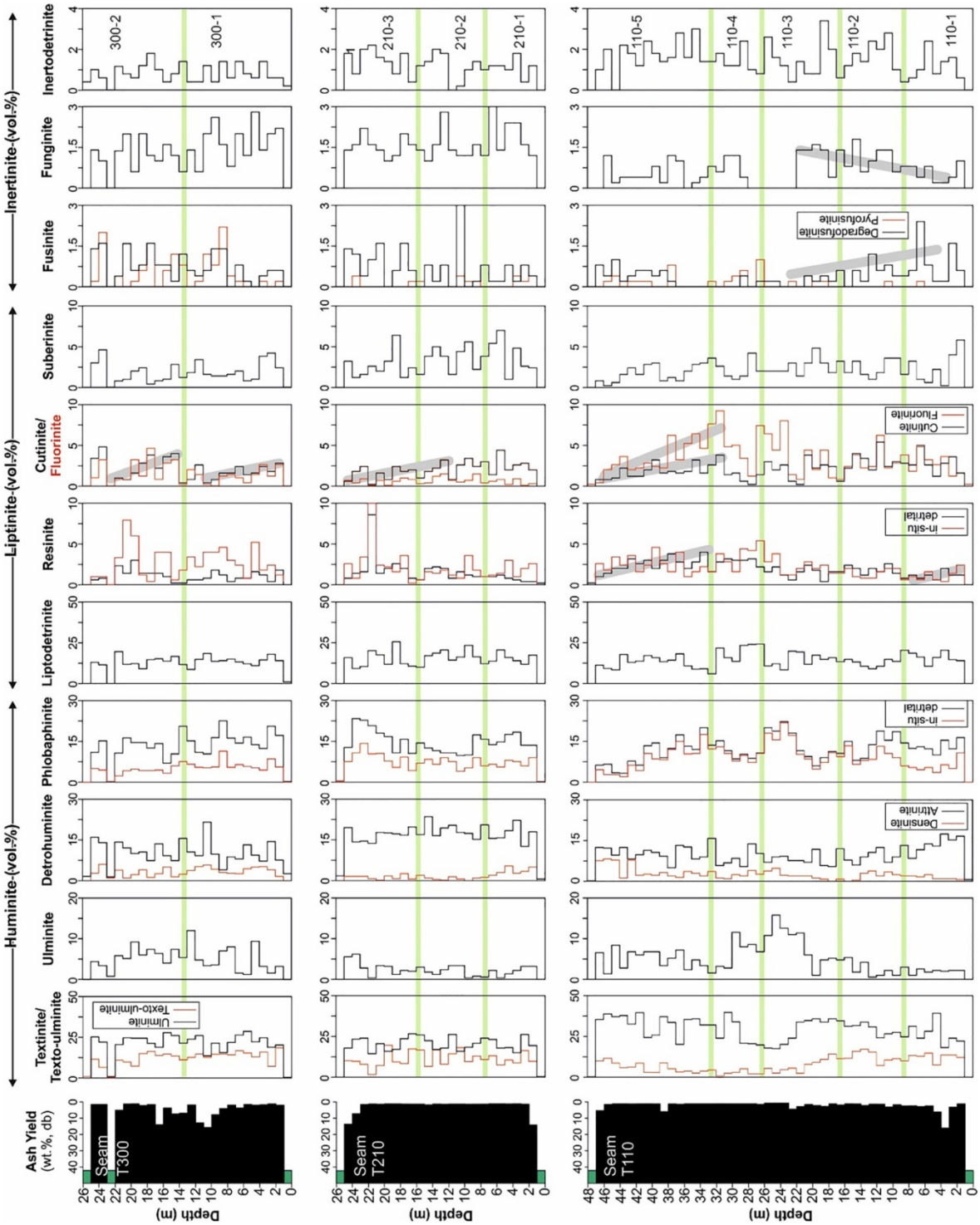

Fig. 11. Variations of maceral percentages in seams T110, T210 and T300. Selected trends are highlighted by grey lines. Cycles defined by geochemical data (see Fig. 5) are labelled 110–1 to 300–2 (see right column). Cycle boundaries are shown by green lines. (For interpretation of the references to colour in this figure legend, the reader is referred to the web version of this article.)

fluorinite/cutinite ratio is about 1. In contrast in the interval between 27 and 34 m, r^2 is 0.90 and the fluorinite/cutinite ratio about 2. Inertinized cutinite is sometimes observed (Fig. 10e,f).

Suberinite represents suberinized tissue in roots and bark (Pickel et al., 2017) and is a prominent liptinite maceral in Tutupan coal (Fig. 9c–f). It is present in considerable quantities in all seams. The highest contents (up to 7 vol%) are observed in seam T210.

Sporinite is very rare (<0.1 vol%). A few lamalginite particles were observed in seam T300. Exsudatinite occurs as impregnations in funginite or cracks.

Inertinite macerals are generally rare. Pyrofusinite (Fig. 10a) was detected in appreciable amounts only in seam T300 (~1 vol%). Degradofusinite is slightly more abundant, but largely absent between 29 and 37 m in the T110 seam (Fig. 11). Funginite occurs in minor amounts (max. 3 vol%). It is often associated with suberinite or cutinite (Fig. 10c–h), but also occurs in humodetrinite (Fig. 9c). Despite its low abundance, funginite in seam T110 shows an interesting vertical distribution: The proportion of funginite increase upwards within the lower part of seam T110 (1–23 m), but between 23 and 27 m funginite is largely absent. In seam T210, funginite is relatively common. The percentages of funginite in seam T300 are in a similar order as in seam T210, but show stronger fluctuations.

5.3.2. Vitrinite reflectance

Vitrinite reflectance was determined for different vitrinite macerals (ulminite, densinite, phlobaphinite). The values range between 0.36 ± 0.02%Rr and 0.41 ± 0.02%Rr. Neither a depth trend nor systematic differences between vitrinite macerals could be detected.

6. Discussion

6.1. Maturity (VR, Tmax, moisture)

Different huminite macerals in low rank coals may show varying reflectance. Therefore, vitrinite (huminite) reflectance of 10 samples was determined for ulminite (0.38%Rr), densinite (0.40%Rr) and phlobaphinite (0.39%Rr). Although seam T300 shows slightly lower values (0.37, 0.38, 0.36%Rr) than the middle and lower seams (0.39, 0.40, 0.40%Rr), neither a depth trend nor systematic differences between vitrinite macerals could be observed.

The low rank of the Tutupan coals is confirmed by Tmax values, although they are strongly influenced by facies. Tmax of coal samples ranges from 372 to 411 °C and are negatively correlated with HI values. Tmax values of mudstone samples typically range from 416 to 425 °C, but significantly lower values (<400 °C) occur as well.

Low maturity is further supported by a strong odd over even predominance of *n*-alkanes (Tissot and Welte, 1984; CPI: 2.8–5.2). This suggests that the distribution of long-chain *n*-alkanes are not significantly influenced by maturity and, therefore, can be used to reconstruct the precursor vegetation type (see below).

Probably the most sensitive maturity parameter for low rank coals is their moisture content. Average moisture contents decrease downwards from 26.3 wt% (seam T300), to 20.6 wt% (T210) and 18.8 wt% (seam T110). As moisture contents mainly reflect compaction due to the weight of overburden rocks (e.g. Holdgate, 2005), this is a strong argument against an overturned succession, as suggested in an internal report (ADARO, 2008).

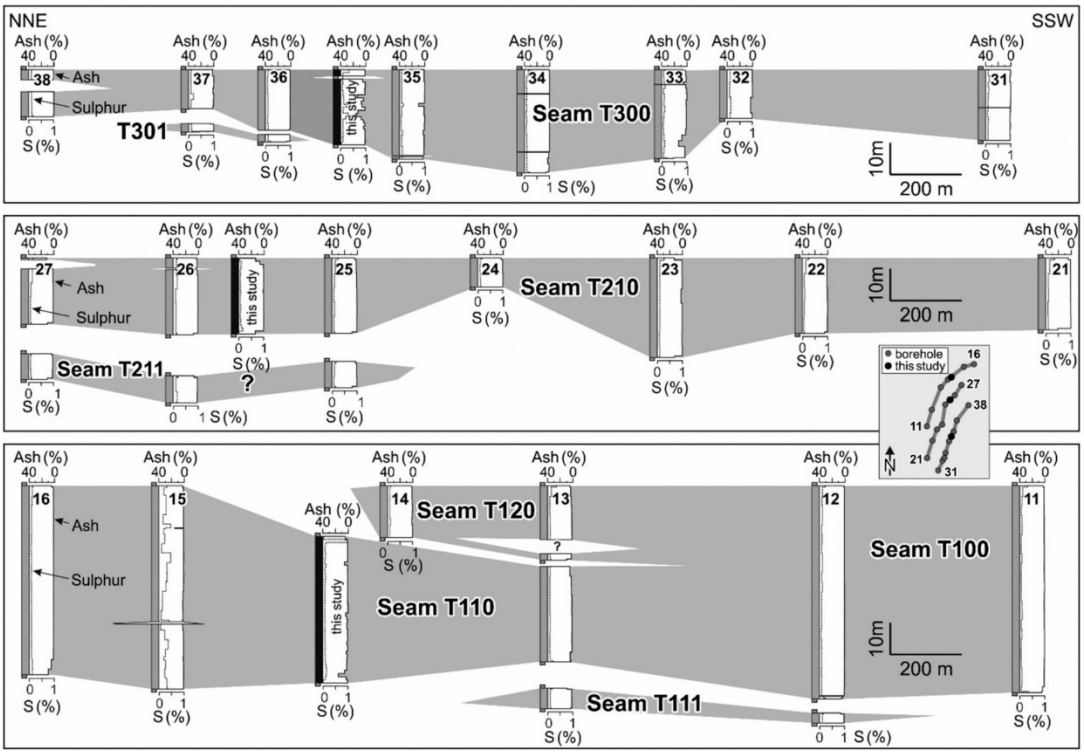

Fig. 12. NNE-SSW trending profiles showing thickness, ash yield and sulphur (S; stippled line) variations of seams T100, T200 and T300 in the South Tutupan mining district. The position of the boreholes and profiles is indicated in the inset. See the rectangle in Fig. 2 for the location of the inset within the Tutupan mine. The profiles have been compiled using data from exploration boreholes and flattened to the top of each seam. Profiles studied in the present paper are shown by coal symbols.

6.2. Lateral continuity of the peat-forming environments

It is beyond the scope of the paper to study the lateral variation of the coal seams in the entire Tutupan area. However, profiles shown in Fig. 12 provide information on the lateral variation of coal thickness and coal properties in the vicinity of the studied sections in order to support the identification of different mire types.

Seam splitting and significant thickness variations are evident in Fig. 12. Ash yields are very low in seams T110 and T210 and slightly enriched yields are restricted to the base and the top of both seams. Sulphur contents are usually as low with a relatively high sulphur content (up to 0.5%) occurring in seam T110 in borehole 15 (Fig. 12). Because no other well shows similar contents, it remains unclear, if this reflects locally less acidic conditions or technical problems. The reduced thickness of seam T210 in borehole 24 probably reflects peat formation on a topographic high.

Seam T300 contains coal with relatively high ash yield in the studied section. In contrast, coals in the neighboring boreholes (35, 36) are relatively clean. However, high-ash coal was encountered in borehole 33, albeit at the base of the coal bed.

6.3. Ombrotrophic versus rheotrophic peat-formation

Coal may originate in rheotrophic (topogenous) and in ombrotrophic (domed) mires (e.g. Clymo, 1987; Diessel, 1992; Gruber and Sachsenhofer, 2001). Ombrothrophic mires develop above the regional (ground)water level and are protected from flooding by surface water by their positive relief. They are fed exclusively by rainfall, which is very poor in sulphate and nutrients (e.g. Clymo, 1987; Moore, 1987). Because humic acids are not efficiently diluted, raised mires are extremely acidic preventing the activity of bacteria. Hence, ombrothrophic peat is typically very low in ash and sulphur, and the plant litter is well preserved.

In this section ash yield and sulphur contents are used to distinguish between ombrothrophic and rheotrophic mires. A more detailed characterization of the mire type based on geochemical and petrographic data follows below.

Seams T110 and T210 contain coal with very low ash yields (2.1 and 2.6 wt%, respectively) and sulphur contents (0.14 and 0.09 wt%). These data imply that seams T110 and T210 formed in ombrotrophic mires (Diessel, 1992; Moore and Shearer, 2003; Dai et al., 2020) similar to present-day domed peats in Kalimantan (e.g. Page et al., 1999; Morley, 2013). The low ash yields, therefore, are mainly due to the fact that the surface of the domed mires never received water-transported mineral matter. In addition, leaching of mineral matter probably further decreased the mineral matter content (Ruppert et al., 1993; Li et al., 2001). Slightly elevated ash yields and sulphur contents near the base of seams T110 (1–5 m; cycle 110–1) and T210 (1–2 m) show that early stages of peat accumulation occurred in a topogenous mire or in a transitional environment. Sulphur contents do not exceed 0.2 wt% even in the topogenous mire stage, a clear indication of a freshwater environment (see also Neuzil et al., 1993).

Although ash yield is very low throughout the T110 seam, it is slightly higher in its lower part (1–23 m; cycles 110–1, 110–2 and lower part of 110–3) than in the upper part (upper part of 110–3, 110–4 and 10–5). This could indicate a more marginal position within the domed mire during the accumulation of the lower part and a more central part during accumulation of the upper part. However, no such trend can be seen in the neighboring boreholes in the T110 and T210 seams (Fig. 12). Peat accumulation ended due to drowning of the domed mire, as indicated by increasing ash yields near the top of the seam. A more gradual increase in ash yields indicates that drowning was more gradual in seam T210 (23–25 m) and more rapid in seam T110 (46–47 m; Fig. 4). Very low sulphur contents in roof rocks (~0.04 wt%) and resulting high TOC/S ratios (Berner, 1984) show that drowning occurred in a freshwater environment, although the uppermost coal sample from seam T110 has a high sulphur content (~2 wt%).

Higher ash yield in parts of the T300 seam (up to 16 wt%) are indicative of peat accumulation in alternating mire types. Peat accumulation probably started in a rheotrophic topogenous mire, but this stage must have been very short, as only the lowest coal sample shows a slightly elevated ash yield. The mire was probably ombrogenous during the early stages of peat formation (1–9 m), which changed later into a rheotrophic topogenous mire (10–12 m). Varying ash yields indicate that ombrotrophic and rheotrophic mire environments alternated during the deposition of the middle and upper parts of the seam (12–24 m). In the upper part of the seam there is a 1-m-thick parting (Fig. 4), but it is not laterally continuous (Fig. 12). Seam splitting, thickness variations and strong lateral variations in ash yields (Fig. 12) reflect unstable conditions during the accumulation of the T300 seam. Eventually, the peat accumulation was terminated by the deposition of freshwater sediments.

Two end-member types of ombrogenous peatlands have been distinguish in the Cenozoic sedimentary successions of SE Asia: 'basinal' (or 'coastal') and 'kerapah' peats (also called 'watershed', 'high' or 'interior' peat) (e.g. Page et al., 2010; Morley, 2013). Basinal peats occur inland from mangrove swamps near the coast, while kerapah peats occur at low elevations (10-30 m above sea level) up to 200 km inland from the coast. Present-day examples of 'interior' peatlands in Kalimantan have been described by Anggara et al. (2021), Moore et al. (1996) and Moore and Shearer (1997). According to our knowledge, there is no evidence for marine sediments nearby the Tutupan seams. Therefore a kerapah-type of peatland is favored.

6.4. Nature of peat-forming vegetation as recorded by geochemical data

It is evident that the organic matter in coal is dominated by terrestrial plants. This is reflected in the distribution of *n*-alkanes, which are dominated by long-chain *n*-alkanes with an odd over even predominance and maximum intensities in the range *n*-C_{27} to *n*-C_{33} (Fig. 5). More detailed information about the peat-forming vegetation can be derived from specific biomarkers and biomarker ratios.

6.4.1. Changes in angiosperm vegetation (n-alkanes and isoprenoids)

Angiosperms produce significantly more *n*-alkanes than gymnosperms (Diefendorf et al., 2011). Furthermore, the low di−/(di- + tri-terpenoid) ratios (Fig. 8) suggest that gymnosperms are generally rare in the Tutupan coal. Therefore, the patterns of long-chain *n*-alkanes mainly provide information on the relative contribution of different angiosperm types.

The ratios of long- to short-chain *n*-alkanes (TAR; Bourbonniere and Meyers, 1996) are very high (5.8–38.4) and show depositional cycles with upward decreasing values. In the T110 seam, five cycles are present, but the uppermost cycle 110–5 is not well developed (Fig. 5). In the T210 seam, three cycles are present (210–1 to 210–3). Widely varying values can be seen in seam T300, but appear random and not cyclic in distribution. Relatively low TAR values at the base of each cycle could be related to increased contributions of algae and aquatic macrophytes (e.g., Silliman et al., 1996; Ortiz et al., 2013), but the presence of algae is not confirmed by maceral analysis.

The Paq ratio was introduced to quantify the relative contribution of submerged and/or floating macrophytes (Ficken et al., 2000). Elevated relative proportions of *n*-C_{23} and *n*-C_{25} alkanes, resulting in increased Paq ratios, have also been reported to be characteristic for the contribution of *Sphagnum* in peat bogs (Nott et al., 2000). However, present-day global distributions and flora of peat bogs indicate that *Sphagnum* prefers a cool to temperate climate. Therefore, the occurrence of *Sphagnum* in Miocene lowlands of Indonesia seems to be unreasonable. The Paq ratios are usually below 0.25, supporting the predominance of terrestrial plants (Ficken et al., 2000; Ronkainen et al., 2013). Paq ratios show a similar cyclicity to TAR in T110 and T210 seams (although the boundary between 110 and 4 and 110–5 may be slightly lower) and have two additional cycles in seam T300 (300–1 to 300–2). The opposing

trends of Paq and TAR in seam T210 support the hypothesis that variations in TAR are mainly due to different contributions of aquatic macrophytes. However, the partly coninciding trends in seam T110 suggest that TAR and/or Paq might be influenced by an additional factor.

Microbial degradation can influence various alkane ratios, including the odd even predominance (e.g. Zech et al., 2009; Buggle et al., 2010; Naafs et al., 2019). The observed high CPI values (2.8–5.2) suggest that any influence by microbial degradation was low. This finding is consistent with the postulated highly acidic ombrotrophic setting reducing microbial activity. Moreover, the CPI shows a very similar cyclicity to TAR and Paq, suggesting that CPI is mainly controlled by plant communities.

The average chain length of long-chain *n*-alkanes (ACL; Poynter and Eglinton, 1990) in peat sediments has been used to reconstruct temperature changes. Higher plants in warmer climates have been shown to synthesize longer-chain compounds, but that humidity also plays a role (e.g. Tipple and Pagani, 2013; Carr et al., 2014; Bush and McInerney, 2015). Overall, the moderate variation in Tutupan coals (28.2–30.2) is within the range observed for modern tree species (26–34; Diefendorf et al., 2011). The greatest variation is observed in seam T110, where the ACL is relatively high near the base of the seam (lower part of cycle 110–1). Relatively low values prevail in the remaining part of the seam. Cycles 210–1 to 210–3 in seam T210 show upward increasing values, and two trends of decreasing values are observed in seam T300. Negative correlations exist between ACL and Paq in seams T110 ($r^2 = 0.64$), T210 ($r^2 = 0.71$) and T300 ($r^2 = 0.77$). This suggests that the growth of aquatic macrophytes is related to slightly cooler conditions or, more likely, a wetter climate. However, as Hoffmann et al. (2013) found opposite trends in ACL with increasing humidity for two different genera in Australia, these interpretations should be viewed with caution.

Apart from climate, the relative abundance of long-chain *n*-alkanes (n-C_{27} to n-C_{33}) is controlled by different plant groups. For example, Schwark et al. (2002) attributed a predominance of n-C_{31} to the input of grasses and herbs, n-C_{27} was found preferentially in birch leaf waxes, and n-C_{29} derived predominantly from deciduous trees (see also Trigui et al., 2019). Thus, high n-C_{29}/n-C_{27} ratios may indicate warm conditions. Zech et al. (2009) found that n-C_{31} and n-C_{33} alkanes predominate in grasslands, while n-C_{27} and n-C_{29} predominate in forest soils. The above results are based on Quaternary sediments in Europe deposited in a cool climate. They must therefore be applied with caution to tropical mires. Despite this ambiguity, the n-C_{29}/n-C_{27} ratio and the ratio of the sum of n-C_{31} and n-C_{33} to the sum of n-C_{27} and n-C_{29} alkanes show clear stratigraphic trends (Fig. 5). A gradual upward increase in the n-C_{29}/n-C_{27} ratio in seam T210 could indicate a general warming during peat accumulation.

The ratio n-C_{31+33}/n-C_{27+29} provides an indication of the relative contribution of grassland vegetation. This ratio is high (2.2) near the base of seam T110 and decreases rapidly within cycle 100–1. This may indicate that the deposition of seam T110 began in a grass-dominated, rheotrophic swamp, an interpretation also supported by the relatively high ash yield and sulphur content (Fig. 4). The n-C_{31+33}/n-C_{27+29} ratio remains low (0.5 on average) in cycles 110–2 to 110–5. In seam T210, the ratios show two upward trends with relatively high values at the top of each trend (2.2). Surprisingly, the boundary between the two trends is located in the middle of cycle 210–2. No other geochemical parameter shows a minimum or maximum value at this depth (12 m). In the T300 seam, the ratio is generally low (average 0.7), suggesting a low contribution from grasses, but there is a slight increase at the boundary between cycles 300–1 and 300–2.

Traditionally, the pristane/phytane (Pr/Ph) ratio is considered to be a redox parameter. Low values (<1) indicate anoxic conditions, while values above 3 are considered indicative of oxic environments (e.g. Didyk et al., 1978). However, very high values are typical for land plants (Brooks et al., 1969; Powell and McKirdy, 1973). Thus, the observed Pr/Ph ratios (3.9–23.6) reflect primarily the land plant input and the low rank of the coal. There is a moderate positive correlation between Pr/Ph and CPI ($r^2 = 0.45$), suggesting that variations in Pr/Ph ratios reflect differences in vegetation type rather than redox conditions.

6.4.2. Relative contribution of gymnosperms and angiosperms (di−/[di- + triterpenoid] ratio)

The ratio of diterpenoid biomarkers (including abietane-, pimarane-, isopimarane-, beyerane-, kaurane-, and phyllocladane-type hydrocarbons) and the sum of diterpenoid and angiosperm-derived triterpenoid hydrocarbons (i.e. oleanane, ursane, lupane-derivatives) is a widely used proxy of the relative contribution of gymnosperms and angiosperms to peat formation (Bechtel et al., 2002a,b, 2008). In Tutupan coals, the average ratio is only 0.04. This shows a clear dominance of angiosperms in the peat-forming vegetation, especially if it is taken into account that the di−/(di- + triterpenoid) ratio may overestimate the amount of gymnosperms (Diefendorf et al., 2014).

Stratigraphic trends in the di−/(di- + triterpenoid) ratio indicate variations in the relative contribution of gymnosperms during peat accumulation (Fig. 8).

The contribution of gymnosperms was low during the accumulation of the lower part of the T110 seam (cycles 110–1 to 110–3; average ratio: 0.02), but increased during formation of cycle 110–4 (0.06). At 33 m, the contribution of gymnosperms decreased sharply and increased again during cycle 110–5 (ratio: 0.02–0.07). The highest ratio, indicating the relative highest contribution of the gymnosperms, occurs near the top of the seam at 45–46 m.

Seam T210 is characterized by the highest average di−/(di- + triterpenoid) ratio (0.07) and the highest single value of all seams (0.12). This indicates a vegetation dominated by angiosperms, but with an increased contribution of gymnosperms. Cycle 210–1 is characterized by upward decreasing gymnosperm contributions. No trends are discernable in the cycles 210–2 and 210–3.

The average di−/(di- + triterpenoid) ratio in the T300 seam is only 0.02, but trends with upwards increasing gymnosperm-derived biomarkers are observed in the cycles 300–1 and 300–2.

Low levels of diterpenoid biomarkers were also detected in middle and upper Miocene coals from the Kutai Basin by Widodo et al. (2009). These authors found a stratigraphic trend of slightly elevated di−/(di- + triterpenoid) ratios in middle and lower upper Miocene seams (0.03–0.07), similar to those in Tutupan coals. In contrast, very low ratios (<0.02) prevailed in upper Miocene seams. Widodo et al. (2009) attributed the observed trend to a cooler climate in the middle and early late Miocene. As this is at odds with global climatic trends, Morley (2013) provided an alternative explanation: they suggested that the diterpenoid biomarkers in tropical peats from SE Asia may be derived from *Dacrydium* (Podocarpaceae) and possibly *Agathis* (Araucariaceae). The presence of *Dacrydium* (together with the angiosperm *Gymnostoma*) is an indicator of *kerapah* swamps (Morley, 2013). Thus, the di−/(di- + triterpenoid) ratios found are a strong argument for the deposition of the Tutupan coals in *kerapah* swamps, which are located at greater distance from the paleo-shore line.

6.4.3. Presence of dipterocarpaceae (cadinanes)

Saturated and aromatic sesquiterpenoids of the cadinane group (Figs. 6, 7) occur in all seams in considerable quantities (Fig. 8). They can be of different origins, including gymnosperms (*Taxodiaceae*) and the angiosperm families *Cornaceae* and *Dipterocarpaceae* (van Aarssen et al., 1990, 1994; Bechtel and Püttmann, 2017). *Taxodiaceae* and *Cornaceae* are not relevant in SE Asia, but *Dipterocarpaceae*, especially the genus *Shorea*, are characteristic elements of present-day forests in ombrogenous mires in SE Asian (e.g. Anderson, 1964, 1983; Anderson and Muller, 1975; Esterle and Ferm, 1994; Esterle et al., 1987, 1989; Cameron et al., 1989; Page et al., 1999; Wüst et al., 2001; Morley, 2013). Dipterocarpaceous pollen has also been detected in Miocene coal in NW Borneo (Anderson and Muller, 1975) and in coal from the Warukin Formation in the Asem–Asem Basin (Sarongga lignite; Demchuk and

Moore, 1993). Furthermore, Widodo et al. (2009) were able to attribute cadalene in Miocene coals from the Kutai Basin to the contribution of *Dipterocarpaceae*. Therefore, it is very likely that cadalenes in the Tutupan coal are derived from this family.

The vertical distribution of the cadalene-type sesquiterpenoids shows maxima in the upper part of the T110 (35–36 m; cycle 110–5) and T210 (21–22 m; cycle 210–3) seams. The latter samples contains the highest resinite content of all samples (19 vol%). In addition, there is a strong positive correlation between cadinane-type sesquiterpenoids and total resinite contents in the T300 seam ($r^2 = 0.85$). These results argue for the presence of dammar resins from *Dipterocarpaceae* (van Aarssen et al., 1990) in these seams.

6.4.4. Contribution of ferns

The presence of aromatic triterpenoids of arborane or fernane type is attributed either to the contribution of organic matter from ferns or to the activity of anaerobic bacteria. Structural identification of aromatic compounds is not possible based on GC–MS spectra. However, since fern spores are commonly found in peat and coal, the identified triterpenoid hydrocarbons are most probably related to the fernane type structural skeleton. In addition, based on palynological data (Demchuk and Moore, 1993), ferns (Polypodium) were identified as part of the understory vegetation that led to the accumulation of Miocene lignite of southeastern Kalimantan. The formation of fernane type triterpenoids is related to fernenol, which is widely distributed in vascular plants (Hauke et al., 1992), including some deciduous species and ferns in particular. However, the compounds may also represent arborane type triterpenoids. According to Hauke et al. (1992), the aromatic compounds with arborane type skeleton found in Permian to modern sedimentary rocks were thought to be of bacterial origin. The highest contents of arborane/fernane type triterpenoids are found in the upper part of the T300 seam (38–45 m).

The dominant hopanoid within the samples is C_{29} neohop-13(18)-ene. The most probable biological precursors are bacteria and cryptogames (e.g. moss, ferns; Bottari et al., 1972, Wakeham, 1990). Chemical processes during early diagenesis may also form this compound from hop-22(29)-ene (Brassell et al., 1980). Hop-22(29)-ene probably originates from diplopterol which is common in several eukaryotic plants and in bacteria (Bottari et al., 1972; Ourrison et al., 1979; Rohmer and Bisseret, 1994). Minor gelification of plant tissues and the low amount of hopanes argue against a bacterial origin and may indicate a fern-related origin.

6.5. Petrography and mire types

Maceral-based facies indicators have been proposed by several authors, including Diessel (1986) (tissue preservation index [TPI]; gelification index [GI]) and Calder et al. (1991) (vegetation index [VI] and groundwater index [GWI]). The TPI is the ratio of preserved to degraded plant tissues and reflects the abundance of decay-resistant plants. The VI is similar to the TPI, but also takes liptinite macerals into acount. The GI and GWI contrast gelified and ungelified macerals and reflect the height of the water table. The main difference between the two proxies is that the GWI also considers detrital minerals. Since the GI and GWI are similar in the low-ash coals, only the GWI is discussed in this paper. All indicators were originally defined for bituminous coals and later adopted for low-rank coals (e.g. Kalkreuth et al., 1991; Markic and Sachsenhofer, 1997). In the present work we have modified the facies indicators:

$$TPI = \frac{humotelinite + phlobaphinite\,(in-situ) + pyrofusinite + degradofusinite}{humodetrinite + phlobaphinite\,(detrital)}$$

$$VI = \frac{humotelinite + phlobaphinite\,(in-situ) + pyrofusinite + degradofusinite + semifusinite + suberinite + resinite\,(in-situ)}{humodetr. + porigelinite + inertodetr. + sporinite + cutinite + liptodetrinite + bituminite + fluorinite + resinite\,(detr.)}$$

$$GWI = \frac{ulminite + densinite + mineral\ matter}{textoulminite + textinite + attrinite}$$

A reliable optical quantification of mineral matter is difficult for the studied low-rank coals with small amounts of dispersed minerals. Therefore, mineral matter (mm) was calculated using the formula of Parr (1928) (mm = [1.08 x ash] + [0.55 x sulphur]) and considering specific gravities of 1.2 and 2.8 for organic and mineral matter, respectively.

In contrast to modern high-latitude peat deposits, tropical ombrotrophic mires are generally forested, although there is a wide variation in forest structure and tree species (Anderson, 1964, 1983; Esterle and Ferm, 1994; Esterle et al., 1987; Page et al., 1999). Variations in TPI and VI may reflect these differences.

Both, TPI and VI are relatively high, reflecting the contribution of trees in all seams. The highest values are observed in seam T110 (average: 3.9 and 1.5). Here, TPI and VI are moderately high in the lower part of the seam (cycle 110–1) and increase upwards in cycle 110–2. The maximum values are reached at the base of cycle 110–3 (TPI: 11.1; VI: 2.4), which is characterized by a general upward decrease of TPI and VI. At 28 m, TPI and VI increase significantly. While TPI decreases again in the upper part of the seam (28–46 m), VI values remain relatively constant (Fig. 13).

TPI and VI in the T210 seam are significantly lower (average: 1.6 and 1.0) than in seam T110 and remarkably uniform. Variations in vegetation indicated by geochemical parameters are not reflected in TPI or VI. Relatively low TPI and VI values also prevail in seam T300 (average: 2.2 and 1.2), but an upward decreasing trend is observed in its upper cycle 300–2.

In Miocene coals from Europe, a strong correlation between the TPI and the di−/(di- + triterpenoid) ratio is often observed, suggesting that tissue preservation is mainly controlled by the contribution of decay-resistant gymnosperms (e.g. Bechtel et al., 2002a, 2002b, 2007a, 2008). No such correlation is observed for the Tutupan coals (compare Figs. 8 and 13). Nevertheless, it is tempting to relate the intervals with the highest TPI and VI values in the T110 seam to forest types with high tree density (e.g. tall interior forest; see Page et al., 1999). However, this interpretation is not supported by the geochemical data.

The groundwater index (GWI) is a proxy for the degree of gelification and thus a relative measure for the microbial activity and the height of the groundwater level (Calder et al., 1991). The generally very low GWI values reflect the extremely acidic conditions typical of ombrotrophic mires, which inhibit microbial activity. Slightly enhanced GWI values in seam T110 (21–31 m) with a maximum between 24 and 25 m indicate temporarily less acidic conditions and a relatively high groundwater level. Interestingly, this interval roughly agrees with the only section in all Tutupan seams where funginite is largely absent (22–28 m; compare Figs. 11 and 13). Hence, this fits with the observation of Moore et al. (1996) that fungal activity (and peat decomposition) is limited during times with high groundwater table (see also Jager and Bruins, 1975;

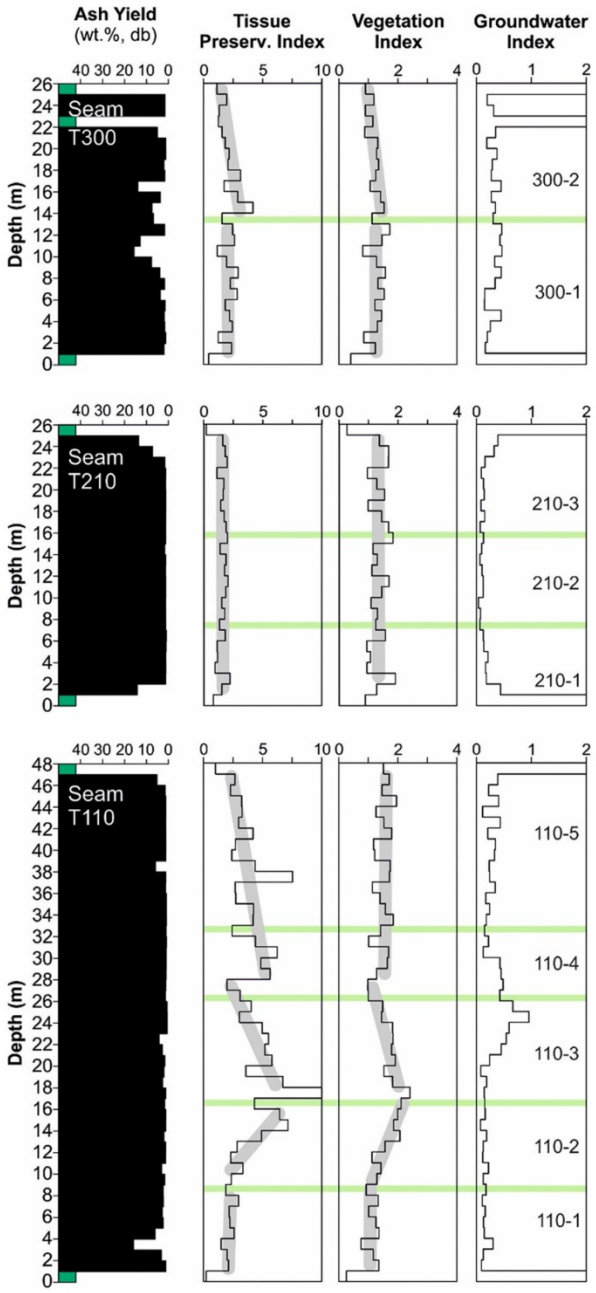

Fig. 13. Variations petrography-based facies indicators in seams T110, T210 and T300. Selected trends are highlighted by grey lines. Cycles defined by geochemical data (see Fig. 5) are labelled 110–1 to 300–2 (see right column). Cycle boundaries are shown by green lines. (For interpretation of the references to colour in this figure legend, the reader is referred to the web version of this article.)

Barber et al., 1998; Moore and Shearer, 2003; Dohong et al., 2017).

Carboniferous coal formed in ombrogenous mires is often rich in inertinite macerals due to drier conditions associated with doming (e.g. Zieger and Littke, 2019). However, Gruber and Sachsenhofer (2001) reported that coal at Leoben (Austria), which formed in a middle Miocene ombrogenous mire, contains only low amounts of inertinite. Moreover, with few exceptions (Moore et al., 1996), inertinite macerals are rare in present-day domed peats in SE Asia (Esterle et al., 1989; Demchuk and Moore, 1993; Esterle and Ferm, 1994). The low proportion of inertinite macerals in Tutupan coals is therefore not inconsistent with peat accumulation in an ombrotrophic mire.

Dehmer (1993) and Esterle and Ferm (1994) reported that funginite is the most abundant inertinite maceral in present-day ombrogenous mires in Borneo and Sumatra. This agrees well with observations in the Miocene Tutupan coal. Demchuk and Moore (1993) found fungal remains in palynological assemblages and concluded that fungal material is typical for present-day tropical ombrogenous mires, where high temperatures, humidity and the peat environment promote fungal activity. Dehmer (1993) and Esterle and Ferm (1994) also observed oxidized cutinite ("oxy-epiderminite"). Inertinized cutinite (Fig. 10e,f) is thus probably a common constituent of ombrogenous peat and coal in SE Asia. Based on the study of Arya et al. (2021) on the fungal attack on plant cuticules, a fungal cause of inertinization is likely. Similar oxidized material with a dentate structure in tropical peat and coal was interpreted as altered epidermal layers of roots by Moore and Swanson (1993) and Moore et al. (1996). The interaction of fungal activity and inertinization has also been described by Moore and Shearer (1997), Hower et al. (2010, 2011a, 2011b) and O'Keefe and Hower (2011).

Suberinite occurs in significant amounts in all seams, but the highest average amount of suberinite content is found in seam T210 (average: 3.3 vol%; max. 6.4 vol%). This is consistent with the results of Wüst et al. (2001), who observed the highest suberinite contents (4%) in forest swamps, while suberinite contents in rheotrophic peats in Malaysia are significantly lower. Suberinite is an important constituent of oil-prone coals in SE Asia (e.g. Hutton et al., 1994; Davis et al., 2007). In addition, suberinite generates oil at very low maturity (~0.35%Rr; Khorasani and Murchison, 1988). Therefore, suberinite (together with resinite) is probably responsible for the presence of exsudatinite, despite the low rank of coal (lignite to subbituminous C).

Leaf-derived macerals are an abundant constituent of Miocene ombrogenous coals in central Europe (Leoben; Gruber and Sachsenhofer, 2001). Cutinite and fluorinite are also abundant in Tutupan coals. While the agreement between petrographic and geochemical data is generally very poor, there is at least some coincidence for these leaf-derived macerals. For example, cycles 110–5, 300–1 and 300–2 are all characterized by upwardly decreasing amounts of cutinite and fluorinite. In addition, cycles 110–4 and 100–5 are characterized by high ratios of fluorinite to cutinite, suggesting that the leaves contained greater amounts of leaf resins during deposition of these cycles. This may reflect a change in vegetation compared to other cycles. However, the obvious change occurred already within cycle 110–3 at 23 m, a level that marks the top of the lower part of seam T110 with slightly increased ash yields.

Overall, the petrographic data from the Tutupan coals do not correspond with the vertical variations in vegetation inferred from the geochemical data. Similar observations were made by Demchuk and Moore (1993), who used palynological data to reconstruct vegetation changes in present-day tropical peats and in Miocene ombrogenous coals in Kalimantan. Similarly, they observed little variation in maceral percentages despite strong variations in the original vegetation. Wüst et al. (2001) studied present-day tropical peat using petrographic techniques and also found little correlations between the petrography, degree of decomposition, and depositional environment. This discrepancy is due to the fact that petrographic data reflect both changes in primary vegetation (e.g. varying amounts of leaf material) and degradation processes, leading to homogenization of the precursor material (Demchuk and Moore, 1993; Wüst et al., 2001; Moore and Shearer, 2003; Dai et al., 2020).

6.6. Factors controlling cyclicality and the duration of peat accumulation

As described above, the geochemical data reveal a distinct cyclicity of the Tutupan seams. This section discusses several possible causes of the observed cyclicity, including sea level oscillations, changes in subsidence rates, autosedimentational processes and climate.

The thickness of the cycles ranges from 6 m (cycle 110–4) to 13 m thick (cycles 110–5, 300–1). Similar cycles have been associated with sea level oscillations (e.g. Holdgate and Clarke, 2000). Seams T110 and T210 were largely formed in oligotrophic mires well above the regional (ground-)water table. In addition, the presence of gymnosperm biomarkers indicates peat accumulation in *kerapah* peats, which form mainly inland (Morley, 2013). This makes a direct link to sea level fluctuations unlikely (Morley, 2013).

The high thickness of the coal seams is evidence of ongoing subsidence during peat accumulation. Therefore, the cyclic coal structure may reflect temporal (and lateral) variations in subsidence and peat accumulation rates as known from extensional fault controlled basin (e.g. De Lange and Lowe, 1990, Maggs, 1997; Shearer, 1997; Thompson et al., 1999; Moore and Shearer, 2003; Ratcliffe et al., 2020). However, the Warukin Formation in the Barito foredeep was deposited in a thermal sag regime (e.g. Friederich et al., 2016), where subsidence rates are probably more uniform. A control by varying subsidence rates, therefore, cannot be excluded, but is considered unlikely.

The watershed position of *kerapah* peat also argues against an influence of autosedimentational processes (e.g. stream avulsion or channel meandering; McCabe, 1984; Esterle and Ferm, 1994; Anggara et al., 2021). Therefore, a climatic driver for depositional cycles is considered more probable. In the following, it is examined whether the duration of the cycles suggests a control by Milankovich-type cycles.

In order to assess the duration of the cycles, a probabilistic approach is used (for details see Moore et al., 2021). Uncertainty of input variables (cycle thickness, peat accumulation rate, compaction ratios) and outputs were estimated using the software @risk, a plug-in to MS Excel (Palisade, 2017).

The thickness of each cycle ranges from 6 to 13 m, which were assumed to be the minimum and maximum values. The average thickness (8.5 m) is taken as best estimate. The mean present-day peat accumulation rate of tropical peat in SE Asia is 1.3 mm/year (data from 266 sites) (e.g. Wüst et al., 2007; Page et al., 2010) with very few data exceeding 4.5 mm/year. For the probabilistic analysis a range of 0.2 to 6.3 mm/year with a best estimate of 1.3 mm/year was considered. Estimates of the compaction rates of coals vary widely (e.g. Widera, 2015; Moore et al., 2021). A lower limit for the Tutupan coals (3.3:1) is suggested by the comparison of the moisture content of tropical low-ash ombrotrophic peat (~ 90 wt%; e.g. Wüst et al., 2001; Wüst and Bustin, 2004) and the moisture content of low-ash Tutupan coals (~20 wt %). Considering that the microbial decay in ombrotrophic mires is minor, an only slightly higher compaction ratio of 3.5:1 is used as the best estimate. Following Widera (2015), a compaction ratio of 11:1 is accepted as maximum value for the Tutupan coal, which reaches the lignite to subbituminous C rank.

The probabilistic analysis shows that there is an 80% chance that the true cycle duration lies between 10.8 kyr (P10) and 61.1 kyr (P90), with 50% probability (P50) that the true value is 22.7 kyr. As expected the time range is high, but the cycles are in any case much shorter than the 405 kyr eccentricity cycles observed by Morley et al. (2021) in middle Miocene sediments offshore Borneo. Obviously, further study is needed, but this simple consideration suggests that the cyclicality observed in Tutupan coals may be related to the 'precession index', which is the combined effects of the Earth's orbital eccentricity and axial precession on the Sun-Earth distance, and has main periods between 17 and 24 kyr (e.g., Hinnov and Hilgen, 2012).

7. Summary and conclusions

In the Tutupan mine (Kalimantan; Barito Basin), three main seams (T100 to T300) of middle Miocene age reach a net thickness of often more than 100 m. Tutupan coal is generally very low in ash and sulphur, although ash yields can vary.

The economically significant T110 (main part of the T100 seam), T210 (part of seam T200) and T300 seams were investigated using a multi-method approach including the analysis of ash yield and moisture content, element analysis (carbon and sulphur), Rock-Eval pyrolysis, organic geochemistry and petrology.

The T110 seam is 46 m thick where sampled. Peat accumulation began in a transitional rheotrophic to ombrotrophic mires, as suggested by slightly enhanced ash yield and sulphur content (1–9 m; cycle 110–1). Geochemical data suggest a relatively high contribution of grassland vegetation. The rest of the seam was accumulated as peat in an ombrotrophic mire. According to the biomarker data, the vegetation was dominated by angiosperms including dipterocarps, while gymnosperm-derived biomarkers are present in variable, but generally low amounts. Nevertheless, the presence of gymnosperm biomarkers is important as it indicates coal formation in a *kerapah*-type swamp. Geochemical data show four cycles (110–2 to 110–5) during accumulation of the *kerapah* peat.

Seam T210 is 24 m thick. Peat accumulation occurred in a similar environment as in seam T110, although the contribution of gymnosperms to the peat-forming vegetation was probably higher. Peat accumulation ended due to deposition of freshwater sediments in both seams, although the drowning of seam T210 was more gradual. Three cycles (210–1 to 210–3) are developed in the T210 seam. The thickness of the individual cycles (6–10 m) is similar to that in seam T110.

The 25 m thick seam T300 was deposited in a more unstable environment, changing from rheotrophic to ombrotrophic. It is characterized by a significantly higher ash yield and seam splitting. Based on geochemical and petrographic data, a subdivision into a lower and an upper part is justified.

Cycles in the ombrotrophic *kerapah* peats are probably controlled by climate variability. Probabilistic assessment indicates that single cycles may represent a time span between 10.8 (P10) and 61.1 kyr (P90) with a 50% probability (P50) of 22.7 kyr. Based on this assessment, a connection between the axial precession of the Earth (17–24 kyr) and the postulated climate variations seems plausible.

The petrographic data do not reflect the cyclic structure of the seams. This is because maceral percentages are controlled by the primary vegetation, and also degradation processes that lead to a homogenization of the plant material. Reduced amounts of gelification reflect the acidic conditions in the ombrotrophic peat. Inertinite macerals are generally rare with funginite being one of the main inertinite macerals. Resinite and the leaf-derived cutinite and fluorinite macerals are abundant and characteristic liptinite macerals. Suberinite and resinite are responsible for the presence of exsudatinie, despite the low rank of the coal (lignite to subbituminous C).

CRediT authorship contribution statement

Hafidz Noor Fikri: Conceptualization, Methodology, Investigation, Writing – original draft, Visualization. **Reinhard F. Sachsenhofer:** Conceptualization, Writing – review & editing. **Achim Bechtel:** Writing – review & editing. **Doris Gross:** Writing – review & editing.

Declaration of Competing Interest

The authors declare that they have no known competing financial interests or personal relationships that could have appeared to influence the work reported in this paper.

Acknowledgments

The first author (FHN) thanks OeAD, Austria's Agency for Education and Internationalization, for an Ernst Mach Grant, ASEA-UNINET scholarship (Reference number: ICM-2019-13766, MPC-2020-01500, MPC-2021-01331). FHN would also like to thank PT. Adaro Indonesia Company for their help in sampling the coal seams. The paper benefitted greatly from the very detailed and positive criticism of the journal reviewers Tim A. Moore and Cortland F. Eble.

References

ADARO, 2008. Feasibility Study for Increasing Production Capacity - 45 Million Tons per Year. PT Adaro Indonesia.

ADARO, 2021. PT Adaro Energy Tbk's Annual Report 2020 Staying Resilent and Reliable through the Headwinds. Corporate Secretary and Investor Relations Division PT Adaro Energy Tbk, p. 427.

Anderson, J.A.R., 1964. The structure and development of the peat swamps of Sarawak and Brunei. J. Trop. Geogr. 18, 7–16.

Anderson, J.A.R., 1983. The tropical peat swamps of western Malesia. In: Gore, A.J.P. (Ed.), Ecosystems of the World, 4B, Mires: Swamp, Bog, Fen and Moor – Regional Studies. Elsevier, Amsterdam, The Netherlands, pp. 181–199.

Anderson, J.A.R., Muller, J., 1975. Palynological study of a Holocene peat and a Miocene coal deposit from N.W. Borneo. Rev. Palaeobot. Palynol. 19, 291–351.

Anggara, F., Muchitawati, G.S., Moore, T.A., Septantia, A., 2021. Spatial variability in macro- and microtextures of a tropical intermontane peatland: Prelimnary investigation in the Kutai peat system, East Kalimantan, Indonesia. Indonesian J. Geosci. 8, 275–296.

Arya, G.C., Sarkar, S., Manasherova, E., Aharoni, A., Cohen, H., 2021. The plant cuticle: an ancient guardian barrier set against long-standing rivals. Front. Plant Sci. 12, 663165 https://doi.org/10.3389/fpls.2021.663165.

ASTM, 2012. D3174-2012. Standard Test Method for Ash in the Analysis Sample of Coal and Coke from Coal, p. 6.

ASTM, 2017. D3173-2017. Standard Test Method for Moisture in the Analysis Sample of Coal and Coke, p. 4.

Barber, K.E., Dumayne-Peaty, L., Hughes, P., Mauquoy, D., Scaife, R., 1998. Replicablity and variability of the recent macrofossil and proxy-climate record from raised bogs: field stratigraphy and macrofossil data from Bolton Fell Moss and Waltn Moss, Cumbria, England. J. Quat. Sci. 13, 515–528. https://doi.org/10.1191/095968300675142023.

Bechtel, A., Püttmann, W., 2017. Biomarkers: Coal. In: White, W. (Ed.), Encyclopedia of Geochemistry. Encyclopedia of Earth Sciences Series. Springer, Cham. https://doi.org/10.1007/978-3-319-39193-9_150-1.

Bechtel, A., Gruber, W., Sachsenhofer, R.F., Gratzer, R., Püttmann, W., 2001. Organic geochemical and stable carbon isotopic investigation of coals formed in low-lying and raised mires within the Eastern Alps (Austria). Org. Geochem. 32, 1289–1310. https://doi.org/10.1016/S0146-6380(01)00101-2.

Bechtel, A., Sachsenhofer, R.F., Kolcon, I., Gratzer, R., Otto, A., Püttmann, W., 2002a. Organic geochemistry of the lower Miocene Oberdorf lignite (Styrian basin, Austria): its relation to petrography, palynology and the palaeoenvironment. Int. J. Coal Geol. 51, 31–57. https://doi.org/10.1016/S0166-5162(02)00079-4.

Bechtel, A., Sachsenhofer, R.F., Gratzer, R., Lücke, A., Püttmann, W., 2002b. Parameters determining the carbon isotopic composition of coal and fossil wood in the early Miocene Oberdorf lignite seam (Styrian Basin, Austria). Org. Geochem. 33, 1001–1024. https://doi.org/10.1016/S0146-6380(02)00054-2.

Bechtel, A., Sachsenhofer, R.F., Markic, M., Gratzer, R., Lucke, A., Püttmann, W., 2003. Paleoenvironmental implications from biomarker and stable isotope investigations on the Pliocene Velenje lignite seam (Slovenia). Org. Geochem. 34, 1277–1298. https://doi.org/10.1016/S0146-6380(03)00114-1.

Bechtel, A., Reischenbacher, D., Sachsenhofer, R.F., Gratzer, R., Lücke, A., 2007a. Paleogeography and paleoecology of the upper Miocene Zillingdorf lignite deposit (Austria). Int. J. Coal Geol. 69, 119–143. https://doi.org/10.1016/j.coal.2006.03.001.

Bechtel, A., Reischenbacher, D., Sachsenhofer, R.F., Gratzer, R., Lücke, A., Püttmann, W., 2007b. Relations of petrographical and geochemical parameters in the middle Miocene Lavanttal lignite (Austria). Int. J. Coal Geol. 70, 325–349. https://doi.org/10.1016/j.coal.2006.07.002.

Bechtel, A., Gratzer, R., Sachsenhofer, R.F., Gusterhuber, J., Lücke, A., Püttmann, W., 2008. Biomarker and carbon isotope variation in coal and fossil wood of Central Europe through the Cenozoic. Palaeogeogr. Palaeoclimatol. Palaeoecol. 262, 166–175. https://doi.org/10.1016/j.palaeo.2008.03.005.

Berner, R.A., 1984. Sedimentary pyrite formation: an update. Geochim. Cosmochim. Acta 48 (4), 605–615. https://doi.org/10.1016/0016-7037(84)90089-9.

Bottari, F., Marsili, A., Morelli, I., Pacchiani, M., 1972. Aliphatic and triterpenoid hydrocarbons from ferns. Phytochemistry 11, 2519–2523. https://doi.org/10.1016/S0031-9422(00)88528-3.

Bourbonniere, R.A., Meyers, P.A., 1996. Sedimentary geolipid records of historical changes in the watersheds and productivities of Lakes Ontario and Erie. Limnol. Oceanogr. 41, 352–359. https://doi.org/10.4319/lo.1996.41.2.0352.

BP, 2021. Statistical Review of World Energy 2021, 70th edition https://www.bp.com/content/dam/bp/business-sites/en/global/corporate/pdfs/energy-economics/statistical-review/bp-stats-review-2021-full-report.pdf.

Brassell, S.C., Comet, P.A., Eglinton, G., Isaacson, P.J., McEvoy, J., Maxwell, J.R., Thompson, I.D., Tibbetts, P.J.C., Volkman, J.K., 1980. The Origin and Fate of Lipids in the Japan Trench. In: Douglas, A.G., Maxwell, J.R. (Eds.), Advances in Organic Geochemistry, 1979. Pergamon Press, Oxford, pp. 375–392.

Bray, E.E., Evans, E.D., 1961. Distribution of n-paraffins as a clue to recognition of source beds. Geochim. Cosmochim. Acta 22, 2–5. https://doi.org/10.1016/0016-7037(61)90069-2.

Brooks, J.D., Gould, K., Smith, J.W., 1969. Isoprenoid Hydrocarbons in coal and Petroleum. Nature 222, 257–259.

Buggle, B., Wiesenberg, G.L., Glaser, B., 2010. Is there a possibility to correct fossil n-alkane data for postsedimentary alteration effects? Appl. Geochem. 25 (7), 947–957. https://doi.org/10.1016/j.apgeochem.2010.04.003.

Bush, R.T., McInerney, F.A., 2015. Influence of temperature and C_4 abundance on n-alkane chain length distributions across the Central USA. Org. Geochem. 79, 65–73. https://doi.org/10.1016/j.orggeochem.2014.12.003.

Calder, J., Gibling, M., Mukhopadhyay, P.K., 1991. Peat formation in a Westphalian B piedmont setting, Cumberland Basin, Nova Scotia: implications for the maceral-based interpretation of rheotrophic and raised paleomires. Bull. Soc. Geol. Fr. 162, 283–298.

Cameron, C.C., Esterle, J.S., Palmer, C.A., 1989. The geology, botany and chemistry of selected peat-forming environments from temperate and tropical latitudes. Int. J. Coal Geol. 12, 105–156. https://doi.org/10.1016/0166-5162(89)90049-9.

Carr, A.S., Boom, A., Grimes, H.L., Chase, B.M., Meadows, M.E., Harris, A., 2014. Leaf wax n-alkane distributions in arid zone South African flora: environmental controls, chemotaxonomy and palaeoecological implications. Org. Geochem. 67, 72–84. https://doi.org/10.1016/j.orggeochem.2013.12.004.

Clymo, R.S., 1987. Rainwater-fed peat as a precursor to coal. In: Scott, A.C. (Ed.), Coal and Coal-Bearing Strata: Recent Advances, 32. Geological Society Special Publications, pp. 17–23. https://doi.org/10.1144/GSL.SP.1987.032.01.03.

Dai, S., Bechtel, A., Eble, C.F., Flores, R.M., French, D., Graham, I.T., Hood, M.M., Hower, J.C., Korasidis, V.A., Moore, T.A., Püttman, W., Wei, Q., Zhao, L., O'Keefe, J. M.K., 2020. Recognition of peat depositional environments in coal: a review. Int. J. Coal Geol. 210, 103383, 67.

Daly, M.C., Cooper, M.A., Wilson, I., Smith, D.G., Hooper, B.G.D., 1991. Cenozoic plate tectonics and basin evolution in Indonesia. Mar. Pet. Geol. 8, 2–21. https://doi.org/10.1016/0264-8172(91)90041-X.

Davis, R.C., Noon, S.W., Harrington, J., 2007. The petroleum potential of Tertiary coals from Western Indonesia: Relationship to mire type and sequence stratigraphic setting. Int. J. Coal Geol. 70, 35–52. https://doi.org/10.1016/j.coal.2006.02.008.

De Lange, P.J., Lowe, D.J., 1990. History of vertical displacement of Kerepehi Fault at Kopouatai bog, Hauraki Lowlands, New Zealand, since c. 10 700 years ago. J. Geol. Geophys. 277–283. https://doi.org/10.1080/00288306.1990.10425685.

Dehmer, J., 1993. Petrology and organic geochemistry of peat samples from a raised bog in Kalimantan (Borneo). Org. Geochem. 20 (3), 349–362. https://doi.org/10.1016/0146-6380(93)90125-U.

Demchuk, T., Moore, T.A., 1993. Palynofloral and organic characteristics of a Miocene bog-forest, Kalimantan, Indonesia. Org. Geochem. 20 (2), 119–134. https://doi.org/10.1016/0146-6380(93)90032-7.

Didyk, B.M., Simoneit, B.R.T., Brassell, S.T., Eglinton, G., 1978. Organic geochemical indicators of palaeoenvironmental conditions of sedimentation. Nature 272 (5650), 216–222.

Diefendorf, A.F., Freeman, K.H., Wing, S.L., Graham, H.V., 2011. Production of *n*-alkyl lipids in living plants and implications for the geologic past. Geochim. Cosmochim. Acta 75, 7472–7485. https://doi.org/10.1016/j.gca.2011.09.028.

Diefendorf, A.F., Freeman, K.H., Wing, S.L., 2014. A comparison of terpenoid and leaf fossil vegetation proxies in Paleocene and Eocene Bighorn Basin sediments. Org. Geochem. 71, 30–42. https://doi.org/10.1016/j.orggeochem.2014.04.004.

Diessel, C.F.K., 1986. The Correlation between Coal Facies and Depositional Environments. Proceeding 20th Symposium of Department Geology. University of New Castle, New South Wales, pp. 11–22.

Diessel, C.F.K., 1992. Coal-Bearing Depositional Systems. Springer, Berlin, Heidelberg. https://doi.org/10.1007/978-3-642-75668-9.

Dohong, A., Aziz, A.A., Dargusch, P., 2017. A review of the drivers of tropical peatland degradation in South-East Asia. Land Use Policy 69, 349–360.

Espitalie, J., Madec, M., Tissot, B., Mennig, J.J., Leplat, P., 1977. Source Rock Characterization Method for Petroleum Exploration. Offshore Technology Conference. https://doi.org/10.4043/2935-MS.

Esterle, J.S., Ferm, J.C., 1994. Spatial variability in modern tropical peat deposits from Sarawak, Malaysia and Sumatra, Indonesia: analogues for coal. Int. J. Coal Geol. 26, 1–41. https://doi.org/10.1016/0166-5162(94)90030-2.

Esterle, J.S., Ferm, J.C., Durig, D.T., Supardi, 1987. Physical and Chemical Properties of Peat near Jambi, Sumatra, Indonesia, International Peat Society, Symposium on Tropical Peat, pp. 1–17.

Esterle, J.S., Ferm, J.C., Tie, Y.L., 1989. A test for the analogy of tropical domed peat deposits to "dulling-up" sequences in coal beds-preliminary results. Org. Geochem. 14, 333–342. https://doi.org/10.1016/0146-6380(89)90060-0.

Ficken, K.J., Li, B., Swain, D., Eglinton, G., 2000. An n-alkane proxy for the sedimentary input of submerged/floating freshwater aquatic macrophytes. Org. Geochem. 31, 745–749. https://doi.org/10.1016/S0146-6380(00)00081-4.

Friederich, M.C., Van Leeuwen, T., 2017. A review of the history of coal exploration, discovery and production in Indonesia: the interplay of legal framework, coal geology and exploration strategy. Int. J. Coal Geol. 178, 56–73. https://doi.org/10.1016/j.coal.2017.04.007.

Friederich, M.C., Moore, T.A., Flores, R.M., 2016. A regional review and new insights into SE Asian Cenozoic coal-bearing sediments: why does Indonesia have such

extensive coal deposits? Int. J. Coal Geol. 166, 2–35. https://doi.org/10.1016/j.coal.2016.06.013.
Gross, D., Bechtel, A., Harrington, G.J., 2015. Variability in coal facies as reflected by organic petrological and geochemical data in Cenozoic coal beds offshore Shimokita (Japan) - IODP Exp. 337. Int. J. Coal Geol. 152, 63–79. https://doi.org/10.1016/j.coal.2015.10.007.
Gruber, W., Sachsenhofer, R.F., 2001. Coal deposition in the Noric Depression (Eastern Alps): raised and low-lying mires in Miocene pull-apart basins. Int. J. Coal Geol. 48, 89–114. https://doi.org/10.1016/S0166-5162(01)00049-0.
Hall, R., Morley, C.K., Kuhnt, W., 2004. Sundaland basins. In: Clift, P., Wang, P., Hayes, D.E. (Eds.), Continent-Ocean Interactions within the East Asian Marginal Seas, vol. 149. Geophysical Monograph, American Geophysical Union, Geophysical Monograph, Washington, D.C., pp. 55–85
Hauke, V., Graff, R., Wehrung, P., Trendel, J.M., Albrecht, P., Riva, A., Hopfgartner, G., Gulacar, F.O., Buchs, A., Eakin, P.A., 1992. Novel triterpene-derived hydrocarbons of the arborane/fernane series in sediments: Part II. Geochim. Cosmochim. Acta 56, 3595–3602. https://doi.org/10.1016/0016-7037(92)90405-8.
Heryanto, R., Sanyoto, P., 1994. Geological Map of the Amuntai Quadrangle, Kalimantan. Geological Agency, Bandung Indonesia (1:250,000).
Hinnov, L.A., Hilgen, F.J., 2012. Cyclostratigraphy and astrochronology. In: Gradstein, F. M., Ogg, J.G., Schmitz, M., Ogg, G. (Eds.), The Geologic Time Scale, p. 2012. https://doi.org/10.1016/B978-0-444-59425-9.00004-4.
Hoffmann, B., Kahmen, A., Cernusak, L.A., Arndt, S.K., Sachse, D., 2013. Abundance and distribution of leaf wax n-alkanes in leaves of Acacia and Eucalyptus trees along a strong humidity gradient in northern Australia. Org. Geochem. 62, 62–67. https://doi.org/10.1016/j.orggeochem.2013.07.003.
Holdgate, G.R., 2005. Geological processes that control lateral and vertical variability in coal seam moisture contents; Latrobe Valley, Gippsland Basin, Australia. Int. J. Coal Geol. 63, 130–155. https://doi.org/10.1016/j.coal.2005.02.010.
Holdgate, G.R., Clarke, J.D.A., 2000. A Review of Tertiary Brown Coal Deposits in Australia: Their Depositional Factors and Eustatic Correlations AAPG Bulletin, 84, pp. 1129–1151.
Hower, J.C., O'Keefe, J.M.K., Volk, T.J., Watt, M.A., 2010. Funginite resinite associations in coal. Int. J. Coal Geol. 83, 64–72. https://doi.org/10.1016/j.coal.2010.04.003.
Hower, J.C., O'Keefe, J.M., Eble, C.F., Raymond, A., Valentim, B., Volk, T.J., Richardson, A.R., Satterwhite, A.B., Hatch, R.S., Stucker, J.D., Watt, M.A., 2011a. Notes on the origin of inertinite macerals in coal: evidence for fungal and arthropod transformations of degraded macerals. Int. J. Coal Geol. 86 (2–3), 231–240. https://doi.org/10.1016/j.coal.2011.02.005.
Hower, J.C., O'Keefe, J.M., Eble, C.F., Volk, T.J., Richardson, A.R., Satterwhite, A.B., Hatch, R.S., Kostova, I.J., 2011b. Notes on the origin of inertinite macerals in coals: Funginite associations with cutinite and suberinite. Int. J. Coal Geol. 85, 186–190. https://doi.org/10.1016/j.coal.2010.11.008.
Hutchison, C.S., 1973. Tectonic evolution of Sundaland: a Phanerozoic synthesis. Geol. Soc. Malaysia, Bull. 6, 61–86.
Hutchison, C.S., 1989. Geological Evolution of South-East Asia, Oxford Monographs on Geology and Geophysics, 13. Oxford University Press, Oxford, p. 368.
Hutchison, C.S., 2014. Tectonic evolution of Southeast Asia. Geol. Soc. Malaysia Bull. 60, 1–18.
Hutton, A., Daulay, B., Herudiyanto, Nas, C., Pujobroto, A., Sutarwan, H., 1994. Liptinite in Indonesian coals. Energy Fuel 1994, 1469–1477. https://doi.org/10.1021/ef00048a037.
ICCP (International Committee for Coal and Organic Petrology), 2001. The new inertinite classification (ICCP System 1994). Fuel 80, 459–471. https://doi.org/10.1016/S0016-2361(00)00102-2.
Jager, G., Bruins, E.H., 1975. Effect of repeated drying at different temperatures on soil organic matter decomposition and characteristics, and on the soil microflora. Soil Biol. Biochem. 7, 153–159. https://doi.org/10.1016/0038-0717(75)90013-9.
Kalkreuth, W.D., Marchioni, D.L., Calder, J.H., Lamberson, M.N., Naylor, R.D., Paul, J., 1991. The relationship between coal petrography and depositional environments from selected coal basins in Canada. Int. J. Coal Geol. 19, 21–76. https://doi.org/10.1016/0166-5162(91)90014-A.
Khorasani, G.K., Murchison, D.G., 1988. Order of generation of petroleum hydrocarbons from liptinic macerals with increasing thermal maturity. Fuel 67, 1160–1162. https://doi.org/10.1016/0016-2361(88)90388-2.
Kusuma, I., Darin, T., 1989. The hydrocarbon potential of the Lower Tanjung Formation, Barito Basin, SE Kalimantan. In: Proceedings Indonesian Petroleum Association 18th Annual Convention. https://doi.org/10.29118/ipa.2166.107.138.
Lambiase, J.J., 1990. A model for tectonic control of lacustrine stratigraphic sequences in continental rift basins. In: Katz, B. (Ed.), Lacustrine Exploration: Case Studies And Modern Analogues, 50. AAPG Memoir, pp. 265–276. https://doi.org/10.1306/M50523C16.
Li, Z., Moore, T.A., Weaver, S.D., 2001. Leaching of inorganics in the cretaceous Greymouth coal beds, South Island, New Zealand. Int. J. Coal Geol. 47, 235–253. https://doi.org/10.1016/S0166-5162(01)00044-1.
Maggs, G.R., 1997. Hydrology of the Kopouatai Peat Dome. J. Hydrol. (NZ) 36, 147–172.
Markic, M., Sachsenhofer, R.F., 1997. Petrographic composition and depositional environments of the Pliocene Velenje lignite seam (Slovenia). Int. J. Coal Geol. 33 (3), 229–254. https://doi.org/10.1016/S0166-5162(96)00043-2.
McCabe, 1984. Depositional environments of coal and coal-bearing strata. In: Rahmani, R.A., Flores, R.M. (Eds.), Sedimentology of Coal and Coal-Bearing Sequences. Blackwell Scientific Publications, Oxford, pp. 13–42.
Moore, P.D., 1987. Ecological and hydrological aspects of peat formation. In: a.C. Scott (ed.), coal and coal-bearing strata: recent advances. Geol. Soc. Spec. Publ. 32, 7–15. https://doi.org/10.1144/GSL.SP.1987.032.01.02.
Moore, T.A., Moroeng, O.M., Shen, J., Esterle, J.S., Pausch, R.C., 2021. Using carbon isotopes and organic composition to decipher climate and tectonics in the Early Cretaceous: An example from the Hailar Basin, Inner Mongolia, China. Cretac. Res. 118, 104674 https://doi.org/10.1016/j.cretres.2020.104674.
Moore, T.A., Shearer, J.C., 1997. Evidence for aerobic degradation and implications for Palangka Raya peat sustainability. In: Rieley, J.O., Page, S.E. (Eds.), Biodiversity and Sustainability of Tropical Peatlands. Samara Publishing, Cardigan, United Kingdom, pp. 157–167.
Moore, T.A., Shearer, J.C., 2003. Coal/peat type and depositional environment – are they related? Int. J. Coal Geol. 56, 233–252. https://doi.org/10.1016/S0166-5162(03)00114-9.
Moore, T.A., Swanson, K.M., 1993. Application of etching and SEM in the identification of fossil plant tissues in coal. Org. Geochem. 20, 769–777. https://doi.org/10.1016/0146-6380(93)90061-F.
Moore, T.A., Shearer, J.C., Miller, S.L., 1996. Fungal origin of oxidised plant material in the Palangkaraya peat deposit, Kalimantan Tengah, Indonesia: Implications for 'inertinite' formation in coal. Int. J. Coal Geol. 30, 1–23. https://doi.org/10.1016/0166-5162(95)00040-2.
Morley, R.J., 2013. Cenozoic ecological history of South East Asian peat mires based on the comparison of coals with present day and Late Quaternary peats. J. Limnol. 72, 36–59. https://doi.org/10.4081/jlimnol.2013.s2.e3.
Morley, R.J., Hasan, S.S., Morley, H.P., Jais, J.H.M., Mansor, A., Aripin, M.R., Nordin, M. H., Rohaizar, M.H., 2021. Sequence biostratigraphic framework for the Oligocene to Pliocene of Malaysia: High-frequency depositional cycles driven by polar glaciation. Palaeogeogr. Palaeoclimatol. Palaeoecol. 561, 110058 https://doi.org/10.1016/j.palaeo.2020.110058.
Naafs, D.F.W., van Bergen, P.F., Boogert, S.J., de Leeuw, J.W., 2019. Solvent-extractable lipids in an acid andic forest soil; variations with depth and season. Soil Biol. Biochem. 36, 297–308. https://doi.org/10.1016/j.soilbio.2003.10.00.
Neuzil, S.G., Supardi, Cecil, C.B., Kane, J.S., Soedjono, K., 1993. Inorganic geochemistry of domed peat in Indonesia and its implication for the origin of mineral matter in coal. In: Cobb, J.C., Cecil, C.B. (Eds.), Modern and Ancient Coal-Forming Environments. Geological Society of America Special Paper, Boulder, Co, pp. 23–44.
Nott, C.J., Xie, S., Avsejs, L.A., Maddy, D., Chambers, F.M., Evershed, F., 2000. *N*-Alkane distribution in ombotrophic mires as indicators of vegetation change related to climatic variation. Org. Geochem. 31, 231–235. https://doi.org/10.1016/S0146-6380(99)00153-9.
O'Keefe, J.M.K., Hower, J.C., 2011. Revisiting Coos Bay, Oregon: a re-examination of funginite-huminite relationships in Eocene subbituminous coals. Int. J. Coal Geol. 85, 34–42. https://doi.org/10.1016/j.coal.2010.09.003.
Ortiz, J.E., Moreno, L., Torres, T., Vegas, J., Ruiz-Zapata, B., García-Cortés, Á., Galán, L., Pérez-González, A., 2013. A 220 ka palaeoenvironmental reconstruction of the Fuentillejo maar lake record (Central Spain) using biomarker analysis. Org. Geochem. 55, 85–97. https://doi.org/10.1016/j.orggeochem.2012.11.012.
Ourrison, G., Albrecht, P., Rohmer, M., 1979. The hopanoids: palaeo-chemistry and biochemistry of a group of natural products. Pure Appl. Chem. 51, 709–729. https://doi.org/10.1351/pac197951040709.
Page, S., Rieley, J.O., Shotyk, O.W., Weiss, D., 1999. Interdependence of peat and vegetation in a tropical peat swamp forest. Philos. Trans. Royal Soc. B Biol. Sci. 354 (1391), 1885–1897. https://doi.org/10.1098/rstb.1999.0529.
Page, S., Wüst, R., Banks, C., 2010. Past and present carbon accumulation and loss in Southeast Asian peatlands. PAGES News 18, 25–27. https://doi.org/10.22498/pages.18.1.25.
Palisade, 2017. @Risk-Risk Analysis and Simulation Add-in for Microsoft Excel, Version 7.5, vol. 798. Palisade Corporation, Cascadilla St., Ithaca, NY, USA. http://www.palisade.com.
Parr, S.W., 1928. The classification of coal. In: University of Illinois, Engineering Experiment Station, Bulletin, 180, pp. 1–62.
Pickel, W., Kus, J., Flores, D., Kalaitzidis, S., Christanis, K., Cardott, B.J., Misz-Kennan, M., Rodrigues, S., Hentschel, A., Hamor-Vido, M., Crosdale, P., Wagner, N., 2017. Classification of liptinite – ICCP System 1994. Int. J. Coal Geol. 169, 40–61. https://doi.org/10.1016/j.coal.2016.11.004.
Powell, T.G., McKirdy, D.M., 1973. Relationship between ratio of pristane to phytane, crude oil composition and geological environment in Australia. Nat. Phys. Sci. 243 (124), 37–39.
Poynter, J., Eglinton, G., 1990. Molecular composition of three sediments from Hole 717C: the Bengal Fan. In: Cochran, J.R., Stow, D.A.V., et al. (Eds.), Proceedings of the Ocean Drilling Program, Scientific Results, College Station, TX (Ocean Drilling Program), 116, pp. 155–161. https://doi.org/10.2973/odp.proc.sr.116.151.1990.
Pubellier, M., Morley, C.K., 2014. The basins of Sundaland (SE Asia): Evolution and boundary conditions. Mar. Pet. Geol. 58, 555–578. https://doi.org/10.1016/j.marpetgeo.2013.11.019.
Radke, M., Schaefer, R.G., Leythaeuser, D., Teichmüller, M., 1980. Composition of soluble organic matter in coals: relation to rank and liptinite fluorescence. Geochim. Cosmochim. Acta 44, 1787–1800. https://doi.org/10.1016/0016-7037(80)90228-8.
Ratcliffe, J.L., Lowe, D.J., Schipper, L.A., Gehrels, M.J., French, A.D., Campbell, D.I., 2020. Rapid carbon accumulation in a peatland following late Holocene tephra deposition, New Zealand. Quat. Sci. Rev. 246, 106505, 14. https://doi.org/10.1016/j.quascirev.2020.106505.
Rohmer, M., Bisseret, P., 1994. Hopanoid and other polyterpenoid biosynthesis in eubacteria. Am. Chem. Soc. Symp. Series 562, 31–43.
Ronkainen, T., McClymont, E.L., Väliranta, M., Tuittila, E.S., 2013. The n-alkane and sterol composition of living fen plants as a potential tool for palaeoecological studies. Org. Geochem. 59, 1–9. https://doi.org/10.1016/j.orggeochem.2013.03.005.
Ruppert, L.F., Neuzil, S.G., Cecil, C.B., Kane, J.S., 1993. Inorganic constituents from samples of a domed and lacustrine peat, Sumatra Indonesia. In: Cobb, J.C., Cecil, C.

B. (Eds.), Modern and Ancient Coal-Forming Environments. Geological Society of America Special Paper, Boulder, Colorado, USA, pp. 83–96.
Sapiie, B., Rifiyanto, A., 2017. Tectonics and geological factors controlling cleat development in the Barito Basin, Indonesia. J. Eng. Technol. Sci. 49 (3), 322–339. https://doi.org/10.5614/j.eng.technol.sci.2017.49.3.3.
Satyana, A.H., Nugroho, D., Surantoko, I., 1999. Tectonic controls on the hydrocarbon habitats of the Barito, Kutei, and Tarakan Basins, Eastern Kalimantan, Indonesia: major dissimilarities in adjoining basins. J. Asian Earth Sci. 17, 99–122. https://doi.org/10.1016/S0743-9547(98)00059-2.
Schwark, L., Zink, K., Lechterbeck, J., 2002. Reconstruction of postglacial to early Holocene vegetation history in terrestrial Central Europe via cuticular lipid biomarkers and pollen records from lake sediments. Geology 30 (5), 463–466. https://doi.org/10.1130/0091-7613(2002)030<0463:ROPTEH>2.0.CO;2.
Shearer, J.C., 1997. Natural and anthropogenic influences on peat development in Waikato/Hauraki Plains restiad bogs. J. R. Soc. N. Z. 27, 295–313. https://doi.org/10.1080/03014223.1997.9517540.
Sikumbang, N., Heryanto, R., 1994. Geological map of the Banjarmasin Sheet, Kalimantan. In: Geological Agency, Bandung, Indonesia (1:250,000).
Silliman, J.E., Meyers, P.A., Bourbonniere, R.A., 1996. Record of postglacial organic matter delivery and burial in sediments of Lake Ontario. Org. Geochem. 24 (4), 463–472. https://doi.org/10.1016/0146-6380(96)00041-1.
Supriatna, S., Djamal, B., Heryanto, R., Sanyoto, P., 1994. Geological Map of Indonesia. Banjarmasin Sheet, Geological Research Centre Bandung, Indonesia.
Sýkorová, I., Pickel, W., Christanis, K., Wolf, M., Taylor, G.H., Flores, D., 2005. Classification of huminite—ICCP System 1994. Int. J. Coal Geol. 62, 85–106. https://doi.org/10.1016/j.coal.2004.06.006.
Taylor, G., Teichmüller, M., Davies, A., Diessel, D., Littke, R., Robert, P., 1998. Organic Petrology: A New Handbook Incorporation some Revised Parts of Stach's Textbook of Coal Petrology. Gebrüder Borntraeger, Berlin.
Thompson, M.A., Campbell, D.I., Spronken-Smith, R.A., 1999. Evaporation from natural and modified raised peat bogs in New Zealand. Agric. For. Meteorol. 95, 85–98. https://doi.org/10.1016/S0168-1923(99)00027-1.
Tipple, B.J., Pagani, M., 2013. Environmental control on eastern broadleaf forest species' leaf wax distributions and D/H ratios. Geochim. Cosmochim. Acta 111, 64–77. https://doi.org/10.1016/j.gca.2012.10.042.
Tissot, B.P., Welte, D.H., 1984. From Kerogen to Petroleum. In: Petroleum Formation and Occurrence. Springer, Berlin, Heidelberg. https://doi.org/10.1007/978-3-642-87813-8_10.
Trigui, Y., Wolf, D., Sahakyan, L., Hovakimyan, H., Sahakyan, K., Zech, R., Fuchs, M., Wolpert, T., Zech, M., Faust, D., 2019. First calibration and application of leaf wax n-alkane biomarkers in loess-paleosol sequences and modern plants and soils in Armenia. Geosciences 9 (6), 263. https://doi.org/10.3390/geosciences9060263.
van Aarssen, B.G.K., Cox, H., Hoogendoorn, N.P., de Leeuw, J.W., 1990. A cadinene biopolymer in fossil and extant dammar resins as a source for cadinanes and bicadinanes in crude oils from South East Asia. Geochim. Cosmochim. Acta 54, 3021–3031. https://doi.org/10.1016/0016-7037(90)90119-6.
van Aarssen, B.G.K., de Leeuw, J.W., Collinson, M., Boon, J.J., Goth, K., 1994. Occurrence of polycadinene in fossil and recent resins. Geochim. Cosmochim. Acta 58, 223–229. https://doi.org/10.1016/0016-7037(94)90459-6.
Wakeham, S.G., 1990. Algal and bacterial hydrocarbons in particulate material and interfacial sediment of the Cariaco trench. Geochim. Cosmochim. Acta 54, 1325–1336. https://doi.org/10.1016/0016-7037(90)90157-G.
Waterhouse, J., Crisostomo, J., Nolan, D., Dutton, A., 2008. An integration of hydrogeology and geotechnical engineering for the design of the Tutupan coal mine T100 low wall, South Kalimantan, Indonesia. In: Proceedings of the 10th IMWA, pp. 81–84. https://www.imwa.info/docs/imwa_2008/IMWA2008_189_Waterhouse.pdf.
Widera, M., 2015. Compaction of lignite: a review of methods and results. Acta Geol. Pol. 65, 367–378. https://doi.org/10.1515/agp-2015-0016.
Widodo, S., Bechtel, A., Komang, A., Püttmann, W., 2009. Reconstruction of floral changes during deposition of the Miocene Embalut coal from Kutai basin, Mahakam delta, East Kalimantan, Indonesia by use of aromatic hydrocarbon composition and stable carbon isotope ratios of organic matter. Org. Geochem. 40, 206–218. https://doi.org/10.1016/j.orggeochem.2008.10.008.
Witts, D., Hall, R., Nichols, G., Morley, R., 2012. A new depositional and provenance model for the Tanjung Formation, Barito Basin, SE Kalimantan, Indonesia. J. Asian Earth Sci. 56, 77–104. https://doi.org/10.1016/j.jseaes.2012.04.022.
Witts, D., Davies, L., Morley, R., 2014. Uplift of the Meratus Complex: Sedimentology, biostratigraphy, provenance and structure. In: Proceedings Indonesian Petroleum Association 38th Annual Convention & Exhibition, IPA14-G-082. https://doi.org/10.29118/ipa.0.14.g.082.
Wüst, R.A.J., Bustin, R.M., 2004. Late Pleistocene and Holocene development of the interior peat-accumulating basin of tropical Tasek Bera, Peninsular Malaysia. Palaeogeogr. Palaeoclimatol. Palaeoecol. 211, 241–270. https://doi.org/10.1016/j.palaeo.2004.05.009.
Wüst, R.A.J., Hawke, M.I., Bustin, R.M., 2001. Comparing maceral ratios from tropical peatlands with assumptions from coal studies: do classic coal petrographic interpretation methods have to be discarded? Int. J. Coal Geol. 48, 115–132. https://doi.org/10.1016/S0166-5162(01)00050-7.
Wüst, R., Rieley, J., Page, S., Kaars, S., Wie-Ming, W., Jacobsen, G., Smith, A., 2007. Peatland evolution in SE Asia over the last 35,000 cal years: Implications for evaluating their carbon storage potential. In: Rieley, J.O., Banks, C.J., Radjagukguk, B. (Eds.), Carbon-Climate-Human Interaction on Tropical Peatland. Proceedings of the International Symposium and Workshop on Tropical Peatland, Yogyakarta. EU CARBOPEAT and RESTORPEAT Partnership. Gadjah Mada University and University of Leicester.
Zahirovic, S., Seton, M., Müller, R.D., 2014. The cretaceous and Cenozoic tectonic evolution of Southeast Asia. Solid Earth 5, 227–273. https://doi.org/10.5194/sed-5-1335-2013.
Zech, M., Buggle, B., Leiber, K., Marković, S., Glaser, B., Hambach, U., Huwe, B., Stevens, T., Sümegi, P., Wiesenberg, G., Zöller, L., 2009. Reconstructing Quaternary vegetation history in the Carpathian Basin, SE-Europe, using n-alkane biomarkers as molecular fossils: problems and possible solutions, potential and limitations. E&G Quat. Sci. J. 58, 148–155. https://doi.org/10.3285/eg.58.2.03.
Zieger, L., Littke, R., 2019. Bolsovian (Pennsylvanian) tropical peat depositional environments: the example of the Ruhr Basin, Germany. Int. J. Coal Geol. 211, 103209 https://doi.org/10.1016/j.coal.2019.103209.

7 Publication II:

Coal deposition in the Barito Basin (Southeast Borneo): The Eocene Tanjung Formation compared to the Miocene Warukin Formation

Chapter 7 was published by the author of this thesis in “International Journal of Coal Geology”. (https://doi.org/10.1016/j.coal.2022.104117)

Author contribution: Conceptualization, methodology, investigation, writing – original draft, and visualization

International Journal of Coal Geology 263 (2022) 104117

Contents lists available at ScienceDirect

International Journal of Coal Geology

journal homepage: www.elsevier.com/locate/coal

Coal deposition in the Barito Basin (Southeast Borneo): The Eocene Tanjung Formation compared to the Miocene Warukin Formation

Hafidz Noor Fikri [a,b], Reinhard F. Sachsenhofer [a,*], Achim Bechtel [a], Doris Gross [a]

[a] Department Applied Geosciences and Geophysics, Montanuniversitaet Leoben, Austria
[b] Department of Mining Engineering, Lambung Mangkurat University, Banjarmasin, South Kalimantan, Indonesia

ARTICLE INFO

Keywords:
Rheotrophic peat
Ombrotrophic peat
Organic Petrography
Organic geochemistry
Kalimantan

ABSTRACT

Coal seams of Late Eocene (Tanjung Formation) and middle Miocene age (Warukin Formation) are present in the Barito Basin of Borneo. The seams are laterally continuous and can be traced over at least 20 km. The thickness of three Eocene seams in the TAJ Pit–1D mine ranges from 1.4 to 3.4 m. These seams (from base to top: D, C, B) were studied to reconstruct their peat–forming environment and to compare the characteristics of Eocene and Miocene coals. The comparison reveals differences in peat types, flora and climate. The study is based on 38 Eocene coal and six non–coal samples, each representing a stratigraphic interval of 0.2 m. The samples were analyzed for ash yield, carbon and sulphur contents, and maceral composition. Organic geochemical parameters (incl. biomarkers) were obtained on every second coal sample to obtain information on the peat-forming vegetation and its diagenetic alteration.

The Eocene seams were deposited in rheotrophic mires with palm/fern–dominated vegetation. Transitions to local ombrotrophic mires cannot be excluded. Very low to low sulphur contents (max. 0.9 wt%) speak against a marine influence, despite a general coastal plain setting. Upward increasing sulphur contents in the lower seam D and the upper seam B are interpreted to reflect transgression, which ended peat accumulation. The seam C formed in a rheotrohpic seam with a relatively high water level. This favored the accumulation of aquatic plants.

Miocene coals from the Warukin Formation in the Barito Basin were studied recently in a companion paper. The comparison of Eocene and Miocene coals shows major differences, which include: Miocene coals are significantly thicker (up to 50 m) and display a cyclic structure. Miocene coals accumulated in ombrotrophic mires dominated by more decay resistant angiosperm trees (and subordinate gymnosperms). Therefore, preserved plant tissues are more abundant in Miocene coals. In addition, Miocene coals contain a significantly higher amount of root–derived macerals (suberinite). Leaf–derived macerals (cutinite, fluorinite) and resinite are ubiquitous in Miocene coals, but even slightly more abundant in Eocene coals. At least part of the resinite in Miocene coals, but not in Eocene coals, is derived from dammar resin produced by Dipterocarpaceae. Fungal activity, recorded by high funginite percentages, was high in low-ash ombrotrophic and high-ash rheotrophic mires both in Eocene and Miocene times.

1. Introduction

Indonesia is one of the most important coal producers in the world (BP, 2022). The most important coals seams are found in Cenozoic sedimentary basins in the islands of Sumatra and Borneo in Miocene and Upper Eocene horizons (Friederich et al., 2016; Friederich and Van Leeuwen, 2017). These large islands belong to the southern part of Sundaland, which has occupied a remarkably stable paleogeographic position ±10° of the equator since Eocene time (Hall and Morley, 2004; Pubellier and Morley, 2014; Friederich et al., 2016). This stable position favored peat formation in ever–wet conditions (Morley, 2012). The sedimentary succession in the Barito Basin in southeastern Borneo (Fig. 1a) contains two coal–bearing units, the Eocene Tanjung Formation (e.g., Siregar and Sunaryo, 1980; Witts et al., 2012) and the Miocene Warukin Formation (Friederich et al., 2016; Fig. 2). Moreover, southern Borneo is currently covered by vast peatlands (e.g., Anderson, 1964, 1983; Rieley et al., 1992; Esterle and Ferm, 1994; Esterle et al., 1987; Page et al., 1999; Wüst et al., 2007). Because of the assumed similar climatic conditions, a comparison of coal parameters and peat–forming environments in the Eocene and the Miocene seems

* Corresponding author.
E-mail address: reinhard.sachsenhofer@unileoben.ac.at (R.F. Sachsenhofer).

https://doi.org/10.1016/j.coal.2022.104117
Received 26 August 2022; Received in revised form 3 October 2022; Accepted 3 October 2022
Available online 12 October 2022

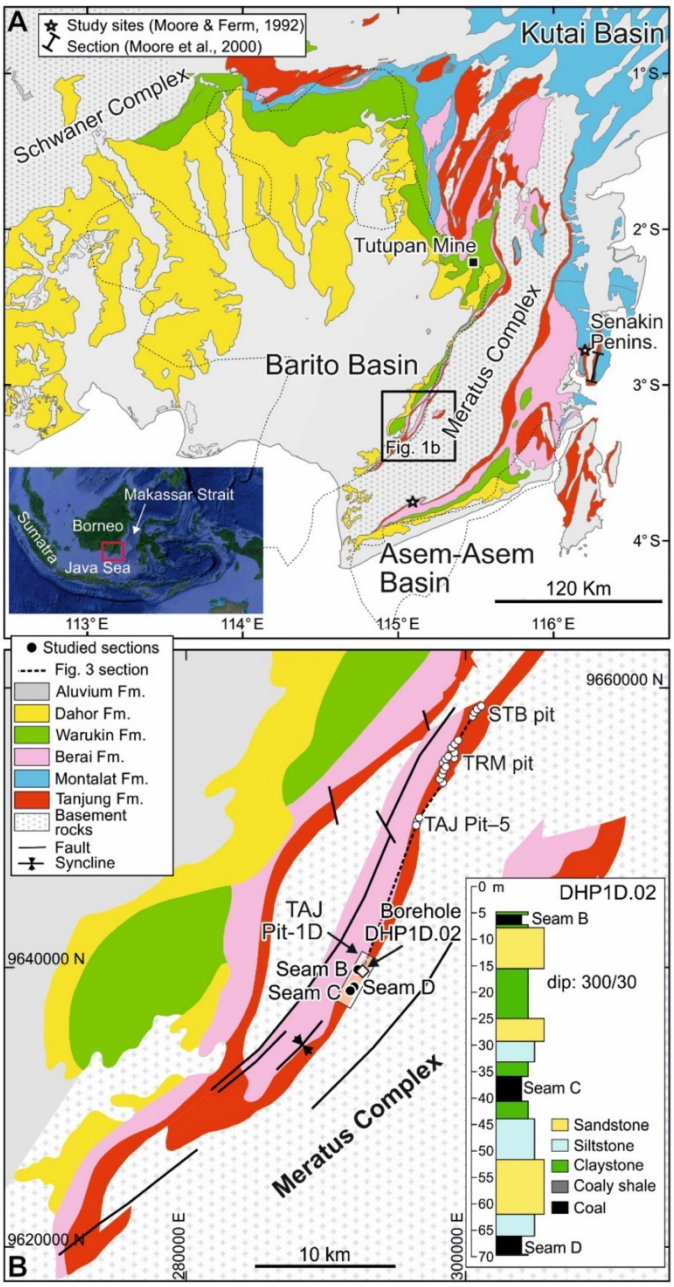

Fig. 1. Geological map of the Barito Basin (a) and of the surroundings of the Tanjung Alam Jaya (TAJ) Pit–1D mine (b; after Supriatna et al., 1994 and Sikumbang and Heryanto, 1994). Sites and cross–section studied by Moore and Ferm (1992) and Moore et al. (2020) are shown in Fig. 1a. The sample locations are shown in Fig. 1b (dots). The inset shows the sedimentary succession of exploration borehole DHP1D.02 in the TAJ PIT–1D mine. The stippled line shows the position of Fig. 3 cross–section connecting borehole DHP1D.02 with the STB pit in the north.

particularly rewarding and may be supported by data from present–day peatlands (e.g., Anderson and Muller, 1975).

Rheotrophic (low-lying) and ombrotrophic (raised, domed) mires are widespread in SE Asia (e.g., Anderson, 1964, 1983; Rieley et al., 1992; Esterle and Ferm, 1994; Esterle et al., 1987; Page et al., 1999; Wüst et al., 2007). Two end-member types of ombrotrophic peatlands have been distinguished: 'basinal' (or 'coastal') peats occur inland from mangrove swamps near the coast, while kerapah peats (also called 'watershed', 'high' or 'interior' peat) occur at low elevations (10–30 m above sea level) up to 200 km inland from the coast peats (e.g., Page et al., 2010; Morley, 2013).

Coal may form in ombrotrophic and in rheotrophic mires (e.g., Diessel, 1992; Gruber and Sachsenhofer, 2001; Morley, 2013). Ombrothropic mires are fed by rainfall and bacterial activity is strongly reduced by very low pH values. Therefore, coal formed in ombrothropic mires is very low in sulphur and (syngenetic) mineral matter and plant litter is well preserved (e.g., Diessel, 1992; Dai et al., 2020). Coals formed in rheotropic mires have variable and partly very high ash and sulphur values, which are controlled by the frequency and extent of flooding events and water chemistry (e.g., Casagrande, 1987; Diessel, 1992; Dai et al., 2020). Plant degradation is dependent on acidity and bacterial activity and may be very high in rheotrophic mires.

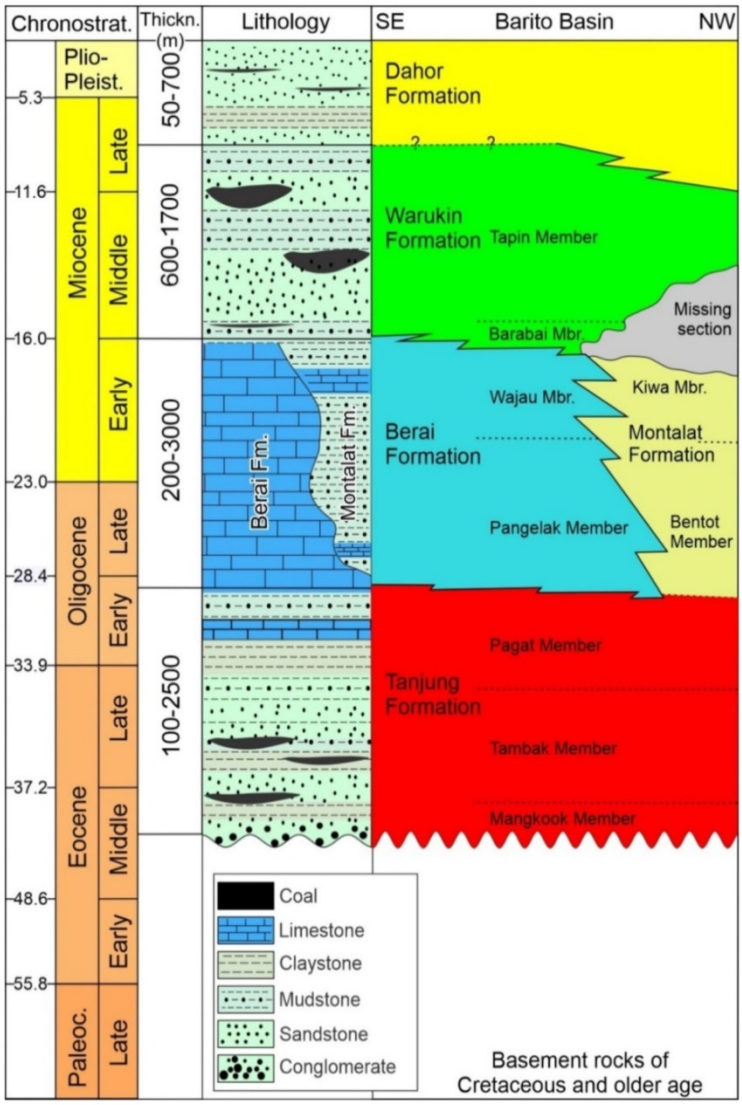

Fig. 2. Stratigraphy and lithology of the basin fill in the Barito Basin (modified after Witts et al., 2012, 2014).

Most previous studies on coal deposits in Borneo focused on Miocene coals (e.g., Anderson and Muller, 1975; Demchuk and Moore, 1993; Widodo et al., 2009; Alias et al., 2012; Morley, 2013). Recently, Fikri et al. (2022) studied Miocene subbituminous coal from Tutupan Mine in the northern part of the Barito Basin (Fig. 1a). The Tutupan Mine is the most important mining site for coal from the Warukin Formation. Three thick seams, labelled from base to top T110 (46 m thick), T210 (24 m) and T300 (24 m) were investigated using geochemical and petrographic techniques. Based on ash yields, sulphur contents, biomarker and maceral data, the authors concluded that the lower seams were deposited in ombrotrophic (kerapah-type) mires, while the upper seam accumulated in alternating ombrotrophic and rheotrophic environments. Geochemical evidence, including *n*-alkane and biomarker ratios, shows that the great thickness of the seams is due to the stacking of individual coal cycles. Seam T110 has five climatically controlled cycles (labelled 110–1 to 110–5 from base to tope) and seam T210 three cycles (210–1 to 210–3). Two less pronounced cycles may exist in seam T300 (300–1 to 300–2).

In contrast to Miocene coals, petrographic or geochemical studies on Eocene coal seams are rare (e.g., Moore and Ferm, 1992; Belkin et al., 2009; Morley, 2013) and often related to their oil and gas potential rather than their depositional environment (e.g., Panggabean, 1991; Hutton et al., 1994; Stankiewicz et al., 1996; Satyana et al., 2001; Davis et al., 2007; Stevens and Hadiyanto, 2004). To fill this gap, we study coal in the Eocene Tanjung Formation at the Tanjung Alam Jaya (TAJ Pit—1D) site in the Barito Basin (Fig. 1a).

A total of four coal seams are known at the TAJ Pit–1D site. They are labelled from base to top, seam D to seam A. The lower three seams (D to B), separated by non–coal sediments, which are several tens of metres thick (Fig. 1b), are considered economic. Seam D is up to 3 m thick. Seam C reaches a thickness of 5 m and is the most important seam. Seams B (~1.5 m) and A (<0.5 m) are relatively thin and their lateral extension is limited (TAJ, 2020; Fig. 3). The economic seams D to B are included in the present study. According to Panggabean (1991), the TAJ site contains subbituminous A to high volatile bituminous C coal with low ash yields (~8 wt% adb), low sulphur contents (~0.36 wt% adb),

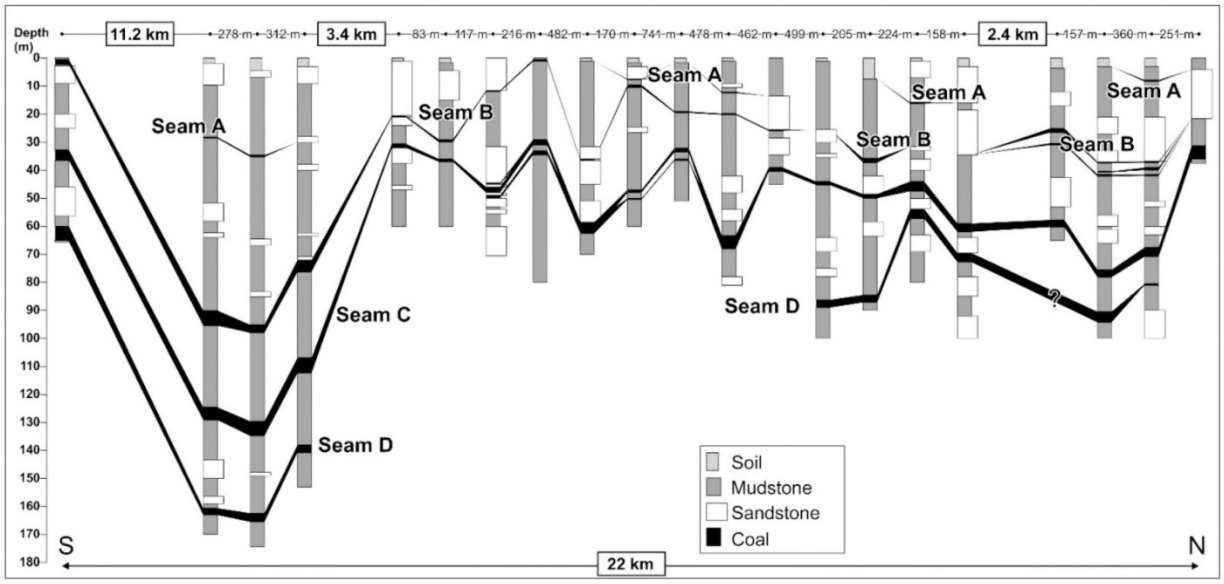

Fig. 3. South–north cross section along the western margin of the Meratus Complex, derived from borehole data from four exploration sites. The distances between the sites are given in kilometres, the distances between boreholes are given in metres. See Fig. 1b for location of the section. The southernmost borehole is located in the TAJ Pit–1D site near the sampling sites.

and a relatively high calorific value (~6900 Kcal/kg, TAJ, 2021).

Thirty-eight Eocene coal and six non–coal samples were collected at the TAJ Pit–1D site across the stratigraphic sequence. These samples were used to determine the vertical distribution of ash yield, moisture, sulphur, total organic carbon (TOC) contents, Rock–Eval parameters, maceral composition, and organic geochemical parameters. The same investigation strategy was applied for the Miocene coal in the Tutupan mine (Fikri et al., 2022). Thus, apart from the investigation of the Eocene paleo-peatland and the factors controlling its distribution over time, the study allows a direct comparison between Eocene and Miocene coals.

2. Geological setting

The Barito Basin is located between two basement units: the continental Schwaner Complex in the northwest and the accreted Meratus Complex in the east (Satyana et al., 1999; Fig. 1a). To the south, the basin extends into the Java Sea. The Meratus Complex separates the Barito Basin from the smaller Asem–Asem Basin. Comparable sedimentary successions suggest that these basins were connected until uplift of the Meratus Complex in the Late Miocene (Satyana et al., 1999; Witts et al., 2014). The thickness of the Cenozoic basin fill in the Barito Basin (Fig. 2) increases from west to east. Structurally, the Barito Basin is a platform near the Schwaner Complex and a foredeep near the thrusted front of the Meratus Complex (Satyana et al., 1999). The Barito Basin was initiated by Eocene rifting of the Makassar Strait (Daly et al., 1991; Pubellier and Morley, 2014; Zahirovic et al., 2014), which led to the formation of NW–SE oriented horst and graben structures along a succession of NW–SE trending strike–slip faults (Satyana et al., 1999). Rifting in the Barito Basin continued until the end of the Early Oligocene (Pubellier and Morley, 2014). Basin inversion commenced in the middle/late Miocene, around the time of the uplift of the Meratus Mountains (Satyana et al., 1999; Witts et al., 2014).

The Cenozoic basin fill consists of Middle Eocene to recent sediments and overlies Cretaceous and older basement rocks. The oldest part of the succession is formed by the transgressive Tanjung Formation. The Tanjung Formation is overlain by the Upper Oligocene to lower Miocene Berai and Montalat formations, the middle and upper Miocene coal–bearing Warukin Formation and the upper Miocene to Pleistocene Dahor Formation (Witts et al., 2012, 2014; Fig. 2).

A comprehensive study of the Tanjung Formation in the eastern side of the Barito Basin was presented by Witts et al. (2012). The following description is based on this paper. The Tanjung Formation was deposited from late Middle Eocene to late Early Oligocene time. The formation comprises three members. The lower Mangkook Member includes alluvial and fluvial deposits (facies association TFA1 of Witts et al., 2012). The Upper Eocene to Lower Oligocene Tambak Member accounts for approximately 80% of the entire formation. It reflects a change from localized alluvial to widespread fluvio–tidal and estuarine deposition in an overall transgressive setting. Witts et al. (2012) distinguished fluvio–tidal coastal floodplain and estuarine settings (TFA2) and lower coastal plain and estuarine settings with strong tidal influence (TFA3). Laterally extensive coals, several-metre thick and extending over >10 km (Fig. 3) occur in TFA2. TFA2 coals are invariably overlain by mudstones, sometimes rhythmically interbedded with siltstone. Sediment transport was mainly in north(east)ern direction. The mudstones contain shallow water foraminifera of Late Eocene age, suggesting that peat accumulation was terminated by transgression. In contrast to TFA2 coals, coals associated with TFA3 are typically thin (<0.25 m). A thin layer of marginal and shallow marine mudstones, siltstones and thin limestone beds (TFA4) forms the Pagat Member.

Palynological investigations revealed that Middle and Upper Eocene coals in SE Asia were formed in palm–dominated brackish and freshwater swamps with a significant contribution of ferns (e.g., Morley, 2013). For example, spore/pollen assemblages in coal from the Tanjung Formation derived almost entirely from palms and ferns (unpublished BHP–Utah Int. report in Moore and Ferm, 1992). Another unpublished report (Dettmann and Playford in Morley, 2013) showed that coal from the Tanjung Formation accumulated in a freshwater setting with a brackish influence in the upper part.

The most detailed studies of coals in the Tanjung Formation have been performed outside of the Barito Basin, east of the Meratus Complex (for location of studied sites and sections see Fig. 1a). Moore and Ferm (1992) noted that Eocene coals consist of small plant parts (< 2 mm) in a

fine–grained or amorphous matrix and related the paucity of large plant material to the strong microbial degradation of the palm– and fern–dominated vegetation. The authors also noted that the coal contains ash yields and sulphur contents of <8 wt% and 1.2 wt% (dry basis), respectively. The main coal seam in the Senakin Peninsular (Senakin seam) is >5-m thick, contains volcanic ash layers as well as pelitic layers transported by water (Ruppert and Moore, 1992), and has a high degree of lateral continuity (>20 km; Moore et al., 2020). The large lateral extent of the seams corroborates previous interpretations that the coal was formed in the early post–rift phase of the Barito Basin (see Friederich et al., 2009, 2016).

Modern swamp forests composed almost exclusively of palms and understory of ferns have been reported from New Guinea (Paijmans, 1990). Additional sites with present–day palm–dominated swamps in SE Asia have been noted by Morley (2013), who postulated that the dominance of palms in coastal mires may be indicative of rheotrophic swamps.

3. Samples

Samples were collected at the TAJ Pit–1D mine (Fig. 1b). At the sample location seams D, C and B are 2.8-m, 3.4-m and 1.4-m thick, respectively. Seam A is missing due to non–deposition. A nearby exploration borehole provides information on the inter–seam sediments (Fig. 1b). Samples were taken vertically in each seam at 20 cm intervals using a continuous series of channel samples, since each seam is considered macroscopically homogeneous. Following the terminology of Moore and Ferm (1992), the coal corresponds to the bright luster, nonbanded type. A total of 38 coal samples were taken together with six rock samples, representing the underlying and overlying sediments of each seam. The fresh samples were placed in gas–tight plastic bags immediately after collection to prevent moisture loss.

4. Methods

All analyses were carried out at Montanuniversitaet Leoben (Austria), except of the determination of the ash yield and moisture content.

Ash yield provides important information on the peat type (Moore and Shearer, 1997). Hence, ash yield was determined for all samples together with the moisture content. Sample preparation was performed at the Mineral and Coal Laboratory of the Mining Department of the Faculty of Engineering (Lambung Mangkurat University), while the analyses were carried out at Coal Laboratory PT Geoservices (Banjarbaru, South Kalimantan) following standard procedures (ASTM, 2012, 2017).

Total organic carbon (TOC), total inorganic carbon (TIC), and sulphur (S) contents were determined in duplicate using an Eltra Helios C/S analyzer. TOC contents are used to normalize Rock–Eval and biomarker data. TIC and S contents are useful indicators of peat facies (e.g., Dai et al., 2020).

Rock–Eval parameters S2 (amount of hydrocarbons generated during pyrolysis, mgHC/g rock), hydrogen index (HI = S2*100/TOC; mgHC/gTOC) and Tmax (°C) provide information on the type of organic matter and its maturity (Espitalie et al., 1977). Rock–Eval pyrolysis was performed in duplicate using a Vinci Rock–Eval 6 instrument.

The petrography of the coal samples was characterized using maceral analysis. The samples were crushed to a maximum size of 1 mm and embedded in epoxy resin. Polished blocks were investigated using a Leica incident light microscope with a 50× oil-immersion objective, reflected white and fluorescent light, and a single–scan approach (Taylor et al., 1998). A total of 500 points on each sample were counted, with macerals assigned according to the ICCP system (ICCP, 1998, 2001; Pickel et al., 2017).

Vitrinite reflectance was measured to determine coal rank of eight samples. A synthetic reflectance standard was applied. Random vitrinite reflectance (%Rr) was measured using standard methods (Taylor et al., 1998) and the Hilgers Fossil software in non–polarized light at a wavelength of 546 nm and a magnification of 50×. Mean values and standard deviation are based on 150 measurement points.

Organic geochemical (biomarker) analyses were performed on approximately every second coal sample to provide information on the peat–forming vegetation. Samples were extracted with dichloromethane for 1 h at 75 °C and 100 bar in a Dionex ASE 350 extractor. After evaporation of the solvent to a total volume of 0.5 ml in a Zymark TurboVap 500 closed–cell concentrator, asphaltenes were precipitated from a hexane–dichloromethane solution (80:1) and separated by centrifugation. The hexane–soluble fractions were separated into NSO compounds, saturated hydrocarbons, and aromatic hydrocarbons using a Köhnen–Willsch medium–pressure liquid chromatography (MPLC) instrument (Radke et al., 1980). *n*–Alkanes and isoprenoids were analyzed using a Trace GC–Ultra gas chromatograph with flame ionization detector (GC–FID). The gas chromatograph was equipped with a 50 m HP–PONA capillary column (0.20-mm inner diameter [i.d.], 0.50–μm film thickness). After sample injection (2 μl at 270 °C), the oven temperature was increased from 70 to 310 °C and kept constant for 35 min. The hydrocarbon fractions were analyzed using a gas chromatograph equipped with a 60 m TG–5MS fused silica capillary column (0.20–mm inner diameter; 0.25-μm film thickness) connected to a ThermoFisher ISQ mass spectrometer (GC–MS). The oven temperature was programmed from 40 to 310 °C at 4 °C/min, followed by an isothermal phase of 30 min. Helium was used as the carrier gas. The sample was injected in split mode (split ratio 20) at an injector temperature of 260 °C. The spectrometer was operated in EI (electron ionization) mode over a scan range from *m/z* 50 to m/z 650 (0.7 s total scan time). The Xcalibur software was used for data processing. Individual compounds were identified based on retention time in the total ion current chromatogram (TIC) and by comparing mass spectra to published reference data. The relative percentages and absolute concentrations of the various compound groups in the saturated and aromatic hydrocarbon fractions were calculated from the peak areas in the TIC chromatograms relative to the internal standards (squalane and 1,1′–binaphthyl, respectively) or by integrating the peak areas in the corresponding mass chromatograms using reaction factors to correct for the intensities of the fragment ion used to quantify total ion abundance. Concentrations were normalized to TOC.

5. Results

5.1. Bulk Parameter

The bulk parameters of the studied samples are listed in Table 1. Their vertical distribution is shown in Fig. 4.

The ash yields vary considerably within the studied seams. Seam D contains low-ash coal in its lower (0.2–1.2 m; average ash yield: 5.25 wt%) and upper part (2.0–2.8 m; av.: 5.70 wt%), and high-ash coal in its middle part (1.2–2.0 m; av.: 10.12 wt%). In seam C, the lower part (0.2–1.6 m) yields less ash (6.11 wt%) than the upper part (1.6–3.6 m; 11.08 wt%). The highest ash yield (29.45 wt%) in seam C is recorded for shaly coal at 2.0–2.2 m. The average ash yield value in seam B is 8.44 wt%. Significant vertical variations cannot be observed in seam B.

The moisture content of all seams are low (seam D: 3.9 wt%; seam C: 3.8 wt%, seam B: 3.3 wt%).

TOC contents of coal samples show a strong negative correlation with ash yields ($r^2 = 0.91$). The slope of the regression line suggests that the TOC content of a hypothetical ash–free coal is 80.8 wt%. The TOC contents of mudstones below and above seam D are low (0.4 wt% and 0.6 wt%), while those related to seams C and B are significantly higher (1.8–3.8 wt%). A total inorganic carbon (TIC) content of 1.32 wt% suggests that the roof of seam D contains about 10 wt% carbonate. All other samples are carbonate–free.

Sulphur contents of coal samples (0.21–0.83 wt%) show significant

Table 1
Bulk Parameter of Eocene TAJ Pit–1D coals.

Sample	Lithology	Position	Ash	Moisture	TOC	Sulphur	HI	Tmax	EOM	NSO	Sat.HC	Arom.HC
		(m above base)	(wt% adb)		(wt% db)		(mgHC/gTOC)	(°C)	(mg/g TOC)			
B–roof	mudstone	1.6	88.14	3.8	2.3	0.06	196	432				
B–1	coal	1.4	7.36	3.0	71.4	0.34	423	427	28.9	11.2	1.3	3.8
B–2	coal	1.2	7.51	3.2	73.3	0.31	432	427				
B–3	coal	1.0	9.52	3.6	70.2	0.30	362	425	30.4	11.7	1.4	3.9
B–4	coal	0.8	8.98	3.6	72.3	0.26	407	426				
B–5	coal	0.6	7.29	3.5	75.9	0.26	452	427	33.4	14.4	1.1	3.0
B–6	coal	0.4	11.23	3.3	72.8	0.28	398	426				
B–7	coal	0.2	7.18	3.1	72.9	0.36	417	425	30.1	12.2	1.1	3.6
B–floor	mudstone	0	87.62	3.0	1.8	0.10	142	432				
C–roof	mudstone	3.6	88.33	3.6	1.8	0.24	134	431				
C–1	coal	3.4	11.89	3.1	67.3	0.26	415	425	34.2	15.7	1.6	3.1
C–2	coal	3.2	7.47	2.9	73.1	0.28	423	426				
C–3	coal	3.0	10.19	2.8	71.6	0.27	457	428	33.8	14.9	1.0	3.0
C–4	coal	2.8	7.07	3.8	72.5	0.39	341	420				
C–5	coal	2.6	5.62	4.9	73.4	0.31	335	422	28.5	10.3	2.3	3.0
C–6	coal	2.4	10.15	2.8	70.3	0.36	432	426				
C–7	coal	2.2	11.81	3.4	69.0	0.40	328	421	35.9	12.4	3.2	4.2
C–8	shaly coal	2.0	29.45	2.6	46.3	0.26	470	428	38.4	17.6	1.6	3.6
C–9	coal	1.8	4.34	4.9	74.6	0.34	340	422				
C–10	coal	1.6	12.80	3.6	65.4	0.34	409	426				
C–11	coal	1.4	5.83	5.0	72.8	0.35	349	425	22.3	7.5	1.7	2.5
C–12	coal	1.2	4.64	4.8	74.0	0.36	332	423				
C–13	coal	1.0	4.64	4.2	74.2	0.35	341	421	29.1	9.1	2.6	3.7
C–14	coal	0.8	7.27	3.6	72.1	0.33	353	425				
C–15	coal	0.6	7.01	3.3	73.2	0.32	382	427	29.3	12.4	1.2	2.9
C–16	coal	0.4	7.08	4.7	71.6	0.32	344	421				
C–17	coal	0.2	6.31	3.9	72.9	0.37	344	426	23.6	8.7	1.4	2.5
C–floor	mudstone	0	89.27	2.7	3.0	0.21	231	426				
D–roof	mudstone	3.0	86.46	2.6	0.6	0.03	81	431				
D–1	coal	2.8	5.01	3.8	76.2	0.72	350	428	27.7	10.1	1.2	2.7
D–2	coal	2.6	6.86	3.4	73.1	0.83	347	427				
D–3	coal	2.4	9.13	4.2	71.5	0.69	330	423	38.2	16.0	1.6	3.2
D–4	coal	2.2	3.70	4.1	76.2	0.57	354	427				
D–5	coal	2.0	3.81	3.8	77.1	0.52	367	427	48.9	31.2	1.4	2.8
D–6	coal	1.8	10.18	3.8	72.1	0.57	366	425				
D–7	coal	1.6	10.03	4.3	71.7	0.56	331	425	37.7	13.9	1.1	3.4
D–8	coal	1.4	10.68	4.6	72.1	0.50	323	424				
D–9	coal	1.2	9.58	4.1	70.9	0.54	347	424				
D–10	coal	1.0	4.94	3.4	75.8	0.38	411	416	42.4	15.7	0.9	2.4
D–11	coal	0.8	5.80	4.2	74.4	0.41	356	423				
D–12	coal	0.6	6.41	3.3	74.9	0.39	402	426	41.4	18.1	0.9	2.6
D–13	coal	0.4	4.40	4.5	74.1	0.44	316	423				
D–14	coal	0.2	4.71	3.8	76.4	0.42	322	424	46.5	17.9	1.0	3.1
D–floor	mudstone	0	95.33	0.7	0.4	0.07	91	430				

TOC – total organic carbon, HI – hydrogen index, EOM – extractable organic matter, NSO – hetero–compounds, Sat.HC – saturated hydrocarbons, Arom.HC – aromatic hydrocarbons.

differences between the seams. Sulphur contents in seam D are moderately high in the lower low–ash part (av.: 0.41 wt%), slightly higher in the middle part (av.: 0.54 wt%) and show a clear upward increasing trend in the upper part (0.52–0.83 wt%; Fig. 4). Sulphur contents in seams C (av.: 0.33 wt%) and B (av.: 0.30 wt%) are lower than in seam D. A subtle increase towards the base and the top of seam B can be recognized. Sulphur contents of floor and roof rocks are typically low (0.03–0.24 wt%).

Hydrogen Index (HI) values are high in all seams and show a subtle increase from seam D (av.: 352 mgHC/gTOC) to seams C (av.: 376 mgHC/gTOC) and B (av.: 413 mgHC/gTOC). The maximum HI (470 mgHC/gTOC) is observed in the coaly shale sample from seam C. HI values of the floor and roof rocks are lower and range from 81 to 231 mgHC/gTOC. Tmax values of coal samples range from 416 to 428 °C (av.: 424 °C). Vertical trends cannot be observed. Tmax values of floor and roof rocks are higher (426–432 °C).

5.2. Biomarker

Biomarker analysis was performed on 20 coal samples. The extractable organic matter (EOM) of these samples is dominated by asphaltenes and NSO compounds, while saturated and aromatic hydrocarbons are subordinate (Fig. 5; Table 2). Chromatograms of the hydrocarbon fractions of selected samples are shown in Fig. 6.

In all samples, the *n*–alkanes are dominated by long–chain *n*–alkanes (*n*–$C_{25–33}$) with a prominent odd–even predominance (Fig. 6). To visualize differences in the composition of the *n*–alkanes and isoprenoids, various parameters were calculated (Table 2). In Fig. 5, these parameters are plotted as a function of stratigraphic position.

The ratio between long and short chain *n*–alkanes (*n*–$C_{27+29+31}$/*n*–$C_{15+17+19}$) is called the terrestrial/ aquatic ratio (TAR; Bourbonniere and Meyers, 1996). An upward trend in TAR is noted in the lower part of seam D (0.2–1.8 m; 21.4–34.7, av.: 27.2). High values, but without a clear vertical trend, are observed in the upper part of seam D (2.0–3.0 m; av.: 32.5; 24.3–41.7). Clear stratigraphic trends are also not evident in seams C and B, but TAR is significantly lower in seam C (av.: 15.7) than

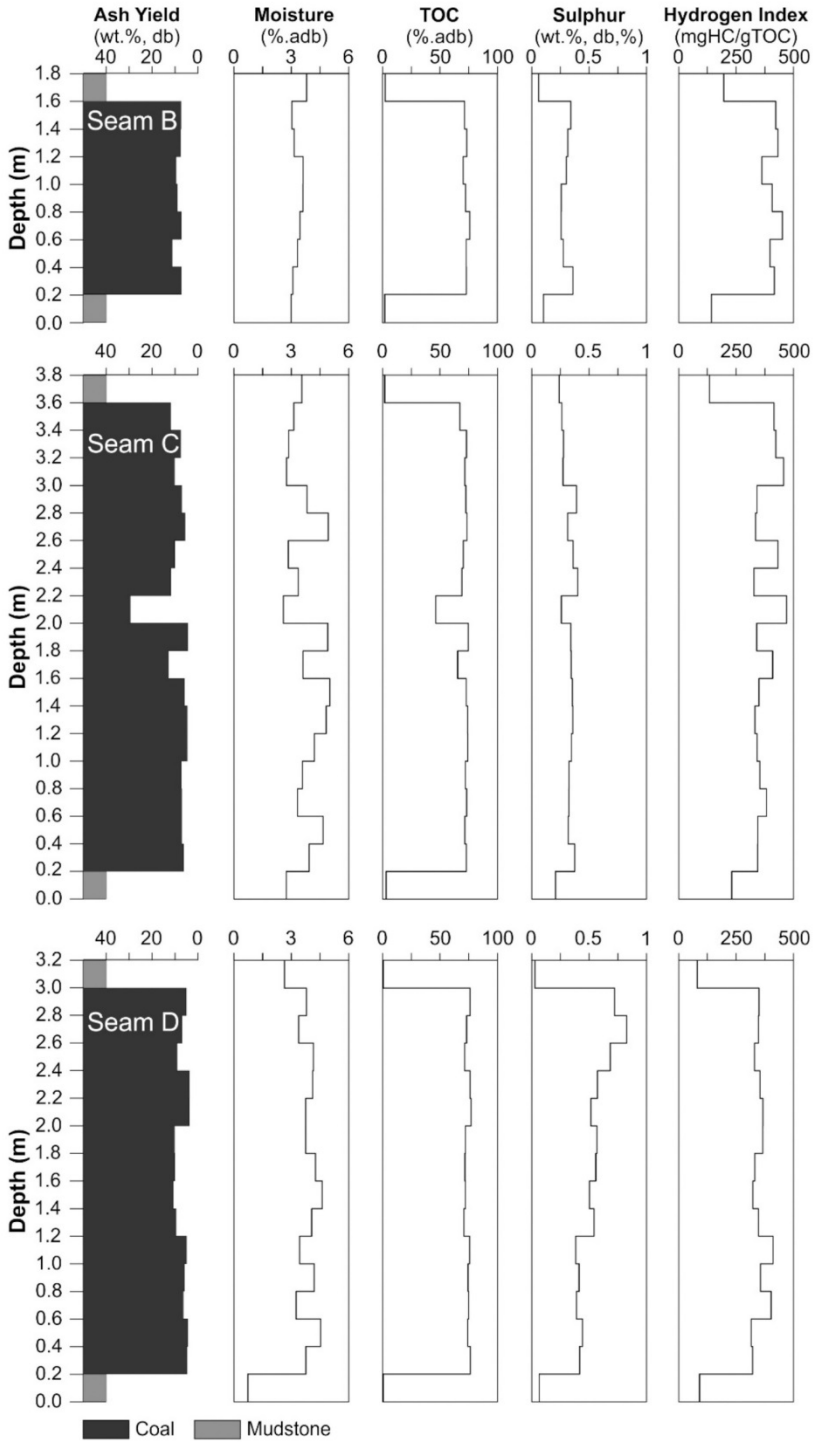

Fig. 4. Vertical variation of bulk data ash yield, moisture content, total organic carbon (TOC) content, sulphur content and hydrogen index in seams D, C and B in the TAJ Pit–1D mine.

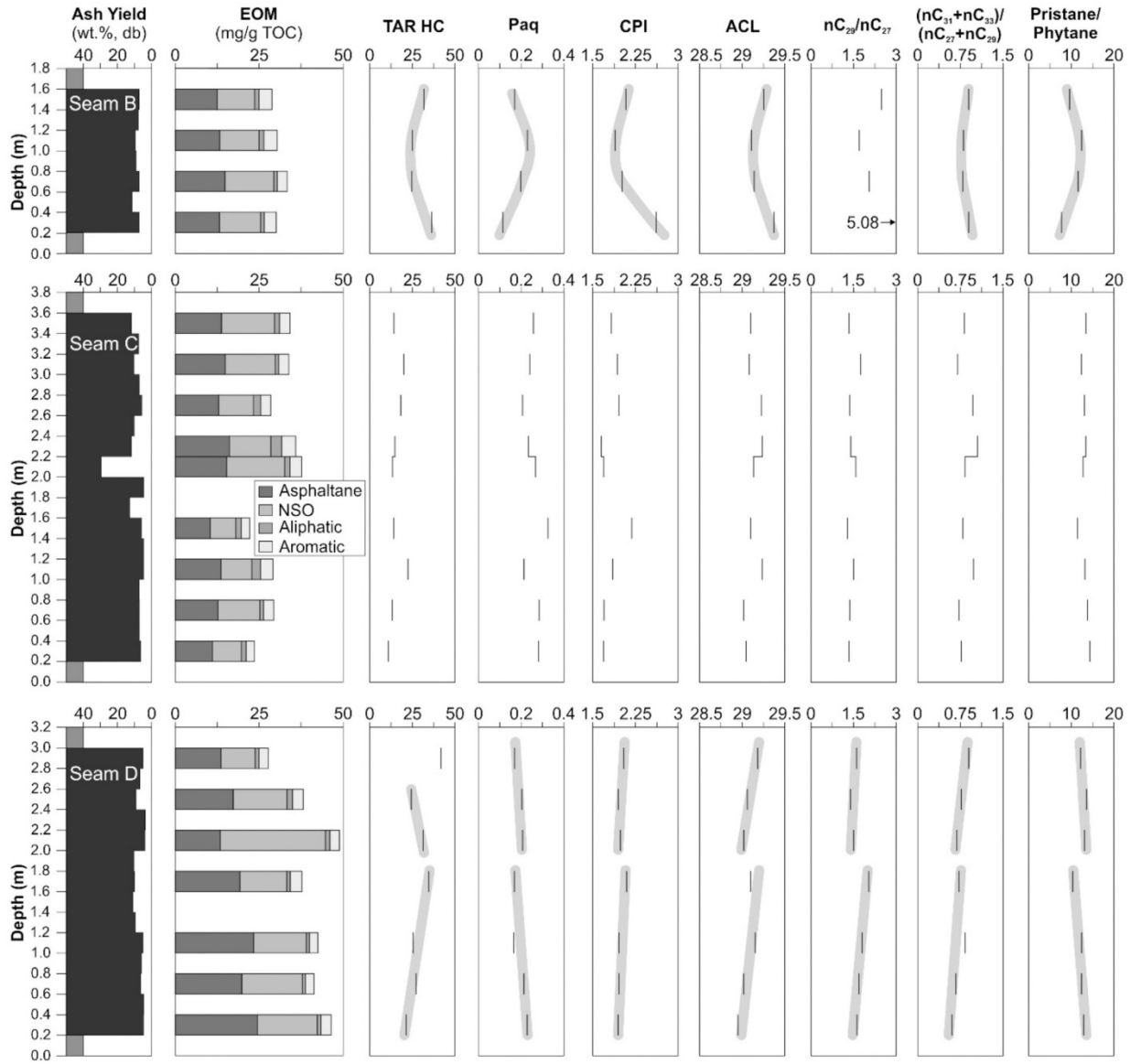

Fig. 5. Variations of EOM, *n*– and iso–alkane ratios in seams D, C and B. EOM – extractable organic matter; TAR – terrestrial/aquatic ratio (Bourbonniere and Meyers, 1996); Paq – P–aqueous (Ficken et al., 2000); CPI – carbon preference index (Bray and Evans, 1961); ACL – average chain length (Poynter and Eglinton, 1990). Selected trends in seams D and B are highlighted by grey lines.

in seam B (av.: 29.5). In the latter seam the maximum values are observed near the base and the top of the seam.

The P–aqueous (Paq) ratio (Ficken et al., 2000) compares the abundance of medium and the sum of medium and long chain *n*–alkanes ((*n*–C_{23} + *n*–C_{25})/(*n*–C_{23} + *n*–C_{25} + *n*–C_{29} + *n*–C_{31})). It was introduced as a proxy for the relative contribution of submerged and/or floating macrophytes. Both, the lower (0.2–1.8 m) and the upper part of seam D (2.0–3.0 m) show decreasing upward trends (0.23–0.17 and 0.21–0.17, respectively). It is evident that Paq is higher in seam C (av.: 0.26) than in seam B (av.: 0.18). A negative correlation between TAR and Paq is observed ($r^2 = 0.72$).

The carbon preference index (CPI; Bray and Evans, 1961) is a maturity indicator, but also reflects relative contributions of land plants (Peters et al., 2005). In the studied coals, the CPI is high (1.7–2.6) and shows opposite trends with Paq. Only the CPI of the sample at 1.4–1.6 m in seam C is unusually high.

The average chain length (ACL) of the long–chain *n*–alkanes was calculated according to Poynter and Eglinton (1990) (ACL = (27*n*–C_{27} + 29*n*–C_{29} + 31*n*–C_{31})/(*n*–C_{27} + *n*–C_{29} + *n*–C_{31})) to detect climatic changes. The determined values range from 29.0 to 29.4 (av.: 29.1). No major differences between the different seams exist, although the average values in seam B (29.2) is slightly higher than in seams D and C (29.1).

The *n*–C_{29}/*n*–C_{27} ratio can indicate changes in vegetation (Buggle et al., 2010). It shows two upward increasing trends in seam D (1.62–2.03 and 1.39–1.60, respectively). In seam C, the ratio ranges from 1.29 to 1.75 (av.: 1.44). The *n*–C_{29}/*n*–C_{27} ratio of the lowermost sample in seam B (av.: 2.83) is very high (5.08), but even the remaining

Table 2
Organic geochemistry.

Sample	TAR HC	Paq	CPI	ACL	nC_{29}/nC_{27}	$(C_{31}+C_{33}/(C_{27}+C_{29})$	Pr/Ph	Sesqui–	Di–	Tri–	Cadi	Drim	Phyl clad	Pim	Olean	Arbor	Di–/(Di– + Tri-) terpenoids	Hop	TMN	TetraMN	MP	PAH
								terpenoids														
								(μg/g TOC)			(μg/g TOC)							(μg/g TOC)				
B–1	31.7	0.2	2.1	29.3	2.5	0.9	9.6	478.6	n.d.	452.8	165.9	19.5	n.d.	n.d.	21.1	165.3	n.d.	840.0	32.1	54.5	41.9	528.3
B–3	25.0	0.2	1.9	29.1	1.7	0.8	12.4	750.5	n.d.	448.5	118.1	10.7	n.d.	n.d.	19.7	146.7	n.d.	591.9	124.4	166.3	56.1	902.5
B–5	24.7	0.2	2.0	29.1	2.1	0.8	11.6	374.3	n.d.	318.4	122.5	19.6	n.d.	n.d.	26.3	111.0	n.d.	678.6	43.8	64.9	37.3	384.5
B–7	36.3	0.1	2.6	29.4	5.1	0.9	7.7	353.3	n.d.	514.9	210.7	31.4	n.d.	n.d.	44.5	184.2	n.d.	1277.5	19.3	22.6	40.1	348.7
C–1	14.2	0.3	1.8	29.1	1.3	0.8	13.4	373.0	n.d.	240.5	87.0	8.4	n.d.	n.d.	15.7	75.1	n.d.	387.4	96.1	110.3	33.1	413.8
C–3	20.1	0.2	1.9	29.1	1.7	0.7	12.4	334.5	n.d.	273.1	98.4	14.4	n.d.	n.d.	8.2	85.0	n.d.	443.3	45.2	63.3	20.7	388.6
C–5	18.3	0.2	2.0	29.2	1.4	1.0	13.1	502.5	n.d.	277.2	46.5	3.2	n.d.	n.d.	13.2	84.5	n.d.	298.8	218.3	229.2	84.2	653.0
C–7	14.8	0.2	1.7	29.2	1.4	1.1	13.4	801.2	n.d.	384.9	84.2	5.4	n.d.	n.d.	16.2	129.4	n.d.	378.6	340.7	318.2	80.4	921.4
C–8	13.4	0.3	1.7	29.1	1.6	0.8	12.8	465.5	n.d.	250.8	99.1	9.9	n.d.	n.d.	12.3	89.4	n.d.	408.1	94.3	108.2	26.1	492.4
C–11	14.2	0.3	2.2	29.1	1.3	0.8	11.5	249.2	n.d.	128.8	29.4	4.3	n.d.	n.d.	6.3	41.0	n.d.	418.8	89.2	95.7	34.3	295.9
C–13	22.5	0.2	1.8	29.2	1.5	1.0	13.2	414.6	n.d.	254.1	61.2	3.4	n.d.	n.d.	9.0	88.7	n.d.	345.7	116.4	138.0	45.8	515.9
C–15	13.2	0.3	1.7	29.0	1.4	0.7	13.7	291.0	n.d.	173.8	59.2	6.8	n.d.	n.d.	10.2	58.8	n.d.	290.3	69.5	90.2	29.4	324.6
C–17	10.8	0.3	1.7	29.0	1.3	0.8	14.3	318.6	n.d.	163.8	55.0	6.1	n.d.	n.d.	8.3	54.7	n.d.	301.3	114.2	120.9	35.3	353.5
D–1	41.7	0.2	2.0	29.2	1.6	0.9	12.2	355.4	1.1	324.6	98.9	9.0	0.6	0.5	20.3	108.8	0.003	361.5	42.7	73.4	47.6	401.6
D–3	24.3	0.2	1.9	29.1	1.4	0.8	13.5	437.7	3.0	285.4	88.6	8.2	1.6	1.5	15.6	96.3	0.011	354.5	65.9	104.8	45.9	476.5
D–5	31.3	0.2	2.0	29.0	1.5	0.7	13.1	345.3	n.d.	251.3	92.8	15.7	n.d.	n.d.	10.3	77.1	n.d.	523.3	43.4	71.2	33.7	374.6
D–7	34.7	0.2	2.1	29.1	2.0	0.7	10.3	279.3	n.d.	478.9	145.2	20.8	n.d.	n.d.	17.5	131.2	n.d.	665.3	18.8	22.9	35.4	336.8
D–10	25.5	0.2	2.0	29.2	1.8	0.8	12.4	446.2	26.9	484.2	220.8	28.1	15.9	11.0	24.0	146.3	0.053	679.4	24.5	33.2	27.9	373.6
D–12	27.1	0.2	2.0	29.0	1.7	0.7	12.4	283.6	n.d.	288.3	117.9	17.1	n.d.	n.d.	15.6	74.1	n.d.	476.8	19.4	34.8	24.8	278.3
D–14	21.4	0.2	1.9	29.0	1.6	0.6	12.9	408.2	n.d.	347.7	150.3	18.6	n.d.	n.d.	16.1	98.3	n.d.	507.9	30.9	53.4	34.2	376.7

TAR – terrestrial/aquatic ratio (Bourbonniere and Meyers, 1996), Paq – P–aqueous ratio (Ficken et al., 2000), CPI – carbon preference index (Bray and Evans, 1961), ACL – average chain length (Poynter and Eglinton, 1990), Pr/Ph – pristane/phytane ratio, Cadi – cadinane–type, Drim – drimane–type, Pim – pimarane–type, Abiet – abietane–type, Lup – lupane derivatives, Olean – oleanane derivatives, Urs – ursane derivatives, Arbor – arborane–type, Hop – hopanes, TMN – Trimethylnapthalenes, TetraMN – Tetramethylnapthalenes, MP – Methylphenanthrene, PAH – polycyclic aromatic hydrocarbons, n.d. – not detected.

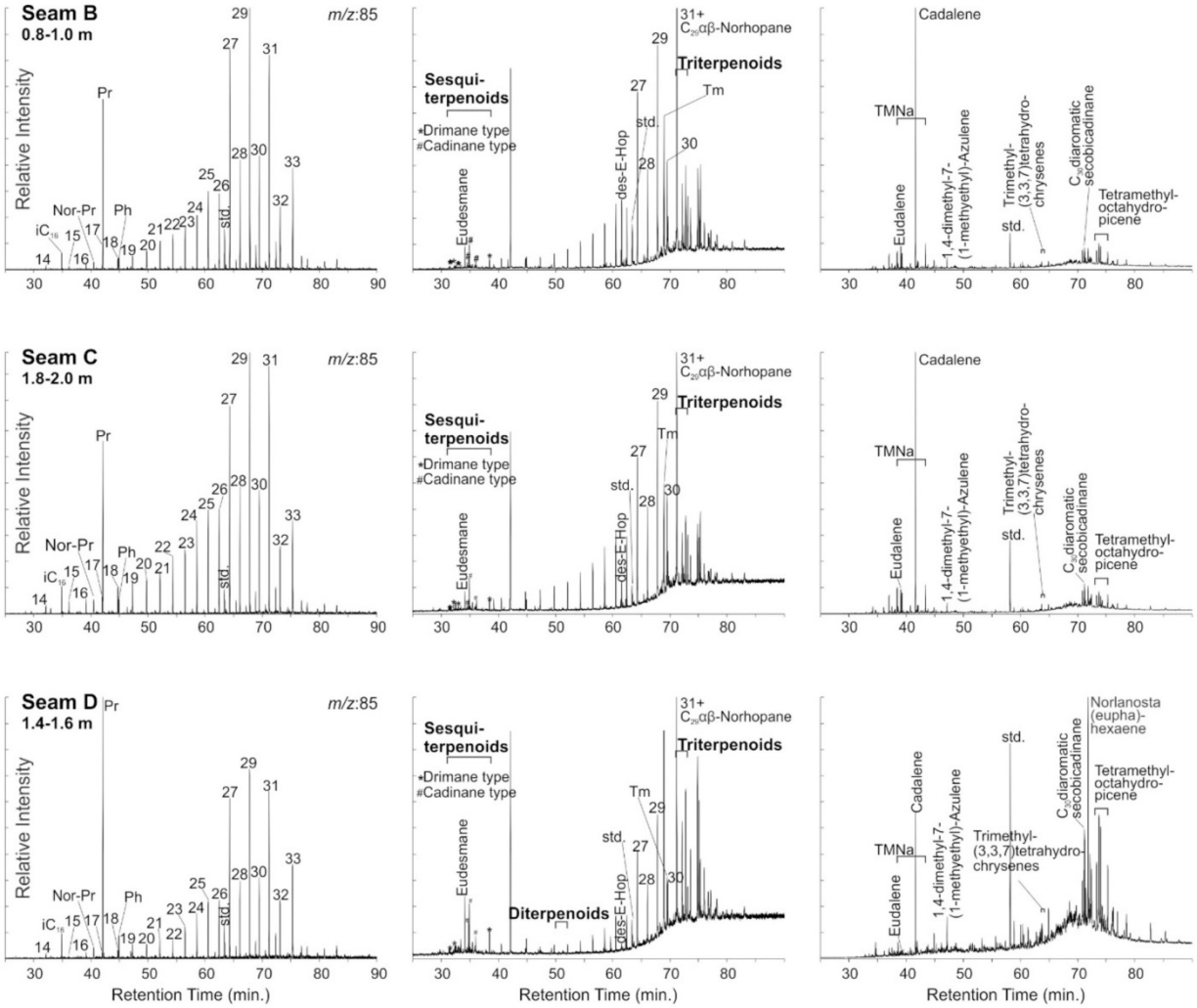

Fig. 6. *M/z* 85 and total ion current (TIC) chromatograms of the aliphatic and aromatic hydrocarbon fractions of selected samples from seam D, C and B. The *m/z* 85 chromatogram shows the distribution of n–alkanes and isoprenoids. Std. standard.

samples have high ratios (1.7–2.5).

The predominant plant species also influence the ratio of (n–C_{31} + $_{33}$)/(n–C_{27} + $_{29}$) (Zech et al., 2009). In the coals studied, the ratio ranges from 0.60 to 1.05. It shows similar trends as ACL. This is reflected by a moderately high correlation coefficient ($r^2 = 0.71$). The ratio of (n–C_{31} + $_{33}$)/(n–C_{27} + $_{29}$) has also the same upward increasing trends in seam D; lower part (0.60–0.83), and upper part (0.69–0.90). Seam C's upper part shows an upward decreasing trend from 1.05 to 0.70, but there is no strong trend in the lower part (0.73–0.98). Seam B has no strong trend (av.: 0.85).

The pristane/phytane (Pr/Ph) ratio is a widely used redox parameter (Didyk et al., 1978), but is also strongly influenced by land plant inputs. Pr/Ph ratios are high (7.7–14.3). The lower and upper parts of Seam D show values that decrease upwards (12.9–10.3 and 13.5–12.2, respectively). Seam C shows no significant trend (11.3–14.3) and has a higher average value (13.1) than seams B (10.3) and D (12.4). A negative correlation exists with CPI ($r^2 = 0.75$).

Among the sesquiterpenoids, a compound-class widely distributed in higher plants, aromatic compounds predominate over aliphatic compounds. They are dominated by cadinane–type (cadinane [Fig. 6], homocadinane; cadinatriene, methyl–cadalene, C_{30}-diaromatic secobicadinane; 29.4–220 μg/gTOC) and drimane–type sesquiterpenoids (drimene, drimane, homodrimane; 3.2–31.4 μg/gTOC).

Gymnosperm-derived diterpenoids were detected only in some intervals from seam D (1.0–1.2 m; 2.4–3.0 m), where saturated pimarane–type (pimarane; 0.5–10.9 μg/gTOC) and phyllocladane–type (α–phyllocladane; 0.6–15.9 μg/gTOC) compounds were observed. Triterpenoids, derived from angiosperms, are present in all sample but only in oleanane derivatives (olean(18)–ene; des–A–seco–noroleana–tetraene; 6.3–44.5 μg/gTOC) and arborane–types (dinor(24,25)arbora(ferna)–5,7,9–triene, dinorarbora(ferna)tetraene, dinorarbora(ferna)pentaene, nor (25)arbora(ferna)pentaene; 40.9–184.2 μg/gTOC). The concentration of triterpenoids in seams D and B is higher than in seam C. Because of the lack of diterpenoids, the di−/(di– + tri–terpenoids) ratio (Bechtel et al., 2003) is mostly 0 and reaches a value of 0.05 only in seam D.

The concentration of different sesquiterpenoids and triterpenoids show positive correlations. The strongest correlation is observed between cadinane– and drimane–type sesquiterpenoids ($r^2 = 0.88$), but cadinane–type sesquiterpenoids also show a positive correlation with oleanane derivatives ($r^2 = 0.61$) and arborane–type triterpenoids (r^2 =

0.67). The correlation between oleanane derivatives and arborane–-triterpenoids yield similar correlation coefficients ($r^2 = 0.68$), whereas the correlations between drimane–type sesquiterpenoids, oleanane derivatives ($r^2 = 0.57$) and arborane–type triterpenoids ($r^2 = 0.45$) are less strong.

The positive correlations reflect similarities in vertical trends. The average concentration of all mentioned landplant–derived components are higher in seam B than in seam C. Seam D occupies an intermediate position. Only diterpenoids are restricted to seam D (Fig. 7).

The concentration of cadinane–type sesquiterpenoids and of arborane–type triterpenoids show strong negative correlations with Paq ($r^2 =$ 0.66 and 0.65, respectively). The positive correlation with the *n*–C_{27}/*n*–C_{29} ratio is less pronounced ($r^2 = 0.53$ and 0.49, respectively). In comparison, the expected positive correlation with TAR is weak ($r^2 =$ 0.38 and 0.37). Whereas the positive correlation between ACL and cadinane–type compounds is weak ($r^2 = 0.21$), the correlation with arborane–type triterpenoids is relatively strong ($r^2 = 0.42$). No good correlation exists between landplant–derived biomarkers and maceral percentages (Table 3).

Steroids occur in concentrations below the detection limit.

Phenanthrene compounds are present in small amounts (0.41–3.88 μg/gTOC) in the upper part of seam D and in seam C, but could not be detected in the lower part of seam D and in seam B. 3–,2–,9–,1– methylphenanthrenes can be observed in all samples (0.95–10.20 μg/gTOC).

Hopanoids in coal are of bacterial origin (Bechtel and Püttmann, 2017). Des–E–hopane is a major compound in seam B, the middle part of seam C, and in low concentrations in the upper part of seam D (3.5–154.3 μg/gTOC). 17α–trisnorhopane (TM; 10.8–191.5 μg/gTOC)

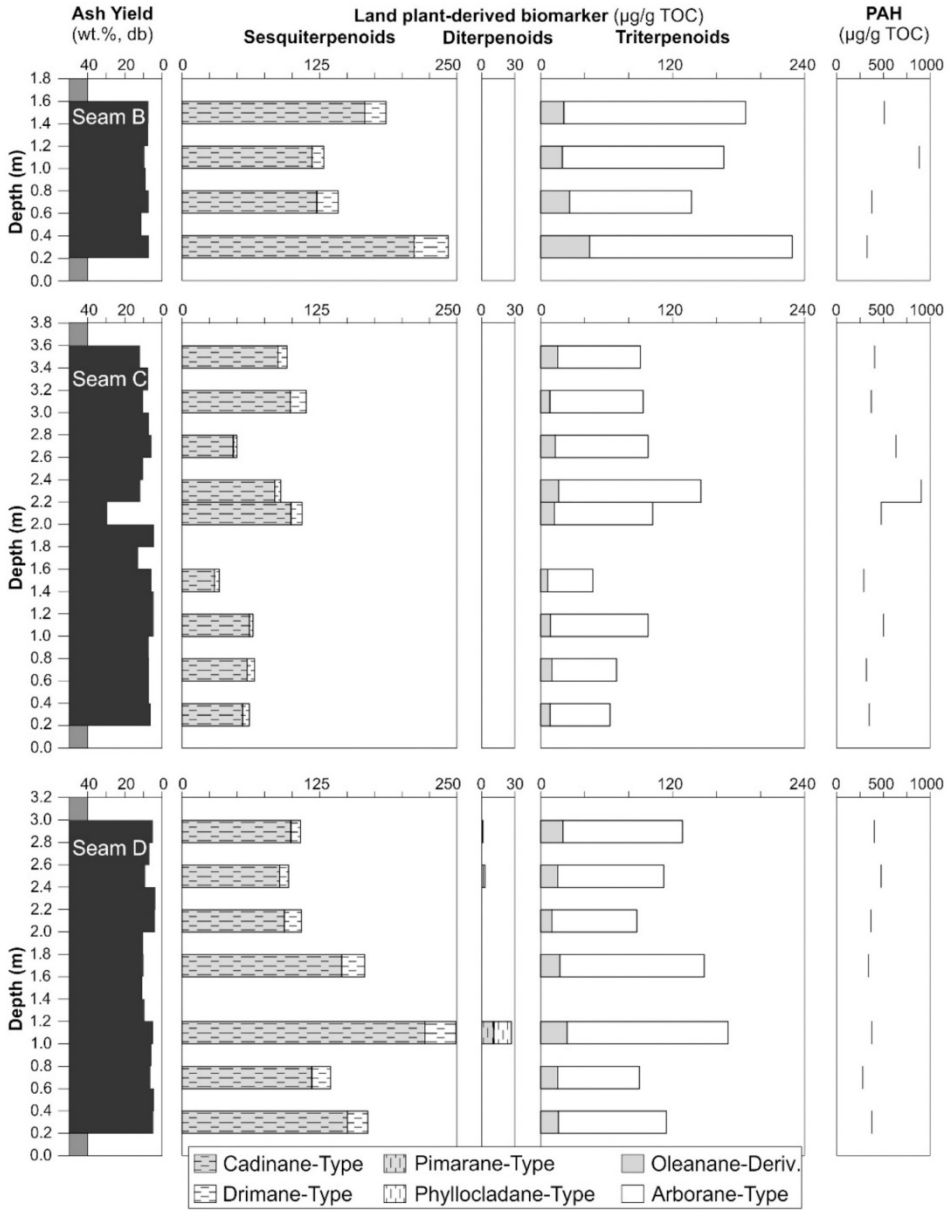

Fig. 7. Variations of land plant–derived terpenoids and polycyclic aromatic hydrocarbons (PAHs) in seams D, C and B.

Table 3
Maceral percentages (in vol%), maceral–based facies indicators (VI, GWI), and random vitrinite reflectance (%Rr).

Sample	Tel.	Coll.	Phyll.	Cld.	Vtd.	Corpogelinite		Liptodet.	Alginite	Resinite		Cutin.	Fluor.	Suber.	Spor.	Exsudat.	Fusinite	Fungi.	Inertodetr.	VI	GWI	% Rr.	Stdev
						in-situ	detr.			in situ	detr.												
B–roof	16.7	0.0	0.0	16.7	66.7	0.0	0.0	0.0	0.0	0.0	0.0	0.0	0.0	0.0	0.0	0.0	0.0	0.0	0.0				
B–1	17.3	7.3	4.0	9.9	8.1	5.0	5.6	15.5	2.0	3.4	5.0	5.0	3.2	1.2	3.8	0.2	1.6	0.8	0.8	0.57	1.36	0.51	± 0.03
B–2	12.5	8.5	3.6	15.3	2.2	4.4	4.6	14.1	2.4	4.4	8.3	8.1	5.6	0.4	2.2	1.2	0.2	1.0	0.4	0.46	2.70		
B–3	17.0	13.6	4.4	12.4	0.8	8.8	8.6	11.8	0.8	3.2	4.2	7.8	3.4	0.6	0.8	0.4	0.0	0.8	0.6	0.78	2.92		
B–4	12.9	12.3	3.0	11.1	3.6	6.7	5.9	12.7	1.0	3.6	8.1	6.1	4.6	1.2	3.0	0.6	0.0	2.8	0.6	0.61	2.66		
B–5	17.8	12.6	4.6	12.4	3.0	4.2	6.2	11.2	0.8	3.8	4.8	8.0	1.8	0.2	4.2	0.6	0.2	1.8	1.6	0.66	2.02	0.52	± 0.03
B–6	17.5	15.9	3.4	13.7	5.0	5.8	5.0	8.8	0.4	5.8	3.8	7.6	1.0	1.6	2.2	0.2	0.2	1.4	0.6	0.91	2.25		
B–7	19.6	14.5	0.6	13.1	6.1	3.2	9.3	16.6	2.0	2.0	3.6	1.8	1.8	1.8	1.6	0.0	0.8	0.6	0.8	0.73	1.82		
B–floor	42.9	0.0	0.0	14.3	35.7	7.1	0.0	0.0	0.0	0.0	0.0	0.0	0.0	0.0	0.0	0.0	0.0	0.0	0.0				
C–roof	46.7	6.7	0.0	6.7	40.0	0.0	0.0	0.0	0.0	0.0	0.0	0.0	0.0	0.0	0.0	0.0	0.0	0.0	0.0				
C–1	6.2	5.6	2.0	18.0	19.2	4.0	9.4	12.8	1.2	3.0	7.6	5.0	0.2	0.0	1.0	0.4	0.0	2.4	1.8	0.24	1.88		
C–2	11.3	9.1	1.6	23.6	9.1	4.4	4.8	13.3	1.2	4.4	3.0	2.4	1.0	1.4	4.4	1.0	0.0	2.6	0.8	0.47	2.39		
C–3	4.4	7.8	0.4	11.5	20.1	7.4	7.2	15.7	1.6	3.2	6.8	1.6	0.0	1.0	6.4	0.4	0.2	3.2	0.8	0.33	1.76	0.56	± 0.04
C–4	11.5	17.6	6.9	16.8	3.6	12.1	3.6	11.3	1.4	1.4	1.8	4.2	3.0	0.0	0.8	0.4	0.0	1.8	1.6	0.77	3.73		
C–5	7.0	21.5	7.0	19.3	3.2	5.8	3.4	13.3	1.6	0.8	3.8	7.0	3.2	0.0	1.2	0.2	0.0	0.8	0.4	0.56	5.40		
C–6	13.3	14.5	1.4	9.0	13.9	6.7	8.6	13.7	0.0	3.9	4.1	3.9	0.2	1.2	2.7	0.2	0.0	2.0	0.8	0.68	1.77		
C–7	12.1	15.4	5.7	19.4	5.3	6.5	5.7	11.9	0.0	2.0	1.4	9.5	0.4	0.2	2.0	0.2	0.0	1.8	0.6	0.58	3.31		
C–8	12.8	9.8	0.4	12.1	18.0	10.0	10.0	11.7	0.0	2.6	5.6	1.7	0.0	1.3	1.3	0.0	0.0	1.3	1.3	0.59	2.22	0.56	± 0.03
C–9	15.5	21.3	6.2	18.3	1.8	6.2	2.0	10.0	0.0	1.2	2.2	7.6	4.6	0.0	0.8	0.2	0.0	1.0	1.0	0.81	3.00		
C–10	9.4	23.7	1.8	18.4	5.3	4.3	6.1	10.6	0.0	1.8	7.3	4.5	0.4	0.4	3.3	0.4	0.2	1.2	0.8	0.68	4.36		
C–11	14.5	16.1	9.3	19.7	1.9	3.1	2.3	9.1	0.4	1.7	2.5	10.6	5.2	0.0	1.0	0.4	0.2	1.2	0.6	0.57	2.84		
C–12	9.4	19.9	9.2	15.8	5.9	1.8	4.9	15.8	2.0	0.2	3.5	7.4	2.3	0.0	0.6	0.2	0.0	0.4	0.2	0.47	3.04		
C–13	13.6	26.0	2.6	13.6	2.4	10.4	4.1	7.7	3.7	1.2	3.5	5.1	1.2	0.0	2.2	0.6	0.0	1.2	0.4	1.11	3.63		
C–14	14.3	14.9	1.2	16.1	7.1	8.7	8.5	9.1	2.8	1.2	4.0	4.2	0.4	0.0	3.0	0.6	0.0	2.4	0.8	0.69	2.57		
C–15	9.6	4.9	1.0	18.7	17.1	5.3	10.0	14.6	2.4	1.6	4.5	3.0	0.0	1.0	2.4	1.0	0.4	1.8	0.2	0.31	1.70	0.58	± 0.04
C–16	23.9	15.7	3.4	13.9	2.2	9.4	4.4	15.3	1.2	1.2	2.4	3.2	1.6	0.0	1.0	0.4	0.0	0.2	0.4	1.02	1.91		
C–17	14.7	18.1	3.4	20.4	3.0	3.0	3.0	18.3	1.8	1.2	6.5	2.8	1.0	0.2	1.0	0.4	0.0	1.0	0.0	0.61	2.84		
C–floor	31.0	2.4	0.0	33.3	33.3	0.0	0.0	0.0	0.0	0.0	0.0	0.0	0.0	0.0	0.0	0.0	0.0	0.0	0.0				
D–roof	5.9	0.0	0.0	0.0	94.1	0.0	0.0	0.0	0.0	0.0	0.0	0.0	0.0	0.0	0.0	0.0	0.0	0.0	0.0				
D–1	13.3	7.6	3.5	23.9	6.7	6.1	4.7	11.5	2.5	1.2	4.1	5.7	2.5	0.0	3.1	1.0	0.2	2.0	0.4	0.41	2.34		
D–2	16.0	6.6	7.6	20.0	10.4	3.4	6.6	10.2	1.2	1.0	3.4	6.0	3.0	0.2	2.2	0.2	0.0	1.2	0.6	0.38	1.63		
D–3	19.2	8.1	3.0	18.2	11.3	4.5	3.6	10.1	2.0	1.8	4.9	4.0	1.0	1.6	4.3	0.4	0.4	0.8	0.6	0.56	1.40	0.60	± 0.05
D–4	17.8	4.4	6.4	21.0	8.8	10.0	4.4	8.4	1.0	1.8	4.2	6.4	2.4	0.0	1.0	0.6	0.0	0.8	0.4	0.53	1.63		
D–5	22.8	6.9	2.6	13.7	10.3	6.3	6.0	12.1	1.4	2.4	5.8	3.6	0.6	0.4	2.2	0.8	0.0	1.8	0.2	0.66	1.10		
D–6	12.0	2.8	0.6	18.1	20.7	5.9	10.5	13.0	1.6	2.6	2.6	2.4	0.0	0.2	2.0	1.2	0.2	2.4	1.0	0.33	1.43		
D–7	21.7	3.8	2.4	19.1	11.7	7.0	5.6	10.3	1.6	1.8	5.8	1.4	0.0	0.2	4.4	1.2	0.8	1.0	0.0	0.57	1.34	0.56	± 0.04
D–8	20.6	16.2	2.2	18.6	13.5	5.7	3.6	7.7	0.8	0.6	3.0	2.4	0.2	0.0	2.4	0.6	0.0	1.2	0.6	0.78	1.57		
D–9	15.2	2.9	0.8	9.9	31.3	4.3	10.9	11.5	1.0	2.5	3.5	0.4	0.0	0.4	2.9	0.8	0.4	1.0	0.2	0.36	0.79		
D–10	17.3	6.5	0.2	13.9	25.8	6.5	10.7	5.0	1.0	3.0	1.6	0.8	0.0	0.4	5.0	0.4	0.4	1.0	0.4	0.53	0.97		
D–11	14.8	4.5	0.4	15.2	20.9	4.7	8.3	16.6	1.6	1.2	3.2	1.2	0.0	0.0	4.9	0.6	0.0	1.2	0.4	0.35	1.06		
D–12	14.5	3.8	0.6	10.1	24.5	13.5	7.6	11.3	0.2	3.6	3.6	1.0	0.0	0.0	4.2	0.4	0.4	0.4	0.2	0.57	1.05		
D–13	21.4	3.2	1.0	9.2	19.2	5.4	12.4	11.0	1.2	0.8	4.0	1.8	0.8	1.2	4.8	0.6	0.2	1.4	0.4	0.49	0.84		
D–14	17.4	5.0	2.8	11.4	22.8	5.6	7.8	9.6	1.4	1.4	3.6	3.0	1.0	0.4	3.2	0.4	0.4	1.8	0.8	0.45	0.85	0.59	± 0.03
D–floor	0.0	3.4	0.0	0.0	93.1	0.0	0.0	0.0	0.0	0.0	0.0	0.0	0.0	0.0	0.0	0.0	0.0	0.0	3.4				

Tel. – telinite, Coll. – collotelinite, Phyll. – phyllovitrinite, Cld. – collodetrinite, Vtd. – vitrodetrinite, Liptodet. – liptodetrinite, Cutin. – cutinite, Fluor. – fluorinite, Suber. – suberinite, Spor. – sporinite, Exsudat. – exsudatinite, Fungi. – funginite, Inertodetr. – inertodetrinite, VI – vegetation index, GWI – groundwater index. Stdev – standard deviation.

and C_{29}–αβ–norhopane (82.6–215.9 μg/gTOC) are aliphatic compounds that occur in significant concentrations in all seams. Concentration of monoaromatic hopanoids and benzohopanes range from 14.4 to 56.3 μg/gTOC.

The presence of trimethylnaphthalenes (TMN) indicate angiosperm input (Roland et al., 1984). Concentrations of TMN range from 18.8 μg/g TOC to 340.7 μg/g TOC.

PAHs, compounds which are formed during wildfires, are abundant (278.3–907.3 μg/gTOC) in all samples (Fig. 7). Aromatic compounds of dibenzofuran, cadalene, dimethyl–methylethyl–azulene, fluoranthene, benzo(*a*)anthracene, methyl–chrysene, trimethyl–tetrahydro–chrysene, and tetramethyl–octahydro–picene contributed to the presence of PAHs.

5.3. Maceral composition and vitrinite reflectance

Photomicrographs of typical macerals in coal from the TAJ mine are shown in Figs. 8 and 9. Maceral percentages are listed in Table 3 and plotted versus depth in Fig. 10.

Vitrinite is the prevailing maceral group in all samples (51–81 vol%). Liptinite occurs in substantial amounts (17–47 vol%), while inertinite is rare (0.8–4.2 vol%). The average vitrinite percentages decreases from seams D (72 vol%) and C (68 vol%) to seam B (60 vol%). In contrast, average liptinite percentages increase upwards from seams D (26 vol%) and C (29 vol%) to seam B (37 vol%). Inertinite percentages do not show differences between the seams.

Vitrinite is dominated by telovitrinite (Fig. 8a,b) and detrovitrinite (Fig. 8c,d). In seams D and B, the percentage of telinite is higher than that of collotelinite, but collotelinite is more abundant than telinite in most seam C samples (Fig. 10). With regard to detrovitrinite, percentages of gelified collodetrinite exceed those of ungelified vitrodetrinite, except in the lower part of seam D, where vitrodetrinite dominates over collodetrinite. Both, *in–situ* corpogelinite (Fig. 8c,d) and attrital corpogelinite (Fig. 8e,f) are equally distributed in each seam. Phyllovitrinite (Fig. 8g,h) occurs in substantial amounts in all seams. Random vitrinite

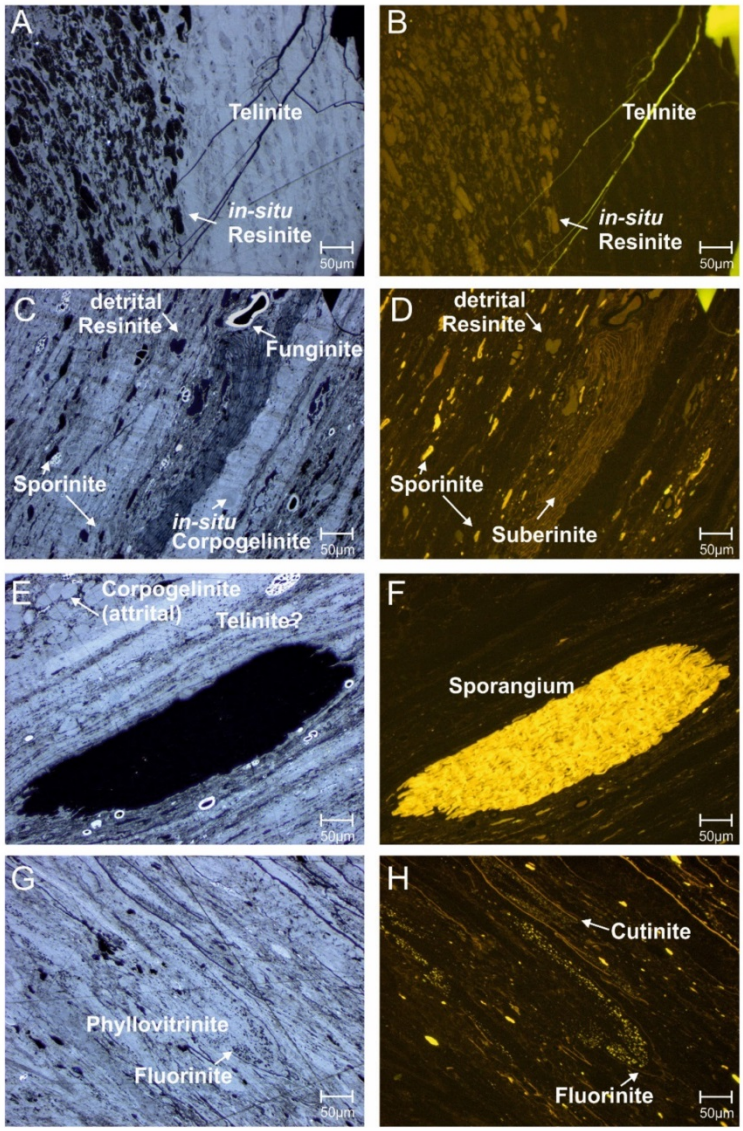

Fig. 8. Representative photomicrographs of coal samples. Left: white light; right: fluorescence light.
a,b) Seam C (2.0–2.2 m); Telinite with *in–situ* resinite.
c,d) Seam C (3.2–3.4 m); Coal with various liptinite macerals (resinite, sporinite, suberinite), corpogelinite, and funginite.
e,f) Seam C (0.4–0.6 m); Sporangium.
g,h) Seam B (0.4–0.6 m); Leaf–derived macerals (fluorinite, cutinite, phyllovitrinite).

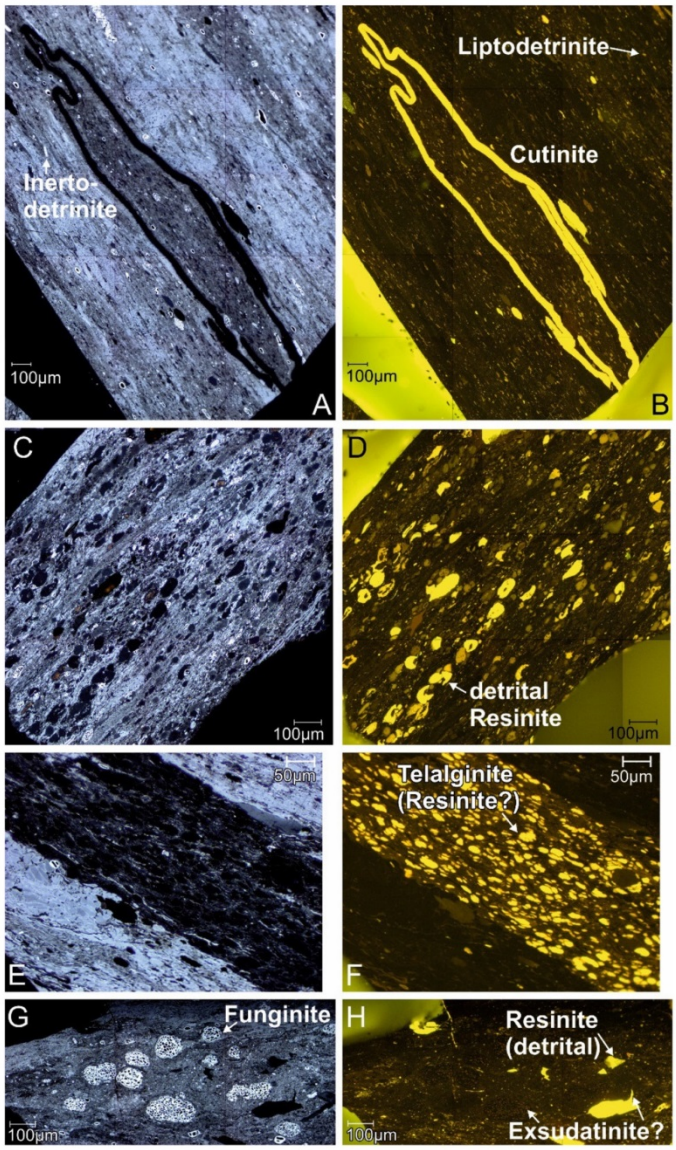

Fig. 9. Representative photomicrographs of coal samples. Left: white light; right: fluorescence light.
a,b) Seam C (3.2–3.4 m); Large cutinite in detrital coal matrix.
c,d) Seam C (0.4–0.6 m); Detrital resinite. Strongly varying fluorescence intensities indicate chemical variation due to different origin of the resins or varying weathering conditions.
e,f) Seam D (2.6–2.8 m); Thin layer rich in telalginite.
g,h) Seam D (1.4–1.6 m); Large funginite bodies in a matrix with detrital resinite.

reflectance increases downwards from the upper seam B (0.52 ± 0.03% Rr) to the middle seam C (0.57 ± 0.04%Rr) and reaches 0.59 ± 0.04%Rr in the lower seam D (Table 3).

Liptinite is the second most abundant maceral group. It is dominated by liptodetrinite (Fig. 9a,b; 5.8–18.3 vol%), which shows an upward increase in seam B (Fig. 10). Resinite is also abundant (3.8–18.3 vol%). It occurs *in–situ* (within telovitrinite; Fig. 8a,b), detrital (associated with detrovitrinite; Fig. 8c,d; Fig. 9c,d), and as the resinite variety fluorinite (Fig. 8g,h). Detrital resinite is typically more abundant than *in–situ* resinite (Fig. 10). Resinite (*in–situ* + detrital) shows a weak positive correlation with HI ($r^2 = 0.49$).

Cutinite (Fig. 8g,h; Fig. 8a,b) occurs in strongly varying, but often high percentages (0.4–10.6 vol%; Fig. 10). In seam D cutinite percentages decrease upwards in the lower part (0.2–1.2 m) and increase upwards in the middle and upper part (1.2–3.0 m). In seam C, cutinite percentages increase upwards in the low-ash lower part (0.2–1.6 m).

Sporinite (Fig. 8c,d) is present throughout the seam (0.6–6.4 vol%). Sporangia were observed in some samples from seams D and C (Fig. 8e, f). Alginite is present in low amounts (max. 2.6 vol%), except in the interval from 1.6 to 2.4 m in seam C; Fig. 10). Lamalginite is more abundant than telalginite (Fig. 9e,f). Suberinite (Fig. 8c,d) is present in all samples from seam B, albeit in low percentages (max. 1.8 vol%). Many seam D and C samples do not contain suberinite. Exsudatinite (up to 1.2 vol%) forms fillings of cavities in funginite or cracks (Fig. 8c,d; Fig. 9g,h).

Inertinite percentages are generally low (av.: 2 vol%). Funginite (Fig. 8c,d; Fig. 9g,h) is the dominant inertinite maceral (up to 3.2 vol%). Inertodetrinite (Fig. 9a,b) occurs in low percentages (max. 1.8 vol%). Pyro– and degradofusinite are very rare (max. 1 vol%). The distributions of inertinite macerals do not show clear vertical trends. Only the percentage of funginite increases upwards in the lower part of seam B (0.2–1.0 m; Fig. 10).

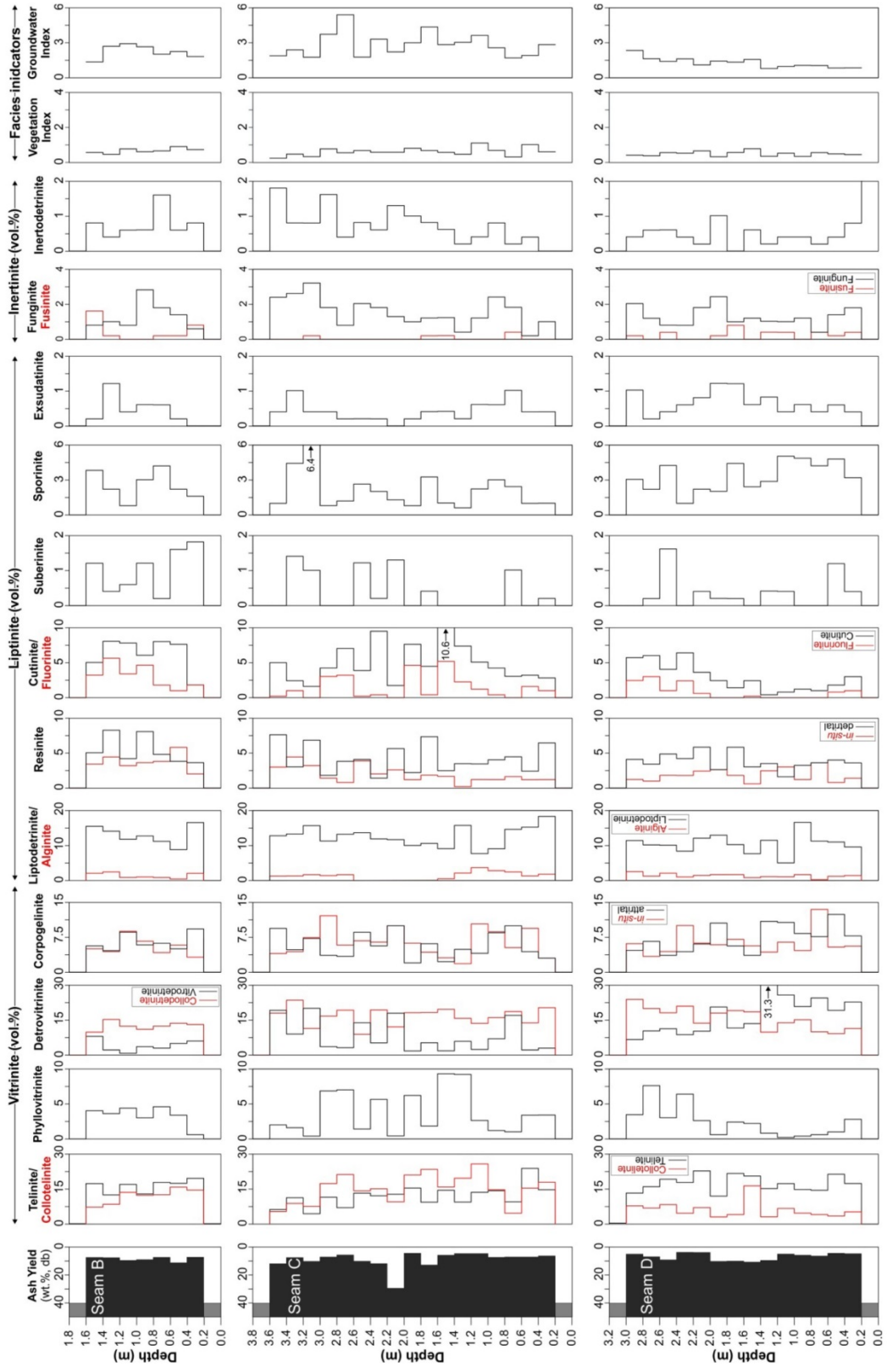

Fig. 10. Variations of maceral percentages and petrography–based facies indicators in seams D, C and B.

6. Discussion

6.1. Maturity

A slight increase of random vitrinite reflectance from the upper seam B (0.52%Rr) to the lower seam D (0.59%Rr) can be observed. Considering the limited thickness of the stratigraphic interval (<100 m; Fig. 1b), it is questionable, if this increase reflects a maturity trend. In any case, no trend is visible in average Tmax, which is 427 °C is seam B and 425 °C in seams C and D. Vitrinite reflectance shows that the coals reached the subbituminous A or high volatile bituminous C coal stage. Low maturity is also indicated by high CPI values of 1.7–2.6 (Tissot and Welte, 1984).

The moisture content is surprisingly low for the given rank, considering that the moisture content at the transition from high volatile bituminous C to B coals is often in the range 8 to 10 wt% (Stach et al., 1982). Moisture contents are related to overburden pressure (e.g., Kothen and Reichenbach, 1981), but may be influenced by tectonic pressure as well (e.g., Teichmüller and Teichmüller, 1975; Gruber and Sachsenhofer, 2001; Holdgate, 2005). Considering the position of the mine close to the thrusted front of the Meratus Complex (Fig. 1a), tectonic pressure is considered a likely explanation.

6.2. Rheotrophic versus ombrotrophic and freshwater versus brackish peat formation

Rheotrophic (low–lying) and ombrotrophic (domed) mires are widespread in SE Asia. Peat accumulation in rheotrophic and ombrotrophic mires has also been suggested for Miocene coals in the Barito Basin (e.g., Demchuk and Moore, 1993; Fikri et al., 2022). Here, we use ash yields and sulphur contents to assess the mire–type of the studied Eocene coals. In following sections, the peat types are characterized in more detail on the basis of biomarker and petrographic evidence.

Ash yields range from 3.7 to 12.8 wt%, with the exception of one shaly coal layer in seam C (29.5 wt% ash). Ash yields <5 wt%, which would be consistent with a possible origin in ombrotrophic mires, are observed in seam D (0.2–0.6 m; 2.0–2.4 m) and seam C (1.0–1.4 m; 1.8–2.0 m). However, the main parts of seams D, C, and B are interpreted to have accumulated in rheotrophic mires based on their higher ash yields. Peatlands influenced by brackish/marine waters are characterized by high sulphur contents (e.g., Casagrande, 1987). Hence, the low sulphur content (<<1.0 wt%) shows that the mires were effectively protected from any marine influence, not only during possible ombrotrophic stages, which by definition are only rain fed, but also during the dominant rheotrophic stages, despite of the general coastal plain setting (Witts et al., 2012). Similar present-day settings were described by Cameron et al. (1989) and Staub and Esterle (1994).

Pollen and spores were not examined in the present study. Elsewhere, regular mangrove elements (e.g., *Nypa, Florchuetzia* spp.) were reported from Tanjung coals, apart from freshwater palm pollen (Witts et al., 2012; Morley, 2013). Thus, the presence of brackish water elements in the studied coals is not impossible. In this case, their occurrence within the palynology data probably would indicate transport from nearby mangrove areas. Within this context it is worth noting that higher sulphur contents (up to 1.2 wt%), consistent with brackish floor or roof rocks, were reported from coals east of the Meratus Complex (Moore and Ferm, 1992).

The sulphur contents in seam D vary upward in a characteristic manner, so that further conclusions about the peat facies are possible. Very low sulphur contents in the lower low–ash part (0.2–1.2 m; av.: 0.41 wt%) are compatible with an ombrotrophic environment, although an origin in a rheotrophic mire protected from detrital input also seems possible. The middle part (1.2–2.0 m) contains higher sulphur contents (av.: 0.54 wt%) and has a higher ash yield (av.: 10.1 wt%). This indicates a change to wetter, certainly rheotrophic conditions at 1.2 m. The highest sulphur contents are observed in the upper part of seam D (2.0–2.8 m), where they show a clear upward increase. This suggests progressing dilution of humic acids due to a rise in water table and that peat accumulation ended due to a transgressive event. A brackish influence was reported for the upper part of a coal seam in the Tanjung Formation by Dettman and Playford (in Morley, 2013). The low sulphur content, which does not exceed 0.9 wt% in seam D, speaks against a brackish influence at the study site. A similar (subtle) upward increase in sulphur contents can be observed in the upper part of seam B (0.8–1.6 m), presumably reflecting that accumulation of seam B also ceased due to a transgression.

6.3. Nature of peat–forming vegetation as recorded by geochemical data

The almost complete absence of diterpenoids (Fig. 7) shows that the peat–forming vegetation was dominated by angiosperms (cf. Bechtel et al., 2003). This is in accordance with palynological data (Morley, 2013). Therefore, differences in *n*–alkane patterns, isoprenoids, sesqui– and triterpenoids provide information on changes in angiosperm vegetation.

6.3.1. N–alkanes and isoprenoids

The very high TAR values (>10) and the low Paq ratios (<0.35) show the expected predominant role of land plants (Bourbonniere and Meyers, 1996; Ficken et al., 2000). Relatively low TAR and high Paq values near the base of seam D and in the entire seam C may reflect enhanced contribution of aquatic macrophytes (e.g., Ficken et al., 2000; Ronkainen et al., 2013) and/or of algal material (e.g., Silliman et al., 1996; Ortiz et al., 2013). However, alginite is absent in the middle part of seam C (Fig. 10).

High CPI values (1.7–2.6) are another consequence of the predominant land plant input. In accordance with the above findings, CPI is slightly lower in seam C than in seams D and B.

The average chain length of long–chain *n*–alkanes (ACL) has been used to reconstruct changes in temperature and/or aridity (e.g., Poynter and Eglinton, 1990; Schouten et al., 2007). However, Hoffmann et al. (2013) found that ACL gives contradictory results for different plant species. No significant changes between the mean ACL values of the three seams can be observed, but strong negative correlations exist between ACL and Paq in seams D ($r^2 = 0.88$) and B ($r^2 = 0.97$). This indicates that variations are largely controlled by the input of aquatic macrophytes. In seam D, ACL shows a strong negative correlation ($r^2 = 0.96$) with the percentage of cutinite and fluorinite suggesting low ACL values are related to samples with high percentages of leaf-derived macerals. However, no such correlation exists in the other seams.

The relative abundance of long–chain *n*–alkanes (*n*–C_{27} to *n*–C_{33}) is also determined by plant groups (Schwark et al., 2002; Zech et al., 2009; Diefendorf et al., 2011). To quantify variations between different trees and the relative proportion of herbs and grasses, the *n*–C_{27}/*n*–C_{29} ratio and the *n*–C_{31+33}/*n*–C_{27+29} ratio were calculated, respectively. The *n*–C_{27}/*n*–C_{29} ratio shows similar trends like ACL. The sample with the highest CPI shows also the highest *n*–C_{27}/*n*–C_{29} ratio. The *n*–C_{31+33}/*n*–C_{27+29} ratio suggests a significant contribution of herbs to the vegetation in the upper part of seam C, but with an upward decreasing trend.

The observed high Pr/Ph ratios (7.7–14.3) are typical for coals (Brooks et al., 1969; Powell and McKirdy, 1973). Strong negative correlations with CPI ($r^2 = 0.75$) and the *n*–C_{27}/*n*–C_{29} ratio ($r^2 = 0.74$) suggest that Pr/Ph ratios reflect different plant communities, rather than redox conditions.

6.3.2. Land plant derived terpenoids

Cadinane–type sesquiterpenoids and arborane–type triterpenoids predominate among the land plant–derived terpenoids. The highest concentrations of cadinane–type sesquiterpenoids (>100 μg/gTOC) occur in the lower part of seam D and in seam B.

Cadinanes (incl. diaromatic secobicadinane) in recent peatlands and Miocene coals in SE Asia are related to dammar resin produced by the

angiosperm family Dipterocarpaceae (e.g., Anderson, 1964, 1983; Anderson and Muller, 1975; Esterle and Ferm, 1994; Esterle et al., 1987, 1989; Cameron et al., 1989; Page et al., 1999; Wüst et al., 2001; van Aarssen et al., 1990, 1994; Morley, 2013; Niyolia et al., 2019). In contrast, the origin of cadinanes (incl. diaromatic secobicadinane) in Eocene coals is less clear, since the oldest dipterocarp fossils in SE Asia come from Oligocene sediments in Borneo (Dutta et al., 2011). Moreover, pyrolysis experiments performed by Stankiewicz et al. (1996) showed that resinite from an Eocene coal in the Tanjung Formation did not produce cadinane compounds. This is also supported by the lack of correlation between resinite and cadalene ($r^2 = 0.03$). Nevertheless, a dammar-resin origin cannot be completely excluded. This is because a land connection between the Indian and Asian plates was already established in the Middle Eocene (Rowley, 1996; Dutta et al., 2011), which could have enabled the migration of dipterocarps from India to Borneo. Alternative potential sources for cadinanes include conifers (e.g., Bechtel and Püttmann, 2017 cum lit.), but palynological data (Morley, 2013) and the almost complete absence of gymnosperm–derived diterpenoids excludes this source. A strong positive correlation ($r^2 = 0.88$) between cadinane–type and drimane–type sequiterpenoids suggests a similar source, but drimane–type sequiterpenoids have been identified in various land plants and may also originate from fungi (e.g., Huang et al., 2021).

The distribution of arborane/fernane–type triterpenoids is more homogenous than that of cadinanes. Arborane/fernane–type triterpenoids are attributed to ferns or bacteria (e.g., Hauke et al., 1992, 1995). Ferns are important components of the Eocene vegetation in SE Asia (Moore and Ferm, 1992; Morley, 2013). Therefore, a fern source is considered likely. The total sum of land plant–derived biomarkers and the arborane/fernane to cadinane ratio are lower in seam C than in seams B and D. Together with the relatively low TAR and high Paq values, this suggests a more open, herbaceous vegetation during accumulation of seam C.

6.4. Petrography and mire types

This section first discusses the significance of specific macerals for the reconstruction of peat facies. Subsequently, petrography–based parameters are used to obtain information about the original vegetation and the height of the water table.

Phyllovitrinite, cutinite, and fluorinite are leaf–related macerals. The percentages of these macerals are positively correlated with high correlation coefficients in seams D ($r^2 = 0.79–0.86$) and C ($r^2 = 0.69–0.79$). Only the sample at 2.2–2.4 m in seam C contains unusually high amount of cutinite (9.5 vol%), but little fluorinite (0.4 vol%). In seam B, the amounts of fluorinite and phyllovitrinite ($r^2 = 0.03$) are not related.

The sum of leaf–related macerals varies strongly from 1.0 to 25.1 vol % and shows simple, but different stratigraphic trends in different seam. In the lower low–ash part of seam D (0.2–1.2 m), the percentage of leaf–related macerals decreases gradually upwards from 6.8 vol% to 1.0 vol%. In the upper part of seam D (1.2–3.0 m) the percentage of leaf–related macerals increases upwards and reaches a maximum of 16.6 vol % near the top of the seam. In seam C, the amount of leaf-derived macerals increases upwards in the lower part (0.2–1.6 m) to a maximum of 25.1 vol%, while leaf- and wood-rich intervals alternate in the upper part (1.6–3.6 m). Seam B contains the highest proportion of leaf–related macerals with an average of 12.8 vol% (max. 17.3 vol%). In contrast to seam D, percentages of leaf–related macerals increase upwards in the lower part and decrease only in the uppermost sample.

Sporinite percentages are generally low (max. 6.4 vol% in the upper part of seam C). Some sporinite in seams D and C occurs in sporangia (Fig. 8e,f). Probably, these sporangia were formed by ferns (cf., Noblin et al., 2012; Guatame and Rincón, 2021).

Botryococcus–related telalginite (Fig. 9e,f) is present in trace amounts in Eocene coals in SE Asia (e.g., Hutton et al., 1994; Amijaya and Littke, 2005) and proves subaquatic deposition.

The proportion of inertinite macerals (except funginite) is very low. This indicates that wildfires were very rare and that oxidation at the peat surface was strongly limited. Even against the background of an ever–wet climate, the very low inertinite percentages are surprising.

Funginite is the dominant inertinite maceral (0.2–3.2 vol%). It occurs as unicellular spherical bodies and multicellular, highly vesicular, objects. The size of funginite ranges from <50 μm (Fig. 8c,d) to 100 μm (Fig. 9g,h). The dominant role of funginite in Eocene coals, its structure and wide size range was already noted by Moore and Ferm (1992). Obviously fungal activity played a major role during the decay and decomposition of dead plants (Adaskaveg et al., 1991; Hower et al., 2011a, 2011b).

Various maceral–based facies indicators are widely used to determine peat facies (e.g., Diessel, 1986; Calder et al., 1991; Kalkreuth et al., 1991; Markic and Sachsenhofer, 1997). However, a poor fit between petrographic, palynological, and geochemical data has often been reported (e.g., Wüst et al., 2001; Moore and Shearer, 2003; Dai et al., 2020; Fikri et al., 2022). Nevertheless, their application is useful, if the critical interpretation considers all available non-maceral data and the fact that petrographic data reflect both changes in primary vegetation and degradation processes leading to homogenization of the precursor plant material (Demchuk and Moore, 1993; Wüst et al., 2001; Moore and Shearer, 2003; Fikri et al., 2022). In the present paper, the vegetation index (VI) and the groundwater index (GWI) of Calder et al. (1991) are applied (Table 3; Fig. 10). These parameters have been invented for Pennsylvanian coal, but seem applicable for coals of different age, as long as trends and not absolute values are considered.

The VI is the ratio between preserved tissues and detrital macerals and considered a proxy for the proportion of decay–resistant plants. In the applied formula, phyllovitrinite is included in the denominator to identify opposing trends between more leaf- and the wood-dominated associations.

VI = (vitrotelinite + phlobaphinite (*in–situ*) + fusinite + suberinite + resinite (*in–situ*)) / (phyllovitrinite + detrovitrinite + phlobaphinite (attr.) + gelinite + inertodetrinite + sporinite + cutinite + liptodetrinite + fluorinite + resinite (detr.) + alginite).

The GWI is the ratio of mineral matter plus gelified macerals to ungelified macerals and is considered to record the wetness of the peat (Calder et al., 1991).

GWI = (collotelinite + collodetrinite + collinite + mineral matter*) / (telinite + vitrodetrinite).

* Mineral matter (mm) has been calculated using the formula of Parr (1928) (mm = [1.08 x ash] + [0.55 x sulphur]).

The vegetation index (VI) is generally very low (0.24–1.11; av.: 0.58) reflecting strong degradation of the precursor plant material and the high amount of leaves. Strong degradation is also supported by the nonbanded character of the coals. This confirms results of Moore and Ferm (1992), who postulated strong degradation of palms and ferns in Eocene coals based on the size of organic particles. VI shows vertical variations in all three seams. These variations cannot be correlated with any geochemical parameters.

In contrast to VI, the groundwater index (GWI) is generally high (0.79–5.40; av.: 2.16). The lowest GWI values (av.: 0.96) occur in the lower part of seam D, which might have been formed in an ombrotrophic mire (0.2–1.2 m). Between 1.2 and 3.0 m, GWI values increase upward, reaching a maximum value of 2.34 at the top of the seam (Fig. 10). This supports the transgressive trend based on sulphur contents postulated above (cf. Fig. 4).

The highest GWI values (av.: 2.84) and ash yields are observed in seam C. Despite the very low sulphur contents (av.: 0.33 wt%) in seam C, the high GWI and ash yields up to 29.5 wt% suggest a rheotrophic mire with relatively high-water level, which became flooded from time to

time. This interpretation is supported by *n*–alkane ratios (low TAR, high Paq; Fig. 5) indicating an elevated contribution of aquatic plants (see above) and relative low concentrations of land plant–derived biomarkers (see Fig. 7).

On average, the GWI in seam B is lower (2.25) than in seam C indicating peat accumulation in a rheotrophic mire with a lower or more fluctuating water level. A slightly lower ash yield in seam B reflects a lower extent of flooding. Relatively dry conditions during deposition of seam B are reflected by high TAR and low Paq ratios (Fig. 5) and by high concentrations of land plant–derived biomarkers (Fig. 7).

Overall, maceral–based facies indicators for the Eocene coals agree reasonably well with the geochemical and biomarker data, which contrasts with the observations of Fikri et al. (2022), who found poorer agreement for the Miocene coals in the Barito Basin. Probably this is due to the origin of the latter in ombrotrophic mires.

6.5. Comparison of Eocene and Miocene coal in the Barito Basin

For comparison to the Miocene, we used coals from the Warukin Formation in the Tutupan mine in the northern part of the Barito Basin (Fig. 1a). Middle Miocene coals from this mine were characterized by Fikri et al. (2022) using similar geochemical and petrographic proxies as applied to Upper Eocene coals in the present work. In addition, the rank of the Miocene coal (subbituminous C) is only slightly lower than that of the Eocene coal (subbituminous A). This allows the comparison of peat facies and the petrographical and geochemical composition of Eocene and Miocene coals (Table 4; Fig. 11).

Although a tropical, ever–wet climate prevailed during both Eocene and Miocene coal accumulation (e.g., Morley, 2012; Friederich et al., 2016), major differences exist between seam geometries and interpreted palaeo peat types. Both mines contain three economic seams with large lateral extent. However, while single Miocene seams are >20-m thick (max. 50 m), the thickness of Eocene coals is typically much lower (up to 5-m at the study location; up to 10-m east of the Meratus Complex; Moore and Ferm, 1992). Geochemical data provides evidence that the large thickness of Miocene seams is the result of stacking of single coal cycles. For example, five stacked cycles (T110–1 to T110–5), each 6 to 13 m thick, were identified in the lower seam T110 in the Tutupan mine and may be controlled by climate cycles (Fikri et al., 2022). The much thinner Eocene seams show some simple parabolic depth trends, but evidence for stacking of individual cycles is missing. The parabolic depth trends are particularly pronounced in seam B (e.g., sulphur content; Fig. 4; *n*-alkane ratios; Fig. 5; leaf-derived macerals; Fig. 10), but are also visible in seam D. In the latter seam, only *n*-alkane ratios may indicate two cycles.

Miocene coal in the Tutupan mine accumulated in ombrotrophic mires (seams T110, T210) or in mixed ombrotrophic/rheotrophic freshwater mires (upper seam T300). In contrast, Eocene coal accumulated mainly in rheotrophic low–lying mires, although short ombrotrophic intervals cannot be excluded. Although palynological studies indicate a brackish influence in the upper part of some Eocene coals, based on sulphur contents, a marine/brackish influence cannot be observed in the Eocene coal from the TAJ Pit–1D mine.

Palynological investigations showed that the precursor vegetation of Eocene and Miocene coals differs significantly. A palm and fern dominated vegetation has been postulated for Eocene coals, while Miocene coals were formed by predominating angiosperm trees, including dammar resin–producing dipterocarps (e.g., Moore and Ferm, 1992; Morley, 2013). The presence of gymnosperms, albeit at lesser extent, has been determined by diterpenoid biomarkers. This indicates that formation of the Tutupan coal occurred in a kerapah (watershed) type peat.

Differences in *n*–alkane based parameters must be evaluated with caution as they may be influenced by the (small) differences in maturity. For example, lower CPI values in Eocene coal (av.: 2.0) than in Miocene Tutupan coal (T110, T210: av.: 4.3; T300: av.: 3.1) may reflect the combined effects of stronger degradation of plant material in rheotrophic settings (e.g., Zech et al., 2009; Buggle et al., 2010; Naafs et al., 2019) and of the higher maturity of the Eocene coal. Other *n*–alkane based parameters vary considerably between Eocene rheotrophic and Miocene ombrotrophic to rheotrophic seams and do not exhibit systematic variations.

Maceral analysis shows that resinite (*in situ* and attrital) is an important constituent in all coals and is slightly more abundant in Eocene coals (6.5 vol%) than in Miocene coals (~4 vol%). In Miocene Tutupan coal, dammar resin, reflected by cadinane–type biomarkers, is present. In contrast, cadinane–type biomarkers in Eocene coal have a different (non–dammar) source (see also Stankiewicz et al., 1996).

Leaf–derived macerals are abundant in Eocene and Miocene coals. Because phyllovitrinite was not counted separately in Tutupan coals, the maceral percentages in Table 4 refer only to cutinite and fluorinite.

Table 4
Summary of similarities and differences between Eocene and Miocene coals in the Barito Basin.

	Eocene (TAJ Pit—1D) This study	Miocene (Tutupan Mine) Fikri et al. (2022)	
Rank	Subbituminous A	Subbituminous C	
Climate (Friederich et al., 2016)	Tropical ever–wet	Tropical ever–wet	
Number of economic seams	3	3	
Lateral continuity	high	high	
Seam names	D, C, B	T110, T210	T300
Thickness of single seams	up to 5 m	up to 50 m	24 m
Stacked successions (cycles)	no	yes (up to 5)	unclear (2?)
Peat–type	rheotrophic	ombrotrophic (kerapah)	ombro– + rheotrophic
Marine/brackish influence	—	—	—
Vegetation (Moore and Ferm, 1992; Morley, 2013)	Palms/ferns	Angiosperm trees (e.g., Shorea) (+gymnosperms)	
Gymnosperms (Di–/(di – +Tri–) Terpenoids)	largely missing	rare	very rare
CPI	2.0 (1.7–2.6)	4.3 (2.8–6.2)	3.1 (2.2–3.8)
TAR	23.3 (10.8–41.7)	10.4 (5.8–23.4)	19.9 (6.0–38.4)
Paq	0.22 (0.12–0.33)	0.14 (0.05–0.24)	0.08 (0.05–0.11)
ACL	29.1 (29.0–29.4)	29.1 (28.2–30.6)	29.5 (29.0–30.0)
n–C_{29}/n–C_{27}	1.79 (1.29–5.08)	1.39 (0.77–2.33)	3.14 (2.09–4.83)
(n–C_{31} + n–C_{33})/(n–C_{27} + n–C_{29})	0.81 (0.60–1.05)	0.85 (0.17–2.23)	0.67 (0.46–0.91)
Pr/Ph	12.3 (7.7–14.3)	12.8 (5.4–23.6)	6.1 (3.9–8.1)
Degradation (Vegetation Index)	High (0.56)	Low (1.56)	Low (1.26)
Water table (GWI) / extent of external influx	low–high (av.: 2.16)	Low (0.17)	Low (0.32)
Resins (*in–situ* + detrital; vol%)	Abundant 6.5 (3.2–12.7)	Abundant 4.1; 1.0–19.1)	Abundant 4.0 (0.8–9.0)
Cadinane–source	Non–dammar?	Dammar resin (dipterocarps)	Dammar resin (dipterocarps)
Leafs (cutinite+fluorinite; vol%)	abundant 6.0 (0.4–15.7)	abundant 4.8 (0.4–13.1)	abundant 3.8 (0.6–8.5)
Roots (suberinite; vol%)	rare 0.5 (0.0–1.8)	abundant 2.6 (0.2–7.0)	abundant 2.0 (0.4–4.6)
Alginite	low (incl. *Botryococcus*)	–	traces
Fungal activity (funginite; vol%)	high 1.4 (0.2–3.2)	high 1.0 (0.0–3.2)	high 1.5 (0.6–2.8)
Inertinite (excl. Funginite; vol%)	0.9 (0.0–2.4)	2.1 (0.0–4.0)	2.3 (0.6–5.0)

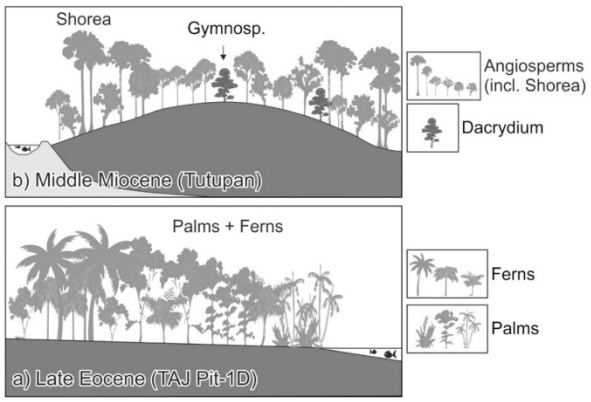

Fig. 11. Cartoons showing a) Eocene (TAJ Pit—1D) and b) Miocene (Tutupan) peat forming environments. Vegetation according Moore and Ferm (1992) and Morley (2013).

Slightly higher percentages of leaves in Eocene coals may be related to the palm– and fern–dominated vegetation. Differences in vegetation are also reflected by a significantly lower fluorinite/cutinite ratio in Eocene coals (av.: 0.29) than in Miocene coals (av.: 1.29). In addition, different stratigraphic trends are observed in Eocene and Miocene coal seams. Eocene seams show either an upward increasing (seams D, C) or decreasing (seam B) trend in their lower part, which is reversed in the upper part of seams D and B, producing the above described parabolic trends. Only the upper part of seam C is characterized by alternating leaf- and wood-rich intervals (Fig. 10). In contrast to the relative simple trends in Eocene coals, the variations in the content of leaf-derived macerals in Miocene coals are more diverse. On the one hand, the percentage of leaf-derived macerals decreases upward in the uppermost cycles of seams T110 (110–5) and T210 (210−3) and in cycles 300–1 and 300–2. On the other hand, no trends are evident in cycles T110–1 to T110–4 and T210–1 to T210–2.

Suberinite, typically related to roots, is abundant only in Miocene coals and reaches the highest percentages in ombrotrophic coals. High percentages of suberinite, therefore, may be characteristic for ombrotrophic peats. The critical role of dense surface layers of fine cluster roots produced by *Empodisma* spp. for the development of ombrotrophic mires in New Zealand has been emphasized by Clarkson et al. (1999) and Robertson et al. (2016).

Alginite occurs in low amounts in Eocene coals and includes some *Botryococcus*–type alginite. In contrast, alginite is not present in ombrotrophic Miocene coals.

Funginite is present in significant amounts (max. 3.2 vol%), reflecting strong fungal activity in rheotrophic Eocene and oligotrophic Miocene coals. Funginite is also the most abundant inertinite maceral in present–day ombrotrophic peats (e.g., Demchuk and Moore, 1993; Dehmer, 1993; Esterle and Ferm, 1994). This shows that Eh and pH conditions favorable to fungal activity can be present in both rheotrophic and oligotrophic peatlands.

Oxydized material (inertinite macerals excluding funginite) is very rare in Eocene (~1 vol%) and in Miocene coals (~2 vol%). The concentration and the variety of PAHs are significantly higher in Eocene coals (447 μg/gTOC) than in Miocene Tutupan coals (37 μg/gTOC). The comparison with inertinite contents suggests that in case of the Eocene coal, PAHs are not derived from wildfires.

Stronger degradation of plant tissues in the Eocene coal is evidenced by petrography–based facies indicators (vegetation index; VI) and is also supported by smaller particle sizes compared to Miocene coals (Moore and Ferm, 1992). Apart from the differences in precursor vegetation, stronger degradation of the Eocene coal may be related to a higher pH value in the rheotrophic mire. Wetter conditions and stronger water influx in the rheotrophic mire are reflected by higher groundwater index (GWI) values.

7. Summary and conclusions

This study of coal seams in the TAJ Pit–1D mine (SE Borneo) was undertaken for two-fold purposes. The first was to reconstruct the environment of peat accumulation in the Late Eocene Barito Basin. The second was to compare Eocene to Middle Miocene peat facies.

In the TAJ Pit–1D mine, three economic, laterally persistent seams (labelled from base to top D, C and B) of Late Eocene age reach a net thickness of about 8 m. The subbituminous A/high volatile bituminous C coal was investigated using a multi–method approach including the analysis of ash yield and moisture content, element analysis (carbon and sulphur), Rock–Eval pyrolysis, organic geochemistry, and petrology.

Seam D is 2.8-m thick. The lower part (0.2–1.2 m) contains low–ash, low–sulphur coal, which might represent peat accumulation in an ombrotrophic or transitional mire. The upper part of the seam (1.2–3.0 m) accumulated in a rheotrophic mire with gradually increasing water level, which finally caused the termination of peat accumulation. The highest sulphur contents (max. 0.9 wt%) are found near the top of seam D, but even these values indicate a freshwater environment, despite of a general coastal plain setting. Seam D is the only seam, which contains identifiable amounts of gymnosperm–derived biomarkers. The geochemical data are in agreement with a palm/fern dominated vegetation, as postulated by previous investigations (Moore and Ferm, 1992; Morley, 2013). The seam C is 3.4-m thick and accumulated in a rheotrophic mire with a relatively high-water level. Hence, ash yields and the proportion of aquatic plants are higher than in any other seam. Seam B is only 1.4-m thick and was formed in a rheotrophic mire, with a lower water level compared to seam C. Sulphur content, which are low (<0.4 wt%), but upward increasing, indicate that peat accumulation ended due to another (non–marine) transgression.

Three seams with Middle Miocene subbituminous C coal in the northern Barito Basin (Tutupan mine) have been investigated by Fikri et al. (2022) using similar geochemical and petrographic proxies. The similar rank of Miocene and Eocene coals facilitates the comparison of peat forming environments. Both Eocene and Miocene coals accumulated in tropical ever–wet climates (e.g., Morley, 2012, 2013; Friederich et al., 2016). Compared to Eocene coals, Miocene coals are significantly thicker (up to 50 m) and display a cyclic structure. Ash yields and sulphur contents of Miocene Tutupan coals are very low. This together with low concentrations of gymnosperm biomarkers reflect peat accumulation in ombrotrophic kerapah-type peats (Fikri et al., 2022). Despite of the presence of gymnosperms, the vegetation was dominated by woody angiosperm including dammar resin producing dipterocarps. The differences in vegetation between Eocene and Miocene coals are reflected by significantly higher percentages of root–derived suberinite in Miocene coals, while resinite and leaf–derived macerals are enriched in Eocene coals and show vertical trends indicative of intervals with increased leaf production. Alginite (including *Botryococcus*–type telalginite) has also been found exclusively in Eocene rheotrophic seams. Funginite percentages up to 3.2 vol% indicate strong fungal activity regardless of age and mire–type. In contrast, fusinite is very rare. The maceral–based vegetation index (Calder et al., 1991) shows greater degradation of plant material in Eocene coals, confirming the observations of Moore and Ferm (1992) that palm/fern–dominated Eocene vegetation is more easily degraded.

CRediT authorship contribution statement

Hafidz Noor Fikri: Conceptualization, Methodology, Investigation, Writing – original draft, Visualization. **Reinhard F. Sachsenhofer:** Conceptualization, Writing – review & editing. **Achim Bechtel:** Writing – review & editing. **Doris Gross:** Writing – review & editing.

Declaration of Competing Interest

The authors declare that they have no known competing financial interests or personal relationships that could have appeared to influence the work reported in this paper.

Data availability

Data will be made available on request.

Acknowledgments

The first author (FHN) thanks OeAD, Austria's Agency for Education and Internationalization, for an Ernst Mach Grant, ASEA-UNINET scholarship (Reference number: ICM-2019-13766, MPC-2020-01500, MPC-2021-01331). FHN would also like to thank PT. Tanjung Alam Jaya Company for their help in sampling the coal seams. The paper benefitted greatly from the positive criticism of Jim Hower and an anonymous reviewer.

References

van Aarssen, B.G.K., Cox, H., Hoogendoorn, N.P., de Leeuw, J.W., 1990. A cadinene biopolymer in fossil and extant dammar resins as a source for cadinanes and bicadinanes in crude oils from South East Asia. GCA. 54, 3021–3031. https://doi.org/10.1016/0016-7037(90)90119-6.

van Aarssen, B.G.K., de Leeuw, J.W., Collinson, M., Boon, J.J., Goth, K., 1994. Occurrence of polycadinene in fossil and recent resins. GCA. 58, 223–229. https://doi.org/10.1016/0016-7037(94)90459-6.

Adaskaveg, J.E., Blanchette, R.A., Gilbertson, R.L., 1991. Decay of date palm wood by white-rot and brown rot fungi. Can. J. Bot. 69, 615–629.

Alias, F.L., Abdullah, W.H., Hakimi, M.H., Azhar, M.H., Kugler, R.L., 2012. Organic geochemical characteristics and depositional environment of the Tertiary Tanjong Formation coals in the Pinangah area, onshore Sabah, Malaysia. Int. J. Coal Geol. 104, 9–21. https://doi.org/10.1016/j.coal.2012.09.005.

Amijaya, H., Littke, R., 2005. Microfacies and depositional environment of Tertiary Tanjung Enim low rank coal, South Sumatra Basin, Indonesia. Int. J. Coal Geol. 61, 197–221. https://doi.org/10.1016/j.coal.2004.07.004.

Anderson, J.A.R., 1964. The structure and development of the peat swamps of Sarawak and Brunei. J. Trop. Geogr. 18, 7–16.

Anderson, J.A.R., 1983. The tropical peat swamps of western Malesia. In: Gore, A.J.P. (Ed.), Ecosystems of the World, 4B, Mires: Swamp, Bog, Fen and Moor - Regional Studies. Elsevier, Amsterdam, The Netherlands, pp. 181–199.

Anderson, J.A.R., Muller, J., 1975. Palynological study of a Holocene peat and a Miocene coal deposit from N.W. Borneo. Rev. Palaeobot. Palynol. 19, 291–351.

ASTM, 2012. D3174-2012. Standard Test Method for Ash in the Analysis Sample of Coal and Coke from Coal, 6 pp.

ASTM, 2017. D3173-2017. Standard Test Method for Moisture in the Analysis Sample of Coal and Coke, 4 pp.

Bechtel, A., Püttmann, W., 2017. Biomarkers: coal. In: White, W. (Ed.), Encyclopedia of Geochemistry, Encycl. Earth Sci. Series. Springer, Cham. https://doi.org/10.1007/978-3-319-39193-9_150-1.

Bechtel, A., Sachsenhofer, R.F., Markic, M., Gratzer, R., Lucke, A., Püttmann, W., 2003. Paleoenvironmental implications from biomarker and stable isotope investigations on the Pliocene Velenje lignite seam (Slovenia). Org. Geochem. 34, 1277–1298. https://doi.org/10.1016/S0146-6380(03)00114-1.

Belkin, H.E., Tewalt, S.J., Hower, J.C., Stucker, J.D., O'Keefe, J.M.K., 2009. Geochemistry and petrology of selected coal samples from Sumatra, Kalimantan, Sulawesi, and Papua, Indonesia. Int. J. Coal Geol. 77, 260–268. https://doi.org/10.1016/j.coal.2008.08.001.

Bourbonniere, R.A., Meyers, P.A., 1996. Sedimentary geolipid records of historical changes in the watersheds and productivities of Lakes Ontario and Erie. Limnol. Oceanogr. 41, 352–359. https://doi.org/10.4319/lo.1996.41.2.0352.

BP, 2022. Statistical Review of World Energy 2021, 71th edition https://www.bp.com/content/dam/bp/business-sites/en/global/corporate/pdfs/energy-economics/statistical-review/bp-stats-review-2022-full-report.pdf.

Bray, E.E., Evans, E.D., 1961. Distribution of n-paraffins as a clue to recognition of source beds. GCA 22, 2–5. https://doi.org/10.1016/0016-7037(61)90069-2.

Brooks, J.D., Gould, K., Smith, J.W., 1969. Isoprenoid Hydrocarbons in coal and Petroleum. Nature 222, 257–259.

Buggle, B., Wiesenberg, G.L., Glaser, B., 2010. Is there a possibility to correct fossil n-alkane data for postsedimentary alteration effects? Appl. Geochem. 25 (7), 947–957. https://doi.org/10.1016/j.apgeochem.2010.04.003.

Calder, J., Gibling, M., Mukhopadhyay, P.K., 1991. Peat formation in a Westphalian B piedmont setting, Cumberland Basin, Nova Scotia: implications for the maceral-based interpretation of rheotrophic and raised paleomires. Bull. Soc. Geol. Fr. 162, 283–298.

Cameron, C.C., Esterle, J.S., Palmer, C.A., 1989. The geology, botany and chemistry of selected peat-forming environments from temperate and tropical latitudes Int. J. Coal Geol. 12, 105–156. https://doi.org/10.1016/0166-5162(89)90049-9.

Casagrande, D.J., 1987. Sulphur in peat and coal. Geol. Soc. Lond., Spec. Publ. 32 (1), 87–105.

Clarkson, B.R., Thompson, K., Schipper, L.A., McLeod, M., 1999. Moanatuatua Bog—proposed restoration of a New Zealand Restiad Peat Bog ecosystem. In: Streever, W. (Ed.), An International Perspective on Wetland Rehabilitation. Springer, Dordrecht. https://doi.org/10.1007/978-94-011-4683-8_13.

Dai, S., Bechtel, A., Eble, C.F., Flores, R.M., French, D., Graham, I.T., Hood, M.M., Hower, J.C., Korasidis, V.A., Moore, T.A., Püttman, W., Wei, Q., Zhao, L., O'Keefe, J. M.K., 2020. Recognition of peat depositional environments in coal: A review. Int. J. Coal Geol. 210, 103383, 67 pp.

Daly, M.C., Cooper, M.A., Wilson, I., Smith, D.G., Hooper, B.G.D., 1991. Cenozoic plate tectonics and basin evolution in Indonesia. Mar. Pet. Geol. 8, 2–21. https://doi.org/10.1016/0264-8172(91)90041-X.

Davis, R.C., Noon, S.W., Harrington, J., 2007. The petroleum potential of Tertiary coals from Western Indonesia: Relationship to mire type and sequence stratigraphic setting. Int. J. Coal Geol. 70, 35–52. https://doi.org/10.1016/j.coal.2006.02.008.

Dehmer, J., 1993. Petrology and organic geochemistry of peat samples from a raised bog in Kalimantan (Borneo). Org. Geochem. 20 (3), 349–362. https://doi.org/10.1016/0146-6380(93)90125-U.

Demchuk, T., Moore, T.A., 1993. Palynofloral and organic characteristics of a Miocene bog-forest, Kalimantan, Indonesia. Org. Geochem. 20 (2), 119–134. https://doi.org/10.1016/0146-6380(93)90032-7.

Didyk, B.M., Simoneit, B.R.T., Brassell, S.T., Eglinton, G., 1978. Organic geochemical indicators of palaeoenvironmental conditions of sedimentation. Nature 272 (5650), 216–222.

Diefendorf, A.F., Freeman, K.H., Wing, S.L., Graham, H.V., 2011. Production of n-alkyl lipids in living plants and implications for the geologic past. GCA. 75, 7472–7485. https://doi.org/10.1016/j.gca.2011.09.028.

Diessel, C.F.K., 1986. The correlation between coal facies and depositional environments. In: Proceeding 20th Symposium of Department Geology. University of New Castle, New South Wales, pp. 11–22.

Diessel, C.F.K., 1992. Coal-Bearing Depositional Systems. Springer Berlin, Heidelberg. https://doi.org/10.1007/978-3-642-75668-9.

Dutta, S., Tripathi, S.M., Mallick, M., Mathews, R.P., Greenwood, P.F., Rao, M.R., Summons, R.E., 2011. Eocene out-of-India dispersal of Asian dipterocarps. Rev. Palaeobot. Palynol. 166 (1–2), 63–68. https://doi.org/10.1016/j.revpalbo.2011.05.002.

Espitalie, J., Madec, M., Tissot, B., Mennig, J.J., Leplat, P., 1977. Source rock characterization method for petroleum exploration. In: Offshore Technology Conference. https://doi.org/10.4043/2935-MS.

Esterle, J.S., Ferm, J.C., 1994. Spatial variability in modern tropical peat deposits from Sarawak, Malaysia and Sumatra, Indonesia: analogues for coal. Int. J. Coal Geol. 26, 1–41. https://doi.org/10.1016/0166-5162(94)90030-2.

Esterle, J.S., Ferm, J.C., Durig, D.T., Supardi, 1987. Physical and chemical properties of peat near Jambi, Sumatra, Indonesia. In: International Peat Society, Symposium on Tropical Peat, pp. 1–17.

Esterle, J.S., Ferm, J.C., Tie, Y.L., 1989. A test for the analogy of tropical domed peat deposits to "dulling-up" sequences in coal beds-preliminary results. Org. Geochem. 14, 333–342. https://doi.org/10.1016/0146-6380(89)90060-0.

Ficken, K.J., Li, B., Swain, D., Eglinton, G., 2000. An n-alkane proxy for the sedimentary input of submerged/floating freshwater aquatic macrophytes. Org. Geochem. 31, 745–749. https://doi.org/10.1016/S0146-6380(00)00081-4.

Fikri, H.N., Sachsenhofer, R.F., Bechtel, A., Gross, D., 2022. Organic geochemistry and petrography in Miocene coals in the Barito Basin (Tutupan Mine, Indonesia): evidence for astronomic forcing in kerapah type peats. Int. J. Coal Geol. 256, 103997 https://doi.org/10.1016/j.coal.2022.103997.

Friederich, M.C., Van Leeuwen, T., 2017. A review of the history of coal exploration, discovery and production in Indonesia: the interplay of legal framework, coal geology and exploration strategy. Int. J. Coal Geol. 178, 56–73. https://doi.org/10.1016/j.coal.2017.04.007.

Friederich, M., Esterle, J., Moore, T., Nas, C., 2009. Variations in the Sedimentological Characteristics of Tertiary Coals in SE Asia; and Climatic Influences on Tertiary Coals and Modern Peats. AAPG Hedberg Conference.

Friederich, M.C., Moore, T.A., Flores, R.M., 2016. A regional review and new insights into SE Asian Cenozoic coal-bearing sediments: why does Indonesia have such extensive coal deposits? Int. J. Coal Geol. 166, 2–35. https://doi.org/10.1016/j.coal.2016.06.013.

Gruber, W., Sachsenhofer, R.F., 2001. Coal deposition in the Noric Depression (Eastern Alps): raised and low-lying mires in Miocene pull-apart basins. Int. J. Coal Geol. 48, 89–114. https://doi.org/10.1016/S0166-5162(01)00049-0.

Guatame, C., Rincón, M., 2021. Coal petrology analysis and implications in depositional environments from upper cretaceous to Miocene: a study case in the Eastern Cordillera of Colombia. Int. J. Coal Sci. Technol. 8 (5), 869–896. https://doi.org/10.1007/s40789-020-00396-z.

Hall, R., Morley, C.K., Kuhnt, W., 2004. Sundaland basins. In: Clift, P., Wang, P., Hayes, D.E. (Eds.), Continent-Ocean Interactions within the East Asian Marginal Seas, Geophysical Monograph, vol. 149. American Geophysical Union, Geophysical Monograph, Washington, D.C., pp. 55–85. https://doi.org/10.1029/149GM04

Hauke, V., Graff, R., Wehrung, P., Trendel, J.M., Albrecht, P., Riva, A., Hopfgartner, G., Gülaçar, F.O., Buchs, A., Eakin, P.A., 1992. Novel triterpene-derived hydrocarbons of the arborane/fernane series in sediments: Part II. GCA 56 (9), 3595–3602. https://doi.org/10.1016/0016-7037(92)90405-8.

Hauke, V., Adam, P., Trendel, J.M., Albrecht, P., Schwark, L., Vliex, M., Hagemann, H., Püttmann, W., 1995. Isoarborinol through geological times: evidence for its presence in the Permian and Triassic. Org. Geochem. 23, 91–93.
Hoffmann, B., Kahmen, A., Cernusak, L.A., Arndt, S.K., Sachse, D., 2013. Abundance and distribution of leaf wax n-alkanes in leaves of Acacia and Eucalyptus trees along a strong humidity gradient in northern Australia. Org. Geochem. 62, 62–67. https://doi.org/10.1016/j.orggeochem.2013.07.003.
Holdgate, G.R., 2005. Geological processes that control lateral and vertical variability in coal seam moisture contents; Latrobe Valley, Gippsland Basin, Australia. Int. J. Coal Geol. 63, 130–155. https://doi.org/10.1016/j.coal.2005.02.010.
Hower, J.C., O'Keefe, J.M., Eble, C.F., Raymond, A., Valentim, B., Volk, T.J., Richardson, A.R., Satterwhite, A.B., Hatch, R.S., Stucker, J.D., Watt, M.A., 2011a. Notes on the origin of inertinite macerals in coal: evidence for fungal and arthropod transformations of degraded macerals. Int. J. Coal Geol. 86 (2–3), 231–240. https://doi.org/10.1016/j.coal.2011.02.005.
Hower, J.C., O'Keefe, J.M., Eble, C.F., Volk, T.J., Richardson, A.R., Satterwhite, A.B., Hatch, R.S., Kostova, I.J., 2011b. Notes on the origin of inertinite macerals in coals: Funginite associations with cutinite and suberinite. Int. J. Coal Geol. 85, 186–190. https://doi.org/10.1016/j.coal.2010.11.008.
Huang, Y., Hoefgen, S., Valiante, V., 2021. Biosynthesis of fungal drimane-type sesquiterpene esters. Angew. Chem. Int. Ed. 2021 (60), 23763–23770.
Hutton, A., Dauley, B., Herriyanto, Nas, Pujobroto, A., Sutarwan, H., 1994. Liptinite in Indonesian Coals. Energy Fuel 1994 (8), 1469–1477.
ICCP, 1998. The new vitrinite classification (ICCP System 1994). Fuel 77, 349–358. https://doi.org/10.1016/S0016-2361(98)80024-0.
ICCP, 2001. The new inertinite classification (ICCP System 1994). Fuel 80, 459–471. https://doi.org/10.1016/S0016-2361(00)00102-2.
Kalkreuth, W.D., Marchioni, D.L., Calder, J.H., Lamberson, M.N., Naylor, R.D., Paul, J., 1991. The relationship between coal petrography and depositional environments from selected coal basins in Canada. Int. J. Coal Geol. 19, 21–76. https://doi.org/10.1016/0166-5162(91)90014-A.
Kothen, H., Reichenbach, K., 1981. Teufenabhängigkeit und gegenseitige Beziehungen von Qualitätsparametern der Braunkohle der Niederrheinischen Bucht. Fortschr. Geol. Rheinland. Westfalen 29, 353–380.
Markic, M., Sachsenhofer, R.F., 1997. Petrographic composition and depositional environments of the Pliocene Velenje lignite seam (Slovenia). Int. J. Coal Geol. 33 (3), 229–254. https://doi.org/10.1016/S0166-5162(96)00043-2.
Moore, T.A., Ferm, J.C., 1992. Composition and grain size of an eocene coal bed in southeastern Kalimantan, Indonesia. Int. J. Coal Geol. 21, 1–30. https://doi.org/10.1016/0166-5162(92)90033-S.
Moore, T.A., Shearer, J.C., 1997. Evidence for aerobic degradation and implications for Palangka Raya peat sustainability. In: Rieley, J.O., Page, S.E. (Eds.), Biodiversity and Sustainability of Tropical Peatlands. Samara Publishing, Cardigan, United Kingdom, pp. 157–167.
Moore, T.A., Shearer, J.C., 2003. Peat/coal type and depositional environment—are they related? Int. J. Coal Geol. 56 (3–4), 233–252. https://doi.org/10.1016/S0166-5162(03)00114-9.
Moore, T.A., Friederich, M.C., Trofimovs, J., Anggara, F., Amijaya, D.H., 2020. Syn-sedimentary Mafic Volcanics in the Eocene Coal-bearing Tanjung Formation, Senakin Peninsula, South Kalimantan (Borneo), Indonesia. Indones. J. Geosci. 7, 65–85.
Morley, R.J., 2012. A review of the Cenozoic climate history of Southeast Asia. In: Gower, D.J., et al. (Eds.), Biotic Evolution and Environmental Change in Southeast Asia. Cambridge University Press, pp. 79–114. © The Systematics Association 2012.
Morley, R.J., 2013. Cenozoic ecological history of South East Asian peat mires based on the comparison of coals with present day and late Quaternary peats. J. Limnol. 72, 36–59. https://doi.org/10.4081/jlimnol.2013.s2.e3.
Naafs, D.F.W., van Bergen, P.F., Boogert, S.J., de Leeuw, J.W., 2019. Solvent-extractable lipids in an acid andic forest soil; variations with depth and season. Soil Biol. Biochem. 36, 297–308. https://doi.org/10.1016/j.soilbio.2003.10.00.
Niyolia, D., Kumar, S., Dutta, S., 2019. Biomarker Signatures Revealed by Gcxgc-Tofms in Eocene Sediments from Cambay Basin, Western India. Conference Proceedings, 29th International Meeting on Organic Geochemistry. https://doi.org/10.3997/2214-4609.201902981.
Noblin, X., Rojas, N.O., Westbrook, J., Llorens, C., Argentina, M., Dumais, J., 2012. The fern sporangium: a unique catapult. Science 335 (6074), 1322. https://doi.org/10.1126/science.1215985.
Ortiz, J.E., Moreno, L., Torres, T., Vegas, J., Ruiz-Zapata, B., García-Cortés, Á., Galán, L., Pérez-González, A., 2013. A 220 ka palaeoenvironmental reconstruction of the Fuentillejo maar lake record (Central Spain) using biomarker analysis. Org. Geochem. 55, 85–97. https://doi.org/10.1016/j.orggeochem.2012.11.012.
Page, S., Rieley, J.O., Shotyk, O.W., Weiss, D., 1999. Interdependence of peat and vegetation in a tropical peat swamp forest. Philos. Trans. Royal Soc. B Biol. Sci. 354 (1391), 1885–1897. https://doi.org/10.1098/rstb.1999.0529.
Page, S., Wüst, R., Banks, C., 2010. Past and present carbon accumulation and loss in Southeast Asian peatlands. PAGES News 18, 25–27. https://doi.org/10.22498/pages.18.1.25.
Paijmans, K., 1990. Wooded swamps of New Guinea. In: Lugo, A.E., Brinson, M., Brown, S. (Eds.), Ecosystems of the World, Forested Wetlands, vol. 15. Elsevier, Amsterdam, pp. 335–355.
Panggabean, H., 1991. Tertiary Source Rocks, Coals and Reservoir Potential in the Asem Asem and Barito Basins, Southeastern Kalimantan, Indonesia. Doctor of Philosophy thesis. Department of Geology-Faculty of Science, University of Wollongong, p. 202. https://ro.uow.edu.au/theses/2113.
Parr, S.W., 1928. The Classification of Coal, 180. University of Illinois, Engineering Experiment Station, Bulletin, pp. 1–62.
Peters, K.E., Walters, C.C., Moldowan, J.M., 2005. The Biomarker Guide, , 2nd2. Cambridge University Press.
Pickel, W., Kus, J., Flores, D., Kalaitzidis, S., Christanis, K., Cardott, B.J., Misz-Kennan, M., Rodrigues, S., Hentschel, A., Hamor-Vido, M., Crosdale, P., Wagner, N., 2017. Classification of liptinite – ICCP System 1994. Int. J. Coal Geol. 169, 40–61. https://doi.org/10.1016/j.coal.2016.11.004.
Powell, T.G., McKirdy, D.M., 1973. Relationship between ratio of pristane to phytane, crude oil composition and geological environment in Australia. Nat. Phys. Sci. 243 (124), 37–39.
Poynter, J., Eglinton, G., 1990. Molecular composition of three sediments from Hole 717C: the Bengal Fan. In: Cochran, J.R., Stow, D.A.V., et al. (Eds.), Proceedings of the Ocean Drilling Program, Scientific Results, College Station, TX (Ocean Drilling Program), 116, pp. 155–161. https://doi.org/10.2973/odp.proc.sr.116.151.1990.
Pubellier, M., Morley, C.K., 2014. The basins of Sundaland (SE Asia): evolution and boundary conditions. Mar. Pet. Geol. 58, 555–578. https://doi.org/10.1016/j.marpetgeo.2013.11.019.
Radke, M., Schaefer, R.G., Leythaeuser, D., Teichmüller, M., 1980. Composition of soluble organic matter in coals: relation to rank and liptinite fluorescence. GCA 44, 1787–1800. https://doi.org/10.1016/0016-7037(80)90228-8.
Rieley, J.O., Sieffermann, R.G., Page, S.E., 1992. The origin, development, present status and importance of the lowland peat swamp forests of Borneo. Suo 42, 241–244.
Robertson, H.A., Clarkson, B.R., Campbell, D.I., Tanner, C.C., 2016. Chapter 16: Wetland biodiversity, ecosystem processes and management. In: Jellyman, P., et al. (Eds.), Advances in New Zealand Freshwater Science. New Zealand Hydrological Society and New Zealand Freshwater Science Society.
Roland, S.J., Alexander, R., Kagi, R.I., 1984. Analysis of trimethylnaphthalenes in petroleum by capillary chromatography. J. Chromatogr. A 294, 407–412. https://doi.org/10.1016/S0021-9673(01)96153-9.
Ronkainen, T., McClymont, E.L., Väliranta, M., Tuittila, E.S., 2013. The n-alkane and sterol composition of living fen plants as a potential tool for palaeoecological studies. Org. Geochem. 59, 1–9. https://doi.org/10.1016/j.orggeochem.2013.03.005.
Rowley, D.B., 1996. Age of initiation of collision between India and Asia; a review of stratigraphic data. Earth Planet. Sci. Lett. 145, 1–13.
Ruppert, L.F., Moore, T.A., 1992. Differentiation of volcanic ash-fall and water-borne detrital layers in the Senakin coal bed (Eocene), Tanjung Formation, Indonesia. Org. Geochem. 20, 233–247.
Satyana, A.H., Nugroho, D., Surantoko, I., 1999. Tectonic controls on the hydrocarbon habitats of the Barito, Kutei, and Tarakan Basins, Eastern Kalimantan, Indonesia: major dissimilarities in adjoining basins. Asian J. Earth Sci. 17, 99–122. https://doi.org/10.1016/S0743-9547(98)00059-2.
Satyana, A.H., Eka, M., Imron, M., 2001. Eocene Coals of the Barito Basin, Southeast Kalimantan: Sequence Stratigraphic Framework and potential for sources of Oil. Berita Sedimentol. 17 III, 1–15.
Schouten, S., Woltering, M., Rijpstra, W.I.C., Sluijs, A., Brinkhuis, H., Damsté, S., 2007. The Paleocene–Eocene carbon isotope excursion in higher plant organic matter: differential fractionation of angiosperms and conifers in the Arctic. Earth Planet. Sci. Lett. 258, 581–592. https://doi.org/10.1016/j.epsl.2007.04.024.
Schwark, L., Zink, K., Lechterbeck, J., 2002. Reconstruction of postglacial to early Holocene vegetation history in terrestrial Central Europe via cuticular lipid biomarkers and pollen records from lake sediments. Geology 30 (5), 463–466. https://doi.org/10.1130/0091-7613(2002)030<0463:ROPTEH>2.0.CO;2.
Sikumbang, N., Heryanto, R., 1994. Geological Map of the Banjarmasin Sheet, Kalimantan. Geological Agency, Bandung, Indonesia (1:250,000).
Silliman, J.E., Meyers, P.A., Bourbonniere, R.A., 1996. Record of postglacial organic matter delivery and burial in sediments of Lake Ontario. Org. Geochem. 24 (4), 463–472. https://doi.org/10.1016/0146-6380(96)00041-1.
Siregar, M.S., Sunaryo, R., 1980. Depositional environment and hydrocarbon prospects, Tanjung Formation, Barito Basin, Kalimantan. In: Proceedings Indonesian Petroleum Association 9th Annual Convention, pp. 379–400.
Stach, E., Mackowsky, M.T., Teichmuller, M., Taylor, G.H., Chandra, D., Teichmuller, R., 1982. Stach's textbook of coal petrology. Gebrüder Borntraeger. 1–535.
Stankiewicz, B.A., Kruge, M.A., Mastalerz, M., 1996. A geochemical study of macerals from a Miocene lignite and an Eocene bituminous coal, Indonesia. Org. Geochem. 24 (5), 531–545. https://doi.org/10.1016/0146-6380(96)00038-1.
Staub, J.R., Esterle, J.S., 1994. Peat-accumulating depositional systems of Sarawak, East Malaysia. Sediment. Geol. 89 (1–2), 91–106.
Stevens, S.H., Hadiyanto, 2004. October. Indonesia: Coalbed methane indicators and basin evaluation. In: SPE Asia Pacific Oil and Gas Conference and Exhibition. OnePetro.
Supriatna, S., Djamal, B., Heryanto, R., Sanyoto, P., 1994. Geological Map of Indonesia, Banjarmasin Sheet. Geological Research Centre Bandung, Indonesia.
TAJ, 2020. Drill Hole DHP1D02 Report. PT Tanjung Alam Jaya.
TAJ, 2021. Internal Report of Coal Analysis. PT Tanjung Alam Jaya.
Taylor, G., Teichmüller, M., Davies, A., Diessel, D., Littke, R., Robert, P., 1998. Organic Petrology: A New Handbook Incorporation some Revised Parts of Stach's Textbook of Coal Petrology. Gebrüder Borntraeger, Berlin.
Teichmüller, M., Teichmüller, R., 1975. Inkohlungsuntersuchungen in der Molasse des Alpenvorlandes. Geol. Bavarica 123–142.
Tissot, B.P., Welte, D.H., 1984. From Kerogen to Petroleum. In: Petroleum Formation and Occurrence. Springer, Berlin, Heidelberg. https://doi.org/10.1007/978-3-642-87813-8_10.
Widodo, S., Bechtel, A., Komang, A., Püttmann, W., 2009. Reconstruction of floral changes during deposition of the Miocene Embalut coal from Kutai basin, Mahakam delta, East Kalimantan, Indonesia by use of aromatic hydrocarbon composition and stable carbon isotope ratios of organic matter. Org. Geochem. 40, 206–218. https://doi.org/10.1016/j.orggeochem.2008.10.008.

Witts, D., Hall, R., Nichols, G., Morley, R., 2012. A new depositional and provenance model for the Tanjung Formation, Barito Basin, SE Kalimantan, Indonesia. Asian J. Earth Sci. 56, 77–104. https://doi.org/10.1016/j.jseaes.2012.04.022.

Witts, D., Davies, L., Morley, R., 2014. Uplift of the Meratus complex: sedimentology, biostratigraphy, provenance and structure. In: Proceedings Indonesian Petroleum Association 38th Annual Convention & Exhibition. https://doi.org/10.29118/ipa.0.14.g.082. IPA14-G-082.

Wüst, R.A.J., Hawke, M.I., Bustin, R.M., 2001. Comparing maceral ratios from tropical peatlands with assumptions from coal studies: do classic coal petrographic interpretation methods have to be discarded? Int. J. Coal Geol. 48, 115–132. https://doi.org/10.1016/S0166-5162(01)00050-7.

Wüst, R., Rieley, J., Page, S., Kaars, S., Wie-Ming, W., Jacobsen, G., Smith, A., 2007. Peatland evolution in SE Asia over the last 35,000 cal years: implications for evaluating their carbon storage potential. In: Rieley, J.O., Banks, C.J., Radjagukguk, B. (Eds.), Carbon-Climate-Human Interaction on Tropical Peatland. Proceedings of the International Symposium and Workshop on Tropical Peatland, Yogyakarta. EU CARBOPEAT and RESTORPEAT Partnership. Gadjah Mada University and University of Leicester.

Zahirovic, S., Seton, M., Müller, R.D., 2014. The cretaceous and Cenozoic tectonic evolution of Southeast Asia. Solid Earth 5, 227–273. https://doi.org/10.5194/se-5-227-2014.

Zech, M., Buggle, B., Leiber, K., Marković, S., Glaser, B., Hambach, U., Huwe, B., Stevens, T., Sümegi, P., Wiesenberg, G., Zöller, L., 2009. Reconstructing Quaternary vegetation history in the Carpathian Basin, SE-Europe, using n-alkane biomarkers as molecular fossils: problems and possible solutions, potential and limitations. EGQSJ 58, 148–155. https://doi.org/10.3285/eg.58.2.03.

8 Publication III:

Organic geochemistry and petrography of Miocene ombrotrophic coals in the tropical Asem-Asem Basin (Kalimantan, Indonesia): Comparison to coeval subtropical coals in the Eastern Alps

Chapter 8 was submitted by the author of this thesis in “Austrian Journal Of Earth Sciences”. (accepted (in press))

Author contribution: Conceptualization, methodology, investigation, writing – original draft, and visualization

Organic geochemistry and petrography of Miocene ombrotrophic coals in the tropical Asem-Asem Basin (Kalimantan, Indonesia): Comparison to coeval subtropical coals in the Eastern Alps

Hafidz Noor Fikri[1,2], Reinhard F. Sachsenhofer[1,*], Achim Bechtel[1] & Doris Gross[1]

[1)] Department Applied Geosciences and Geophysics, Montanuniversitaet Leoben, 8700 Leoben, Austria

[2)] Department of Mining Engineering, Lambung Mangkurat University, Banjarmasin, South Kalimantan, Indonesia

[*)] Corresponding author, reinhard.sachsenhofer@unileoben.ac.at

Abstract

The middle Miocene Warukin Formation in the Asem-Asem Basin (Kalimantan) contains a 20-m-thick coals seam (BL1) that is mined at the Jumbang mine. The seam, formed in a tropical peat, was studied to reconstruct the peat–forming environment and to compare its characteristics with those of similarly aged tropical coals from the Tutupan mine in the Barito Basin (Kalimantan) and similarly aged (~15 Ma) subtropical coal from the Leoben Basin in the Eastern Alps (Austria). Although all coals were formed in ombrotrophic peatlands, the comparison reveals differences in biomarker and maceral composition due to the different climate and flora.

The study is based on 22 coal and three non–coal samples, each representing a stratigraphic interval of 0.2 to 1.0 m. The samples were analyzed for ash yield, carbon and sulphur contents, and maceral composition. Organic geochemical parameters were obtained on eight coal sample to obtain information on the peat-forming vegetation. The low-ash, low-sulphur BL1 seam was deposited in an ombrotrophic basinal (coastal) mire. Locally increased sulphur contents in the lower coal bench BL1L demonstrate brackish influence and a near-shore environment. The vegetation was dominated by angiosperms including abundant dammar resin producing *Dipterocarpaceae*, while the contribution of gymnosperms was negligible.

The Tutupan seams T110 and T210, which were formed in kerapah (inland) ombrotrophic mires, have similar ash yields and sulphur contents but contain higher, although still low, concentrations of gymnosperm-derived diterpenoids. In addition, lower amounts of cadinane-type biomarkers and resinite suggest that *Dipterocarpaceae* were less dominant in kerapah peats. While

differences between tropical coals from Kalimantan are minor, major differences exist between the tropical coals and the subtropical ombrotrophic Leoben coal. These include significantly higher concentrations of gymnosperm-derived biomarkers in subtropical peat, lower amounts of resinite due to the absence of *Dipterocarpaceae*, as wells as lower amounts of leaf- and rootlet-derived macerals. Apparently, fungal activity was also reduced in the subtropical Leoben peat. Surprisingly, the average amount of oxidized plant remains is also lower in the subtropical peat.

Keywords: ombrotrophic peat, basinal mire, climate, Borneo, tropical, subtropical

1. Introduction

Coal is an abundant and relatively cheap fuel, but its combustion produces huge amounts of the greenhouse gas carbon dioxide. In 2021, CO_2 emissions from coal combustion reached an all-time high of 15.2 gigatonnes (Gt) contributing about 40 % of the entire energy-related CO_2 emissions (36.3 Gt; IEA, 2022). Similarly, coal production in 2021 (8173 million tonnes [Mt]) was close to the all-time high reached in 2013 (8256 Mt; BP, 2022). Following China (4126 Mt) and India (811 Mt), Indonesia is the third largest producer of coal (614 Mt) equivalent to 7.5 % of world production. Most of Indonesia's coal reserves are located in Cenozoic basins on the islands of Sumatra and Kalimantan (Indonesian part of Borneo) (Friedrich et al., 2016; Fig. 1).

While coal combustion poses a significant threat to global climate, coal is an excellent archive for reconstructing terrigenous depositional settings. Important statements on the peat-forming environments (e.g., ombrotropic [raised] vs. rheotrophic [low-lying] mire; brackish influence) are possible based solely on basic coal parameters such as seam geometry, ash yield and sulphur content (e.g., Gruber and Sachsenhofer, 2001). Palynological studies are often used to reconstruct paleovegetation (e.g., Demchuk and Moore, 1993; Rich, 2015; Korasidis et al., 2016; Dai, 2020). Petrographic and geochemical parameters provide additional information on the depositional environment and diagenetic processes (e.g., Bechtel et al., 2003a; 2007; 2008; Naafs et al., 2019).

Peat-forming environments of Upper Eocene and middle Miocene coals in the Barito Basin (southern Kalimantan; for location see Figs 1, 2) were studied recently by Fikri et al. (2022a,b) using bulk geochemical parameters, biomarker and maceral data. Eocene coal seams in the Tanjung Formation from the Tanjung Alam Jaya (TAJ) Pit 1-D mine are 1.4 to 3.4 m thick and originated in rheotrophic low-lying mires dominated by palm and fern vegetation (Fikri et al., 2022b). In contrast, Miocene coal seams in the Warukin Formation from the Tutupan mine are up to 50 m thick and were deposited predominantly in ombrotrophic raised mires (Fikri et al., 2022a). In addition, Miocene coal seams in the Warukin Formation display a remarkable cyclic structure.

In the present study, we investigate a 20-m-thick coal seam in the Warukin Formation (BL1) exposed in the Jumbang open pit mine in the Asem-Asem Basin. The Asem-Asem Basin, located near the southern tip of Kalimantan Island, is considered a sub-basin of the larger Barito Basin, from which it is separated today by the Meratus Complex (Witts et al., 2014; Fig. 2). Similar to Tutupan, coal from the Jumbang mine has very low ash yields (5.5 wt.% adb) and total sulphur contents (0.4 wt.% adb) (Bumi Resources, 2021) making deposition in an ombrotrophic mire likely. The calorific value of Jumbang coal is about 4,200 Kcal/kg (as received, ar) and the average total moisture ~35 wt.% (ar) (Arutmin, 2015). Thus, the coal is classified as lignite.

The paper has three main objectives: (1) reconstruction of environmental conditions during the accumulation of the BL1 seam; (2) comparison of Miocene peat forming conditions in the Asem-Asem Basin (Jumbang mine) and in the Barito Basin (Tutupan mine); and (3) comparison of the characteristics of Miocene ombrotrophic coals from tropical and subtropical regions to investigate the effects of climate on maceral and biomarker compositions.

For this comparison, middle Miocene coals from Kalimantan and from the Leoben Basin in the Eastern Alps of Central Europe are used (Fig. 1a; Gruber and Sachsenhofer, 2001). A considerable number of Miocene coal deposits in the Eastern Alps were formed under subtropical conditions (e.g., Weber and Weiss, 1983), but only the coal in the Leoben Basin was deposited in an ombrotrophic mire (Bechtel et al., 2001; Gruber and Sachsenhofer, 2001; Sachsenhofer et al., 2003).

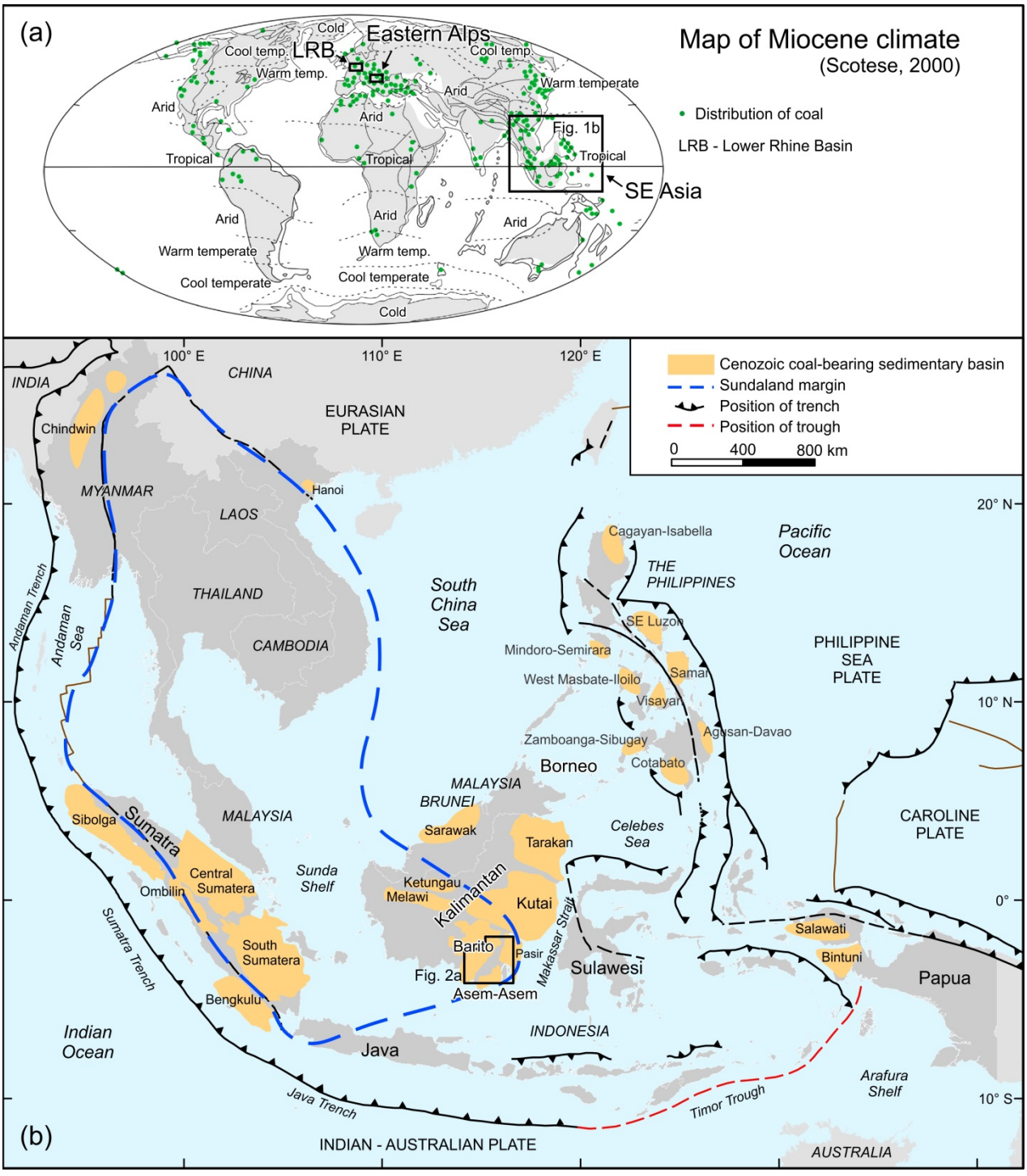

Figure 1: (a): Map of Miocene climate with position of coal deposits (from Scotese, 2000). The locations of Southeast Asia, the Eastern Alps and the Lower Rhine Basin are indicated. **(b):** The main on-shore Cenozoic coal-bearing basins in Southeast Asia (from Friederich et al., 2016).

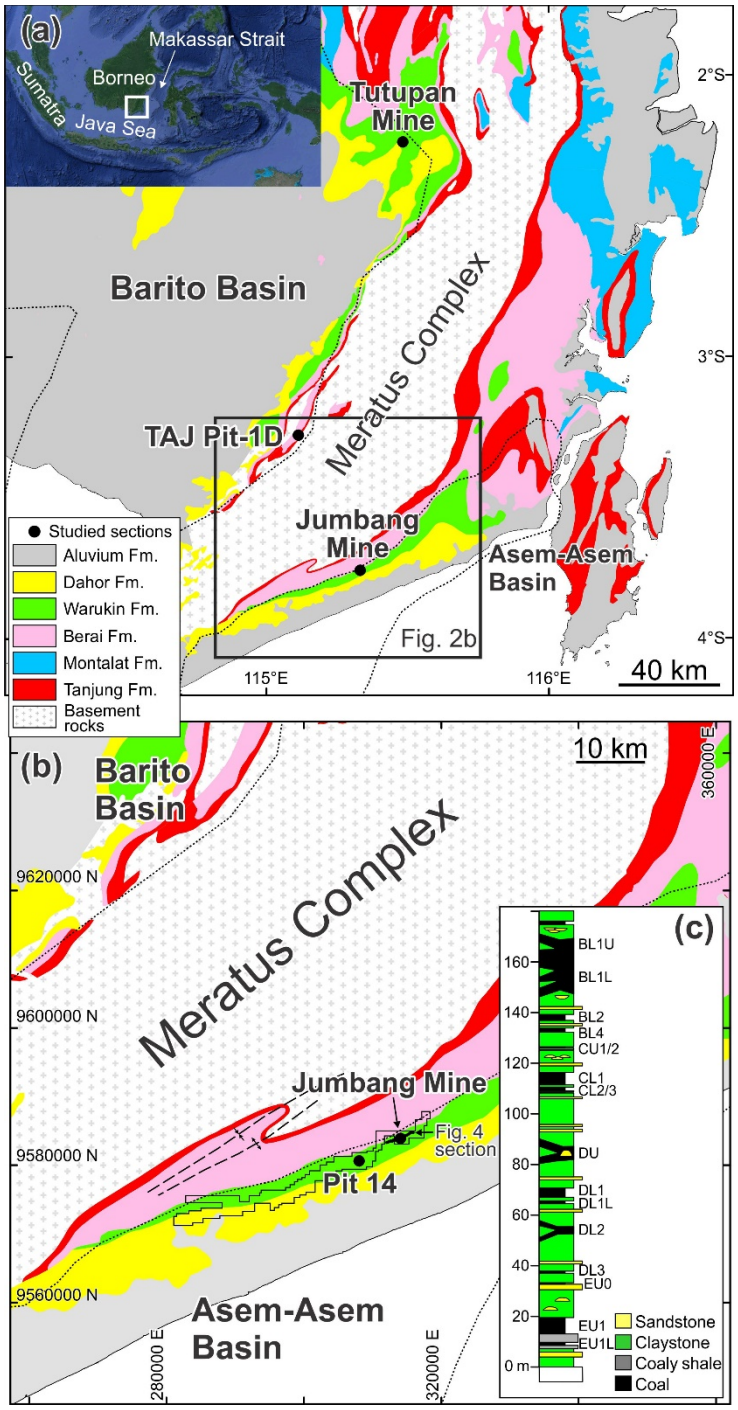

Figure 2: (a): Geological map of the Barito and Asem-Asem basins showing the location of the study site (Jumbang mine) and mines with Eocene (TAJ Pit-1D) and Miocene coals (Tutupan) studied in companion papers (Fikri et al., 2022a,b). **(b):** Geological map of the Asem-Asem Basin showing the location of the study site and the position of the cross-section shown in Figure 4. **(c):** Profile through the Warukin Formation in the study area with seam names (from Achmad, 2018).

2. Geological setting

The Asem-Asem Basin is located at the eastern margin of Sundaland, the southeastern promontory of Eurasia (Fig. 1b; Hall and Morley, 2004; Pubellier and Morley, 2014). Sundaland was formed by Permian and Triassic amalgamation of continental blocks and arc fragments (Hutchison, 1989; 2014; Hall and Morley, 2004; Advokaat et al., 2018). Other fragments of oceanic, arc and continental origin accreted to Sundaland during the Cretaceous (e.g., Hall, 2012) and formed the southwestern part of Borneo. The Meratus Complex in southern Borneo (Fig. 2) is interpreted as a Cretaceous subduction complex, which forms the suture between SW Borneo and East Java-West Sulawesi (e.g., Hall, 2012; Witts et al., 2014).

An extensional regime was initiated in eastern Borneo by the rifting of the Makassar Strait in the Eocene (e.g., Pubellier and Morley, 2014; Zahirovic et al., 2014; for location see Fig. 1). This extensional event led to the formation of NW-SE oriented horst and graben structures along a succession of NW-SE trending strike-slip faults (Satyana et al., 1999). Rifting ended towards the end of the Early Oligocene (Pubellier and Morley, 2014). Basin inversion commenced in the middle Miocene, around the time of the uplift of the Meratus Mountains (Satyana et al., 1999; Witts et al., 2014).

The Cenozoic basin fill in the Barito Basin and the Asem-Asem Basin is comparable, suggesting that they once formed uniform depocenter (Witts et al., 2014). The basin fill overlies Cretaceous and older basement rocks unconformably and comprises, from base to top, the Middle Eocene to Lower Oligocene Tanjung Formation, the Upper Oligocene to lower Miocene Berai and Montalat Formations, the middle to upper Miocene Warukin Formation, and the upper Miocene to Pleistocene Dahor Formation (Witts et al., 2012; 2014; Fig. 3). Coal seams occur in the Tanjung Formation and in the Warukin Formation (Friederich et al., 2016). The transgressive Tanjung Formation starts with alluvial and fluvial plain deposits filling a pre-existing relief (Mangkook Member) and continues with fluvio-tidal and estuarine deposits containing several-m-thick and laterally extensive coal seams (Tambak Member). The upper part of the Tanjung Formation consists of marginal to shallow marine rocks dominated by calcareous mudstones (Pagat Member; Witts et al., 2012). The Tanjung Formation is overlain by shallow marine carbonates

(Berai Formation) in the Asem-Asem Basin and the southern Barito Basin, and by fluvio-deltaic strata in the northern Barito Basin (Montalat Formation). The regressive Warukin Formation comprises marginal marine rocks with thin coal seams (typically <2 m; Sapiie and Rifiyanto, 2017) in its lower part (Barabai Member of Witts et al., 2012). The overlying Tapin Member (Witts et al., 2012) represents (south-)eastward prograding fluvio-deltaic sedimentary rocks with thick coal seams (Satyana et al., 1999; Witts et al., 2012). A change in paleocurrent directions during deposition of the uppermost part of the Tapin Member in the Barito Basin indicates the middle/late Miocene onset of uplift of the southern part of the Meratus Complex (Witts et al., 2014). In contrast, paleocurrent directions in the Asem-Asem Basin remained southeastward (Witts et al., 2014). Regression and basin inversion continued during deposition of the Dahor Formation (Witts et al., 2014), which consists mainly of alluvial to shallow marine reddish sandstone, polymict conglomerate, and siltstone (Sapiie and Rifiyanto, 2017). In the Asem-Asem Basin, coal seams are locally present in the lower part of the Dahor Formation (Arutmin, 2015).

A significant number of coal seams grouped into seam groups are present in the Warukin Formation in the Asem-Asem Basin. Near the study area the seam groups are labelled from top to bottom with A to E (Fig. 2b). Individual seams are identified by an addition (U for “upper”, L for “lower”). The most important seam in the Jumbang mine is seam BL1, which reaches a thickness of 20 m and dips gently (6-14°) towards the southeast (125°). A southwest-northeast trending cross-section of the BL1 seam is shown in Figure 4 based on data from exploration boreholes provided by the mine. It shows that the BL1 seam is split into individual coal benches, labelled BL1U and BL1L. Seams A1 and A2 are present with an average thickness of 1.6 m. Seam D2 has an average thickness of 4 m, while seam C2 is thin and discontinuous.

The seams are separated by prevailing mudstones and subordinate sandstone beds. The sediments overlying the BL1 seam in the Pit 14 (see Fig. 2b for location) represent floodplain, fluvial channel-belt, estuarine and tidal flat settings (Achmad, 2018). Sediment transport was directed southeastwards (107-160°; Achmad, 2018).

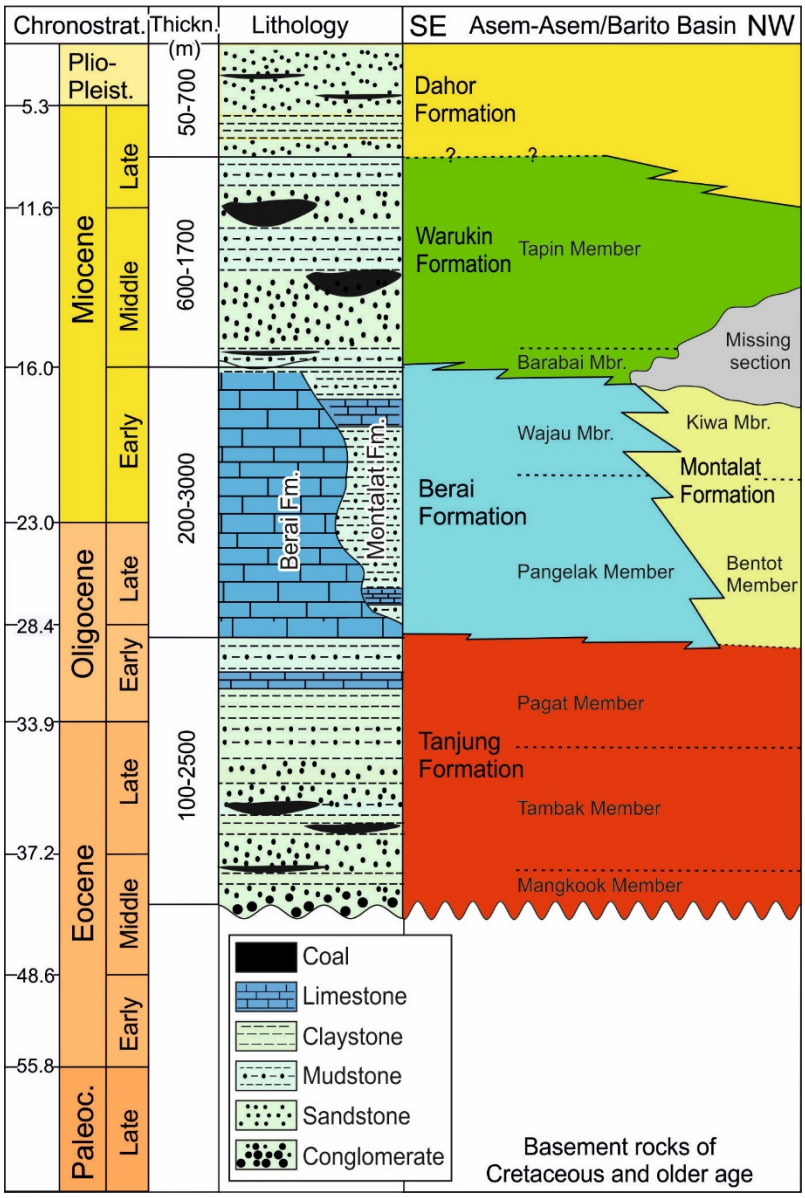

Figure 3: Stratigraphy and lithology of the basin fill in the Asem-Asem Basin (modified after Witts et al., 2012; 2014).

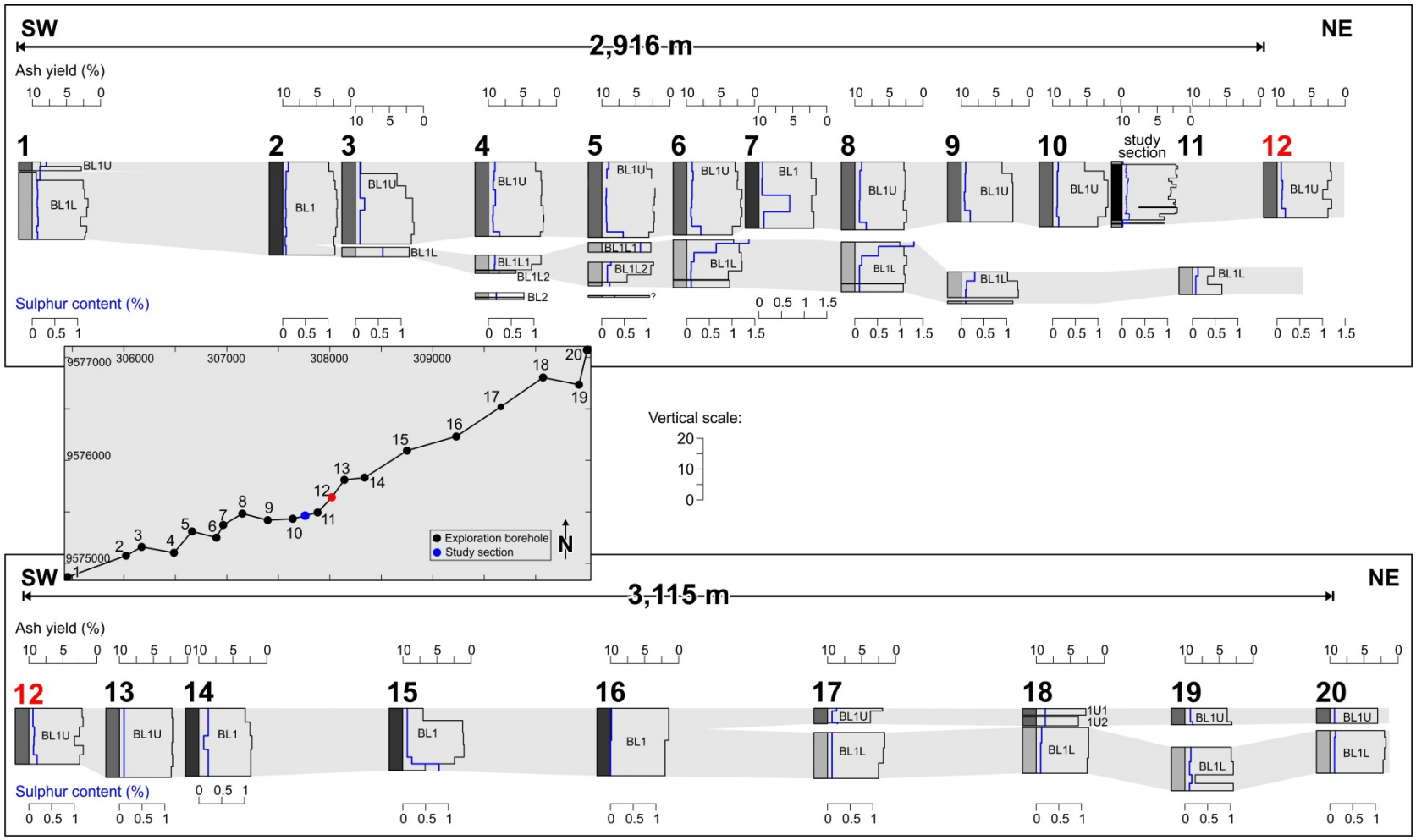

Figure 4: Southwest-northeast trending cross section of the BL1 seam in the Jumbang open pit showing thickness, ash yield (black line) and sulphur content (blue line). Laterally, the BL1 seam splits into an upper (BL1U) and a lower (BL1L) coal bench. The location of the profile is indicated in the inset and in Figure 2b. The profile was compiled using data from exploration boreholes and flattened to the top of the BL1 seam. Position and data from the section studied in the present paper (between boreholes 10 and 11) are shown.

3. Material and methods

Samples were collected at the Jumbang mine (Fig. 2b). At the sampling site, the BL1 seam is 19.4 m thick. Samples were taken from the deposits below and above the seam (2 mudstone samples) and from the seam (22 coal samples, 1 mudstone parting). The samples represent a continuous series of channel samples. Megascopically distinct coal layers were taken separately. Consequently, channel samples in the more diverse lower part of the seam (0-7.9 m) are only 0.2 to 1 m long, whereas in the more homogenous upper part of the seam (7.9-19.4 m) they are typically 1 m long. Fresh samples were placed in gas–tight plastic bags immediately after collection to prevent moisture loss.

Samples were prepared at the Mineral and Coal Laboratory of the Mining Department of the Faculty of Engineering (Lambung Mangkurat University). Ash yield and moisture analyses were conducted at the PT Geoservices coal laboratory (Banjarbaru, South Kalimantan) using standard procedures (ASTM, 2012; 2017). Ash yield provides valuable information on peat type (Moore and Shearer, 1997). All other analyses were carried out at Montanuniversitaet Leoben (Austria).

Bulk parameters: Sulphur (S), total inorganic carbon (TIC), and total organic carbon (TOC) contents are useful indicators of peat facies (e.g., Dai et al., 2020). Rock-Eval parameters S2 (amount of hydrocarbons generated during pyrolysis, mgHC/g rock), hydrogen index (HI = S2×100/TOC; mgHC/gTOC), and T_{max} (°C) provide information on the type and maturity of the organic matter (Espitalie et al., 1977). An Eltra Helios C/S analyzer and a Vinci Rock-Eval 6 instrument were used to determine these parameters in duplicate.

Organic petrography: The maceral composition of coal samples allows inferences on peat facies and diagenetic alterations. For maceral analysis, all samples were crushed to a maximum size of 1 mm and embedded in epoxy resin. The polished blocks were investigated using a Leica incident light microscope with a 50× oil-immersion objective, reflected white and fluorescent light, and a single–scan approach (Taylor et al., 1998). A total of 500 points were counted on each sample, with macerals assigned according to the ICCP system (ICCP, 1998, 2001; Pickel et al., 2017).

Huminite reflectance was measured to determine the coal rank of three samples. Random huminite reflectance (%Rr) was measured in non-polarized light at a wavelength of 546 nm and a magnification of 50× using the Hilgers Fossil software. Mean values and standard deviation are based on 150 measurement points per sample.

Organic geochemical (biomarker) analyses were performed on eight coal samples to obtain information on the peat–forming vegetation. Samples were extracted with dichloromethane for 1 h at 75 °C and 100 bar in a Dionex ASE 350 extractor. After evaporation of the solvent to a total volume of 0.5 ml in a Zymark TurboVap 500 closed–cell concentrator, asphaltenes were precipitated from a hexane–dichloromethane solution (80:1) and separated by centrifugation. The hexane–soluble fractions were separated into aliphatic hydrocarbons, aromatic hydrocarbons and NSO compounds using a Köhnen–Willsch medium–pressure liquid chromatography (MPLC) instrument (Radke et al., 1980). *n*-Alkanes and isoprenoids in the aliphatic fractions were analyzed using a Trace GC–Ultra gas chromatograph with flame ionization detector (GC–FID). The gas chromatograph was equipped with a 50 m HP–PONA capillary column (0.20-mm inner diameter [i.d.], 0.50–µm film thickness). After sample injection (2 µl at 270 °C), the oven temperature was increased from 70 to 310 °C and kept constant for 35 min. The hydrocarbon fractions were analyzed using a gas chromatograph equipped with a 60 m TG–5MS fused silica capillary column (0.20–mm inner diameter; 0.25 µm film thickness) connected to a ThermoFisher ISQ mass spectrometer (GC–MS). The oven temperature was programmed from 40 to 310 °C at 4 °C/min, followed by an isothermal phase of 30 min. Helium was used as the carrier gas. The sample was injected in split mode (split ratio 20) at an injector temperature of 260 °C. The spectrometer was operated in EI (electron ionization) mode over a scan range from m/z 50 to m/z 650 (0.7 s total scan time). The Xcalibur software was used for data processing. Individual compounds were identified based on retention time in the total ion current chromatogram (TIC) and by comparing mass spectra to published reference data. The relative percentages and absolute concentrations of the various compound groups in the aliphatic and aromatic hydrocarbon fractions were calculated from the peak areas in the TIC chromatograms relative to the internal standards (squalane and 1,1′–binaphthyl, respectively) or by integrating the peak areas in the corresponding mass chromatograms using reaction factors to correct for the

intensities of the fragment ion used to quantify total ion abundance. Concentrations were normalized to TOC.

Bulk carbon isotope data were determined on twelve coal samples. Portions of each sample (0.4 to 0.7 mg) were packed in tin capsules and burned in excess oxygen at 1080 °C using an elemental analyzer (Thermo Scientific Flesh EA). The CO_2 produced was analyzed online using a Thermo Scientific Delta-V isotopic ratio mass spectrometer. The $^{13}C/^{12}C$ isotope ratio of CO_2 from a sample was compared to a reference ratio calibrated against the PDB standard. The overall reproducibility of the analytical procedure is in the 0.1 to 0.2 range.

4. Results

4.1 Bulk parameters

The bulk parameters of the studied samples are listed in Table 1. Their vertical distribution is shown in Figure 5. The ash yield in the BL1 seam is very low (1.8-8.8 wt.% adb). Slightly higher values are restricted to 20-cm-thin layers beneath the main seam (8.8 wt.%) and between 6.2 and 6.4 m (7.5 wt.%). Moisture contents range from 23 to 30.7 wt.%, with three samples from the lower part of the seam having significantly lower contents (≤18 wt.%). Since moisture contents of coals in boreholes is typically around 35 wt.%, it is likely that the moisture content was reduced by air-drying.

The TOC content of the coal samples averages 52.7 wt.%. The TOC values of mudstones near the base of the coal seam (~2.2 wt.%) and above the seam (0.73 wt.%) are low. Sulphur contents are very low in all coal samples (0.07-0.16 wt.%) and even lower in the mudstone samples (0.01-0.02 wt.%). Despite the low sulphur contents, some vertical trends are visible: relatively high sulphur contents are observed in the lowermost part of the seam (1.0-4.2 m; ~0.15 wt.%), while a steady upward increase in sulphur content is observed between 4.2 and 15.9 m (0.07-0.14 wt.%). Above 15.9 m, the sulphur content is constant (~0.09 wt.%).

The hydrogen Index (HI) of coal samples averages 236 mgHC/gTOC (154-539 mgHC/gTOC). The highest HI values occur at 4.2-4.4 m (539 mgHC/gTOC) and 17.9-18.9 m (413 mgHC/gTOC). Mudstone samples near the base of the seam have HI values around 200 mgHC/gTOC, while the

organic-poor sample from the roof has a lower HI (39 mgHC/gTOC). T_{max} values of non-coal layers are in the range of 412-425 °C, while T_{max} values of coal samples are very low (370-399 °C).

Stable carbon isotope ($\delta^{13}C$) ratios of organic carbon range from -28.26 ‰ to -27.54 ‰. While $\delta^{13}C$ values of samples with HI <190 mgHC/gTOC cover the entire range of values, $\delta^{13}C$ values of samples with HI ≥190 mgHC/gTOC show a strong negative correlation with HI (r^2=0.93).

Table 1: Bulk Parameters of Miocene Pit Jumbang coal.

Sample	Lithology	Position (m above base)	Ash (wt.% adb)	Moisture (wt.% adb)	TOC (wt.% db)	Sulphur (wt.% db)	T_{max} (°C)	HI (mgHC/gTOC)	$\delta^{13}C$ (‰)	EOM (mg/gTOC)	NSO (mg/gTOC)	Ali.HC (mg/gTOC)	Arom.HC (mg/gTOC)
BL1-roof	mudstone	20.4	89.07	4.2	0.73	0.02	425	39					
BL1-2	coal	19.9	2.12	27.6	49.3	0.10	390	170	-27.86				
BL1-3	coal	18.9	1.85	28.3	52.7	0.09	371	218					
BL1-4	coal	17.9	2.13	23.7	54.9	0.08	375	413	-27.99	441.0	8.5	0.5	0.4
BL1-5	coal	16.9	2.11	26.2	56.4	0.10	370	202					
BL1-6	coal	15.9	1.94	24.4	55.3	0.09	372	310	-27.81	301.6	11.8	0.8	0.4
BL1-7	coal	14.9	3.17	24.6	54.1	0.14	372	234					
BL1-8	coal	13.9	2.68	23.2	52.3	0.12	371	255	-27.82	273.6	8.4	0.7	0.6
BL1-9	coal	12.9	2.08	24.8	54.0	0.11	370	272					
BL1-10	coal	11.9	2.90	26.1	51.3	0.11	374	184	-27.54	221.4	6.6	0.7	0.4
BL1-11	coal	10.9	2.81	25.3	51.1	0.11	378	154					
BL1-12	coal	9.9	2.91	29.0	48.5	0.11	371	229	-27.68	231.8	3.9	0.3	0.2
BL1-13	coal	8.9	3.20	27.6	49.3	0.08	374	184					
BL1-14	coal	7.9	2.18	25.5	52.6	0.09	376	189	-28.06				
BL1-15	coal	7.4	2.45	27.0	51.3	0.09	371	204					
BL1-16a	coal	6.4	2.14	27.0	51.2	0.10	376	164	-28.04	217.2	6.4	0.7	0.4
BL1-16b	coal	6.2	7.54	22.1	51.3	0.09	371	240					
BL1-17	coal	5.4	1.90	27.5	52.5	0.10	372	185	-28.22				
BL1-18a	coal	4.4	1.94	27.8	53.0	0.09	375	230					
BL1-18b	coal	4.2	2.26	14.6	62.4	0.07	373	539	-28.26	305.4	4.2	0.3	0.1
BL1-19a	coal	3.2	4.52	17.9	55.4	0.16	395	195					
BL1-19b	coal	2.2	3.82	18.0	55.6	0.15	395	190	-27.74	246.0	5.4	1.2	0.8
BL1-20	mudstone	1.2	92.56	3.0	2.27	0.01	412	196					
BL1-21	coal	1	8.77	30.7	45.2	0.14	399	228	-27.70				
BL1-floor	mudstone	0	91.55	6.1	2.13	0.01	419	209					

TOC – total organic carbon, HI – hydrogen index, EOM – extractable organic matter, NSO – hetero–compounds, adb – air-dried basis, db – dry basis, Ali.HC – aliphatic hydrocarbons, Arom.HC – aromatic hydrocarbons.

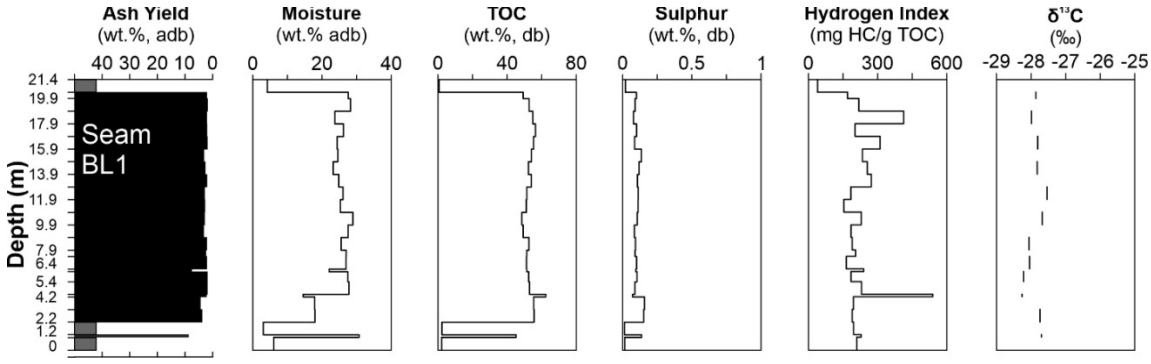

Figure 5: Vertical variation of bulk data: ash yield, moisture content, total organic carbon (TOC) content, sulphur content, hydrogen index, and stable carbon isotope ($\delta^{13}C$) ratios in seam BL1.

4.2 Biomarkers

Biomarker analysis was performed on eight coal samples. The extractable organic matter (EOM) of these samples is dominated by asphaltenes and NSO compounds, while aliphatic and aromatic hydrocarbons are subordinate (Fig. 6; Table 1). Chromatograms of the hydrocarbon fractions from samples taken from the lower, middle and upper parts of the BL1 seam are shown in Figure 7.

In all samples, the distribution of *n*–alkanes is dominated by long–chain *n*–alkanes (*n*–$C_{25–33}$), with a prominent odd–even predominance (Fig. 7). The concentration of *n*–C_{31} is remarkably high in most samples (Fig. 7). To visualize the differences in the composition of the *n*–alkanes, various parameters were calculated (Table 2). In Figure 6, these parameters are plotted as a function of stratigraphic position.

The ratio between long- and short-chain *n*–alkanes (*n*–$C_{27+29+31}$/*n*–$C_{15+17+19}$) is referred to as the terrestrial/aquatic ratio (TAR; Bourbonniere and Meyers, 1996). It ranges from 15 to 23 in most samples but is strongly elevated (37) in the upper sample (17.9-18.9 m). The P–aqueous ratio (Paq) is the ratio between medium- and long-chain *n*–alkanes ((*n*–C_{23}+*n*–C_{25})/(*n*–C_{23}+*n*–C_{25}+*n*–C_{29}+*n*–C_{31})) (Ficken et al., 2000). It is considered an indicator of the relative contribution of submerged and/or floating macrophytes. Between 2.2 and 16.9 m, the ratio varies between 0.21 and 0.27 with an overall slight upward increasing trend, while in the sample at 17.9-18.9 m it is significantly lower (0.17).

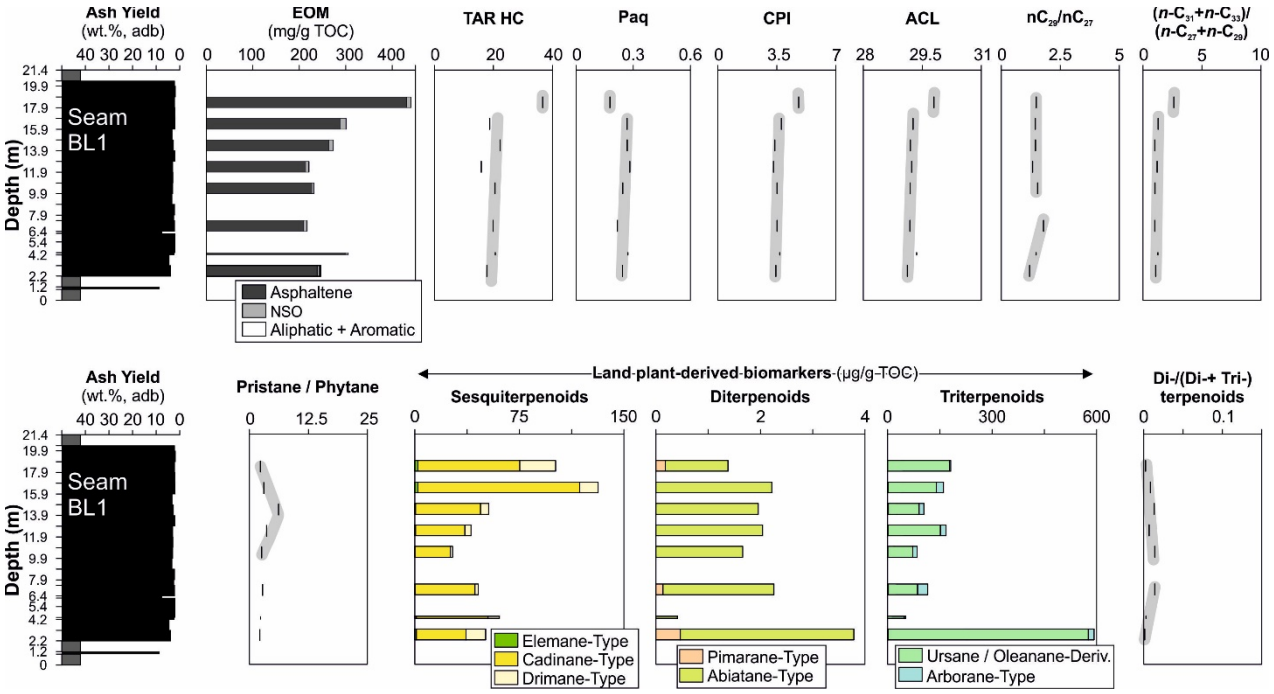

Figure 6: Variations of EOM, *n*–alkane and isoprenoid ratios and land plant–derived terpenoids in seam BL1. EOM – extractable organic matter; TAR – terrestrial/aquatic ratio (Bourbonniere and Meyers, 1996); Paq – P–aqueous (Ficken et al., 2000); CPI – carbon preference index (Bray and Evans, 1961); ACL – average chain length (Poynter and Eglinton, 1990)

The carbon preference index (CPI; Bray and Evans, 1961) reflects the relative contributions of land plants, but also maturity (Peters and Moldowan, 1993). In the BL1 coals, the average CPI is 3.7. Similar to TAR, CPI values are uniform in the main part of the seam (3.3-3.8), but elevated (4.8) in the sample at 17.9-18.9 m.

The average chain length (ACL) of the long–chain *n*–alkanes was calculated according to Poynter and Eglinton (1990) (ACL = ($27n$–C_{27}+$29n$–C_{29}+$31n$–C_{31})/(n–C_{27}+n–C_{29}+n–C_{31})) to detect climatic changes. The values obtained range from 29.1 to 29.8 with the maximum value in the uppermost sample.

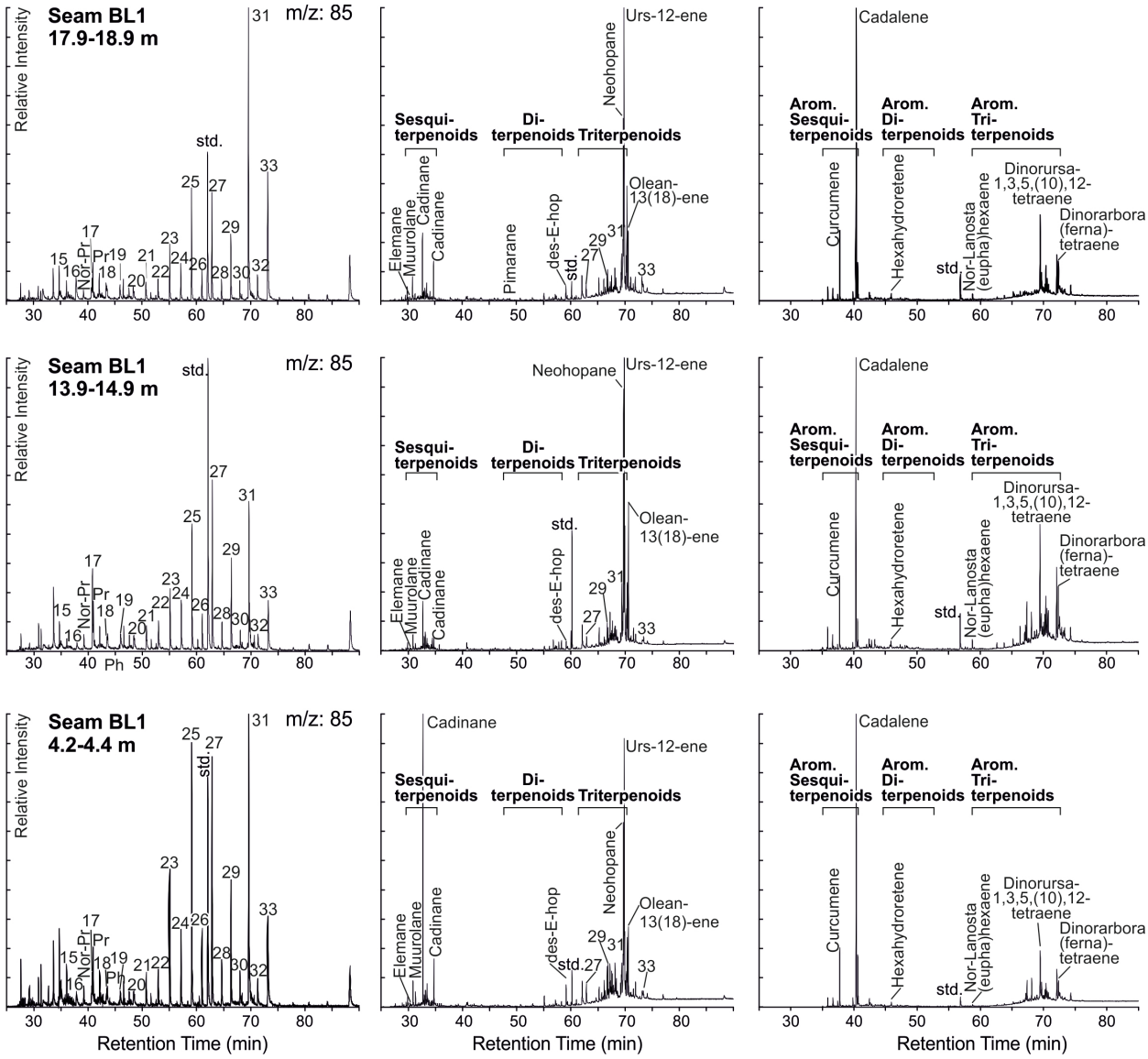

Figure 7: M/z 85 and total ion current (TIC) chromatograms of the aliphatic and aromatic hydrocarbon fractions of selected samples from seam BL1. The m/z 85 chromatogram shows the distribution of *n*–alkanes and isoprenoids. *n*–alkanes are labelled according to their carbon number; Pr – Pristane; Nor-Pr – Norpristane; Ph – Phytane; des-E-hop – des-E-hopane Std – standard.

The *n*–C_{29}/*n*–C_{27} ratio (Buggle et al., 2010) and the *n*–C_{31+33}/*n*–C_{27+29} ratio (Zech et al., 2009) can indicate changes in vegetation. The *n*–C_{29}/*n*–C_{27} ratio increases from 1.2 to 1.8 in the lower part of the seam (2.2-7.4 m) and varies between 1.3 and 1.5 in the upper part. The *n*–C_{31+33}/*n*–C_{27+29} ratio generally ranges between 1.0 and 1.3, but is significantly higher in the uppermost sample (2.6). The depth trends of ACL and of the *n*–C_{31+33}/*n*–C_{27+29} ratio are almost identical (Fig. 6). The pristane/phytane (Pr/Ph) ratio is a widely used redox parameter (Didyk et al., 1978), but it is also strongly influenced by land plant input. The Pr/Ph ratio generally ranges from 2.2 to 3.6, but reaches a maximum (6.2) in the sample at 13.9-14.9 m depth.

Steranes occur in very low amounts and were not quantified, but land plant-derived tetra- and pentacyclic terpenoids are present in significant amounts (Table 2; Fig. 6). The dominant hopanoid compound is neohop-13(18)-ene (11.5-357.0 µg/gTOC). Aromatic hopanoids (D-ring monoaromatic hopane and benzohopanes) occur in minor amounts (0.16-2.09 µg/gTOC). Polyaromatic hydrocarbons (PAHs) were not detected.

Saturated, unsaturated, and aromatic sesquiterpenoids of the cadinane (21.8-97.1 µg/gTOC) and drimane (1.3-22.6 µg/gTOC) types are observed in varying amounts (Fig. 7). The predominant cadinane types are muurolane, cadinane, cadinene, calamene, calamanene, tetrahydrocadalene, cadalene, and cadinatriene. Aliphatic drimane types are longifolene, eudesmane, and drimane. Elemane type sesquiterpenoids occur in small amounts (0.1-1.9 µg/gTOC).

Gymnosperm-derived diterpenoids occur in very low concentrations (Table 2). The occurrence of pimarane is limited to the lower part of the seam (≤0.3 µg/gTOC) and the uppermost sample (0.1 µg/gTOC). Abietane type diterpenoids (norabiete-triene and norabiete-tetraene) are present in all samples, albeit at very low concentrations (0.3-2.0 µg/gTOC). Angiosperm-derived triterpenoids are much more abundant than diterpenoids (Table 2; Fig. 7). They are dominated by ursane (urs-12-ene, dinorursa- 1,3,5(10),12-tetraene, tetramethyl-octahydropicene, dinor-oleana(ursa)-triene) and oleanane types (olean-12(18)-ene, olean-13(18)-ene, monoaromatic 8,14-seco-oleanane, dinoroleana-tetraene) (47.9-574.3 µg/gTOC). Arborane type (aromatic des-A-arbora-triene, norarbora(ferna)-triene, arbora(ferna)triene, dinorarbora(ferna)tetraene, dinoarbora(ferna)pentaene; 3.53-28.79 µg/gTOC) and lupine-derived (aromatic dinorlupatriene;

0.16-2.09 µg/gTOC) triterpenoids are less abundant. The di-/(di- + triterpenoids) ratio, a measure of the proportion of conifers versus angiosperms (Bechtel et al., 2003b), is very low (<0.02). Ratios >0.01 are restricted to the middle part of the seam (Fig. 6).

Table 2: Organic geochemistry of selected samples in seam BL1

Sample	TAR HC	Paq	CPI	ACL	nC_{29}/nC_{27}	nC_{31+33}/nC_{27+29}	Pr/Ph	Sesqui-	Di-	Tri-	Elem	Cadi	Drim	Pim	Abietane	Lupane	Olean - Urs	Arbor	Di-/(Di- + Tri-) terpenoids
								terpenopids (µg/g TOC)			(µg/g TOC)								
BL1-4	36.7	0.17	4.8	29.8	1.5	2.6	2.3	101.0	1.4	181.3	1.9	64.2	22.6	0.1	0.8	0.5	43.9	3.5	0.008
BL1-6	18.7	0.26	3.8	29.3	1.4	1.3	3.1	131.5	2.2	160.3	1.9	97.1	11.0	0.0	1.8	1.6	38.9	19.8	0.014
BL1-8	22.3	0.26	3.4	29.2	1.5	1.0	6.2	53.0	2.0	104.4	0.4	39.7	5.0	0.0	1.8	2.0	23.8	13.9	0.018
BL1-10	15.9	0.27	3.3	29.2	1.3	1.2	3.6	40.3	2.0	167.7	0.4	30.4	3.7	0.0	1.9	1.5	45.6	15.9	0.012
BL1-12	20.5	0.24	3.5	29.2	1.5	1.0	2.6	27.0	1.7	85.0	0.1	21.8	1.3	0.0	1.5	1.0	17.2	12.4	0.019
BL1-16a	19.9	0.21	3.5	29.2	1.8	1.0	2.8	45.4	2.3	115.1	0.2	37.1	2.0	0.1	2.0	2.1	22.8	28.8	0.019
BL1-18b	20.6	0.26	3.7	29.4	1.5	1.3	2.4	60.7	0.4	51.7	1.0	47.1	7.4	0.0	0.3	0.2	12.3	3.6	0.008
BL1-19b	17.8	0.24	3.4	29.1	1.2	1.0	2.2	50.8	3.8	592.5	1.1	33.5	13.2	0.3	1.9	1.8	574.3	16.4	0.006

TAR – terrestrial/aquatic ratio (Bourbonniere and Meyers, 1996); Paq – P-aqueous ratio (Ficken et al., 2000); CPI – carbon preference index (Bray and Evans, 1961); ACL – average chain length (Poynter and Eglinton, 1990); Pr/Ph – pristane/phytane ratio; Elem – elemane-type; Cadi – cadinane-type; Drim – drimane-type; Pim – pimarane-type; Abiet – abietane-type; Lup – lupane derivatives; Olean-Urs – oleanane-ursane derivatives; Arbor – arborane-type

4.3 Maceral composition and huminite reflectance

Maceral percentages are listed in Table 3 and are plotted as a function of depth in Figure 8. Photomicrographs of typical macerals are shown in Figures 9 and 10.

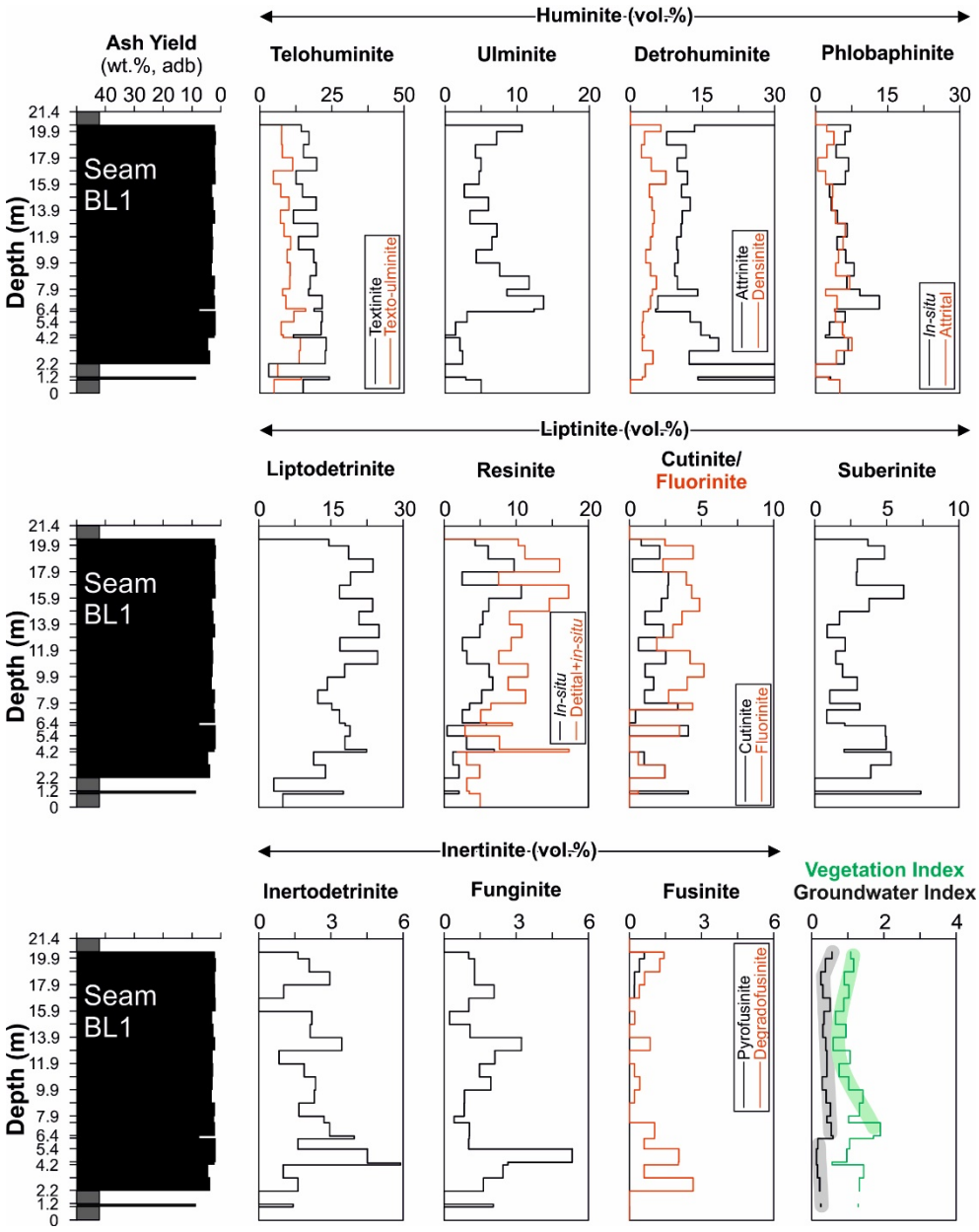

Figure 8: Variations of maceral percentages and petrography–based facies indicators in seam BL1.

Huminite, derived from lignin and cellulose, is the predominant maceral group in most samples (47–75 vol.%). Huminite percentages (63-75 vol.%) are relatively high in the lower part of the BL1 seam (2.2-4.2 m), but decrease sharply (47 vol.%) in the thin layer between 4.2 to 4.4 m depth, which is characterized by the HI maximum. Above this level, the huminite content increases again and a reaches another maximum between 6.4 and 7.4 m (72 vol.%). The interval between 7.4 and 15.9 m is characterized by a general upward decrease in huminite to 47 vol.%. In the upper part of the seam (15.9-20.4 m), huminite percentages vary considerably, but display a general upward increase. Telohuminite (Fig. 9a-f) is the dominant huminite maceral. Detrohuminite (Fig. 9c-f) and gelohuminite occur in lower amounts. Phyllohuminite was recognized, but not counted separately (Fig. 9g). Phlobaphinite (cell fillings) is present both *in–situ* (in telohuminite; Fig. 9a) and attrital (Fig. 10e). Ungelified macerals (textinite, attrinite; Fig. 10g) are more abundant than gelified macerals (e.g., ulminite, densinite; Fig. 9c,e). Random huminite reflectance of three samples ranges from 0.33 to 0.35 %Rr (Table 3).

Liptinite, derived from hydrogen-rich plant components (e.g., resins, cuticules, etc.), occurs in significant amounts (21–50 vol.%) and shows an opposite depth trend compared to huminite. Thus, liptinite is most abundant in the thin layer between 4.2 to 4.4 m depth (42 vol.%) and in the layer between 14.9 and 15.9 m (49 vol.%), where the amount of liptinite is even higher than that of huminite. Liptinite is dominated by liptodetrinite (Figs 8, 9f, 10d; 11–25 vol.%). Resinite (fossil resins; Figs 9, 10) is also abundant (3–22 vol.%) and shows the same depth trend as the sum of liptinite macerals. It occurs *in–situ* (within telohuminite; Fig. 9a-b), detrital (Fig. 10e-h), and as the resinite variety fluorinite (leaf resins) (Fig. 9h). Detrital and *in–situ* resinite occur in similar amounts (Fig. 8). Resinite (*in–situ* + detrital) shows weak positive correlation with HI (r^2=0.48). Cutinite (Fig. 9g-h) occurs in varying proportions (max. 4 vol.%; Fig. 8), but its content is low in the coal layer beneath the BL1 seam and in its lower part. Sporinite occurs only in traces (max. 0.2 vol.%). Suberinite (fossil cork) (Figs 9g-h, 10a-b) is present in all samples in considerable amounts (0.8-7.3 vol.%).

Macerals of the inertinite group are less abundant (often 2-7 vol.%). Higher proportions (10-14 vol.%) are restricted to two intervals (4.2-5.4 m; 12.9-13.9 m). Inertodetrinite (Fig. 10g; up to 5.9 vol.%) and funginite (Figs 9c,g, 10c; up to 5.4 vol.%) are the dominant inertinite macerals. Pyrofusinite (Fig. 10e) occurs in notable amounts only in the uppermost seam (16.9-20.4 m; 0.2-0.6 vol.%). Degradofusinite is more abundant (up to 2.7 wt.%). Similar to pyrofusinite, its proportion increases in the uppermost part of the seam (up to 1.4 vol.%), but it is also present near the base of the seam (2.7 vol.%; Fig. 8).

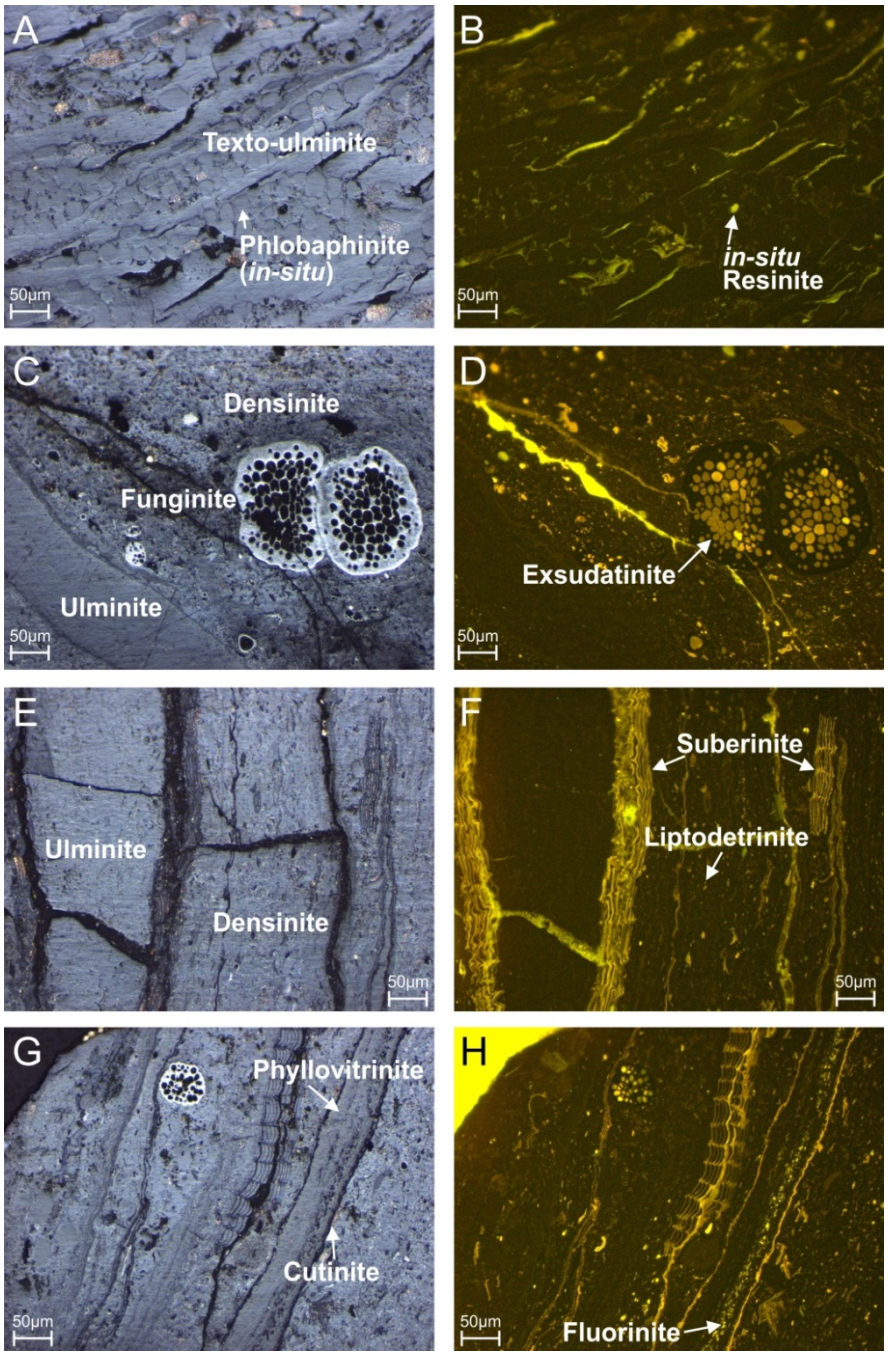

Figure 9: Representative photomicrographs of sample BL1 (3.2-4.2 m). Left: white light, right: blue light. **(a,b):** Texto-ulminite with *in-situ* phlobaphinite and resinite. **(c,d):** Ulminite and densinite with large funginite particles. Exsudatinite fills cavities inside of funginite. **(e,f):** Ulminite and densinite separated by suberinite. Liptodetrinite occurs together with humodetrinite. **(g,h):** Leaf with phyllohuminite, fluorinite, and cutinite in detrital coal with suberinite and funginite.

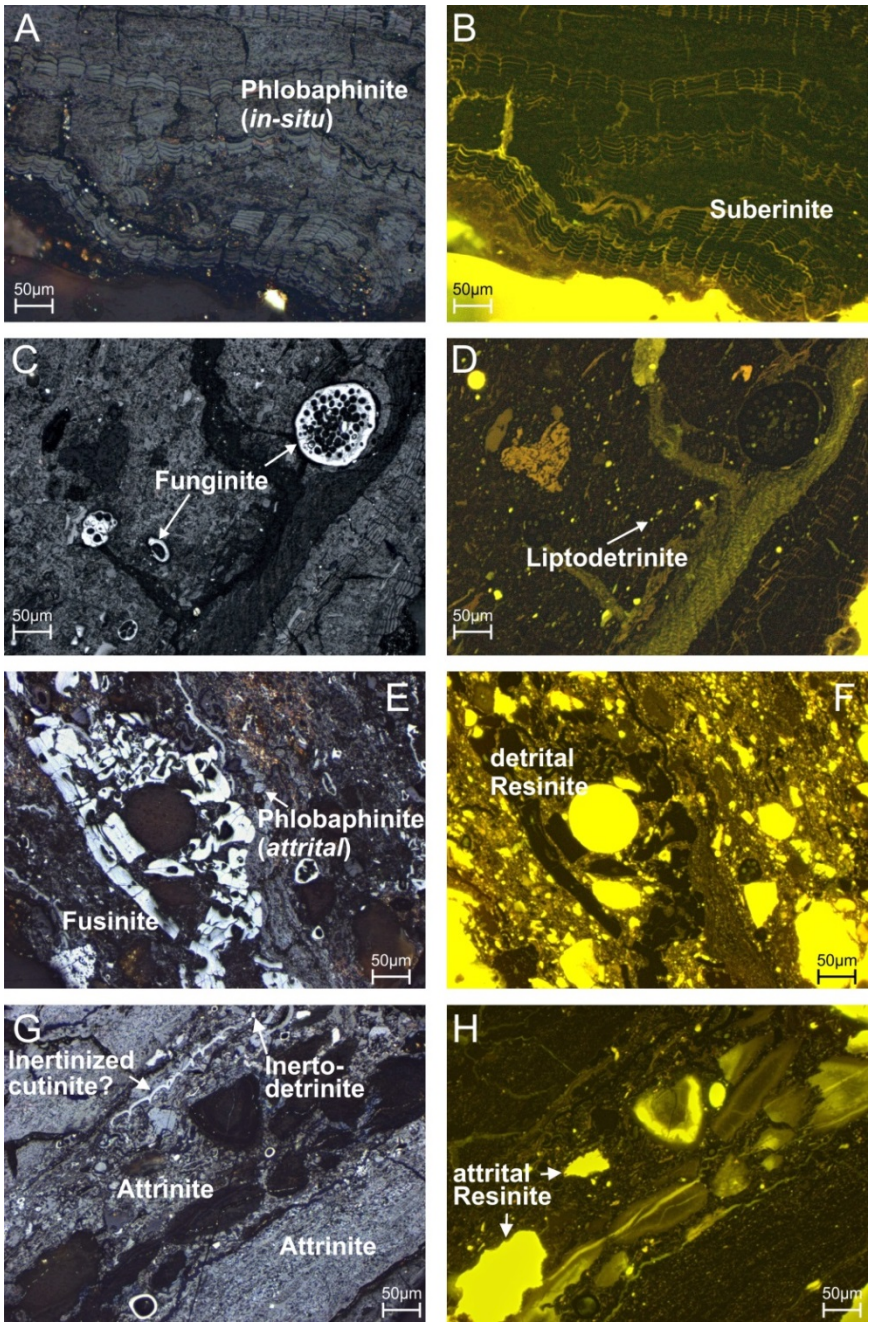

Figure 10: Representative photomicrographs of various samples from seam BL1. Left: white light, right: blue light. **(a,b):** 19.9-20.4 m; Coal rich in suberinite. Phlobaphinite occurs between suberinite. **(c,d):** 18.9-19.9 m; Attrinite matrix with funginite showing difference sizes and shapes. **(e,f):** 4.2-4.4 m; Coal with high amounts of detrital resinite, fusinite and attrital phlobaphinite. The HI of this sample is exceptionally high (539 mgHC/gTOC). **(g,h):** 4.2-4.4 m; Attrinite and detrital resinite with inertodetrinite fragments. Inertinized cutinite(?) may be related to pathogenic fungi (cf. Arya et al., 2021; Fikri et al., 2022a). Alternatively, the oxidized structure may be interpreted as altered epidermal layers of roots (Moore et al., 1996).

Table 3: Maceral percentages (in vol.%), maceral–based facies indicators (VI, GWI), and random huminite reflectance (%Rr).

Sample	Text.	Text-ulmi	Ulmi.	Attr.	Dens.	Pholabaphinite		Lipto det.	Resinite		Cutin.	Fluor.	Suber.	Spor.	Pyro	Degra.	Fungi.	Inerto detr.	VI	GWI	%Rr.	Stdev
						in-situ	detr.		*in situ*	detr.					Fusinite							
BL1-roof	0.0	0.0	0.0	100.0	0.0	0.0	0.0	0.0	0.0	0.0	0.0	0.0	0.0	0.0	0.0	0.0	0.0	0.0				
BL1-2	14.3	7.6	10.7	13.3	6.4	7.2	2.3	14.5	4.3	5.9	0.8	2.5	3.7	0.0	0.6	1.4	1.0	1.6	1.1	0.6		
BL1-3	17.0	7.6	7.1	7.6	2.9	6.1	3.8	18.7	6.1	5.0	2.1	4.4	4.8	0.0	0.4	1.3	1.3	2.1	1.2	0.4		
BL1-4	15.2	7.8	4.2	11.6	2.3	4.2	2.3	23.8	9.7	6.3	0.2	2.3	2.9	0.0	0.2	0.6	1.3	2.9	0.9	0.3		
BL1-5	19.7	11.4	5.0	9.8	4.4	6.8	0.4	19.1	2.5	5.0	2.7	3.9	2.9	0.0	0.2	0.4	2.1	1.0	1.0	0.3	0.35	0.02
BL1-6	12.5	4.7	4.7	11.9	7.4	6.2	2.1	16.8	10.7	6.6	2.7	4.3	6.2	0.0	0.0	0.0	1.0	0.0	0.9	0.5		
BL1-7	14.8	7.3	2.7	10.6	4.0	2.9	3.5	23.7	6.2	8.4	2.2	4.9	3.8	0.0	0.0	0.2	0.2	2.2	0.7	0.3		
BL1-8	19.5	10.1	6.0	12.4	4.5	3.2	3.4	20.8	5.4	3.6	1.1	3.6	1.7	0.0	0.0	0.0	1.1	2.1	0.9	0.3		
BL1-9	11.6	7.1	3.4	10.8	5.0	4.5	4.1	25.0	5.0	5.8	2.4	3.0	0.9	0.0	0.0	0.9	3.2	3.4	0.6	0.4		
BL1-10	20.0	8.4	7.2	10.5	4.6	6.5	6.1	16.9	2.5	6.8	0.6	1.9	2.1	0.0	0.0	0.0	2.1	0.8	1.1	0.4		
BL1-11	13.4	10.7	6.5	9.6	4.2	4.4	5.7	24.7	3.1	4.4	2.5	4.2	1.5	0.0	0.0	0.2	1.5	1.9	0.8	0.4	0.33	0.02
BL1-12	18.7	9.5	4.3	9.9	3.2	6.2	4.7	17.8	6.2	5.4	1.1	5.2	1.9	0.0	0.0	0.4	1.9	2.4	1.0	0.3		
BL1-13	19.5	10.5	7.6	9.2	4.2	8.0	4.2	14.3	6.7	2.1	1.7	4.0	2.9	0.0	0.0	0.2	0.8	2.3	1.4	0.4		
BL1-14	17.5	10.4	11.7	9.8	5.4	6.5	7.1	12.3	5.2	6.0	1.0	2.7	1.0	0.0	0.0	0.0	0.8	1.7	1.3	0.5		
BL1-15	16.9	7.9	8.6	14.0	4.6	9.2	2.1	15.2	3.5	2.9	3.3	4.4	3.1	0.0	0.0	0.0	0.4	2.7	1.0	0.4		
BL1-16a	21.6	9.0	13.7	5.7	4.2	13.2	4.4	16.8	2.5	2.5	0.4	0.0	0.8	0.0	0.0	1.1	1.1	2.9	1.9	0.5	0.35	0.02
BL1-16b	18.8	15.9	12.3	5.2	3.8	4.0	4.0	18.0	5.8	3.5	0.0	0.0	2.1	0.0	0.0	1.0	1.0	4.0	1.7	0.6		
BL1-17	21.6	11.8	3.1	12.4	2.7	6.1	4.1	19.0	0.4	2.4	4.1	3.5	4.9	0.0	0.0	0.6	1.0	1.6	1.1	0.2		
BL1-18a	21.2	7.4	1.4	14.6	2.5	2.9	5.6	17.9	3.1	4.5	0.0	0.0	4.9	0.0	0.0	2.1	5.4	4.5	1.0	0.1		
BL1-18b	11.6	8.1	0.0	16.5	2.9	2.0	5.9	22.4	6.9	10.4	0.0	0.0	2.0	0.0	0.0	2.0	2.6	5.9	0.6	0.1		
BL1-19a	23.0	14.1	2.0	18.3	2.4	6.7	7.5	11.4	1.2	1.8	1.0	0.6	5.3	0.0	0.0	0.6	2.4	1.0	1.4	0.2		
BL1-19b	22.7	13.7	2.4	12.2	4.7	5.9	4.3	13.9	2.0	2.9	2.4	2.4	3.9	0.2	0.0	2.7	1.6	1.6	1.3	0.2		
BL1-20	3.1	6.3	0.0	81.3	3.1	0.0	0.0	3.1	0.0	3.1	0.0	0.0	0.0	0.0	0.0	0.0	0.0	0.0				
BL1-21	24.1	14.3	2.9	14.1	2.4	3.1	2.7	17.6	2.0	1.4	4.1	0.6	7.3	0.0	0.0	0.0	2.0	1.4	1.3	0.3		
BL1-floor	15.0	5.0	5.0	55.0	0.0	5.0	5.0	5.0	0.0	5.0	0.0	0.0	0.0	0.0	0.0	0.0	0.0	0.0				

Text. – textinite, Ulmi. – ulminite, Attr. – attrinite, Dens. – densinite, Liptodet. – liptodetrinite, Cutin. – cutinite, Fluor. – fluorinite, Suber. – suberinite, Spor. – sporinite, Fungi. – funginite, Inertodetr. – inertodetrinite, VI – vegetation index, GWI – groundwater index. stdev – standard deviation.

5. Discussion

5.1 Maturity

Huminite reflectance (0.33-0.35 %Rr) and T_{max} values (<400 °C in coal samples, avg. 418 °C in non-coal layers) show the low maturity of the BL1 seam. This is supported by the high moisture content (~35 wt.% as received) and low calorific value of the coal, which classify the coal as lignite. Comparison with Miocene coal from the Tutupan mine in the Barito Basin, indicates that the Tutupan coal (0.36-0.41 %Rr; moisture: 18.8-26.3 wt.% in different seams) is slightly more mature.

5.2 Rheotrophic versus ombrotrophic and freshwater versus brackish peat formation

Rheotrophic (low–lying) and ombrotrophic (domed) mires are widespread in Southeast Asia. Peat accumulation in rheotrophic and ombrotrophic mires has also been proposed for Eocene and Miocene coals in south Kalimantan (e.g., Demchuk and Moore, 1993; Morley, 2013; Fikri et al., 2022a,b). Different mire-types can be distinguished based on basic parameters such as ash yield and sulphur content (e.g., Gruber and Sachsenhofer, 2001). These parameters are used in this section. In following sections, peat types are characterized in more detail based on biomarker and petrographic evidence.

Ash yields in the studied section range from 1.9 to 8.8 wt.%, with ash yields above 5 wt.% limited to the coal layer beneath the main seam (1.0-2.0 m) and a thin layer at 6.2-6.4 m (Fig. 5). Sulphur contents are also very low (0.08-0.16 wt.%). The borehole panel shown in Figure 4 indicates that low ash yield and low sulphur content are characteristic of the BL1 seam throughout the Jumbang mine. Low ash yields and low sulphur contents suggest deposition in a rainwater-fed ombrotrophic mire.

Slightly increased ash yields near the base of the seam could indicate a transition from an initial rheotrophic to an ombrotrophic setting. In the early stages of ombrotrophic mires, when roots were still reaching the nutrient-rich substrate, a slight increase in ash yield may also be due to uptake of inorganic substances. In some boreholes (5-6, 8-11, 16) not only ash yields, but also sulphur contents are increased in the lowermost part of seam BL1U.

In several boreholes (e.g., 3, 11, 16 in Fig. 4), but not in the study section (Fig. 5), ash yields are also increased near the top of the seam. This may indicate a flooding event that finally terminated peat accumulation. Interestingly, this flooding is hardly reflected in the sulphur contents, which remain very low even in the uppermost samples (Fig. 4).

While sulphur contents in the BL1 seam are typically very low (<<0.5 wt.%), locally strongly elevated sulphur contents (1.0-1.5 wt.%) occur near the top of the lower coal bench (BL1L). This sharp increase in sulphur content is most evident in the lower coal bench in boreholes 5 to 8, which are located approximately 1 km southwest of the study section (Fig. 4). The high sulphur content in this area is a strong argument for the deposition of BL1L in a rheotrophic low-lying mire. Here, sulphur content is controlled by sulfate availability of and the presence of sulfate-reducing bacteria, which is mainly controlled by acidity (e.g., Casagrande, 1987). The observed sulphur levels are consistent with deposition in a freshwater rheotrophic mire, where high water levels resulted in dilution of humic acids and an increase in pH. However, given the low ash yield of the sulphur-rich coals (Fig. 4) and the coastal depositional environment of the host rocks (e.g., Achmad, 2018), the high sulphur contents are most likely due to the influence of brackish water, underscoring the near-shore environment of the BL1 seam in the Jumbang mine.

It should be added that sulphur contents greater than 0.4 wt.% were not detected in Tutupan coals deposited in ombrotrophic or rheotrophic environments (Fikri et al., 2022a). This is likely due to their greater distance from the paleo-shoreline. In fact, Fikri et al. (2022a) postulated the formation of Tutupan seams T110 and T210 in kerapah (inland or watershed) swamps.

5.3 Nature of the peat–forming vegetation as recorded by geochemical data

The dominance of terrigenous plants in the coal organic matter is reflected in the distribution of *n*-alkanes and isoprenoids (Fig. 6). The *n*-alkane based parameters TAR (~19), Paq (~0.25) and CPI (~3.5) are quite uniform in the main part of the BL1 seam (2.2-16.9 m) showing the expected dominant role of land plants (Bourbonniere and Meyers, 1996; Ficken et al., 2000). An even stronger dominance of land plant is indicated by the biomarker data from the uppermost sample (17.9-18.9 m; Fig. 6). The dominant role of land plants is also confirmed by the Pr/Ph ratios (~3.2; e.g., Brooks et al., 1969; Powell and McKirdy, 1973), with the highest ratios are found in the middle part of the seam (13.9-14.9 m).

A notable feature of the BL1 coal is the high concentration of *n*-C_{31} alkanes (Fig. 7), which is responsible for very high *n*–C_{31+33}/*n*–C_{27+29} ratios (average 1.3; Fig. 6). Following Schwark et al. (2002) and Zech et al. (2009), the dominance of *n*-C_{31} is attributed to the input of grasses and herbs.

Very low di- /(di- + triterpenoids) ratios (<0.02; Fig. 6) indicate that gymnosperms were rare in the peat-forming vegetation (cf. Bechtel et al., 2003b). Still low, but higher values were detected for Miocene coal in the Tutupan mine (0.01-0.12). Morley (2013) suggested that diterpenoid biomarkers in tropical peats from Southeast Asia may be derived from Dacrydium (Podocarpaceae) and possibly Agathis (Araucariaceae). He also noted that the presence of Dacrydium (together with the angiosperm Gymnostoma) is an indicator of kerapah swamps located at a greater distance from the paleo-shore line than basinal (or coastal) domed peats. Based on this information, Fikri et al. (2022a) postulated the deposition of Tutupan coal in kerapah swamps. In contrast to kerapah swamps, gymnosperms are largely absent from basinal mires (Morley, 2013). Therefore, the observed very low di- /(di- + triterpenoids) ratios in the BL1 coals support the deposition in a basinal peat growing behind mangrove swamps. This interpretation is further supported by the postulated near-shore environment.

Low di- /(di- + triterpenoids) ratios (0.1-0.07) were also detected in middle and upper Miocene coals from the Kutai Basin by Widodo et al. (2009). These authors found a positive relation between $\delta^{13}C$ values (-28 to -27 ‰) and the di- /(di- + triterpenoids) ratios. Thus, the range of $\delta^{13}C$ values determined for the BL1 coals (-28.3 to -27.5 ‰), reflects the largely missing contribution of gymnosperms.

Among terpenoids derived from land plants, sesquiterpenoids of the cadinane type and triterpenoids of the ursane/oleanane type predominate. Cadinanes in present-day peats and Miocene coals in Southeast Asia are related to dammar resin produced by the angiosperm family *Dipterocarpaceae*, particularly the genus *Shorea* (e.g., Anderson, 1963; 1964; Anderson and Muller, 1975; Esterle and Ferm, 1994; Esterle et al., 1989; Cameron et al., 1989; Page et al., 1999; Wüst et al., 2001; van Aarssen et al., 1990, 1994; Widodo et al., 2009; Morley, 2013). A positive correlation between cadinane type sesquiterpenoids and the amount of *in-situ* resinite (r^2=0.63) provides additional support for the presence of dammar resin in the BL1 seam. The

vertical distribution of the cadinane type sesquiterpenoids shows an upward increase in the upper part of the seam (~9-17 m) with a maximum (98 µg/gTOC) at 15.9-16.9 m (Fig. 6).

Sequiterpenoids of the elemane type occur in small amounts. They may originate from gymnosperms (Otto and Wilde, 2001) or Magnoliaceae (Ding et al., 2019). Since their concentration shows a negative correlation with the di- /(di- + triterpenoids) ratio, a relation to Magnoliaceae is considered likely.

The concentration of arborane/fernane type triterpenoids is low. Arborane/fernane type triterpenoids are attributed to ferns or bacteria (e.g., Hauke et al., 1992). A fern source is considered likely because ferns are ubiquitous components of tropical vegetation in Southeast Asia (Demchuk and Moore, 1993; Morley, 2013).

Based on the near-shore environment and the virtual absence of gymnosperm biomarkers, the BL1 seam is presumed to have been deposited in a basinal peat swamp. Basinal peat swamps were studied in detail by Anderson (1963; 1964), who distinguished six phasic communities depending on decreasing soil fertility and increasing waterlogging. Phase 1 shows similarities with lowland rain forests, phase 2 shows less diversity with abundant *Shorea albida*, while phase 3 consists almost entirely of very large specimens of *Shorea albida*. Phase 4 and 5 lack emergent size trees and phase 5 lacks *Shorea albida*. Phase 6 represents open woodland or savanna where herbs are common (see also Morley, 2013). Given the above biomarker results, it is tempting to relate the maximum in cadinane type sesquiterpenoids (derived from dammar resin) at 15.9-16.9 m with phase 3 or 4 and the highest n–C_{31+33}/n–C_{27+29} ratio (indicating herbaceous vegetation) at 17.9-18.9 m to phase 6. Of course, palynological data are needed to support or refute this interpretation.

5.4 Petrography and mire types

The biomass of the original peat can be inferred from the abundance of specific macerals and of maceral ratios (e.g., Dai et al., 2020). The sum of the leaf–related macerals cutinite and fluorinite varies strongly from 0.0 to 7.7 vol.% (average 4.3 vol.%), but only samples from the lower part of the seam contain less than 0.1 vol.%. The percentages of cutinite and fluorinite are positively correlated in the lower part of the seam (2.2-7.9 m: r^2=0.92) and in the upper part (10.9-20.4 m: r^2=0.63) (Fig. 11), but the ratio between fluorinite and cutinite is much higher in the upper part of the seam (7.9-20.4 m; Fig. 8). This indicates a change in leaf-forming vegetation at 7.9 m depth. It may be a coincidence, but some biomarker trends (e.g., Paq, *n*-C_{29}/*n*-C_{27}) show a break at roughly the same depth (cf. Fig. 6).

Suberinite is mainly derived from rootlets and occurs in high proportions in rheotrophic and ombrotrophic tropical mires (Fikri et al., 2022a,b). Suberinite contents are also very high in the Jumbang mine (0.9-7.3 vol.%; average 3.2 vol.%), especially in the lower and upper part of the BL1 seam (Fig. 8).

Resins, both *in-situ* (4.6 vol.%) and detrital (4.7 vol.%), occur in high amounts in the BL1 seam. Their content increases upward in the seam, but the maximum percentage (17.7 vol.%) occurs in the thin layer between 4.2 and 4.4 m depth with very high HI (539 mgHC/gTOC). Resinite is also abundant in the clastic parting near the base of the seam. At least partly, resinite is derived from dammar resin (see section 5.3). In contrast to leaf- and root-derived macerals and resinite, sporinite is largely absent.

The proportion of inertinite macerals (excl. funginite) is low (1.2-8.6 vol.%; average 3.8 vol.%). This indicates that wildfires were very rare and that oxidation at the peat surface was limited. Small amounts of pyrofusinite in the uppermost part of the seam (Fig. 8) were probably wind-transported. Funginite is an inertinite maceral derived from fungal remains (0.2–5.4 vol%; average 1.6 vol.%). It occurs as unicellular spherical bodies and multicellular objects whose size can be well over 100 µm (Fig. 9c,d). Substantial amounts of funginite have been found in Miocene tropical coals (Demchuk and Moore, 1993; Fikri et al., 2022a) and in present-day ombrotrophic mires (Dehmer, 1993; Esterle and Ferm, 1994). Apparently, fungal activity played

an important role in the decay and decomposition of dead plants (Adaskaveg et al., 1991; Hower et al., 2011a,b).

Various maceral–based facies indicators have been introduced to determine peat facies (e.g., Diessel, 1986; Calder et al., 1991; Markic and Sachsenhofer, 1997). Although poor agreement between petrographic, palynological, and geochemical data has been frequently reported (e.g., Wüst et al., 2001; Moore and Shearer, 2003; Dai et al., 2020; Fikri et al., 2022a), the use of these indicators is reasonable if all available non-maceral data and the fact that petrographic data reflect both changes in primary vegetation and degradation processes are taken into account (Demchuk and Moore, 1993; Wüst et al., 2001; Moore and Shearer, 2003; Fikri et al., 2022a,b). In the present paper, the vegetation index (VI) and groundwater index (GWI) of Calder et al. (1991) are applied. These parameters were developed for Pennsylvanian coal but appear to be applicable to coals of different ages, provided trends rather than absolute values are considered (Table 3; Fig. 8).

VI is the ratio of preserved tissues to detrital macerals and is considered a proxy of the proportion of decay–resistant plants.

VI = (humotelinite + phlobaphinite (*in–situ*) + fusinite + suberinite + resinite (*in–situ*)) / (detrovitrinite + phlobaphinite (attr.) + gelinite + inertodetrinite + sporinite + cutinite + liptodetrinite + fluorinite + resinite (detr.) + alginite)

GWI is the ratio of mineral matter plus gelified macerals to ungelified macerals and is considered an indicator of the wetness of the peat (Calder et al., 1991).

GWI = (ulminite + densinite + collinite + mineral matter*) / (textinite + attrinite)

* Mineral matter (mm) has been calculated using the formula of Parr (1928) (mm = [1.08 x ash] + [0.55 x sulphur]).

The vegetation index (VI) is low (0.56–1.90; av. 1.10), reflecting moderate decomposition of the precursor plant material. The highest values (>1.7) are observed between 6.2 and 7.4 m. Above this level, VI decreases to 12.9 to 13.9 m, showing a slight increase only in the upper 7 m of the seam. The groundwater index (GWI) is very low (0.14-0.25) in the lower part of the seam (1.0-6.4 m) and low (0.25–0.59) in the upper part (6.4-20.4 m). Neither VI nor GWI can be correlated

with geochemical parameters. Only GWI shows a weak positive correlation with the di- /(di- + triterpenoid) ratios (r^2=0.34), which might indicate that gymnosperms, if present, preferred moist conditions.

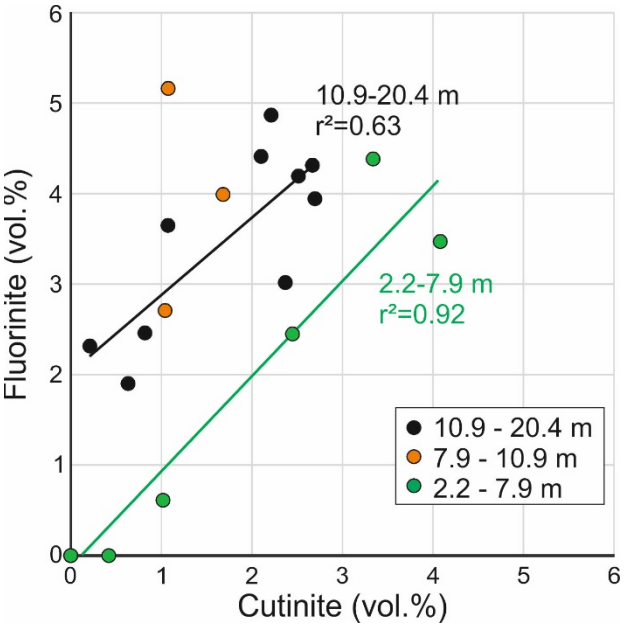

Figure 11: Plot of fluorinite versus cutinite percentages. Positive correlations exist for both samples from the lower part of the seam (2.2-7.9 m; r^2=0.92) and samples from the upper part (10.9-20.4 m; r^2=0.63), but the ratio of fluorinite to cutinite is higher in the upper part.

5.5 Comparison of Miocene ombrotrophic coals in Kalimantan and the Eastern Alps

Middle Miocene ombrotrophic coals are widespread in the Warukin Formation in Kalimantan, which formed during the post-rift/thermal sag stage of the Asem-Asem and Barito basins (e.g., Friedrich et al., 2016). Coals of the same age formed in warm-temperate to subtropical climate in small pull-apart basins in the Eastern Alps (Fig. 12a). The coal in the Leoben Basin was formed in an ombrotrophic setting (Gruber and Sachsenhofer, 2001). This allows comparison of ombrotrophic coals of the same age, but formed in different climates and basin types. Key parameters of these coals are summarized in Table 4 and shown in a cartoon-like illustration in Figure 13.

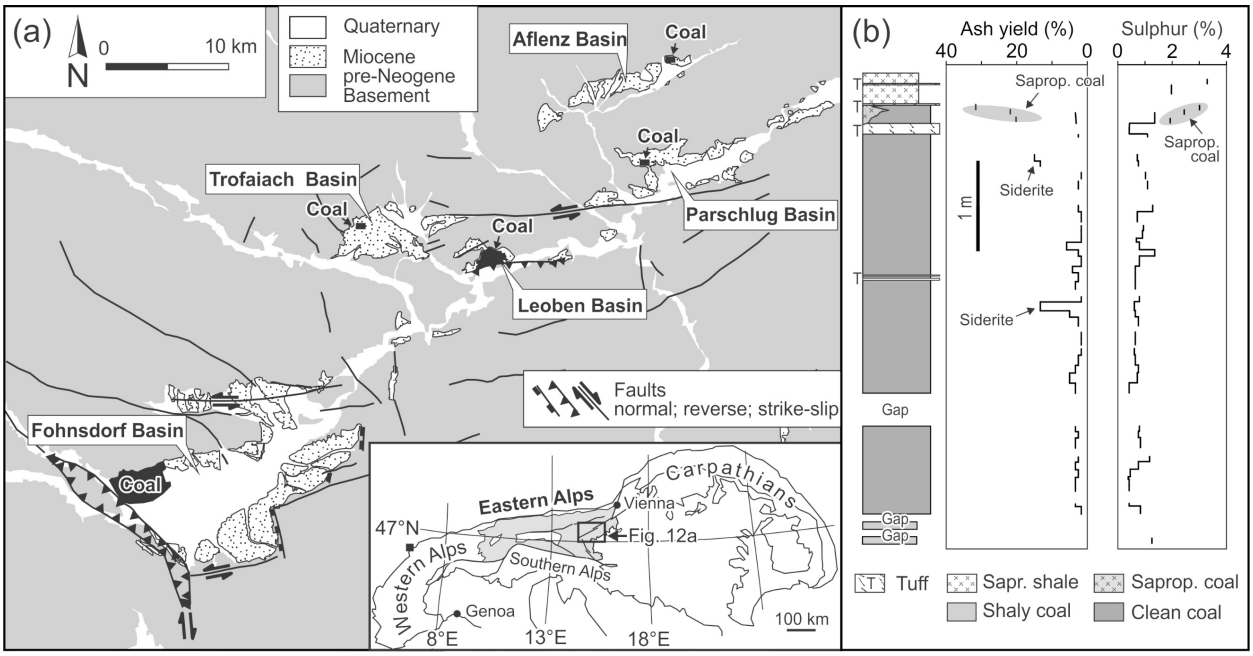

Figure 12: (a): Position of Miocene coal-bearing pull-apart in the Eastern Alps. Coal in the Fohnsdorf, Trofaiach, Aflenz and Parschlug basins was formed in low-lying mires, while coal in the Leoben Basin was formed in an ombrotropihc domed mire (Sachsenhofer et al., 2003). **(b):** Ash yields and sulphur contents of the coal seam in the Leoben Basin (after Gruber and Sachsenhofer, 2001).

Table 4: Summary of similarities and differences between middle Miocene ombrotrophic coals in Kalimantan and the Eastern Alps. Data from the Tutupan and Leoben mines are from Fikri et al. (2022a) and Gruber and Sachsenhofer (2001) and Bechtel et al. (2001), respectively.

	Jumbang Mine	**Tutupan Mine**		**Leoben Mine**
Peat–type	ombrotrophic (basinal)	ombrotrophic (kerapah)	ombrotrophic + rheotrophic	ombrotrophic
Rank	Lignite A	Subbituminous C		Subbituminous A
Climate (Friedrich et al., 2016; Kovar-Eder, pers. comm., 2023)	Tropical ever–wet	Tropical ever–wet		Warm temperate (Cfa)
Number of economic seams	1 (-3)	3		1
Lateral continuity	high	high		Restricted
Seam names	BL1	T110, T210	T300	Leoben seam
Thickness of single seams	20 m	up to 50 m	24 m	up to 16 m
Stacked successions (cycles)	no	yes (up to 5)	unclear (2?)	no
Marine/brackish influence	Local brackish influence in BL1U	—	—	—
Vegetation (Morley, 2013)	Angiosperm trees (e.g., Shorea)	Angiosperm trees (e.g., Shorea) (+gymnosperms)		??
Gymnosperms (Di–/(di- +Tri-)Terpenoids)	Very rare (0.01-0.02)	Rare (0.01-0.12)	Very rare (0.01-0.04)	High (0.63-0.92)
CPI	3.7 (3.3–4.8)	4.3 (2.8–6.2)	3.1 (2.2–3.8)	1.4 (1.1-2.8)
TAR	21.6 (15.9-36.7)	10.4 (5.8–23.4)	19.9 (6.0–38.4)	~15
Paq	0.24 (0.17-0.27)	0.14 (0.05–0.24)	0.08 (0.05–0.11)	~0.6
ACL	29.3 (29.1-29.8)	29.1 (28.2–30.6)	29.5 (29.0–30.0)	~28.8
n–C_{29}/n–C_{27}	1.47 (1.20-1.80)	1.39 (0.77–2.33)	3.14 (2.09–4.83)	~1.2
n–C_{31+33}/n–C_{27+29}	1.3 (1.0-2.6)	0.85 (0.17–2.23)	0.67 (0.46–0.91)	~0.45
Pr/Ph	3.2 (2.2-6.2)	12.8 (5.4–23.6)	6.1 (3.9–8.1)	5.4 (2.0-7.1)
Degradation (Vegetation Index)	Moderate (1.10)	Low (1.56)	Low (1.26)	Moderate (1.0)
Water table (GWI) / extent of external influx	Low (0.35)	Low (0.17)	Low (0.32)	Low (~0.1)
Resins (*in–situ*+detrital; vol.%)	Very abundant 9.3 (2.9-17.3)	Abundant 4.1 (1.0–19.1)	Abundant 4.0 (0.8–9.0)	Rare 0.6 (0.0-2.7)
Cadinane–source	Dammar resin (dipterocarps)	Dammar resin (dipterocarps)	Dammar resin (dipterocarps)	Conifer resins
Leafs (cutinite+fluorinite; vol.%)	abundant 4.3 (0.0–7.7)	abundant 4.8 (0.4–13.1)	abundant 3.8 (0.6–8.5)	rare to abundant 2.6 (0-20.8)
Roots (suberinite; vol.%)	very abundant 3.2 (0.0-7.3)	abundant 2.6 (0.2–7.0)	abundant 2.0 (0.4–4.6)	rare to abundant 0.7 (0.0-5.8)
Alginite	—	—	traces	—
Fungal activity (funginite; vol.%)	high 1.6 (0.2–5.4)	high 1.0 (0.0–3.2)	high 1.5 (0.6–2.8)	Low 0.2 (0.0-1.2)
Inertinite (excl. funginite; vol.%)	3.8 (1.2-8.6)	2.1 (0.0–4.0)	2.3 (0.6–5.0)	0.5 (0.0-2.4)

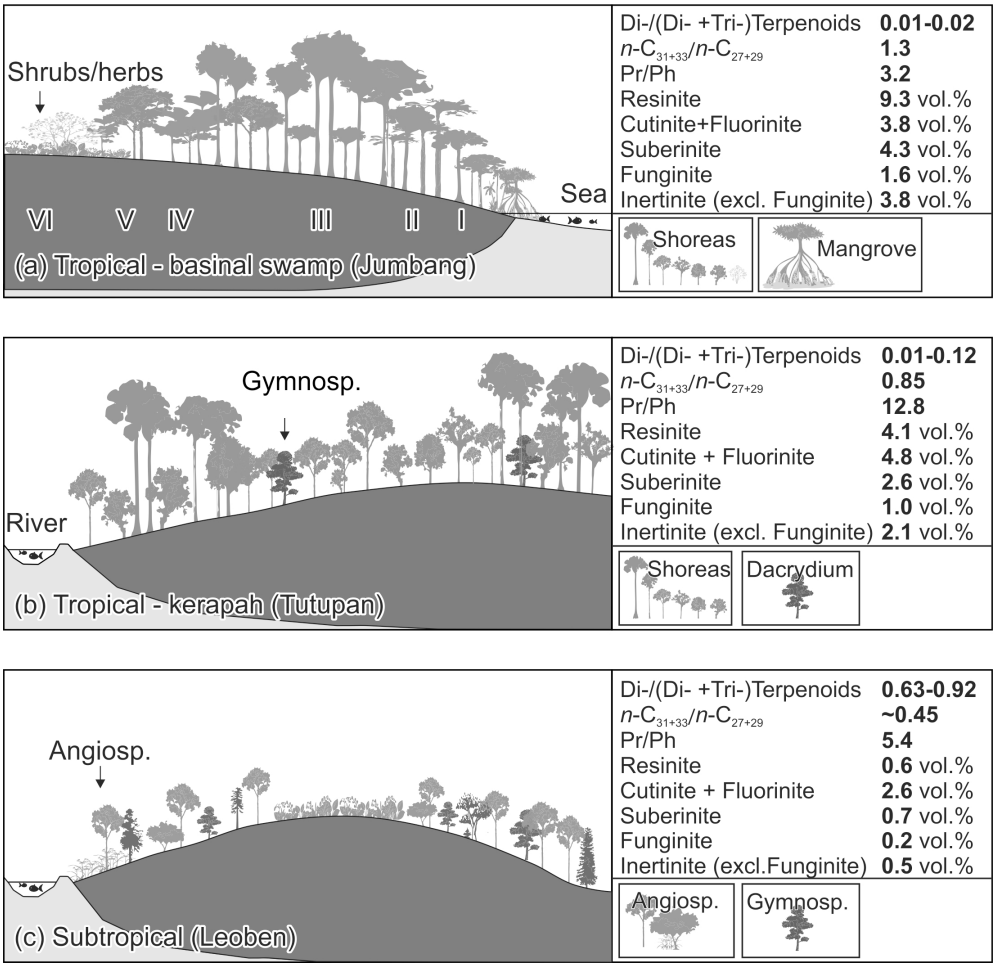

Figure 13: Cartoons showing middle Miocene peat forming environments in **(a)** tropical basinal swamp (Jumbang), **(b)** tropical kerapah swamp (Tutupan) and **(c)** in subtropical ombrotrophic mire (Leoben). Tropical vegetation in basinal swamp (phasic communities I-VI) according to Anderson (1963; 1964), Anderson and Muller (1975) and Morley (2003).

5.5.1 Climate and mire types

The tropical wet climate that prevailed in Kalimantan since Eocene time (Morley, 2012) favored middle Miocene coal accumulation in basinal and kerapah domed mires and in rheotrophic mires. Data published in this paper suggest that the Jumbang coal (seam BL1) was formed in a basinal mire (Fig. 13a). In contrast, coal exploited at the Tutupan mine was formed in kerapah mires (seams T110, T210; Fig. 13b) or in mixed rheotrophic/ombrotrophic mires (seam T300; Fikri et al., 2022a,b).

A warm, subtropical climate prevailed in the Eastern Alps during the (early) middle Miocene (e.g., Jiménez-Moreno et al., 2008). A rich flora has been described from the Leoben Basin (e.g., Ettingshausen, 1888) and the nearby Parschlug Basin (Kovar-Eder et al., 2022; see Fig. 12 for location). The Parschlug flora indicates a subtropical climate with pronounced seasonality (Csa, Csb according to Peel et al., 2007; Kovar-Eder et al., 2022). In contrast, a humid subtropical warm-temperate climate without distinct seasonality is indicated for the Leoben area (Cfa according to Peel et al., 2007; Kovar-Eder, pers. comm., 2023). We suspect that local climatic conditions in the Leoben area may have favoured the formation of an ombrotrophic mire (Fig. 13c), whereas ombrotrophic mires did not form in other areas in the Eastern Alps. Ash yield in the Leoben coal is very low and increased only in coal benches with diagenetic siderite concretions (Fig. 12b).

Peat accumulation rates may be influenced by climate. The average present-day peat accumulation rate of tropical peat in Southeast Asia is 1.3 mm/year (e.g., Page et al., 2010), with very few data exceeding 4.5 mm/year. However, average ombrotrophic peat accumulation rates in cool climates in northern Europe are in a similar range (0.5-3.5 mm/year; Stivrins et al., 2017), indicating that ombrotrophic peat growth rates are not necessarily higher in tropical areas.

5.5.2 Basin type, seam geometry and peat accumulation rates

Major differences exist between number, thickness, and lateral continuity of seams. The Miocene coal seams in Kalimantan formed during the post-rift/thermal sag stage of basin evolution (e.g., Friedrich et al., 2016). During this basin stage, faulting is minor and subsidence often moderate, favouring the accumulation of multiple, laterally extensive coal seams. Three seams of exceptional thickness are present at the Tutupan mine (Fikri et al., 2022a) and many

seams, although not all mined, are present in the Jumbang area (Fig. 2b). In contrast, coal in the Eastern Alps formed in late-orogenic pull-apart basins with limited lateral extent (Fig. 12a; Sachsenhofer et al., 2003). A single thick seam overlain by sapropelic coals and shales (Fig. 12b) is characteristic of this setting characterized by very high subsidence rates (Sachsenhofer, 2000).

The very large thickness of single Tutupan seams (up to 50 m) shows that subsidence rates were in equilibrium with peat accumulation for a long time. Geochemical data demonstrate that the large thickness of the Tutupan coals is the result of stacking of several coal cycles (Fikri et al., 2022a). No such stacking was observed in the Jumbang or Leoben coals. In case of coals in pull-apart basins, the high subsidence rates prevent the evolution of multiple cycles (cf., Markic and Sachsenhofer, 1997).

5.5.3 Sulphur contents and brackish/marine influence

All coals considered accumulated in freshwater mires. However, sulphur contents are locally elevated in the lower coal bench BL1L in the Jumbang mine (Fig. 4; section 5.2) suggesting deposition in a near-shore environment, possibly behind coastal mangroves (Fig. 13a). Coal layers with locally increased sulphur contents, therefore, may be used as marker for ombrotrophic basinal coals.

The average sulphur content in the Leoben coal is 0.65 wt.%. Relatively high sulphur contents in the lowermost ash-rich samples represent an early rheotrophic stage, whereas sulphur contents >1 wt.% in the uppermost 20 cm (Fig. 12b) may be related to volcanic activity rather than a brackish environment (Gruber and Sachsenhofer, 2001; Widodo et al., 2010).

5.5.4 Differences in vegetation between tropical and subtropical ombrotrophic mires as reflected by geochemical and petrographic data

Miocene vegetation in tropical ombrotrophic mires is dominated by angiosperms, but small amounts of gymnosperms are present in kerapah peat (e.g., Anderson and Muller, 1975; Morley, 2013; Fig. 13a,b). The peat-forming vegetation of the Leoben coal is unknown. Considering results from the ombrotrophic coal in the Lower Rhine Basin (e.g., Figueiral et al., 1999; Stock et al., 2016; LRB in Fig. 1a), angiosperm-dominated vegetation with substantial amounts of gymnosperms, rich in shrubs and mosses can be assumed (Fig. 13c). Differences in gymnosperm

abundance are clearly reflected in the di–/(di– + triterpenoids) ratios, which are very low in basinal and tropical rheotrophic coal, low to moderately high in kerapah coals, and high in subtropical Leoben coals (Table 4, Fig. 13).

Other geochemical differences include significantly lower Pr/Ph and significantly higher *n*–C_{31+33}/*n*–C_{27+29} ratios in coals from basinal peats (Fig. 13a) compared to kerapah peat (Fig. 13b). Because of the lower maturity of the Jumbang coal, these differences are attributed to differences in primary vegetation rather than maturity. The Pr/Ph ratio in the Leoben coal occupies an intermediate position. The *n*–C_{31+33}/*n*–C_{27+29} ratio in the Leoben coal is not discussed, as it may be reduced by the slightly higher maturity of this coal. The same is applies to the CPI, which is significantly lower in Leoben coal than in other coals.

Dammar resin-producing *Dipterocarpaceae* (e.g., *Shorea*) are characteristic floristic elements in Miocene coals from Southeast Asia. A positive correlation between cadinane type biomarkers and total resinite content for 56 Miocene coals from Kalimantan (r^2=0.62) supports the relation between cadalene and dammar resin in the tropical coals. Therefore, the higher cadinane concentration and higher resinite percentage in the Jumbang coal compared to the Tutupan coal support a higher contribution of *Dipterocarpaceae* in basinal peats. Cadinane type biomarkers are also present in the Leoben coal. As dipterocarps are restricted to the tropical zone, cadinanes in Leoben coal must have a different source. Bechtel et al. (2001) linked cadinanes in the Leoben coal to members of the Coniferales families.

There are also large differences in the maceral composition between tropical and subtropical ombrotrophic coals (Table 4, Fig. 13). Resinite is significantly more abundant in tropical coals than in subtropical coals. This could be due to the absence of dammar resin-producing dipterocarps outside the tropical zone. Among tropical coals, the average resinite percentage is more than twice as high in basinal compared to kerapah coal. Rootlet-derived suberinite is an important constituent in all tropical coals, but is much less abundant in subtropical coal. Some layers in the subtropical Leoben coal are very rich in leaf-derived macerals (max. 21 vol.%), but on average the amount of leaf-derived macerals is higher in tropical coals.

Funginite is present in significant amounts in tropical coals from Kalimantan (average 1.0-1.6 vol.%) and in present–day tropical peats (e.g., Demchuk and Moore, 1993; Dehmer, 1993; Esterle and Ferm, 1994), but in low amounts in subtropical Leoben coal (average: 0.2 vol.%). This indicates that Eh and pH conditions were less favourable to fungal activity in subtropical peatlands. The amount of oxidized plant material in tropical coals is low (average 2.1-3.8 vol.%), but even lower in the subtropical Leoben coal.

6. Conclusions

The purpose of studying the BL1 coal seam in the Jumbang mine (south Kalimantan) was threefold. First, to reconstruct the depositional environment of peat in the middle Miocene Asem-Asem Basin. Secondly, to compare the middle Miocene peat facies in the Asem-Asem and Barito basins based in coal data from the Tutupan mine. Finally, the tropical coals should be compared with the subtropical Leoben coal of the same age in the Eastern Alps.

Several middle Miocene coal seams are present in the Jumbang mine, but only the BL1 seam, up to 20 m thick, is mined. The lignite seam was investigated using a multi–method approach including analysis of ash yield, carbon and sulphur content, Rock–Eval pyrolysis, organic geochemistry, and petrology.

The BL1 seam is locally underlain by a coal bench (BL1L) that has a high sulphur content. Together with the facies of the host rocks, this indicates a near-shore environment. In contrast to the lower coal bench, the main seam contains low–ash, low–sulphur coal that represents peat accumulation in an ombrotrophic mire. According to biomarker data, the vegetation was dominated by angiosperms, including a large number of dammar resin-producing dipterocarps. Biomarkers for gymnosperms are very rare, suggesting deposition in a basinal (coastal) domed mire.

Ash yields, sulphur contents and geochemical and petrographic parameters of the BL1 seam are similar to those of the tropical Tutupan T110 and T210 seams in the Barito Basin, which accumulated in a kerapah (or inland) swamp. However, the concentration of cadinane type biomarker and the percentage of resinite are significantly higher in the BL1 seam, which is probably related to the abundance od *Shorea albida* in the basinal mire.

The comparison of the tropical ombrotrophic coals (Jumbang, Tutupan) with the subtropical ombrotrophic Leoben coal shows that the latter contains a significantly higher amount of gymnosperm-derived biomarkers. Moreover, the percentage of resinite, leaf- and rootlet derived macerals is significantly lower in the subtropical coal. The low amount of resinite is at least partly due to the absence of dipterocarps. The low amounts of funginite show that fungal activity was reduced in the subtropical peat. In addition, the amount of oxidized plant tissues (inertinite without funginite) is much lower in the subtropical coal studied.

Overall, the comparison of the Jumbang, Tutupan, and Leoben coals shows minor differences between ombrotrophic coals from kerapah and basinal mires, but major differences between tropical coals from Kalimantan and the subtropical ombrotrophic Leoben coal. Further investigations and a larger database are needed to show whether these differences are site-specific or general.

Acknowledgments

The first author (FHN) thanks OeAD, Austria´s Agency for Education and Internationalization, for an Ernst Mach Grant, ASEA-UNINET scholarship (Reference number: ICM-2019-13766, MPC-2020-01500, MPC-2021-01331, MPC-2021-01480). FHN would also like to thank PT Jhonlin Baratama and PT Arutmin Indonesia for their help in sampling the coal seams. We thank Johanna Kovar-Eder for as yet unpublished paleoclimate data on the Leoben site. The paper benefited from constructive reviews by Sri Widodo (Hasanuddin University, Indonesia) and Ksenija Stojanovics (University of Belgrade).

References

Achmad, A., 2018. Key of Meratus Complex Uplift: Sedimentological approachment of Ophiolitic Fragments within Warukin Sandstones in Asem - Asem Basin. Proceedings Pekan Ilmiah Tahunan IAGI, 28th Oct-1st Nov, 2018

Adaskaveg, J.E., Blanchette, R.A., Gilbertson, R.L., 1991. Decay of date palm wood by white-rot and brown rot fungi. Canadian Journal of Botany, 69/3, 615–629. https://doi.org/10.1139/b91-083

Advokaat, E. L., Marshall, N. T., Li, S., Spakman, W., Krijgsman, W., van Hinsbergen, D. J., 2018. Cenozoic rotation history of Borneo and Sundaland, SE Asia revealed by paleomagnetism, seismic tomography, and kinematic reconstruction. Tectonics, 37/8, 2486–2512. https://doi.org/10.1029/2018TC005010

Anderson, J.A.R., 1963. The flora of the peat swamp forests of Sarawak and Brunei, including a catalogue of all recorded species of flowering plants, ferns and fern allies. The Gardens´ Bulletin, Singapore, 20/2, 131–238.

Anderson, J.A.R., 1964. The structure and development of the peat swamps of Sarawak and Brunei. Journal of Tropical Geography, 18, 7–16.

Anderson, J.A.R., Muller, J., 1975. Palynological study of a Holocene peat and a Miocene coal deposit from N.W. Borneo. Review of Palaeobotany and Palynology, 19/4, 291–351. https://doi.org/10.1016/0034-6667(75)90049-4

Arutmin, 2015. Internal report on coal mining development of PT Arutmin Indonesia 2015–2020). PT Arutmin Indonesia, Jakarta, 441 pp. (in Indonesian)

Arya, G.C., Sarkar, S., Manasherova, E., Aharoni, A., Cohen, H., 2021. The Plant Cuticle: An Ancient Guardian Barrier Set Against Long-Standing Rivals. Frontiers in Plant Science, 12, 663165. https://doi.org/10.3389/fpls.2021.663165

ASTM, 2012. D3174-2012. Standard Test Method for Ash in the Analysis Sample of Coal and Coke from Coal, 6 pp.

ASTM, 2017. D3173-2017. Standard Test Method for Moisture in the Analysis Sample of Coal and Coke, 4 pp.

Bechtel, A., Gruber, W., Sachsenhofer, R.F., Gratzer, R., Püttmann, W., 2001. Organic geochemical and stable carbon isotopic investigation of coals formed in low-lying and raised mires within the Eastern Alps (Austria). Organic Geochemistry, 32/11, 1289–1310. https://doi.org/10.1016/S0146-6380(01)00101-2

Bechtel, A., Gruber, W., Sachsenhofer, R.F., Gratzer, R., Püttmann, W., 2003a. Depositional environment of the Late Miocene Hausruck lignite (Alpine Foreland Basin): Insights from petrography, organic geochemistry, and stable carbon isotopes. International Journal of Coal Geology, 53, 153–180. https:// doi.org/10.1016/S0166-5162(02)00194-5

Bechtel, A., Sachsenhofer, R.F., Markic, M., Gratzer, R., Lucke, A., Püttmann, W., 2003b. Paleoenvironmental implications from biomarker and stable isotope investigations on the Pliocene Velenje lignite seam (Slovenia). Organic Geochemistry, 34/9, 1277–1298. https://doi.org/10.1016/S0146-6380(03)00114-1

Bechtel, A., Reischenbacher, D., Sachsenhofer, R.F., Gratzer, R., Lücke, A., Püttmann, W. 2007. Relations of petrographical and geochemical parameters in the middle Miocene Lavanttal lignite (Austria). International Journal of Coal Geology, 70/4, 325–349. https://doi.org/10.1016/j.coal.2006.07.002

Bechtel, A., Gratzer, R., Sachsenhofer, R.F., Gusterhuber, J., Lücke, A., Püttmann, W., 2008. Biomarker and carbon isotope variation in coal and fossil wood of Central Europe through the Cenozoic. Palaeogeography, Palaeoclimatology, Palaeoecology, 262/3–4, 166–175. https://doi.org/10.1016/j.palaeo.2008.03.005

Bourbonniere, R.A., Meyers, P.A., 1996. Sedimentary geolipid records of historical changes in the watersheds and productivities of Lakes Ontario and Erie. Limnology and Oceanography, 41/2, 352–359. https://doi.org/10.4319/lo.1996.41.2.0352

BP, 2022. bp Statistical Review of World Energy 2022, 71st edition. https://www.bp.com/content/dam/bp/business-sites/en/global/corporate/pdfs/energy-economics/statistical-review/bp-stats-review-2022-full-report.pdf (accessed on 23 April 2023)

Bray, E.E., Evans, E.D. 1961. Distribution of *n*-paraffins as a clue to recognition of source beds. Geochimica et Cosmochimica Acta, 22/1, 2–5. https://doi.org/10.1016/0016-7037(61)90069-2

Brooks, J.D., Gould, K., Smith, J.W., 1969. Isoprenoid Hydrocarbons in Coal and Petroleum. Nature, 222, 257–259. https://doi.org/10.1038/222257a0

Buggle, B., Wiesenberg, G.L., Glaser, B., 2010. Is there a possibility to correct fossil n-alkane data for postsedimentary alteration effects? Applied Geochemistry, 25/7, 947–957. https://doi.org/10.1016/j.apgeochem.2010.04.003

Bumi Resources, 2021. Annual Report 2021. http://www.bumiresources.com/index.php/en/investor-relations#report (accessed on 01 January 2023).

Calder, J., Gibling, M., Mukhopadhyay, P.K., 1991. Peat formation in a Westphalian B piedmont setting, Cumberland Basin, Nova Scotia: implications for the maceral-based interpretation of rheotrophic and raised paleomires. Bulletin Societe Geologique de France, 162/2, 283–298.

Cameron, C.C., Esterle, J.S., Palmer, C.A., 1989. The geology, botany and chemistry of selected peat-forming environments from temperate and tropical latitudes. International Journal of Coal Geology, 12/1–4, 105–156. https://doi.org/10.1016/0166-5162(89)90049-9

Casagrande, D.J., 1987. Sulphur in peat and coal. Geological Society, London, Special Publications, 32/1, pp. 87–105. https://doi.org/10.1144/GSL.SP.1987.032.01.07

Dai, S., Bechtel, A., Eble, C.F., Flores, R.M., French, D., Graham, I.T., Hood, M.M., Hower, J.C., Korasidis, V.A., Moore, T.A., Püttman, W., Wei, Q., Zhao, L., O'Keefe, J.M.K., 2020. Recognition of peat depositional environments in coal: A review. International Journal of Coal Geology, 219, 103383. https://doi.org/10.1016/j.coal.2019.103383

Dehmer, J., 1993. Petrology and organic geochemistry of peat samples from a raised bog in Kalimantan (Borneo). Organic Geochemistry, 20/3, 349–362. https://doi.org/10.1016/0146-6380(93)90125-U

Demchuk, T., Moore, T.A., 1993. Palynofloral and organic characteristics of a Miocene bog-forest, Kalimantan, Indonesia. Organic Geochemistry, 20/2, 119–134. https://doi.org/10.1016/0146-6380(93)90032-7

Didyk, B.M., Simoneit, B.R.T., Brassell, S.T., Eglinton, G., 1978. Organic geochemical indicators of palaeoenvironmental conditions of sedimentation. Nature, 272, 216–222. https://doi.org/10.1038/272216a0

Diessel, C.F.K., 1986. The correlation between coal facies and depositional environments. Proceedings of the 20th Symposium of Department Geology, University of New Castle, New South Wales, pp. 11–22.

Ding, L.-F., Liu, J.-X., Xie, Z.-Q., Wang, S.S., Nie, W., Song, L.-D., Wu, X.-D., Zhao, Q.-S., 2019. Magnograndins J-M, elemane sesquiterpenoids from the leaves of *Magnolia grandiflora* and their inhibitory effects on nitric oxide production. Phytochemistry Letters 31, 121–124. https://doi.org/10.1016/j.phytol.2019.03.021

Espitalie, J., Madec, M., Tissot, B., Mennig, J.J., Leplat, P., 1977. Source Rock Characterization Method for Petroleum Exploration. Offshore Technology Conference. https://doi.org/10.4043/2935-MS

Esterle, J.S., Ferm, J.C., 1994. Spatial variability in modern tropical peat deposits from Sarawak, Malaysia and Sumatra, Indonesia: analogues for coal. International Journal of Coal Geology, 26/1–2, 1–41. https://doi.org/10.1016/0166-5162(94)90030-2

Esterle, J.S., Ferm, J.C., Tie, Y.L., 1989. A test for the analogy of tropical domed peat deposits to “dulling-up” sequences in coal beds-preliminary results. Organic Geochemistry, 14/3, 333–342. https://doi.org/10.1016/0146-6380(89)90060-0

Ettingshausen, C., 1888. Die fossile Flora von Leoben in Steiermark. 1., 2. Theil. – Denkschriften kaiserliche Akademie der Wissenschaften. mathematisch-naturwissenschaftliche Classe, 54, 261–318, 319–384. https://doi.org/10.5962/bhl.title.118927

Ficken, K.J., Li, B., Swain, D., Eglinton, G., 2000. An n-alkane proxy for the sedimentary input of submerged/floating freshwater aquatic macrophytes. Organic Geochemistry, 31/7–8, 745–749. https://doi.org/10.1016/S0146-6380(00)00081-4

Figueiral, I., Mosbrugger, V., Rowe, N.P., Ashraf, A.R., Utescher, T., Jones, T.P., 1999. The Miocene peat-forming vegetation of northwestern Germany: an analysis of wood remains and comparison with previous palynological interpretations. Review of Palaeobotany and Palynology, 104/3–4, 239–266. https://doi.org/10.1016/S0034-6667(98)00059-1

Fikri, H.N., Sachsenhofer, R.F., Bechtel, A., Gross, D., 2022a. Organic geochemistry and petrography in Miocene coals in the Barito Basin (Tutupan Mine, Indonesia): Evidence for astronomic forcing in kerapah type peats. International Journal of Coal Geology, 256, 103997. https://doi.org/10.1016/j.coal.2022.103997

Fikri, H.N., Sachsenhofer, R.F., Bechtel, A., Gross, D., 2022b. Coal deposition in the Barito Basin (Southeast Borneo): The Eocene Tanjung Formation compared to the Miocene Warukin Formation. International Journal of Coal Geology, 263, 104117. https://doi.org/10.1016/j.coal.2022.104117

Friederich, M.C., Moore, T.A., Flores, R.M., 2016. A regional review and new insights into SE Asian Cenozoic coal-bearing sediments: why does Indonesia have such extensive coal deposits? International Journal of Coal Geology, 166, 2–35. https://doi.org/10.1016/j.coal.2016.06.013

Gruber, W., Sachsenhofer, R.F., 2001. Coal deposition in the Noric Depression (Eastern Alps): raised and low-lying mires in Miocene pull-apart basins. International Journal of Coal Geology, 48/1–2, 89–114. https://doi.org/10.1016/S0166-5162(01)00049-0

Hall, R., 2012. Late Jurassic–Cenozoic reconstructions of the Indonesian region and the Indian Ocean. Tectonophysics, 570–571, 1–41. https://doi.org/10.1016/j.tecto.2012.04.021

Hall, R., Morley, C.K., 2004. Sundaland basins. In: Clift, P., Wang, P., Kuhnt, W., Hayes, D.E. (eds.), Continent-Ocean Interactions within the East Asian Marginal Seas. Geophysical Monograph Series, 149, American Geophysical Union, Washington, D.C., pp. 55–85. https://doi.org/10.1029/149GM04

Hauke, V., Graff, R., Wehrung, P., Trendel, J.M., Albrecht, P., Riva, A., Hopfgartner, G., Gülaçar, F.O., Buchs, A., Eakin, P.A., 1992. Novel triterpene-derived hydrocarbons of the arborane/fernane series in sediments: Part II. Geochimica et Cosmochimica Acta, 56/9, 3595–3602. https://doi.org/10.1016/0016-7037(92)90405-8

Hower, J.C., O'Keefe, J.M., Eble, C.F., Raymond, A., Valentim, B., Volk, T.J., Richardson, A.R., Satterwhite, A.B., Hatch, R.S., Stucker, J.D., Watt, M.A., 2011a. Notes on the origin of inertinite macerals in coal: evidence for fungal and arthropod transformations of degraded macerals. International Journal of Coal Geology, 86/2–3, 231–240. https://doi.org/10.1016/j.coal.2011.02.005

Hower, J.C., O'Keefe, J.M., Eble, C.F., Volk, T.J., Richardson, A.R., Satterwhite, A.B., Hatch, R.S., Kostova, I.J., 2011b. Notes on the origin of inertinite macerals in coals: Funginite associations with cutinite and suberinite. International Journal of Coal Geology; 85/1, 186–190. https://doi.org/10.1016/j.coal.2010.11.008

Hutchison, C.S., 1989. Geological evolution of South-East Asia, Oxford Monographs on Geology and Geophysics, 13. Oxford University Press, Oxford, 368 pp.

Hutchison, C.S., 2014. Tectonic evolution of Southeast Asia. Geological Society of Malaysia Bulletin, 60, 1–18. https://doi.org/10.7186/bgsm60201401

ICCP (International Committee for Coal and Organic Petrology), 1998. The new vitrinite classification (ICCP System 1994). Fuel, 77/5, 349–358. https://doi.org/10.1016/S0016-2361(98)80024-0

ICCP (International Committee for Coal and Organic Petrology), 2001. The new inertinite classification (ICCP System 1994). Fuel, 80/4, 459–471. https://doi.org/10.1016/S0016-2361(00)00102-2

IEA, 2022. World Energy Outlook 2002. International Energy Agency. https://iea.blob.core.windows.net/assets/830fe099-5530-48f2-a7c1-11f35d510983/WorldEnergyOutlook2022.pdf (accessed on 09 February 2023)

Jiménez-Moreno, G., Fauquette, S., Suc, J.-P., 2008. Vegetation, climate and palaeoaltitude reconstructions of the Eastern Alps during the Miocene based on pollen records from Austria, Central Europe. Journal of Biogeography, 35/9, 1638–1649. https://doi.org/10.1111/j.1365-2699.2008.01911.x

Korasidis, V.A., Wallace, M.W., Wagstaff, B.E., Holdgate, G.R., Tosolini, A.-M.P., Jansen, B., 2016. Cyclic floral succession and fire in a Cenozoic wetland/peatland system. Palaeogeography, Palaeoclimatology, Palaeoecology, 461, 237–252. https://doi.org/10.1016/j.palaeo.2016.08.030

Kovar-Eder, J., Kcacek, Z., Teodoridis, V., Mazouch, P., Collinson, M.E., 2022. Floristic, vegetation and climate assessment of the early/middle Miocene Parschlug flora indicates a distinctly seasonal climate. Fossil Imprint, 78/1, 80–144. https://doi.org/10.37520/fi.2022.005

Markic, M., Sachsenhofer, R.F., 1997. Petrographic composition and depositional environments of the Pliocene Velenje lignite seam (Slovenia). International Journal of Coal Geology, 33/3, 229–254. https://doi.org/10.1016/S0166-5162(96)00043-2

Moore, T.A., Shearer, J.C., 1997. Evidence for aerobic degradation and implications for Palangka Raya peat sustainability. In: Rieley, J.O., Page, S.E. (eds.), Biodiversity and Sustainability of Tropical Peatlands. Samara Publishing, Cardigan, United Kingdom, 157-167.

Moore, T.A., Shearer, J.C., 2003. Peat/coal type and depositional environment—are they related? International Journal of Coal Geology, 56/3-4, 233–252. https://doi.org/10.1016/S0166-5162(03)00114-9

Moore, T.A., Shearer, J.C., Miller, S.L., 1996. Fungal origin of oxidised plant material in the Palangkaraya peat deposit, Kalimantan Tengah, Indonesia: Implications for 'inertinite' formation in coal. International Journal of Coal Geology, 30/1–2, 1–23. https://doi.org/10.1016/0166-5162(95)00040-2

Morley, R.J., 2012. A review of the Cenozoic climate history of Southeast Asia. In: Gower, D., Johnson, K., Richardson, J., Rosen, B., Rüber, L., Williams, S. (eds.), Biotic Evolution and Environmental Change in Southeast Asia. Cambridge University Press, Cambridge, pp. 79–114. https://doi.org/10.1017/CBO9780511735882.006

Morley, R.J., 2013. Cenozoic ecological history of South East Asian peat mires based on the comparison of coals with present day and Late Quaternary peats. Journal of Limnology, 72/S2, 36–59. https://doi.org/10.4081/jlimnol.2013.s2.e3

Naafs, B.D.A., Inglis, G.N., Blewett, J., McClymont, E.L., Lauretano, V., Xie, S., Evershed, R.P., Pancost, R.D., 2019. The potential of biomarker proxies to trace climate, vegetation, and biogeochemical processes in peat: A review. Global and Planetary Change, 179, 57–79. https://doi.org/10.1016/j.gloplacha.2019.05.006

Otto, A., Wilde, V., 2001. Sesqui-, di-, and triterpenoids as chemosystematic markers in extant conifers - A Review. The Botanical Review, 67/2, 141–238

Page, S., Rieley, J.O., Shotyk, O.W., Weiss, D., 1999. Interdependence of peat and vegetation in a tropical peat swamp forest. Philosophical Transactions of The Royal Society B - Biological Sciences, 354/1391, 1885-1897. https://doi.org/10.1098/rstb.1999.0529

Page, S., Wüst, R., Banks, C., 2010. Past and present carbon accumulation and loss in Southeast Asian peatlands. PAGES News, 18/1, 25–27. https://doi.org/10.22498/pages.18.1.25

Parr, S.W., 1928. The Classification of Coal. University of Illinois, Engineering Experiment Station, Bulletin, 180, 1–62

Peel, M.C., Finlayson, B.L., McMahon, T. A., 2007. Updated world map of the Köppen-Geiger climate classification. Hydrology and Earth System Sciences, 11, 1633–1644. https://doi.org/10.5194/hess-11-1633-2007

Peters, K.E., Moldowan, J. M., 1993. The biomarker guide: interpreting molecular fossils in petroleum and ancient sediments. 363 pp.

Pickel, W., Kus, J., Flores, D., Kalaitzidis, S., Christanis, K., Cardott, B.J., Misz-Kennan, M., Rodrigues, S., Hentschel, A., Hamor-Vido, M., Crosdale, P., Wagner, N., 2017. Classification of liptinite – ICCP System 1994. International Journal of Coal Geology, 169, 40–61. https://doi.org/10.1016/j.coal.2016.11.004

Powell, T.G., McKirdy, D.M., 1973. Relationship between ratio of pristane to phytane, crude oil composition and geological environment in Australia. Nature Physical Science, 243, 37–39. https://doi.org/10.1038/physci243037a0

Poynter, J., Eglinton, G. 1990. Molecular composition of three sediments from Hole 717C: the Bengal Fan. In: Cochran, J.R., Stow, D.A.V., et al. (eds.), Proceedings of the Ocean Drilling Program, Scientific Results, College Station, TX (Ocean Drilling Program), 116, 155–161. https://doi.org/10.2973/odp.proc.sr.116.151.1990

Pubellier, M., Morley, C.K., 2014. The basins of Sundaland (SE Asia): Evolution and boundary conditions. Marine and Petroleum Geology, 58/Part B, 555–578. https://doi.org/10.1016/j.marpetgeo.2013.11.019

Radke, M., Schaefer, R.G., Leythaeuser, D., Teichmüller, M., 1980. Composition of soluble organic matter in coals: relation to rank and liptinite fluorescence. Geochimica et Cosmochimica Acta, 44/11, 1787–1800. https://doi.org/10.1016/0016-7037(80)90228-8

Sachsenhofer, R.F., 2000. Geodynamic controls on deposition and maturation of coal in the Eastern Alps. In: F. Neubauer, V. Höck (eds.), Aspects of Geology in Austria, Mitteilungen der Österreichischen Geologischen Gessellschaft, 92, 185–194

Sachsenhofer, R.F., Bechtel A., Reischenbacher D., Weiss A., 2003. Evolution of lacustrine systems along the Miocene Mur-Mürz fault system (Eastern Alps) and implications on source rocks in pull-apart basins. Marine and Petroleum Geology, 20/2, 83–110. https://doi.org/10.1016/S0264-8172(03)00018-7

Sapiie, B., Rifiyanto, A., 2017. Tectonics and Geological Factors Controlling Cleat Development in the Barito Basin, Indonesia. Journal of Engineering & Technological Sciences, 49/3, 322–339. https://doi.org/10.5614/j.eng.technol.sci.2017.49.3.3

Satyana, A.H., Nugroho, D., Surantoko, I., 1999. Tectonic controls on the hydrocarbon habitats of the Barito, Kutei, and Tarakan Basins, Eastern Kalimantan, Indonesia: major dissimilarities in adjoining basins. Journal of Asian Earth Sciences, 17/1–2, 99–122. https://doi.org/10.1016/S0743-9547(98)00059-2

Schwark, L., Zink, K., Lechterbeck, J., 2002. Reconstruction of postglacial to early Holocene vegetation history in terrestrial Central Europe via cuticular lipid biomarkers and pollen records from lake sediments. Geology, 30/5, 463–466. https://doi.org/10.1130/0091-7613(2002)030<0463:ROPTEH>2.0.CO;2

Scotese, C.R., 2000. PALEOMAP Project [DB/OL]. http://www.scotese.com/ (accessed on 03 February 2023).

Stivrins, N., Ozola, I., Galka, M., Kuske, E., Alliksaar, T., Andersen, T.J., Lamentowicz, M., Wulf, S., Reitalu, T., 2017. Drivers of peat accumulation rate in a raised bog: impact of drainage, climate, and local vegetation composition. Mires and Peat, 19, 1–19. https://doi.org/10.19189/MaP.2016.OMB.262

Stock, A.T., Littke, R., Lücke, A., Zieger, L., Thielemann, T., 2016. Miocene depositional environment and climate in western Europe: The lignite deposits of the Lower Rhine Basin, Germany. International Journal of Coal Geology, 157, 2–18. http://dx.doi.org/10.1016/j.coal.2015.06.009

Taylor, G., Teichmüller, M., Davis, A., Diessel, C.F.K., Littke, R., Robert, P., 1998. Organic Petrology. Gebrüder Borntraeger, Berlin.704 pp.

van Aarssen, B.G.K., Cox, H., Hoogendoorn, N.P., de Leeuw, J.W., 1990. A cadinene biopolymer in fossil and extant dammar resins as a source for cadinanes and bicadinanes in crude oils from South East Asia. Geochimica et Cosmochimica Acta, 54/11, 3021–3031. https://doi.org/10.1016/0016-7037(90)90119-6

van Aarssen, B.G.K. de Leeuw, J.W., Collinson, M., Boon, J.J., Goth, K., 1994. Occurrence of polycadinene in fossil and recent resins. Geochimica et Cosmochimica Acta, 58/1, 223–229. https://doi.org/10.1016/0016-7037(94)90459-6

Weber L., Weiss A., 1983. Bergbaugeschichte und Geologie der österreichischen Braunkohlevorkommen. Archiv für Lagerstättenforschung der Geologischen Bundesanstalt, 4, 1–217.

Widodo, S., Bechtel, A., Komang, A., Püttmann, W., 2009. Reconstruction of floral changes during deposition of the Miocene Embalut coal from Kutai basin, Mahakam delta, East Kalimantan, Indonesia by use of aromatic hydrocarbon composition and stable carbon isotope ratios of organic matter. Organic Geochemistry, 40/2, 206–218. https://doi.org/10.1016/j.orggeochem.2008.10.008

Widodo, S., Oschmann, W., Bechtel, A., Sachsenhofer, R.F., Komang, A., Püttmann, W., 2010. Distribution of sulfur and pyrite in coal seams from Kutai Basin (East Kalimantan, Indonesia): Implications for paleoenvironmental conditions. International Journal of Coal Geology, 81/3, 151–162. https://doi.org/10.1016/j.coal.2009.12.003

Witts, D., Davies, L., Morley, R., 2014. Uplift of the Meratus Complex: Sedimentology, biostratigraphy, provenance and structure. Proceedings Indonesian Petroleum Association 38th Annual Convention & Exhibition, IPA14-G-082

Witts, D., Hall, R., Nichols, G., Morley, R., 2012. A new depositional and provenance model for the Tanjung Formation, Barito Basin, SE Kalimantan, Indonesia. Journal of Asian Earth Sciences, 56, 77–104. https://doi.org/10.1016/j.jseaes.2012.04.022

Wüst, R.A.J., Hawke, M.I., Bustin, R.M., 2001. Comparing maceral ratios from tropical peatlands with assumptions from coal studies: do classic coal petrographic interpretation methods have to be discarded? International Journal of Coal Geology, 48/1-2, 115–132. https://doi.org/10.1016/S0166-5162(01)00050-7

Zahirovic, S., Seton, M., Müller, R.D., 2014. The Cretaceous and Cenozoic tectonic evolution of Southeast Asia. Solid Earth, 5, 227–273. https://doi.org/10.5194/se-5-227-2014

Zech, M., Buggle, B., Leiber, K., Marković, S., Glaser, B., Hambach, U., Huwe, B., Stevens, T., Sümegi, P., Wiesenberg, G., Zöller, L., 2009. Reconstructing Quaternary vegetation history in the Carpathian Basin, SE-Europe, using n-alkane biomarkers as molecular fossils: Problems and possible solutions, potential and limitations. E&G Quaternary Science Journal, 58/2, 148–155. https://doi.org/10.3285/eg.58.2.03

9 Publication IV:

Factors controlling oil potential in Eocene and Miocene coals from Borneo: Implications for the petroleum system in the Barito Basin

Chapter 9 was submitted for publication to the “International Journal of Coal Geology”.

Author contribution: Conceptualization, methodology, investigation, writing – original draft, and visualization

Factors controlling oil potential in Eocene and Miocene coals from Borneo: Implications for the petroleum system in the Barito Basin

Hafidz Noor Fikri[1,2], Reinhard F. Sachsenhofer[1,*], Doris Gross[1], Brian Horsfield[3], Nicolaj Mahlstedt[3], David Misch[1]

[1)] Department Applied Geosciences and Geophysics, Montanuniversitaet Leoben, 8700 Leoben, Austria
[2)] Department of Mining Engineering, Lambung Mangkurat University, Banjarmasin, South Kalimantan, Indonesia
[3)] Geos4, 14552 Michendorf, Germany

[*)] Corresponding author, reinhard.sachsenhofer@unileoben.ac.at

Abstract

Eocene to Miocene coals are the most likely source rock for oil in several Indonesian sedimentary basins, but the factors controlling their oil potential are still poorly understood.

Depositional environments of rheotrophic coals in the Eocene Tanjung Formation and prevailing ombrotrophic coals in the Miocene Warukin Foramtion (Barito and Asem-Asem basins in southern Borneo) have been studied recently, based on organic geochemical and organic petrographic data from more than 150 coal samples. In the present study, we use this wealth of information together with new pyrolysis data from solvent-extracted coals, pyrolysis-gas chromatography and carbon isotope data to determine the factors controlling the oil potential of the coals, as well as to correlate different oil families in the Barito Basin to specific coal intervals.

The study revealed that Miocene coals from the Barito Basin (Tutupan mine) and the Asem-Asem Basin (Jumbang Mine) are immature, while Eocene coals in the Barito Basin (TAJ Pit-1 mine) reached the stage of early oil generation. Both, Eocene and Miocene contain significant amounts of heavy, oxygen-rich bitumen components, which form part of the Rock-Eval S2 peak

($S2_{bitumen}$). This bitumen has a slightly lower thermal stability than the kerogen part is mainly derived from resins.

The type of hydrocarbons generated from Eocene coals (high wax paraffinic oil) and Miocene coals (paraffinic-napthenic-aromatic mixed oil with moderately high wax content) differs significantly. It is concluded that the oil type is mainly controlled by the prevailing resin producing vegetation, this is palms in Eocene coals and dammar resin producing dipterocarps in the Miocene coals.

Two oil families have been distinguished in the Barito Basin by previous authors and have been termed Tanjung and Warukin families, based on the prevailing reservoir horizons. The differences in oil type produced by Eocene and Miocene coals together with differences in bulk carbon isotope ratios allow the correlation of the Tanjung family with Eocene coals and the Warukin family with Miocene coals. Most of the oil detected in the Barito Basin so far belongs to the Tanjung family, although the Miocene coals have the higher oil potential. However, the Miocene coals reach the oil window only in the deepest parts of basin.

Keywords: resinite, oil potential, Rock-Eval, Pyrolysis-Gas chromatography, Kalimantan, biomarker

Highlights:

- Amount and origin of resinite control the oil potential of coals in Kalimantan
- Miocene coals from southern Kalimantan produce a high wax paraffinic oil
- Eocene coals produce a paraffinic-napthenic-aromatic-mixed oil
- Differences in oil type are due to changes in Eocene and Miocene vegetation
- Two oil families in the Barito Basin are related to Eocene and Miocene coals

1 Introduction

It has long been known that coal is an important source rock for gas deposits (e.g., Lutz et al., 1975). However, some coal can generate also commercial amounts of liquid hydrocarbons (e.g., Durand and Paratte, 1983; Horsfield et al., 1988; Hunt, 1991; Clayton et al., 1991; Bojesen-Koefoed et al., 1996; Newman et al., 1997; Isaksen et al., 1991; Killops et al., 1998; Wilkins and George, 2002). Petersen et al. (1998) provided a summary of areas with oil generated from coals. According to this list, basins with oil generated from Paleozoic to Mesozoic coals include the Tarim, Junggar and Turpan basins in northwest China (Huang et al., 1991; Hendrix et al., 1995), the Bowen and Eromanga basins in Australia (Thomas, 1982; Khorasani, 1987; Murchison, 1987), and the Greater Green River Basin in the U.S. (García-González et al. 1997). Basins with oil generated from (Upper Cretaceous to) Cenozoic coals include the Beaufort-Mackenzie basins in Canada (Snowdon 1980; Snowdon and Powell 1982; Issler and Snowdon 1990), the Niger Delta (Bustin, 1988), as well as the Gippsland and Taranaki basins in Australia and New Zealand (Shibaoka et al. 1978; Shanmugam 1985; Johnston et al., 1991; Killops et al., 1994). Petroliferous basins in Indonesia sourced by Cenozoic coals include from southwest to northeast the Ardjuna (offshore Java), Barito, Kutai (Mahakam Delta), and Tarakan basins (on- and offshore eastern Borneo; Fig. 1) (Durand and Oudin 1979; Gordon, 1985; Horsfield et al., 1988; Noble et al., 1991; 1997).

Eocene and Miocene coal seams in the Barito and Asem-Asem basins in southern Borneo have been studied recently to obtain information on their depositional environment (Fikri et al., 2022a,b,; Fikri et al., submitted). For this purpose, a total of 153 coal samples have been studied for bulk parameters (e.g., ash yield, sulphur content, total organic carbon), maceral composition, and Rock-Eval parameters. Organic geochemical data including biomarker concentrations have been determined for 76 samples. These investigations showed that the coals have been deposited in different ombrotrophic and rheotrophic settings and that the coal rank ranges from lignite A (Miocene coal in the Asem-Asem Basin) to subbituminous A / high volatile bituminous C coal (Eocene coal in the Barito Basin).

This paper has two main objectives: (i) to use the extensive Eocene and Miocene coal data set to investigate the effect of maturity, depositional environment and coal composition on the oil

potential of the coals, and (ii) to support source-to-oil correlation in the Barito Basin. For the latter purpose, Rock-Eval pyrolysis on extracted coals and pyrolysis-gas chromatography (Py-GC) measurements were carried out on selected coal samples and stable carbon isotope ratios of whole coals were determined.

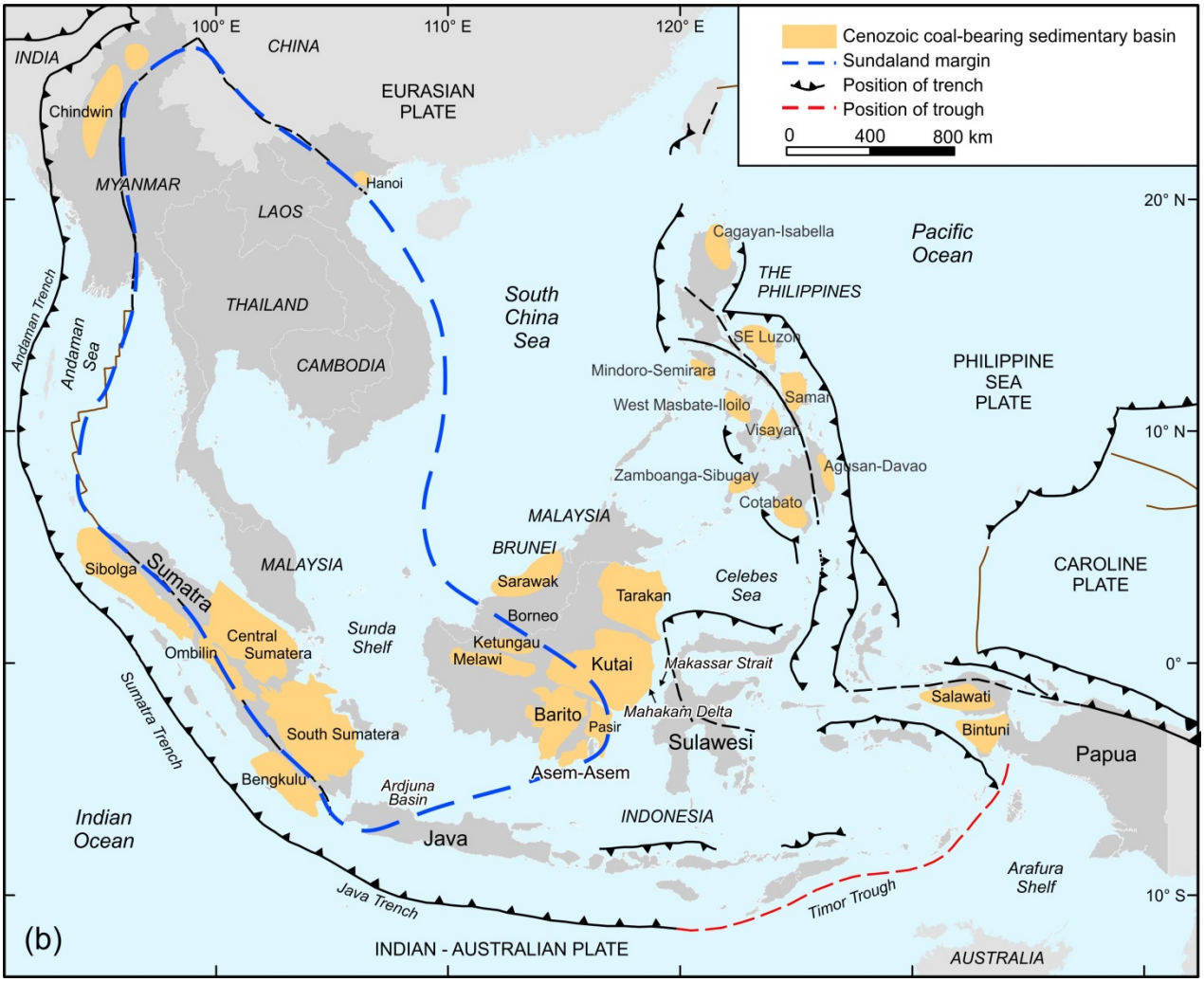

Fig. 1. The main on-shore Cenozoic coal-bearing sedimentary basins in SE Asia (from Friederich et al., 2016). The Ardjuna, Barito, Kutai and Tarakan basins contain coal-derived liquid hydrocarbons (e.g., Doust and Noble, 2008).

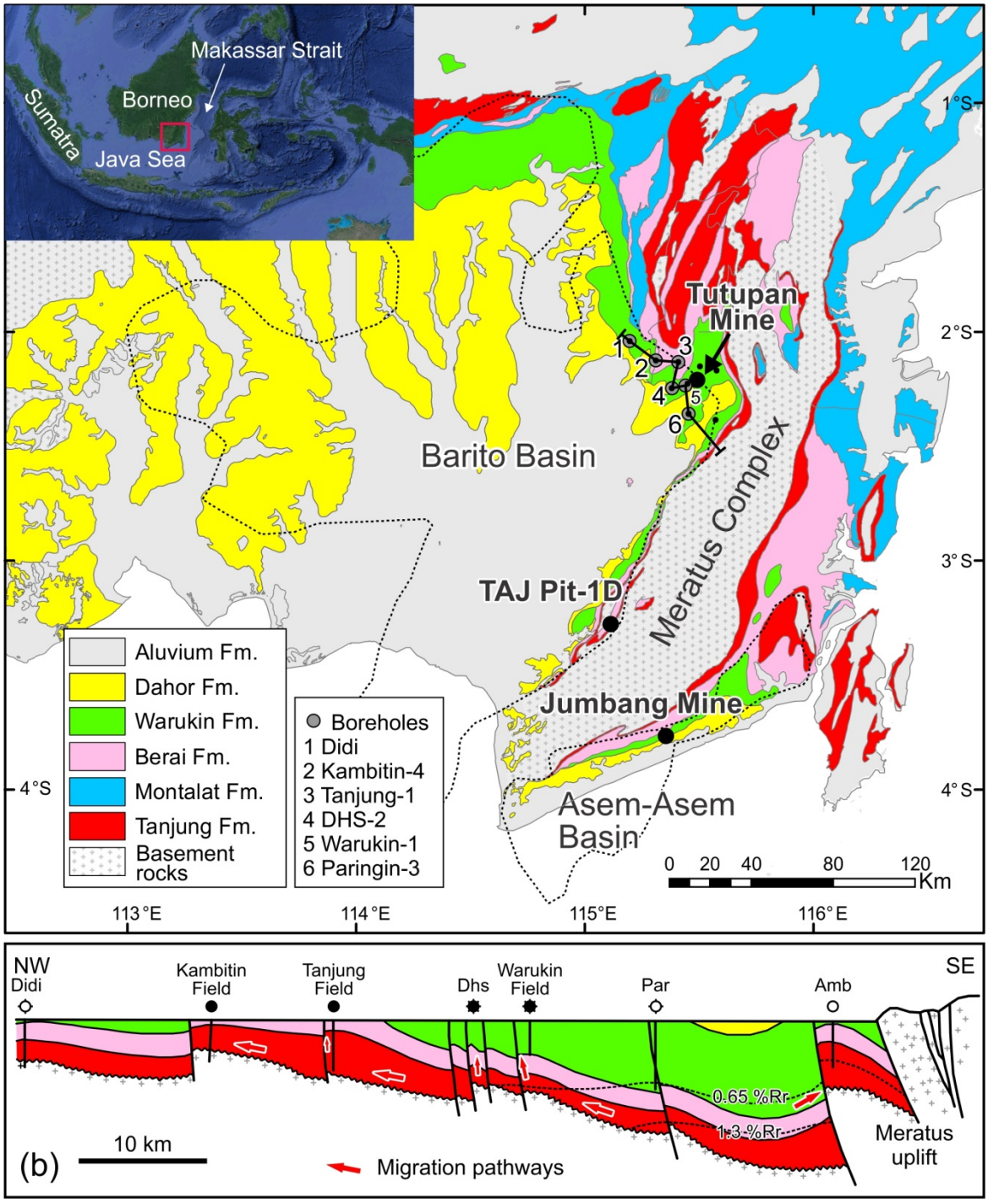

Fig. 2. (a) Geological map of the Barito and Asem-Asem basins with location of the studied Eocene (TAJ Pit-1D) and Miocene coal samples (Tutupan; Jumbang mines) (Fikri et al., 2022a,b). Oil fields are located in the northern part of the Barito Basin near the Tutupan mine. (b) Cross-section through the northern Barito Basin with position of oil fields (modified after Wibowo and Sutrisno, 2013).

2 Geological setting

The southeastern promontory of Eurasia is called Sundaland (Hall and Morley, 2004; Pubellier and Morley, 2014) and contains a significant number of coal-bearing Cenozoic basins (Fig. 1). Coal occurs in the northern part of Sundaland, but the most significant coal seams formed in southern Sundaland (Sumatra and Borneo) (Friedrich et al., 2016).

The South Sumatra Basin is an Eocene to Oligocene back-arc basin and includes mineable coal in the upper Miocene to early Pliocene Muara Enim Formation (Amijaya and Littke, 2005; Friederich et al., 2016). However, lower delta plain coals also occur in the Oligocene succession (Talang Akar Formation; Noble et al., 1991). This coal is the main source rock for petroleum found in the Ardjuna Basin, NW Java, Indonesia (Gordon, 1985; Horsfield et al., 1988; Doust and Noble, 2008).

Sedimentary basins in eastern Borneo reflect a Middle Eocene extensional regime initiated by the rifting of the Makassar Strait between Borneo and Sulawesi (Daly et al., 1991; Pubellier and Morley, 2014; Zahirovic et al., 2014; for location see Fig. 1). This extensional event led to the formation of NW-SE oriented horst and graben structures (Satyana et al., 1999). Rifting ended towards the end of the Early Oligocene (Pubellier and Morley, 2014) and basin inversion commenced in the middle Miocene.

The Barito Basin and the Asem-Asem Basin are located in southern Borneo (Figs. 1, 2). The sediments in these basins are comparable suggesting that they once formed a uniform depocenter (Witts et al., 2014). The Cenozoic basin fill includes, from base to top, the Middle Eocene to Lower Oligocene Tanjung Formation, the Upper Oligocene to lower Miocene Berai and Montalat Formations, the middle to upper Miocene Warukin Formation, and the upper Miocene to Pleistocene Dahor Formation (Witts et al., 2012, 2014; Fig. 3). A change in paleocurrent directions during the deposition of the upper part of the Warukin Formation in the Barito Basin indicates the middle/late Miocene onset of uplift of the southern part of the Meratus Complex and the start of the separation of the Barito and Asem-Asem basins (Witts et al., 2014).

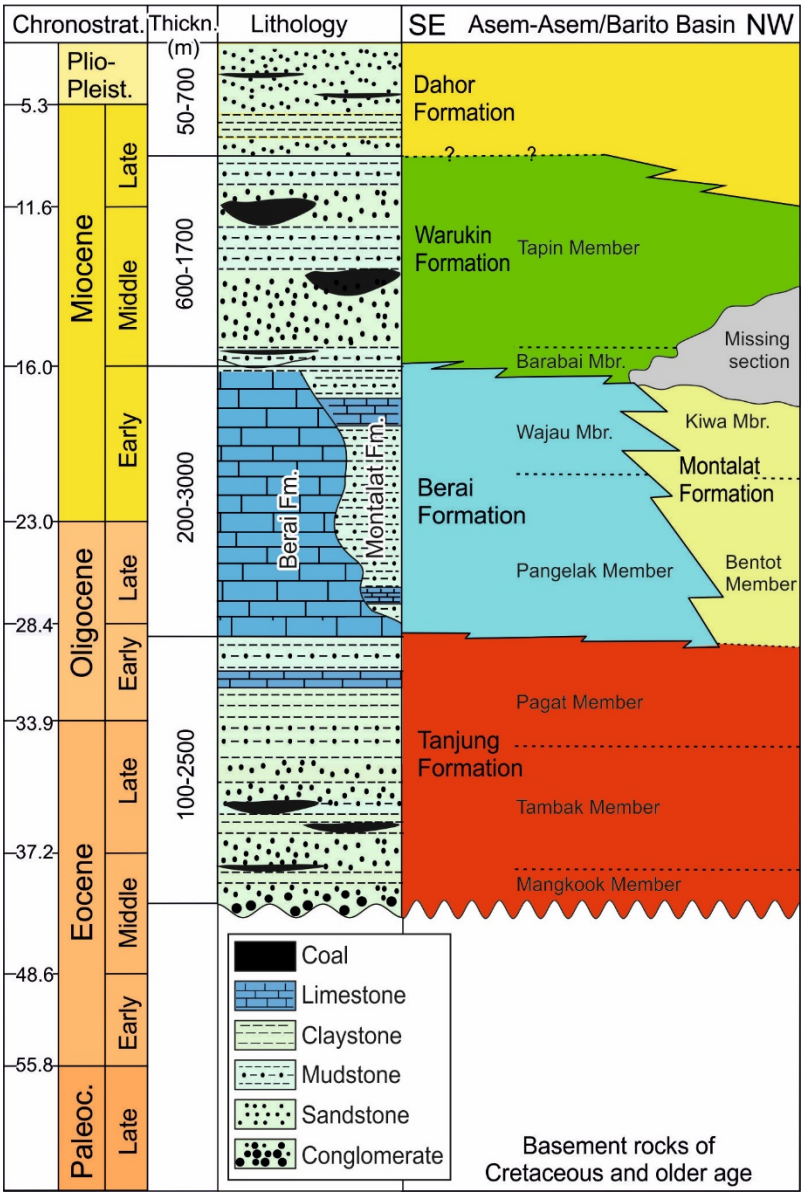

Fig. 3. Stratigraphy and lithology of the basin fill in the Barito and Asem-Asem Basin (modified after Witts et al., 2012, 2014).

2.1 Coal Geology of the Barito Basin

Coal seams occur in the Upper Eocene part of the Tanjung Formation and in the middle Miocene part of the Warukin Formation (Friederich et al., 2016). The transgressive Tanjung Formation includes fluvio-tidal and estuarine deposits containing several-m-thick and laterally extensive coal seams (Upper Eocene Tambak Member; Witts et al., 2012). Three coal seams (from base to top: D, C, B) are mined in the TAJ Pit-1D mine, where they are 1.4 to 3.4 m thick (Fikri et al.,

2022b). The seams were deposited in rheotrophic mires with palm/fern–dominated vegetation (Moore and Ferm, 1992). Transitions to local ombrotrophic mires cannot be excluded. Despite a general coastal plain setting, very low to low sulphur contents (max. 0.9 wt%) speak against a marine influence (Fikri et al., 2022b).

The regressive Warukin Formation comprises fluvio-deltaic sedimentary rocks with thick coal seams in the Middle Miocene Tapin Member (Satyana et al., 1999; Witts et al., 2012). Three very thick coal seams (up to 50 m), exposed in the Tutupan mine, have been studied by Fikri et al. (2022a). The two lower seams (T110 and T210) accumulated in ombrotrophic kerapah (inland or watershed) mires, while the upper seam (T300), which contains slightly more mineral matter, accumulated in a mixed rheotrophic-ombrotrophic mire. The coal seam BL1 in the Jumbang mine in the Asem-Asem Basin formed in an ombrotrophic basinal (coastal) mire. The vegetation in Miocene mires was dominated by angiosperms. A relatively high contribution of gymnosperms, typical for kerapah mires, is only recorded for seams T110 and T210 (cf. Morley, 2013). All coals are very low in sulphur. However, locally elevated sulphur contents (~1.5 wt.%) a lower coal bench in the BL1 seam (BL1L) suggest a brackish water influence.

Moisture contents and vitrinite reflectance data show that the Eocene coal has a higher maturity (subbituminous A / high volatile bituminous C coal) than the Tutupan coal (subbituminous C) and the Jumbang coal (lignite A; Fikri et al., 2022a,b; Fikri et al., submitted). Differences in geochemical parameters and maceral percentages are summarized in Table 1.

While all coals contain high amounts of resinite, the maximum amounts are found in ombrotrophic Miocene coals. At least part of the resinite in Miocene coals, but not in Eocene coals, is derived from dammar resin produced by *dipterocarpaceae* (Demchuk and Moore, 1993; Stankiewicz et al., 1996). Leaf-derived macerals (cutinite and fluorinite) are also abundant in all coals, but more abundant in Eocene than in Miocene coals. In contrast, root-derived suberinite occurs in higher percentages in Miocene coals. Fungal activity, recorded by high funginite percentages, was high in ombrotrophic and rheotrophic mires both in Eocene and Miocene times. In contrast to funginite, percentages of other inertinite macerals are low.

Table 1. Summary of similarities and differences between Eocene and Miocene coals from Borneo. Data from the TAJ Pit-1D, Tutupan and Jumbang mines are from Fikri et al. (2022b), Fikri et al. (2022a), and Fikri et al. (submitted), respectively.

	TAJ Pit-1D Mine	**Tutupan Mine**		**Jumbang Mine**
	Eocene	**Miocene**		**Miocene**
Peat–type	rheotrophic	ombrotrophic (kerapah)	ombro- + rheotrophic	ombrotrophic (basinal)
Rank	Subbituminous A/ high vol. bitum. C	Subbituminous C		Lignite A
Climate (Morley, 2012)	Tropical ever–wet	Tropical ever–wet		Tropical ever–wet
Number of economic seams	3	3		1 (-3)
Seam names	D, C, B	T110, T210	T300	BL1
Thickness of single seams	Up to 5 m	up to 50 m	24 m	20 m
Stacked successions (cycles)	no	yes (up to 5)	no (unclear)	no
Marine/brackish influence	—	—	—	local (bench BL1U)
Vegetation (Moore and Ferm, 1992; Morley, 2013)	Palms/ferns	Angiosperm trees (e.g., Shorea) (+gymnosperms)		Angiosperm trees (e.g., Shorea)
Gymnosperms (Di–/(di- +Tri-)Terpenoids)	largely missing	Rare (0.01-0.12)	Very rare (0.01-0.02)	Very rare (0.01-0.02)
CPI	2.0 (1.7–2.6)	4.3 (2.8–6.2)	3.1 (2.2–3.8)	3.7 (3.3–4.8)
TAR	23.3 (10.8–41.7)	10.4 (5.8–23.4)	19.9 (6.0–38.4)	21.6 (15.9-36.7)
Paq	0.22 (0.12–0.33)	0.14 (0.05–0.24)	0.08 (0.05–0.11)	0.24 (0.17-0.27)
n–C_{29}/n–C_{27}	1.79 (1.29–5.08)	1.39 (0.77–2.33)	3.14 (2.09–4.83)	1.47 (1.20-1.80)
n–C_{31+33}/n–C_{27+29}	0.81 (0.60–1.05)	0.85 (0.17–2.23)	0.67 (0.46–0.91)	1.3 (1.0-2.6)
Pr/Ph	12.3 (7.7–14.3)	12.8 (5.4–23.6)	6.1 (3.9–8.1)	3.2 (2.2-6.2)
Degradation (VI; Calder et al., 1991)	High (0.56)	Low (1.56)	Low (1.26)	Moderate (1.10)
Extent of external influx (GWI; Calder et al., 1991)	low–high (av. 2.16)	Low (0.17)	Low (0.32)	Low (0.35)
Resins (*in–situ*+detrital; vol.%)	Abundant 6.5 (3.2–12.7)	Abundant 4.1 (1.0–19.1)	Abundant 4.0 (0.8–9.0)	Very abundant 9.3 (2.9-17.3)
Cadinane–source	Non–dammar?	Dammar resin (dipterocarps)	Dammar resin (dipterocarps)	Dammar resin (dipterocarps)
Leafs (cutinite+fluorinite; vol%)	abundant 6.0 (0.4–15.7)	abundant 4.8 (0.4–13.1)	abundant 3.8 (0.6–8.5)	abundant 4.3 (0.0–7.7)
Roots (suberinite; vol%)	rare 0.5 (0.0–1.8)	abundant 2.6 (0.2–7.0)	abundant 2.0 (0.4–4.6)	very abundant 3.2 (0.0-7.3)
Alginite	low (incl. *Botryococcus*)	—	traces	—
Fungal activity (funginite; vol. %)	high 1.4 (0.2–3.2)	high 1.0 (0.0–3.2)	high 1.5 (0.6–2.8)	high 1.6 (0.2–5.4)
Inertinite (excl. funginite; vol. %)	0.9 (0.0–2.4)	2.1 (0.0–4.0)	2.3 (0.6–5.0)	3.8 (1.2-8.6)
HI (mgHC/gTOC)	374 (316-470)	195 (115-331)	226 (133-349)	236 (154-539)
Tmax (°C)	424 (416-428)	393 (372-411)	381 (371-405)	377 (370-399)
Oil-type	Paraffinic oil, high wax	P-N-A mixed oil, high wax	P-N-A mixed oil, high wax	P-N-A mixed oil, high wax?

CPI - carbon preference index (Bray and Evans, 1961); TAR - terrestrial-aquatic ratio (n-$C_{27+29+31}$/n-$C_{15+17+19}$) (Bourbonniere and Meyers, 1996); Paq- P-aqueous ratio (n-C_{23+25})/(n-$C_{23+25+29+31}$) (Ficken et al., 2000); Pr/Ph – pristane/phytane ratio ((Didyk et al., 1978); VI – vegetation index; GWI – groundwater index

2.2 Petroleum Geology of the Barito Basin

Apart from coal, the Barito Basin also contains petroleum (Tanjung-Tanjung petroleum system of Doust and Noble, 2008). However, to date only a single large field (Tanjung discovered in 1937; ~180 MMBOE) and a few smaller oil fields (Kambitin [1959], Warukin [1965], Tapian Timur [1967]), all located in the northern part of the basin near the Tutupan mine, were discovered (see position of oil fields in Fig. 2a). A cross-section of the main oil fields together with the position of the oil window is shown in Fig. 2b after Wibowo and Sutrisno (2013).

The Tanjung and Kambitin fields produce from Eocene (Tanjung) sandstones and, in Tanjung, also from fractures in the pre-Cenozoic basement (IPA, 1991; Doust and Noble, 2008; Kleibacker et al, 2015). The Bagok-1 well, drilled in 1986 on the southerly plunging nose of the Kambitin structure, tested oil from Tanjung sandstones, but Tanta-1, drilled on the southern extension of the Tanjung anticline, found small amounts of oil in fractured Oligocene Berai limestone (Kusuma and Darin, 1989). The Warukin and Tapian Timur fields produce oil from sandstones in the Miocene Warukin Formation (IPA, 1991). Traps are provided by thrusted and highly faulted anticlinal structures (Doust and Noble, 2008; Fig. 2b).

3 Material and methods

The study is based on Eocene coals from the TAJ Pit-1D mine (38 samples) and Miocene coals form the Tutupan (93 samples) and Jumbang mines (22 samples). Information on ash yield, TOC and sulphur contents, as wells as petrographic data is available in tabular form for all samples in Fikri et al. (2022b; TAJ Pit-1D), Fikri et al. (2022a; Tutupan), and Fikri et al. (submitted; Jumbang). Hydrogen index (HI = S2×100/TOC; mgHC/gTOC) and Tmax (°C) also have also been reported by the above authors, but S1 and S2 (mgHC/g rock) as well as bitumen index (BI = 100×S1/TOC) and quality index (QI = 100×(S1+S2)/TOC) are reported here for the first time (Tables 2-4). Organic geochemical data for roughly every second sample (TAJ Pit-1D mine: 20 samples; Tutupan: 48 samples; Jumbang: 8 sample) have also been reported previously (Fikri et al., 2022a,b, submitted).

While the study is based mainly on the interpretation of data, which became available recently, some additional analyses were performed specifically for this study. These analyses include Rock-Eval pyrolysis (Espitalié et al., 1977) on nine solvent-extracted coal samples, pyrolysis-gas

chromatography (Py-GC) measurements (Horsfield, 1984; 1989; 1997) on five coals samples, and stable carbon isotope measurements on 68 whole coal samples.

Nine coal samples were extracted twice with dichloromethane for 1 h at 75°C and 100 bar in a Dionex ASE 350 extractor. After each extraction step, the solvent was reduced to a total volume of 0.5 ml by evaporation in a Zymark TurboVap 500 closed–cell concentrator. Asphaltenes were precipitated from a hexane–dichloromethane solution (80:1) and separated by centrifugation. The hexane–soluble fractions were separated into NSO compounds, saturated hydrocarbons, and aromatic hydrocarbons using a Köhnen–Willsch medium–pressure liquid chromatography (MPLC) instrument (Radke et al., 1980).

Rock-Eval pyrolysis was performed on all coal samples using a Vinci Rock-Eval 6 instrument. Rock-Eval parameters S2 (amount of hydrocarbons generated during pyrolysis; mgHC/g rock), hydrogen index (HI = S2×100/TOC; mgHC/gTOC) and Tmax (°C) of whole coal samples were reported by Fikri et al. (2022a,b) and Fikri et al. (submitted). The Rock-Eval parameters S1 (amount of free hydrocarbons; mgHC/g rock), bitumen index (BI = S1×100/TOC; mgHC/gTOC) and quality index (QI = [S1+S2]×100/TOC; mgHC/gTOC) are reported here for the first time. In this study, Rock-Eval pyrolysis was repeated on extracted coal samples. The difference between the S2 of the unextracted and extracted coal is called as $S2_{bitumen}$ (e.g., Ziegs et al., 2017; Misch et al., 2019).

Pyrolysis gas chromatography (Py-GC) was performed using the Quantum MSSV-2 Thermal Analysis System®. Material of the five crushed coal samples was heated in a flow of helium, and products released over the temperature range 300-600°C (40K/min) were focussed using a cryogenic trap, and then analysed using a 50m x 0.32mm BP-1 capillary column equipped with a flame ionisation detector. The GC oven temperature was programmed from 40°C to 320°C at 8°C/minute. Boiling ranges (C1, C2-C5, C6-C14, C15+) and individual compounds (*n*-alkenes, *n*-alkanes, alkylaromatic hydrocarbons and alkylthiophenes) were quantified by external standardisation using *n*-butane. Response factors for all compounds were assumed the same, except for methane whose response factor was 1.1.

Bulk carbon isotope data were determined on 68 coal samples from the TAJ Pit-1D and Tutupan mines. Portions of each sample (0.4 to 0.7 mg) were packed in tin capsules and burned in excess oxygen at 1080°C using an elemental analyzer (Thermo Scientific Flesh EA). The CO_2 produced was analyzed online using a Thermo Scientific Delta-V isotopic ratio mass spectrometer. The $^{13}C/^{12}C$ isotope ratio of CO_2 from a sample was compared to a reference ratio calibrated against the PDB standard. The overall reproducibility of the analytical procedure is in the 0.1 to 0.2 range.

4 Results and Interpretation

4.1 Rock-Eval data of whole coals

Bulk geochemical parameters of Eocene and Miocene coals are listed in Tables 2-4. Their vertical distribution is shown in Fig. 5.

4.1.1 Eocene coals (TAJ Pit-1D mine)

The amount of free hydrocarbons (S1) in coal samples ranges from 2.6 to 9.8 mgHC/g rock (Table 2). The average S1 of each coal seam increases upwards from 4.2 (seam D) to 5.6 (seam C) and 6.5 mgHC/g rock (seam B). The BI shows the same trend and increases from 5.7 (seam D) to 8.1 (seam C) and 8.9 mgHC/gTOC (seam B). S2 (217-343; average 269 mgHC/g rock), HI (316-470; average 374 mgHC/gTOC) and QI (321-481; average 381 mgHC/gTOC) are very high and show a similar subtle upward increase. Consequently, the highest HI values are observed in samples from the upper seam B (average 413 mgHC/gTOC). Tmax values of coal samples are rather uniform (424±2.5 °C) and slightly lower than the average Tmax of six non-coal samples (430±2.2 °C).

4.1.2 Miocene coals (Tutupan mine)

The amount of S1 hydrocarbons (0.4-5.8 mgHC/g rock) and the BI (0.7-10.7; Table 3) in Tutupan coals are significantly lower than in Eocene coals. The average values increase again from the lower seam T110 (1.4 mgHC/g rock; 2.4 mgHC/gTOC) to the middle seam 210 (1.9 mgHC/g rock; 3.2 mgHC/gTOC) and to the upper seam T300 (2.7 mgHC/g rock; 5.1 mgHC/gTOC). S2 (54-202; average 114 mgHC/g rock), HI (115-349; average 203 mgHC/gTOC) and QI (115-359; average 206 mgHC/gTOC) do not show a clear depth trend. Tmax values of coal samples show two cluster with values around 375 °C and values around 405 °C. Relatively high Tmax values prevail in the

lower part of the lower seam T110, while low Tmax values dominate in the upper seam T300. Non-coal layers typically show higher Tmax values (425 °C).

4.1.3 Miocene coals (Jumbang mine)

Jumbang coals contain significant amounts of S1 hydrocarbons (2.8-15.5; average 6.2 mgHC/g rock). Consequently, the BI values (5.5-24.8; average 11.6 mgHC/gTOC) are higher than in any other studied coal. S2 (79-336; average 126 mgHC/g rock); HI (154-539; average 236 mgHC/gTOC) and QI (160-564; average 248 mgHC/gTOC) are nearly as high as high as in Eocene seams. Tmax values of coal samples are often very low (373±2.3 °C). Slightly higher values (390-400 °C) are limited to the lowermost and uppermost samples. In contrast, Tmax values of non-coal layers are significantly higher (412-425 °C).

Table 2. Bulk parameter of Eocene TAJ Pit – 1D coals.

Sample	Position	Ash	TOC	Sulphur	S1	S2	HI	BI	QI	Tmax	Resinite (Total|Detr.)		EOM	Asph.	NSO	S+A	$\delta^{13}C$
	(m a.b.)		(wt% db)		(mgHC/g rock)		(mgHC/gTOC)			(°C)	(vol %)		(mgHC/gTOC)				‰
Mudstone	1.6	88.14	2.3	0.06	0.05	4.5	196			432	0.0	0.0					
B–1	1.4	7.36	71.4	0.34	6.47	301.7	423	9.1	432	427	8.5	5.0	28.9	12.55	11.2	5.1	-26.65
B–2	1.2	7.51	73.3	0.31	5.77	316.7	432	7.9	440	427	12.7	8.3					
B–3	1.0	9.52	70.2	0.30	6.49	254.3	362	9.2	372	425	7.4	4.2	30.4	13.32	11.7	5.4	-26.57
B–4	0.8	8.98	72.3	0.26	4.88	294.0	407	6.7	413	426	11.7	8.1					
B–5	0.6	7.29	75.9	0.26	5.74	342.7	452	7.6	459	427	8.6	4.8	33.4	14.89	14.4	4.1	-26.70
B–6	0.4	11.23	72.8	0.28	9.77	289.5	398	13.4	411	426	9.6	3.8					
B–7	0.2	7.18	72.9	0.36	6.35	303.7	417	8.7	425	425	5.7	3.6	30.1	13.21	12.2	4.7	-26.64
Mudstone	0	87.62	1.8	0.10	0.04	2.6	142			432	0.0	0.0					
Mudstone	3.6	88.33	1.8	0.24	0.03	2.4	134			431	0.0	0.0					
C–1	3.4	11.89	67.3	0.26	5.99	279.3	415	8.9	424	425	10.6	7.6	34.2	13.81	15.7	4.7	-26.40
C–2	3.2	7.47	73.1	0.28	5.47	309.0	423	7.5	430	426	7.5	3.0					
C–3	3.0	10.19	71.6	0.27	5.24	327.2	457	7.3	464	428	10.1	6.8	33.8	14.93	14.9	4.0	-26.56
C–4	2.8	7.07	72.5	0.39	6.98	247.0	341	9.6	350	420	3.2	1.8					
C–5	2.6	5.62	73.4	0.31	5.06	245.9	335	6.9	342	422	4.6	3.8	28.5	12.99	10.3	5.2	-26.18
C–6	2.4	10.15	70.3	0.36	7.44	303.8	432	10.6	443	426	8.0	4.1					
C–7	2.2	11.81	69.0	0.40	7.93	226.1	328	11.5	339	421	3.4	1.4	35.9	16.14	12.4	7.4	-26.56
C–8	2.0	29.45	46.3	0.26	5.33	217.3	470	11.5	481	428	8.2	5.6	38.4	15.68	17.6	5.1	-26.42
C–9	1.8	4.34	74.6	0.34	4.84	253.2	340	6.5	346	422	3.4	2.2					
C–10	1.6	12.80	65.4	0.34	5.26	267.8	409	8.0	417	426	9.2	7.3					
C–11	1.4	5.83	72.8	0.35	4.27	254.4	349	5.9	355	425	4.1	2.5	22.3	10.47	7.5	4.2	-26.18
C–12	1.2	4.64	74.0	0.36	4.91	245.9	332	6.6	339	423	3.7	3.5					
C–13	1.0	4.64	74.2	0.35	5.77	253.3	341	7.8	349	421	4.7	3.5	29.1	13.67	9.1	6.3	-26.49
C–14	0.8	7.27	72.1	0.33	5.73	254.5	353	7.9	361	425	5.2	4.0					
C–15	0.6	7.01	73.2	0.32	5.32	279.7	382	7.3	390	427	6.1	4.5	29.3	12.79	12.4	4.1	-26.60
C–16	0.4	7.08	71.6	0.32	4.72	246.5	344	6.6	351	421	3.6	2.4					
C–17	0.2	6.31	72.9	0.37	5.64	250.5	344	7.7	351	426	7.7	6.5	23.6	11.08	8.7	3.9	-26.40
Mudstone	0	89.27	3.0	0.21	0.14	7.0	231			426	0.0	0.0					
Mudstone	3.0	86.46	0.6	0.03	0.01	0.5	81			431	0.0	0.0					
D–1	2.8	5.01	76.2	0.72	3.66	266.3	350	4.8	354	428	5.3	4.1	27.7	13.72	10.1	3.9	-26.12
D–2	2.6	6.86	73.1	0.83	4.29	253.8	347	5.9	353	427	4.4	3.4					
D–3	2.4	9.13	71.5	0.69	3.37	236.1	330	4.7	335	423	6.7	4.9	38.2	17.28	16.0	4.8	-25.63
D–4	2.2	3.70	76.2	0.57	3.50	269.8	354	4.6	359	427	6.0	4.2					
D–5	2.0	3.81	77.1	0.52	4.05	282.7	367	5.2	372	427	8.3	5.8	48.9	13.48	31.2	4.2	-26.16
D–6	1.8	10.18	72.1	0.57	3.50	264.1	366	4.8	371	425	5.3	2.6					
D–7	1.6	10.03	71.7	0.56	3.49	237.6	331	4.9	336	425	7.6	5.8	37.7	19.33	13.9	4.5	-26.08
D–8	1.4	10.68	72.1	0.50	2.60	232.7	323	3.6	327	424	3.6	3.0					
D–9	1.2	9.58	70.9	0.54	3.97	245.9	347	5.6	353	424	6.0	3.5					
D–10	1.0	4.94	75.8	0.38	7.77	311.5	411	10.3	421	416	4.6	1.6	42.4	23.40	15.7	3.4	-25.82
D–11	0.8	5.80	74.4	0.41	5.78	265.2	356	7.8	364	423	4.5	3.2					
D–12	0.6	6.41	74.9	0.39	4.29	301.3	402	5.7	408	426	7.2	3.6	41.4	19.81	18.1	3.5	-26.06
D–13	0.4	4.40	74.1	0.44	4.12	233.8	316	5.6	321	423	4.8	4.0					
D–14	0.2	4.71	76.4	0.42	4.81	246.0	322	6.3	328	424	5.0	3.6	46.5	24.45	17.9	4.1	-26.24
Mudstone	0	95.33	0.4	0.07	0.01	0.4	91			430	0.0	0.0					

TOC – total organic carbon, HI – hydrogen index, BI – bitumen index, QI – quality index, EOM – extractable organic matter, Asph. - asphaltenes, S+A – saturated + aromatic hydrocarbons, a.b. – above base, Tot. – total, Detr. – detrital. Data are partly from Fikri et al. (2022b)

Table 3. Bulk parameter of Miocene Tutupan coals.

Sample	Position (m a.b.)	Ash	TOC (wt% db)	Sulphur (wt% db)	S1 (mgHC/g rock)	S2 (mgHC/g rock)	HI (mgHC/gTOC)	BI (mgHC/gTOC)	QI (mgHC/gTOC)	Tmax (°C)	Resinite (Total|Detr.) (vol %)		EOM (mgHC/gTOC)	Asph. (mgHC/gTOC)	NSO (mgHC/gTOC)	S+A (mgHC/gTOC)	$\delta^{13}C$ ‰
Mudstone	25	88.03	1.8	0.33	0.02	0.9	51			425	0.0	0.0					
T300-1	24	1.54	51.6	0.09	2.02	103.4	201	3.9	204	383	1.6	0.6					
T300-2	23	1.54	50.8	0.09	0.95	84.6	167	1.9	168	402	1.8	0.8	122.4	67.1	52.2	3.1	-28.36
T300-3	22	88.25	1.4	0.06	0.03	1.2	82			422	0.0	0.0					
T300-4	21	5.03	51.3	0.10	4.38	141.3	275	8.5	284	372	5.7	2.4	235.4	139.8	90.4	5.2	-28.23
T300-5	20	1.20	52.8	0.07	4.97	166.3	315	9.4	325	374	9.4	1.4					
T300-6	19	1.12	53.6	0.07	5.73	187.0	349	10.7	359	373	9.0	3.0	316.1	190.9	119.7	5.5	-27.85
T300-7	18	2.09	50.0	0.10	1.70	100.1	200	3.4	204	375	2.6	1.4					
T300-8	17	1.64	48.8	0.10	0.48	64.8	133	1.0	134	403	1.8	1.4	75.8	56.8	16.6	2.5	-28.23
T300-9	16	13.88	34.4	0.12	2.05	65.1	189	5.9	195	403	5.5	1.4	159.4	81.4	73.9	4.2	-28.27
T300-10	15	3.69	51.8	0.11	1.67	124.3	240	3.2	243	375	5.0	1.0					
T300-11	14	7.39	45.9	0.11	0.84	72.6	158	1.8	160	405	0.8	0.2	89.4	41.1	45.1	3.2	-28.31
T300-12	13	6.74	49.1	0.26	1.75	95.1	194	3.6	197	372	2.0	0.2					
T300-13	12	1.73	54.6	0.11	3.03	133.5	244	5.5	250	373	4.0	0.6	162.2	116.2	42.3	3.7	-28.33
T300-14	11	12.85	41.7	0.09	1.79	84.1	201	4.3	206	373	2.8	0.6	120.7	76.0	40.3	4.4	-28.10
T300-15	10	15.61	43.1	0.30	1.34	103.9	241	3.1	244	378	4.8	0.8					
T300-16	9	7.69	49.9	0.21	3.26	142.5	286	6.5	292	372	5.9	1.8					
T300-17	8	3.96	53.6	0.10	1.67	76.7	143	3.1	146	371	5.9	1.2	99.8	72.2	25.1	2.6	-29.02
T300-18	7	1.76	54.6	0.09	4.81	140.5	257	8.8	266	375	3.5	0.4					
T300-19	6	3.69	49.2	0.09	1.64	93.7	190	3.3	194	382	3.3	0.8					
T300-20	5	1.49	49.6	0.09	1.11	92.6	187	2.2	189	399	1.6	0.8	96.9	69.1	24.5	3.3	-28.46
T300-21	4	1.86	56.1	0.09	4.99	163.4	291	8.9	300	374	6.8	1.6					
T300-22	3	1.68	56.1	0.11	3.45	126.6	226	6.1	232	376	3.0	1.2	105.2	88.0	15.5	1.8	-28.60
T300-23	2	1.19	60.0	0.08	4.26	161.6	269	7.1	276	375	2.8	0.4					
T300-24	1	1.94	52.5	0.09	3.03	121.8	232	5.8	238	378	3.1	1.8	122.6	85.6	33.7	3.3	-28.44
Mudstone	0	85.46	2.35	0.04	0.10	2.8	119			416	2.3	0.0					
mudstone	25	89.47	1.31	0.03	0.02	0.9	68			423	0.0	0.0					
T210-1	24	13.55	36.7	0.11	0.96	77.9	213	2.6	215	377	3.5	0.8	254.4	98.9	152.5	3.0	-28.55
T210-2	23	7.16	49.2	0.10	0.78	76.6	156	1.6	157	407	2.2	1.4					
T210-3	22	1.60	56.8	0.10	0.64	77.2	136	1.1	137	403	5.0	1.6	93.7	57.9	33.7	2.1	-27.46
T210-4	21	1.21	60.9	0.07	5.58	201.2	331	9.2	340	377	19.2	8.7	179.3	103.4	73.7	2.2	
T210-5	20	1.31	56.4	0.08	1.17	114.1	202	2.1	204	379	3.8	1.4					-27.80
T210-6	19	1.14	55.7	0.07	0.70	92.1	165	1.3	167	387	4.3	2.0					
T210-7	18	1.14	58.3	0.07	1.93	121.8	209	3.3	212	375	4.2	2.6	180.3	90.4	86.8	3.0	-28.02
T210-8	17	1.24	63.1	0.07	4.83	189.8	301	7.6	308	377	5.7	2.0	219.5	131.3	84.5	3.7	-27.94
T210-9	16	1.26	58.2	0.08	0.77	92.5	159	1.3	160	405	1.0	0.8					
T210-10	15	1.26	61.1	0.06	1.41	120.4	197	2.3	199	378	1.2	0.6					
T210-11	14	1.70	58.9	0.08	1.21	109.5	186	2.1	188	376	3.6	2.0	126.8	109.2	16.1	1.6	-28.02
T210-12	13	1.22	59.3	0.08	1.20	104.2	176	2.0	178	403	3.6	2.2					
T210-13	12	1.34	60.5	0.08	1.86	119.0	197	3.1	200	375	2.0	0.8	164.1	92.2	68.6	3.3	-28.22
T210-14	11	1.22	61.1	0.08	3.59	154.6	253	5.9	259	374	2.0	0.8					
T210-15	10	1.24	59.3	0.08	1.59	109.4	185	2.7	187	376	2.4	1.6	129.1	72.9	53.5	2.7	-27.97
T210-16	9	1.32	60.6	0.08	5.07	162.6	268	8.4	277	372	4.9	1.2					
T210-17	8	1.28	59.8	0.08	2.27	148.8	249	3.8	253	374	2.8	1.0	186.4	119.7	63.5	3.2	-27.97
T210-18	7	1.26	59.6	0.08	1.03	93.4	157	1.7	158	397	2.0	1.0					
T210-19	6	0.98	59.0	0.07	0.93	110.7	188	1.6	189	399	2.2	1.0	77.0	65.3	10.1	1.6	-28.58
T210-20	5	1.05	59.6	0.07	0.91	114.8	193	1.5	194	392	2.6	1.2					
T210-21	4	1.19	61.2	0.09	3.03	154.3	252	4.9	257	374	3.8	0.8	216.9	116.8	94.8	5.4	-27.87
T210-22	3	1.08	60.8	0.08	1.50	108.9	179	2.5	181	378	1.6	0.6					
T210-23	2	1.30	54.2	0.11	1.49	93.3	172	2.7	175	397	2.4	0.4					-28.40
T210-24	1	14.15	40.7	0.17	1.05	77.7	191	2.6	194	403	3.0	0.4	110.3	79.1	27.6	3.6	-28.17
Mudstone	0	88.90	1.18	0.02	0.03	1.6	131			364	1.6	1.6					

Table 3. (continued)

Sample	Position (m a.b.)	Ash	TOC (wt% db)	Sulphur (wt% db)	S1 (mgHC/g rock)	S2 (mgHC/g rock)	HI (mgHC/gTOC)	BI (mgHC/gTOC)	QI (mgHC/gTOC)	Tmax (°C)	Resinite (Total|Detr.) (vol %)		EOM (mgHC/gTOC)	Asph. (mgHC/gTOC)	NSO (mgHC/gTOC)	S+A (mgHC/gTOC)	$\delta^{13}C$ ‰
Mudstone	47	91.13	0.73	0.04	0.01	0.6	89			372	0.0	2.8					
T110-1	46	5.19	53.5	2.03	4.10	143.8	269	7.7	276	375	1.0	3.7	214.7	118.7	92.7	3.3	-27.63
T110-2	45	1.44	62.8	0.12	4.07	185.3	295	6.5	301	378	1.4	3.2	139.2	53.5	83.9	1.8	-27.60
T110-3	44	1.12	63.8	0.10	3.03	174.5	273	4.7	278	376	2.0	5.5					
T110-4	43	1.12	62.7	0.09	1.09	144.5	230	1.7	232	377	2.1	4.5	133.0	68.8	62.0	2.3	-27.94
T110-5	42	1.18	59.7	0.12	3.20	156.4	262	5.4	267	376	3.2	6.9					
T110-6	41	1.12	62.7	0.10	1.18	130.4	208	1.9	210	392	2.6	4.3	182.4	80.1	99.0	3.2	-27.24
T110-7	40	1.08	61.9	0.09	0.92	105.1	170	1.5	171	399	3.1	5.6					
T110-8	39	1.16	60.7	0.09	0.65	85.0	140	1.1	141	401	2.1	6.8	108.5	63.8	42.6	2.0	-27.45
T110-9	38	5.87	55.3	0.13	1.79	123.0	222	3.2	225	377	3.1	5.7					
T110-10	37	1.18	60.8	0.10	1.70	123.0	202	2.8	205	403	3.9	5.6	110.2	81.0	26.1	3.1	-27.60
T110-11	36	1.33	58.1	0.09	0.80	90.6	156	1.4	157	384	2.9	6.9					
T110-12	35	0.98	62.5	0.10	1.08	100.5	161	1.7	163	404	2.1	3.1	172.6	60.8	107.8	4.0	-26.81
T110-13	34	0.98	62.5	0.11	2.25	151.4	242	3.6	246	382	2.9	4.6					
T110-14	33	0.96	60.8	0.09	1.32	105.8	174	2.2	176	401	4.1	6.4	99.0	95.1	2.0	1.9	-27.23
T110-15	32	1.04	60.5	0.10	1.28	114.2	189	2.1	191	399	1.6	3.3					
T110-16	31	0.92	63.1	0.08	4.19	195.3	310	6.6	316	376	2.9	6.8	260.6	114.6	140.1	6.0	-27.22
T110-17	30	1.02	60.7	0.08	1.56	138.1	228	2.6	230	379	3.3	6.1					
T110-18	29	1.02	59.0	0.09	0.77	99.5	169	1.3	170	405	3.1	4.7	65.2	51.8	11.6	1.8	-27.37
T110-19	28	1.05	60.4	0.10	1.33	126.5	209	2.2	212	383	3.2	8.0					
T110-20	27	1.10	60.5	0.09	2.15	138.6	229	3.5	233	377	3.3	7.6	254.1	135.7	113.0	5.4	-27.58
T110-21	26	1.37	58.8	0.09	1.52	105.5	179	2.6	182	403	2.2	7.8					
T110-22	25	0.64	59.5	0.08	1.17	107.5	181	2.0	182	401	1.7	4.6	157.5	75.1	79.0	3.4	-27.65
T110-23	24	0.60	58.9	0.08	0.96	109.9	187	1.6	188	405	2.2	6.1					
T110-24	23	0.61	61.5	0.09	1.03	106.8	174	1.7	175	404	1.2	2.5	106.8	76.7	28.1	1.9	-27.25
T110-25	22	4.27	51.7	0.08	0.75	87.2	169	1.5	170	399	0.6	1.9					
T110-26	21	2.78	53.3	0.08	1.29	105.9	199	2.4	201	398	1.6	3.7	116.1	101.7	11.9	2.5	-28.03
T110-27	20	1.58	60.4	0.09	1.43	136.5	226	2.4	228	384	2.4	5.3					
T110-28	19	2.08	57.2	0.10	1.98	108.3	189	3.5	193	404	1.8	3.9	92.6	68.3	21.3	3.1	-27.74
T110-29	18	2.56	54.2	0.10	1.27	100.3	185	2.3	187	402	0.4	2.8					
T110-30	17	1.17	59.1	0.09	1.26	113.8	193	2.1	195	401	1.6	3.0	126.0	83.0	40.8	2.2	-27.78
T110-31	16	1.73	58.4	0.09	0.70	83.4	143	1.2	144	400	1.6	3.0					
T110-32	15	1.10	59.4	0.08	1.40	114.8	193	2.3	196	401	2.4	4.4	116.8	76.2	37.9	2.7	-28.16
T110-33	14	1.18	59.3	0.09	0.90	91.4	154	1.5	156	405	2.0	3.1					
T110-34	13	2.08	54.2	0.10	0.42	66.7	123	0.8	124	408	1.2	2.0	117.0	59.5	54.1	3.4	-28.08
T110-35	12	1.28	58.2	0.10	0.61	73.9	127	1.0	128	406	2.0	2.8					
T110-36	11	1.32	59.2	0.10	1.14	99.3	168	1.9	170	406	1.6	3.3	76.4	61.5	11.3	3.6	-27.90
T110-37	10	3.03	51.7	0.09	0.71	91.6	177	1.4	178	404	2.6	4.6					
T110-38	9	1.69	53.0	0.10	0.83	84.7	160	1.6	161	405	1.4	3.4	125.4	61.2	58.5	5.8	-28.28
T110-39	8	2.35	54.5	0.10	1.29	97.3	178	2.4	181	406	0.8	1.4					
T110-40	7	2.24	56.6	0.10	2.49	111.5	197	4.4	202	405	1.2	2.2	98.6	68.6	25.9	4.1	-28.42
T110-41	6	2.81	55.4	0.12	1.24	88.9	160	2.2	163	404	0.8	1.4					
T110-42	5	2.37	56.4	0.13	0.43	80.9	144	0.8	144	408	1.2	2.9	69.6	45.3	21.2	3.1	-28.16
T110-43	4	6.04	47.8	0.16	0.40	54.8	115	0.8	115	411	0.6	1.2					
T110-44	3	15.91	38.7	0.14	0.50	59.6	154	1.3	155	408	2.0	2.4	71.7	52.4	16.6	2.7	-28.14
T110-45	2	3.22	54.5	0.13	0.94	99.2	182	1.7	184	405	1.2	2.6					
T110-46	1	1.16	59.3	0.10	1.00	101.4	171	1.7	173	403	1.2	3.6	78.6	54.3	19.9	4.4	-28.09
Mudstone	0	92.78	0.61	0.01	0.01	0.3	55			421	0.0	0.0					

Data are partly from Fikri et al. (2022a).

Table 4. Bulk parameter, resinite percentages and bulk isotope data of Miocene Jumbang coals.

Sample	Position (m a.b.)	Ash	TOC (wt% db)	Sulphur (wt% db)	S1 (mgHC/g rock)	S2 (mgHC/g rock)	HI (mgHC/gTOC)	BI (mgHC/gTOC)	QI (mgHC/gTOC)	Tmax (°C)	Resinite (Total|Detr.) (vol %)		EOM (mgHC/gTOC)	Asph. (mgHC/gTOC)	NSO (mgHC/gTOC)	S+A (mgHC/gTOC)	$\delta^{13}C$ ‰
Mudstone	20.4	89.07	0.73	0.02	0.02	0.3	39			425	0.0	0.0					
BL1-2	19.9	2.12	49.3	0.10	3.25	83.5	170	6.6	176	390	10.2	5.9					-27.86
BL1-3	18.9	1.85	52.7	0.09	6.65	114.9	218	12.6	231	371	11.1	5.0					
BL1-4	17.9	2.13	54.9	0.08	10.51	226.8	413	19.1	432	375	16.0	6.3	441.0	431.5	8.5	0.9	-27.99
BL1-5	16.9	2.11	56.4	0.10	7.14	114.1	202	12.7	215	370	7.5	5.0					
BL1-6	15.9	1.94	55.3	0.09	11.08	171.7	310	20.0	330	372	17.2	6.6	301.6	288.5	11.8	1.2	-27.81
BL1-7	14.9	3.17	54.1	0.14	7.15	126.6	234	13.2	247	372	14.6	8.4					
BL1-8	13.9	2.68	52.3	0.12	9.15	133.6	255	17.5	273	371	9.0	3.6	273.6	263.9	8.4	1.3	-27.82
BL1-9	12.9	2.08	54.0	0.11	9.21	147.1	272	17.0	289	370	10.8	5.8					
BL1-10	11.9	2.90	51.3	0.11	6.36	94.4	184	12.4	196	374	9.3	6.8	221.4	213.7	6.6	1.1	-27.54
BL1-11	10.9	2.81	51.1	0.11	3.18	78.6	154	6.2	160	378	7.5	4.4					
BL1-12	9.9	2.91	48.5	0.11	4.01	111.3	229	8.3	238	371	11.6	5.4	231.8	227.3	3.9	0.6	-27.68
BL1-13	8.9	3.20	49.3	0.08	4.31	90.9	184	8.7	193	374	8.8	2.1					
BL1-14	7.9	2.18	52.6	0.09	3.87	99.7	189	7.4	197	376	11.3	6.0					-28.06
BL1-15	7.4	2.45	51.3	0.09	3.25	104.8	204	6.3	210	371	6.5	2.9					
BL1-16a	6.4	2.14	51.2	0.10	2.84	84.2	164	5.5	170	376	5.0	2.5	217.2	209.7	6.4	1.1	-28.04
BL1-16b	6.2	7.54	51.3	0.09	5.23	123.3	240	10.2	250	371	9.4	3.5					
BL1-17	5.4	1.90	52.5	0.10	5.26	96.8	185	10.0	195	372	2.9	2.4					-28.22
BL1-18a	4.4	1.94	53.0	0.09	6.04	122.1	230	11.4	242	375	7.6	4.5					
BL1-18b	4.2	2.26	62.4	0.07	15.45	336.2	539	24.8	564	373	17.3	10.4	305.4	300.8	4.2	0.4	-28.26
BL1-19a	3.2	4.52	55.4	0.16	4.81	108.2	195	8.7	204	395	3.1	1.8					
BL1-19b	2.2	3.82	55.6	0.15	3.63	105.4	190	6.5	196	395	4.9	2.9	246.0	238.5	5.4	2.0	-27.74
Mudstone	1.2	92.56	2.27	0.01	0.13	4.5	196			412	3.1	3.1					
BL1-21	1	8.77	45.2	0.14	4.21	103.1	228	9.3	238	399	3.5	1.4					-27.70
Mudstone	0	91.55	2.13	0.01	0.17	4.5	209			419	5.0	5.0					

Data are partly from Fikri et al. (submitted).

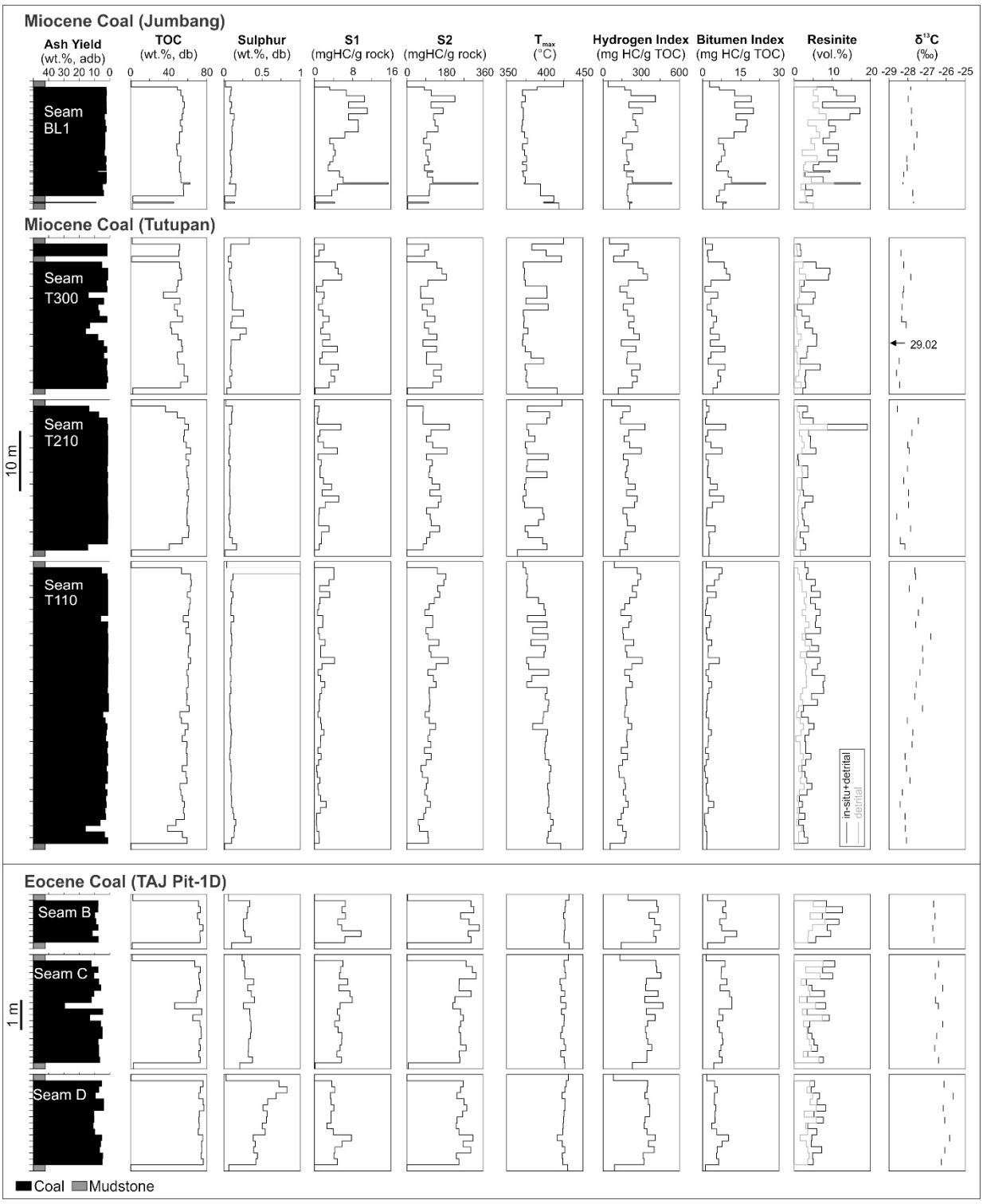

Fig. 4. Depth plots of ash yield, total organic carbon (TOC) and sulphur contents together with Rock-Eval parameters and isotope ratios of bulk organic carbon. Note different depth scales for Miocene and Eocene coal seams.

4.1.4 Shape of Rock-Eval pyrograms

Pyrograms of Eocene coals show a unimodal, largely symmetrical S2 peak with a maximum at about 425 °C (Fig. 5a). In contrast, pyrograms of low-rank Miocene coals are more diverse and vary considerably, even within a single seam (Fig. 5b-e). They show either unimodal S2 peaks at ~370 °C (e.g., T210-04) or ~400 °C (e.g., T210-02), unimodal S2 peaks with a clear "shoulder" (e.g., T300-22), or a bimodal S2 peak (e.g., T300-09).

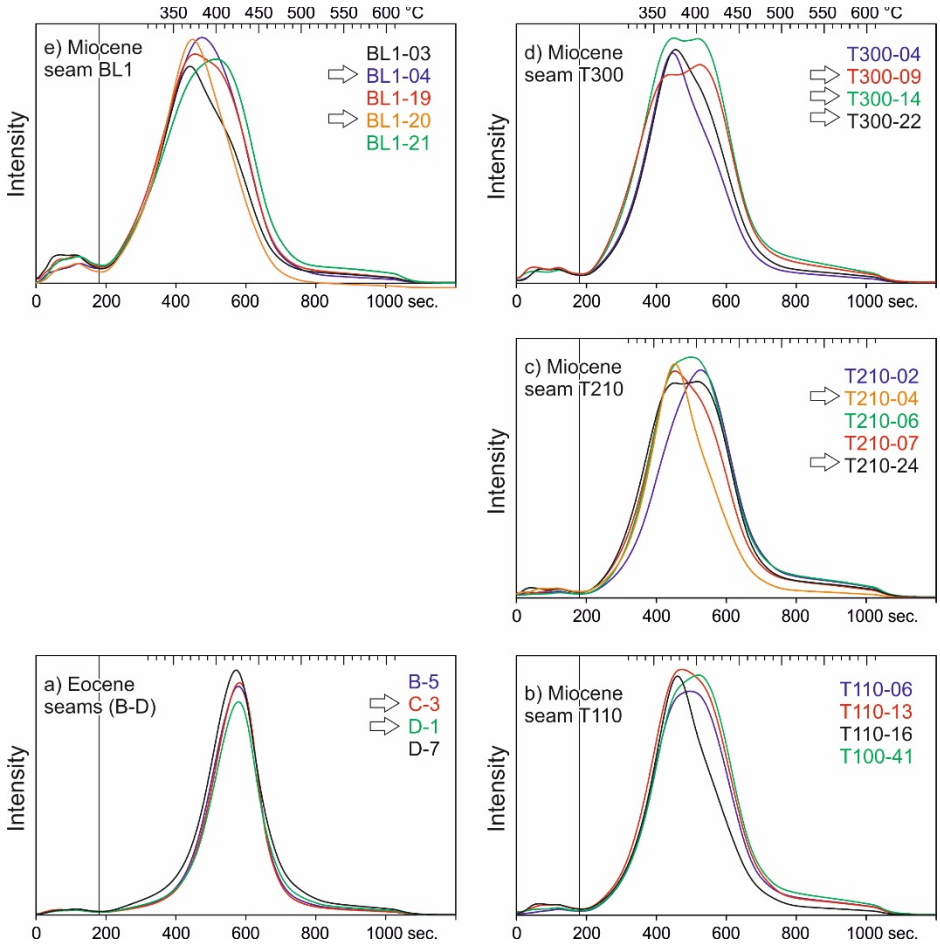

Fig. 5. Pyrograms of (a) Eocene samples and of Miocene samples from seams (b) T-110, (c) T-210, (d) T300, and (e) BL1. The pyrograms show a unimodal peak, peaks with a strong shoulder, or a bimodal peak. The given temperatures are corrected pyrolysis temperatures. Nine samples which were selected for Rock-Eval pyrolysis after extraction are highlight by an arrow.

4.2 Rock-Eval data of extracted coals

Two Eocene (D-1, C-3) and seven Miocene coals have been selected for Rock-Eval analysis on extracted coals. The Miocene coals include three samples with distinct bimodal S2 peaks (T210-24; T300-09; T300-14) and four samples with a unimodal S2 peak and low Tmax. Two of these samples (BL1-4, BL1-20) have symmetric S2 peaks, while the other samples have S2 peaks with a mild (T210-04) or a strong shoulder (T300-22; Fig. 6), respectively.

Each sample was extracted twice. The amount of the extractable organic matter (EOM) of the original coal and the extracted coal is listed in Table 5. The amounts and the compositions of the first and second extract are shown graphically in Fig. 6d. It can be seen that the amount of extract decreased significantly after the first extraction. It is also evident that the second extract, unlike the first one, contains almost no NSO compounds.

Rock-Eval parameters of the original samples (S2, HI, Tmax) are listed in Table 5 together with S2 and Tmax after the first and second extraction. $S2_{bitumen}$ has been calculated using the data after the second extraction. The effects of the second extraction on the shape of the pyrograms are small (Fig. 6a,b).

The S2 peak of the extracted Eocene coals (Fig. 6a) is about 30 % lower than that of the original coal, but the Tmax is similar. The change in the shape of the S2 peaks suggests that thermally labile compounds have been extracted. $S2_{bitumen}$ of Eocene coals is about 85 mgHC/g rock.

Major changes are evident in the pyrograms of Miocene coals (Fig. 6b,c). In coals with bimodal S2 peaks, the low Tmax peak disappeared completely (Fig. 6b). For samples with a unimodal S2 peak, S2 decreased significantly during extraction (by more than 60 % in T210-04 and BL-20) and Tmax increased to values between 407 and 415 °C (Table 5). $S2_{bitumen}$ in Miocene coals ranges from 16 to 208 mgHC/g rock.

Table 5. Rock-Eval parameters of coal samples before (original coal) and after extraction.

Sample	original coal						after first extraction			after second extraction		
	TOC	S1	S2	HI	Tmax	EOM	S2	Tmax	EOM	S2	$S2_{bitumen}$	Tmax
	wt%	mgHC/g rock		mgHC/gTOC	°C	mg/gTOC	mgHC/g rock	°C	mg/gTOC	mgHC/g rock		°C
BL1-04	54.9	10.5	226.8	413	375	441.0	116.7	407	13.2	96.3	130.5	409
BL1-20	62.4	15.5	336.2	539	373	305.4	158.8	410	26.7	131.5	204.7	414
T300-09	34.4	2.05	65.1	189	403	159.4	58.6	414	26.1	48.8	16.3	413
T300-14	41.7	1.79	84.1	201	373	120.7	48.3	417	17.1	40.3	43.8	416
T300-22	56.1	3.45	126.6	226	376	105.2	67.1	408	13.8	64.1	62.5	407
T210-04	60.9	5.58	201.2	331	377	179.3	72.8	409	15.0	76.1	125.1	411
T210-24	40.7	1.05	77.7	191	403	110.3	52.9	416	19.3	49.1	28.6	415
C-3	71.6	5.2	327.2	457	428	86.4	234.5	429	10.9	240.1	87.1	428
D-1	76.2	3.7	266.4	350	428	70.8	175.4	428	10.5	183.8	82.6	429

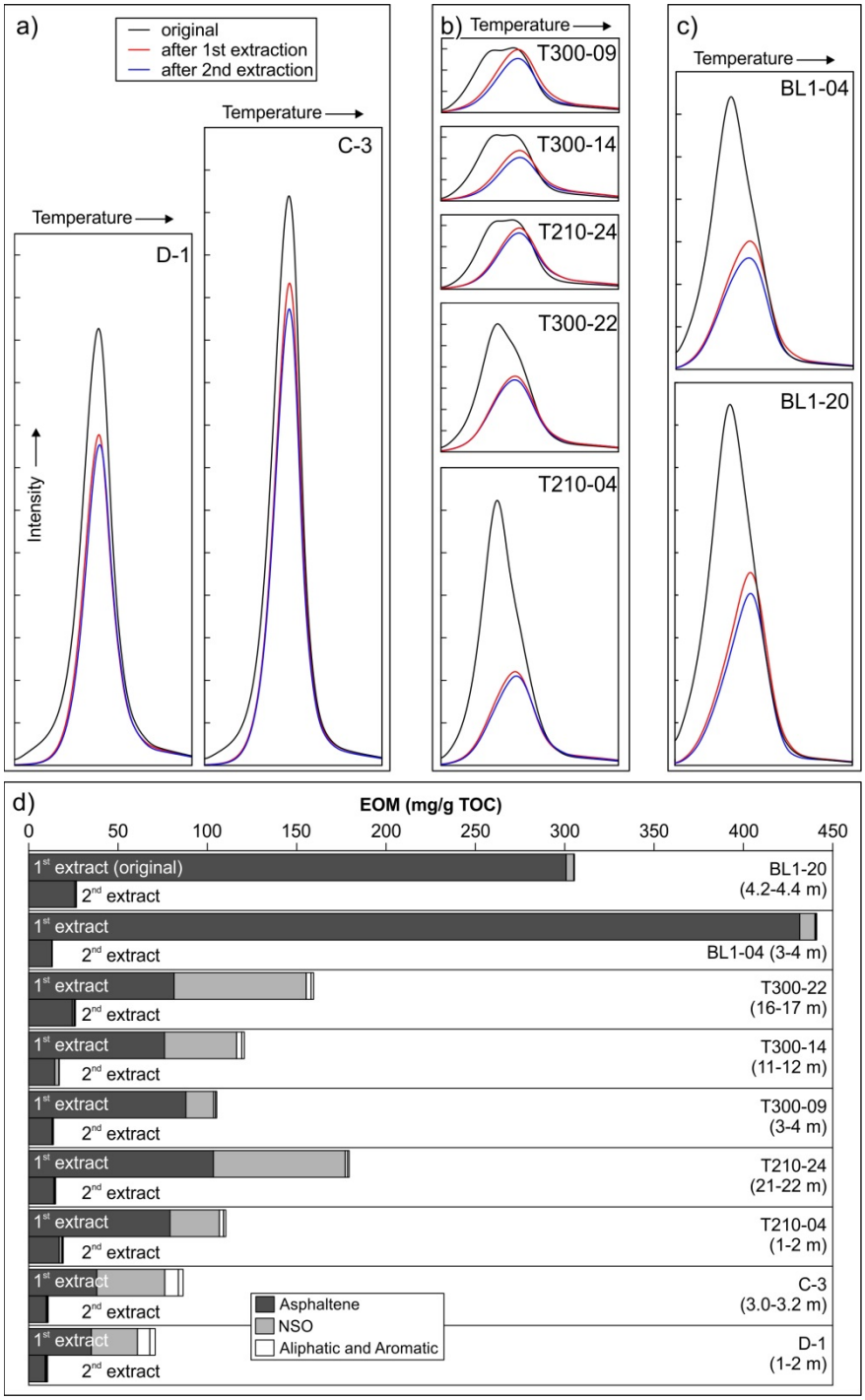

Fig. 6. Pyrograms of selected (a) Eocene and Miocene (b) Tutupan and (c) Jumbang coals showing the shape of the S2 peak before and after extraction with an organic solvent. (d) Amount and composition of extracts from Eocene and Miocene coals (first and second extract).

4.2 Pyrolysis-gas chromatography (Py-GC)

Two Eocene and three Miocene samples from the Tutupan mine have been selected for open-system Py-GC analysis. The pyrolysis gas chromatograms show significant differences between Eocene and Miocene coals (Fig. 7). In contrast, the variability between samples with the same age are minor, despite of varying HI values and varying amounts of resinite.

Fig. 8a shows the carbon chain lengths distribution of the samples plotted in the Petroleum Type Organofacies triangle of Horsfield (1989). For further molecular description of the organic matter structure (phenol abundance, aromaticity, organic sulphur abundance) the triangular plots of Larter (1984) and Eglinton et al. (1990) are shown in Figs. 8b and 8c, respectively.

The pyrolysis products of Eocene and Miocene samples differ significantly. Based on the distribution of chain lengths of *n*-alkenes and *n*-alkanes, it is likely that Eocene coals will generate a paraffinic oil with high wax content, while Miocene coals will generate a high wax paraffinic-naphthenic-aromatic (P-N-A) mixed oil (Fig. 8a).

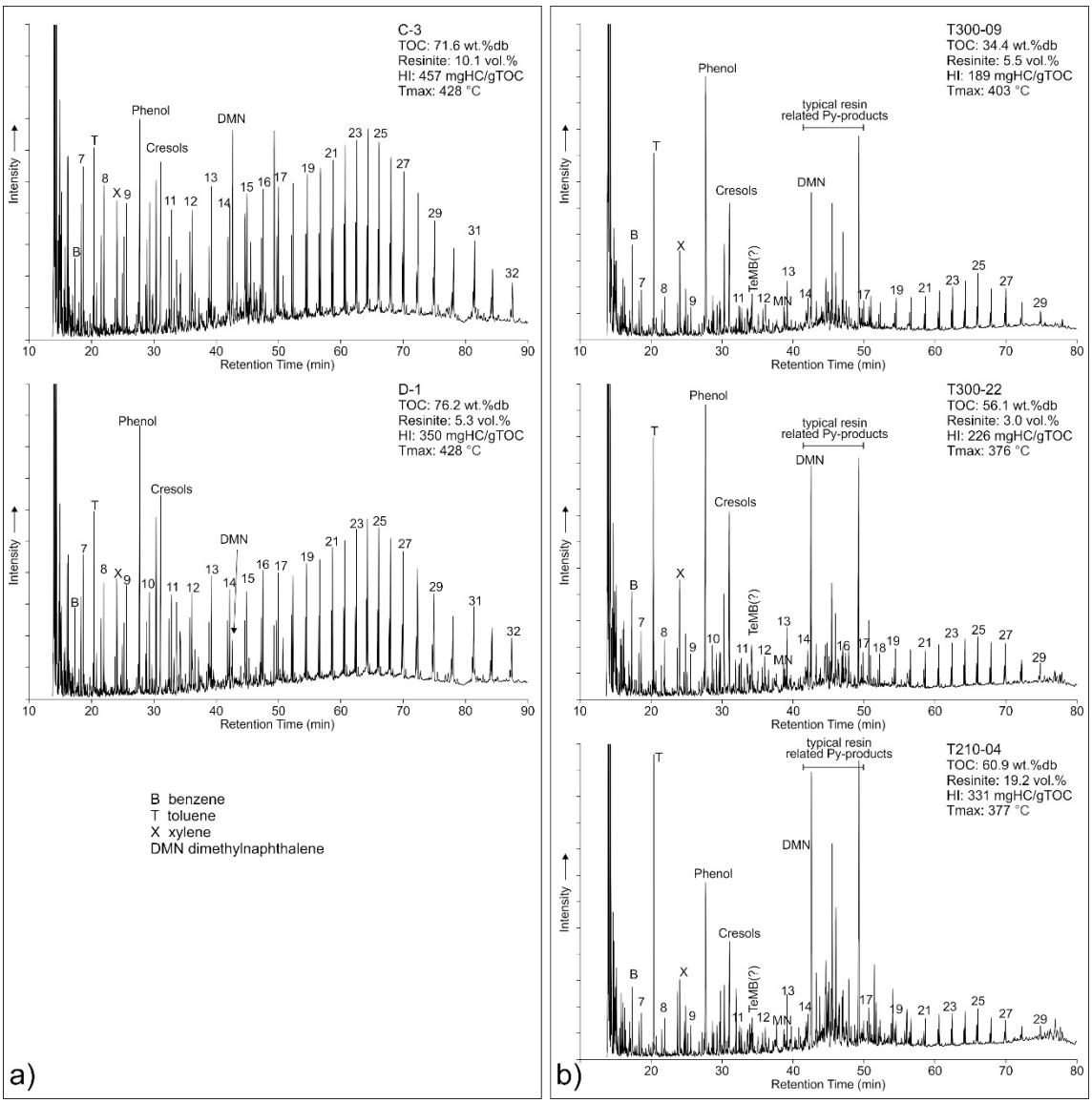

Fig. 7. Gas chromatograms of pyrolysis products of (a) Eocene and (b) Miocene coals.

In the scheme of Larter (1984), both Eocene and Miocene coals plot in that part of the broad field for terrestrial organic matter where phenol is high (Fig. 8b), but the proportion of phenol, typical of land plant lignocellulosic pyrolysis products (van de Meent et al., 1980; Vu et al., 2008), is slightly lower for Eocene coals.

The proportion of thiophenes is low in products from all coals, while the concentration of *n*-C_9 is higher and the concentration of o-xylene is lower in pyrolysates from Eocene coals. Therefore, Eocene and Miocene coals plot in the diagram after Eglinton et al. (1990) into the field of Type II and Type III kerogen, respectively (Fig. 8c).

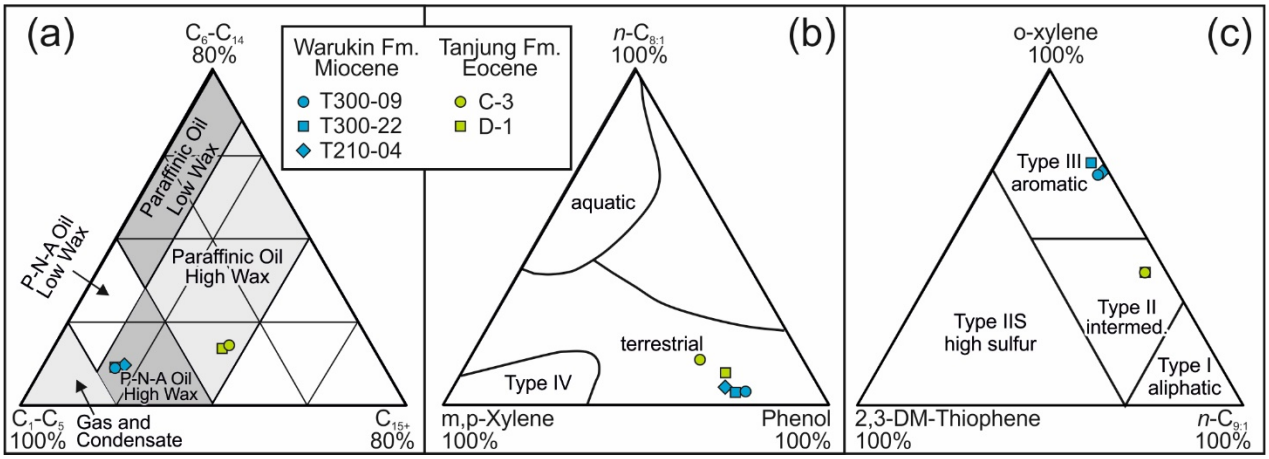

Fig. 8. Screening data from pyrolysis gas chromatography for the most important source-rock units: (a) normal alkyl chain length distribution (petroleum type after Horsfield, 1989), (b) phenol abundance (diagram after Larter, 1984) and (c) sulphur discriminator (Eglinton et al., 1990).

4.3 Stable carbon isotopes

Stable carbon isotope ($\delta^{13}C$) ratios of bulk organic carbon in Eocene coals fall into the range of -26.70 ‰ to -25.63 ‰. Organic carbon in Miocene is isotopically lighter (-29.04 to -26.81 ‰).

5 Discussion

In the discussion of the hydrocarbon potential of Indonesian Cenozoic coals, both maturity and facies aspects have to be considered.

5.1 Maturity

As testified by moisture content (~35 wt.% H_2O_{af}) and vitrinite reflectance (0.33-0.35 %Rr), the Miocene lignite from the BL1 seam from the Jumbang Mine (Asem-Asem Basin) is the studied coal with the lowest rank (Fikri et al., submitted). In the Tupupan Mine (Barito Basin), rank of Miocene coals increases from the upper seam T300 (26.3 wt.% H_2O_{af}; 0.36 %Rr) to the lower seam T110 (18.8 wt.% H_2O_{af}; ~0.40 %Rr; Fikri et al., 2022a). The Eocene coals from the TAJ mine in the Barito Basin have a slightly higher maturity (3-4 wt.% H_2O_{af}; 0.52-0.59 %Rr; Fikri et al., 2022b). Thus, the coals cover the maturity range of diagenesis (<0.40 %Rr) to early catagenesis (0.40-0.55 %Rr) according to Vu et al. (2009; 2013). The higher rank of Eocene coals is also supported by relatively high Tmax values (416-428; average 424 °C; Fig. 4; Table 2).

Sykes and Snowdon (2002) proposed a series of diagrams to determine the maturity and source potential of coals. According to these diagrams, Eocene coal is at a maturity stage corresponding to the onset of oil generation (Fig. 9a), while oil expulsion or even gas generation has not yet occurred (Fig. 9c).

Low Tmax values (≤411 °C) show that Miocene coals from the Jumbang and Tutupan mines are immature (Fig. 9). The Tmax values of the coals from both mines vary considerably and form clusters with Tmax values around 370 to 380 °C and at ~400 °C, with BL1 coals tending to have the lower Tmax values in both clusters. This reflects the lower maturity of the BL1 coals, which is also supported by on average higher S1 contents and bitumen index (BI=100*S1/TOC) values (Figs. 4, 9a). However, Tmax values of solvent-extracted coals are similar for Jumbang (409-414 °C) and Tutupan coals (407-416 °C; Table 5).

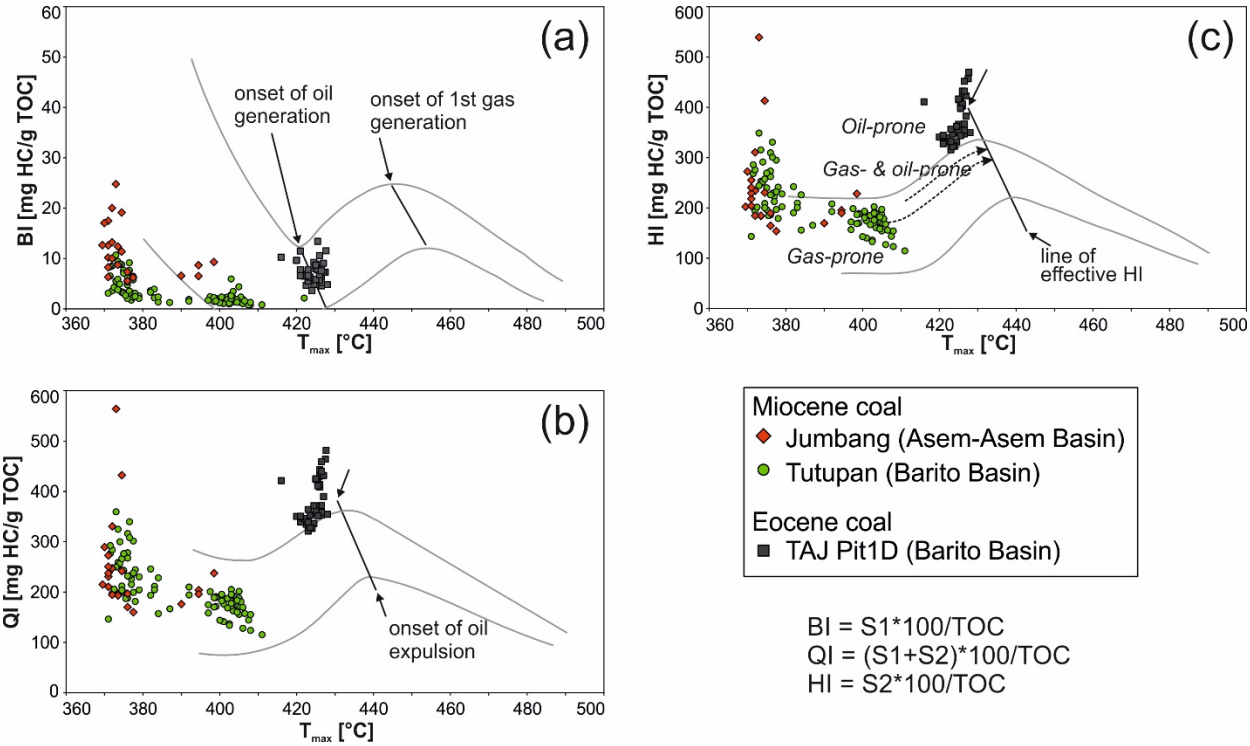

Fig. 9. Source potential of coals: Position of Miocene and Eocene coals in plots of Tmax versus (a) bitumen index (BI), (b) hydrogen index (HI) and (c) quality index (QI; after Sykes and Snowdon, 2002).

5.2 Presence and origin of in-situ bitumen

The shape of S2 peaks from Miocene coals varies greatly (Fig. 5). Within single seams, symmetrical peaks (with Tmax between 370-380 or 390-410 °C), strongly asymmetrical peaks or even bimodal peaks can be observed. Such variability may show the presence in-situ bitumen, which contributes to the S2 peak ($S2_{bitumen}$; e.g. Peters et al., 1981). This assumption is supported by the results of solvent-extracted Miocene coals, which show significantly reduced S2 peaks with increased and more uniform Tmax values (407-416 °C; Fig. 6). The results of solvent-extracted Eocene coals demonstrate that significant amounts of $S2_{bitumen}$ also exist in these slightly more mature coals. The presence of high amounts of heavy bitumen components in immature coals, especially in the lignite stage, has been observed by previous studies (e.g., Bechtel et al., 2005; Vu et al., 2009).

A good positive correlation exists between $S2_{bitumen}$ and the percentage of resinite macerals (r^2=0.72), which is even stronger if only detrital resinite is considered (r^2=0.84; Fig. 10a). *In-situ* resinite (r^2=0.41) and liptodetrinite (r^2=0.47) show moderate positive correlations, while other

liptinite macerals do not show any correlation with $S2_{bitumen}$. It should be noted that the correlation coefficients between $S2_{bitumen}$ and detrital resinite (r^2=0.89) and liptodetrinite (r^2=0.69) are even higher, if only Miocene coals are considered. In any case, the results suggest that the amount of *in-situ* bitumen is mainly controlled by the amount of (detrital) resinite. A positive correlation between $S2_{bitumen}$ and cadinene (r^2=0.72 for Miocene coals) further supports the significant role of resins on the amount of in-situ bitumen.

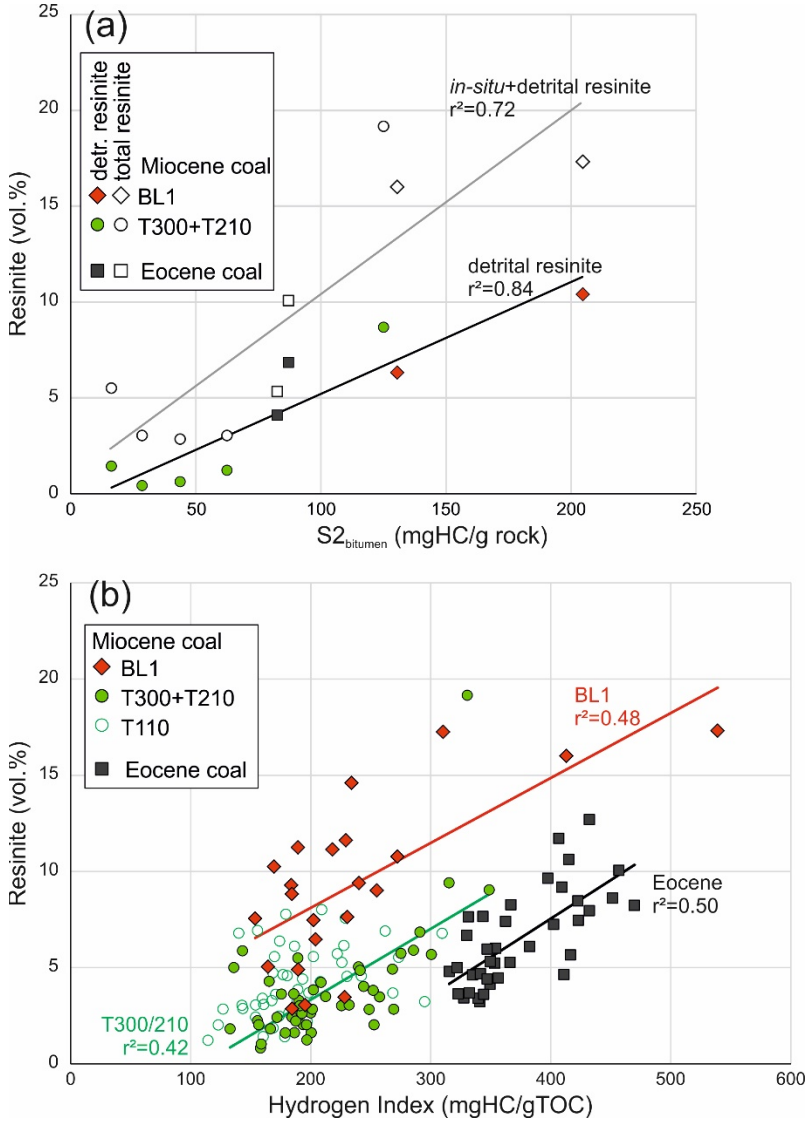

Fig. 10. Plot of resinite percentages versus (a) $S2_{bitumen}$ and (b) hydrogen index. The positive correlations suggest a dominant role of resins for the amount of heavy bitumen components and the hydrocarbon potential.

A general trend can be observed that with increasing original Tmax, the total EOM (Fig. 11a) and its asphaltene content (Fig. 11b) decrease. The amount of NSO compounds in Tutupan and Eocene coals shows a similar trend, but immature BL1 coals contain very low amounts of NSOs (see Table 4 and Fig. 6d). This suggests that the $S2_{bitumen}$ bitumen fraction is composed of heavy, probably oxygen-rich compounds with a slightly lower thermal stability to the kerogen part.

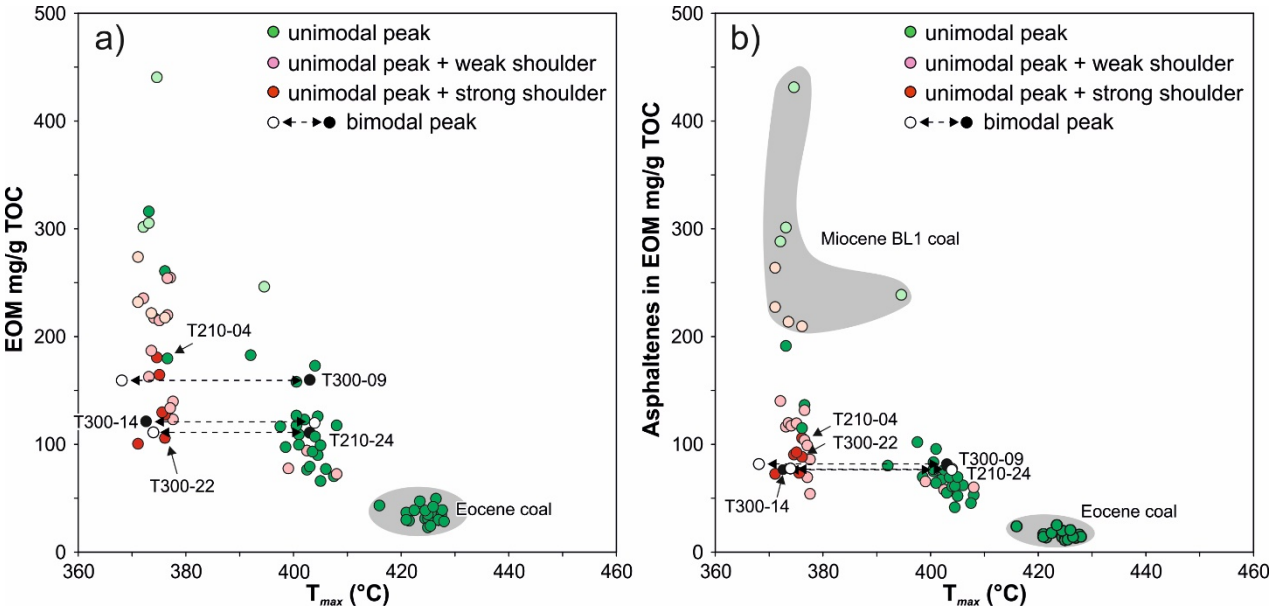

Fig. 11. Plot of Tmax versus extractable organic matter (EOM) content with description of the shape of the pyrograms. For samples with a double-peak pyrogram, the values of both peaks are shown.

The fate of the in-situ bitumen in low rank coals and its contribution to hydrocarbon generation is not completely understood, as pointed out by Vu et al. (2008). Perhaps, the bitumen simply contributes in an additive sense to the petroleum generation potential (e.g. Schenk et al., 1997). Alternatively, the in-situ bitumen may be progressively made insoluble by reactions with the kerogen (e.g., Levine, 1993). In any case, pyrolysis experiments of whole coal and extracted coal showed that the presence of bitumen during pyrolysis enhanced the oil yield of coals (Vu et al., 2008).

5.3 Hydrocarbon potential and type of generated hydrocarbons

The position of the Eocene coals in the diagram of HI versus Tmax (Fig. 9c) shows that these coals are highly oil-prone. Pyrolysis-GC data show that the coals will generate a low-sulphur paraffinic oil with high wax content (Fig. 8a). The source potential index (SPI=thickness*[S1+S2]*bulk density/1000) was introduced to provide an estimate on the amount of hydrocarbons which can be generated under a surface area of 1 m² (Demaison and Huizinga, 1991). Considering the average generation potential of Eocene coals (S1+S2: 274 mgHC/g rock), an average density of 1.32, and thickness of 7.6 m (net coal thickness in the TAJ mine), the SPI is estimated as 2.75 t/m².

Miocene coals are also oil-prone, but probably will generate a high wax paraffinic-naphthenic-aromatic (P-N-A) mixed oil (Figs. 8a, 9c), as they generate a remarkably broad range of naphthalenic compounds besides the usual phenolic and paraffinic compounds. Naturally, the thickness of coal seam in the Miocene Warukin Formation changes laterally. But, considering the net coal thickness in the Tutupan mine (94 m), the average generation potential (116 mgHC/g rock), and a density of 1.32, shows the theoretically enormous big SPI (~16 t/m²).

The pyrolysis products of the Oligocene Talang Akar coal in the Ardjuna Basin (Horsfield et al., 1988) are similar to those from the Miocene coal in the Barito Basin, but differ significantly from those from Eocene coals. Indeed, the field of high P-N-A mixed oil (cf., Fig. 8a) was defined originally by Horsfield (1989) based on Talang Akar coal.

5.4 Factors controlling different oil types

Stankiewicz et al. (1996) performed a detailed study on macerals concentrates from Eocene and Miocene coals from southeastern Kalimantan (Asem-Asem basin), which are comparable in rank and depositional environment to the Miocene BL1 coal and the Eocene coals investigated in the present paper. Pyrolysis-GC-MS results obtained on resinite concentrates from Miocene coals show very strong peaks of 1,6-dimethylnaphthalene, cadalene and other cadinene monomers characteristic for dammar resins (Stankiewicz et al., 1996; cf. van Aarssen et al., 1990; 1994), apart from moderate amounts of C_6-C_{32} *n*-alk-1-enes/*n*-alkanes pairs. In contrast, the pyrolyzate of resinite concentrates from Eocene coals was of a strongly aliphatic nature with a minor amount of cadelene, which is typical for non-dammar resins.

Resinite contents are high in Eocene (5.3-10.1 vol.%) and Miocene coals (3.0-19.2 vol.%) investigated in the present study for Py-GC. Thus, the diversity and high concentrations of naphtalenes in pyrolyzates from Miocene coals reflect the origin of the resins from dammar-producing diterocarapceae in Miocene coals (e.g. Fikri et al., 2022a), while the very high amount of *n*-alk-1-enes/*n*-alkanes in pyrolyzates from Eocene coals reflects the origin of the resins from the palm and fern dominated vegetation of the Eocene (e.g. Moore and Ferm, 1992; Morley, 2013; Fikri et al., 2022b; see also Table 1). This suggests that the different oil types are strongly related to the change in vegetation between the Eocene and the Miocene, while different mire types do not play a significant role.

5.5 Factors controlling the hydrocarbon potential of Eocene and Miocene coals

An in-depth investigation of the factors controlling the petroleum potential of Paleogene and Neogene coals from different Indonesian basins has been performed by Davis et al. (2007). These authors investigated 432 coal samples and found a very poor correlation between hydrogen index (HI) and liptinite content, but a better relationship between HI and petrographic indices for tissue preservation/degradation. They also observed an increase in HI with increasing rank.

Since Eocene and Miocene coals generate oil with significant chemical differences, the controls on hydrocarbon potential are discussed separately for coals with different ages. This approach also avoids difficulties related to the higher maturity of the Eocene coals.

As expected, moderate positive correlations are obtained between HI and (total) resinite percentages, both for Eocene (r^2=0.50) and Miocene coals (r^2=0.36). In case of Miocene coals, the relatively poor correlation is mainly due to seam T110 in the Tutupan mine (r^2=0.17), while the coefficients for seams T210 and T110 (r^2=0.42) and the BL1 seam (r^2=0.48) are significantly higher. In case of Eocene coals and the Miocene seams T210/300 the correlation is better for *in-situ* resinite (r^2=0.54 and 0.49, respectively) than for detrital resinite (r^2=0.21 and 0.17, respectively). No such relation is observed for the BL-1 seam, where correlation coefficients are similar for both in-situ (r^2=0.36) and detrital (r^2=0.39) resinite. This is remarkable in that the bitumen content is mainly controlled by detrital resinite.

The special role of resinite in the oil potential of coals was also noted by Snowdon (1991), who found that resinite yields oil at relatively low maturity. Horsfield et al. (1988) investigated the Oligocene Talang Akar coal in the Ardjuna Basin. These authors noted that the early formed oil from resinite may be essential for oil expulsion, as it has the capability of saturating pores and surfaces by oleophilic chemical species.

In contrast to resinite, HI is neither related to other abundant macerals of the liptinite group (e.g., rootlet-derived suberinite; leaf-derived cutinite and fluorinite), nor the sum of liptinite macerals. This shows the predominant role of resins for the hydrocarbon potential of the studied coals.

This relation is apparently also supported by a positive correlation between cadinane concentrations and HI (r^2=0.55). However, if Eocene (r^2=0.12) and Miocene (r^2=0.26) are considered separately, the correlation coefficients are much lower. Hence, the good correlation observed for the entire sample set probably simply reflects the significantly higher cadinane concentrations in Eocene coals with high HI values.

Interestingly, for Miocene coals the correlations between BI and resinite (r^2=0.55) and BI and cadinane (r^2=0.63) are better than for HI. These correlations, however, are poor for Eocene coals, reflecting either the different plant origin of resins in Eocene coals or – more likely - their higher maturity.

Davis et al. (2007) observed a relation between the degree of degradation (e.g. detrovitrinite index) and HI. Using the entire sample set from the present study, a correlation coefficient of r^2=0.40 is observed. However, no correlation is observed, if Eocene (r^2=0.01) and Miocene coals (r^2=0.10) are investigated separately. Thus, the correlation is probably an apparent correlation reflecting the higher HI of Eocene coals and the higher degree of plant degradation in the Eocene rheotrophic peats.

5.6 Oil-source correlation in the Barito Basin

Oil in the Barito Basin is produced from the Eocene Tanjung Formation and the pre-Cenozoic basement (e.g., Tanjung Field). In the Warukin and Tapian Timur fields, oil is also produced from the Miocene Warukin Formation (IPA, 1991; Doust and Noble, 2008). Moreover oil shows occur in the Berai Formation (Tanta-1) and in oil seeps (Kusuma and Darin, 1989). All oils recovered from wells and surface seeps in the Barito basin are similar in having high wax contents and high pristane/phytane ratios, proving a terrigenous origin of the oils (Kusuma and Darin, 1989; Doust and Noble, 2008; Kleibacker et al., 2015).

Despite of the similarities, differences in carbon isotope ratios allow the distinction of an isotopically heavy Tanjung oil family and an isotopically light Warukin oil family (Kusuma and Darin, 1989). The difference between $\delta^{13}C$ values from both families is about 2 ‰ (Table 6). In addition, the wax contents of Tanjung oils is significantly higher (22-25 vol.%) than that of Warukin oils (7-13 vol.%; IPA, 1991; Table 6). Thus, it is not surprising that a major paraffin problem occurs in the Tanjung field (e.g., Wibowo and Sutrisno, 2013).

Table 6. Bulk and isotope data from oil samples from the Barito Basin (IPA, 1991; Kusuma and Darin, 1989)

Borehole	Formation	Oil Gravity (API)	Pour Point (°C)	Wax (% Vol.)	Borehole	Formation	$\delta^{13}C_{aro}$ (‰)	$\delta^{13}C_{sat}$ (‰)
Warukin oil family								
Warukin Selatan-1	Warukin	28.0	4.0	7.0	Warukin Selatan-17	Warukin	-27.8	-30.3
Warukin Tengah-1	Warukin	30.3	24.0	11.2	Warukin Selatan-19	Warukin	-27.9	-30.4
Tapian Timur-1	Warukin (Zone-B)	39.0	24.0	12.8	Tapian Timur-13	Warukin	-28.0	-30.5
					Tapian Timur-14	Warukin	-28.1	-30.2
					Tanta-1	Berai		-30.6
Tanjung oil family								
Tapian Timur-1	Tanjung (Zones C-D)	38.8	30.0	22.4				
Kambitin-2	Tanjung Z-710	39.5	38.9	23.6	Kambitin-2	Tanjung	-26.2	-28.5
Tanjung-1	Upper Tanjung	40.1	40.6	22.4	Tanjung-58	Tanjung	-26.0	-28.6
Tanjung-1	Low. Tanjung & Pre-Cenoz.	39-41	42.2	24.6	Tanjung-76	Tanjung	-26.5	-28.4
Tanjung-1	Low. Tanjung & Pre-Cenoz.	40.1-41.5	39.0		Bagok-1	Tanjung		-28.3

A good fit exists between the predicted petroleum type generated from Eocene (paraffinic oil with very high wax content) and Miocene coals (P-N-A oil with moderately high wax; Fig. 8a) and the character of the high-wax Tanjung oils and the less waxy Warukin oils (Table 6). In addition,

in correspondence to the Tanjung and Warukin oils, Eocene coals have less negative $\delta^{13}C$ values (-26.3 ‰) than Miocene coals ($\delta^{13}C$: -28.0 ‰).

Consequently, the new results provide additional support to the assumption that the Tanjung field was sourced by Eocene coals, while Warukin oil was produced by Miocene coals (Kusuma and Darin, 1989).

The small amount of oil detected so far in the Warukin Formation is probably related to the fact that the Miocene coals hardly reach the oil window in the depocenter of the basin (Kusuma and Darin, 1989, Fig. 2b).

6 Conclusions

Indonesian coals are well-known for their oil potential. This study focuses on Eocene and Miocene coals from southern Kalimantan (Borneo) and was undertaken to determine the factors controlling the oil potential and to support oil to source correlations. The main results are summarized in the following:

- Miocene coals from the northern Barito Basin (Tutipan mine) and the southern Asem-Asem Bain (Jumbang Mine) are immature, while Eocene coals in the Barito Basin (TAJ-1 mine) reached the stage of early oil generation.
- Miocene and Eocene coals contain significant amounts of heavy, oxygen-rich bitumen components, which are mainly derived from resins.
- Miocene coals generate a paraffinic-napthenic-aromatic mixed oil with (moderately) high wax content, while Eocene coals generate a high wax paraffinic oil. This difference is attributed to the different resin-producing plant in the Miocene (dammar-producing dipterocarps) and the Eocene (mainly palms).
- The HI of the coals is mainly controlled by the resinite content. Other abundant liptinite macerals (e.g., cutinite, suberinite), the degree of plant degradation or the peat-type do not play any discernable role.
- Oil in the Eocene Tanjung Formation (and in the pre-Cenozoic basement) was generated from Eocene coals, while oil in the Miocene Warukin Formation was generated from Miocene coals.

- Mainly due to the very large thickness of Miocene coal seams, the oil potential of coal in the Warukin Formation is higher than that of coal in the Eocene Tanjung Formation. However, since Miocene coals have only reached the oil window in the deepest parts of the basin, only a small amount of Warukin oils has been detected so far.

Acknowledgments

The first author (FHN) thanks OeAD, Austria´s Agency for Education and Internationalization, for an Ernst Mach Grant, ASEA-UNINET scholarship (Reference number: ICM-2019-13766, MPC-2020-01500, MPC-2021-01331, MPC-2021-01480). FHN would also like to thank PT Adaro Indonesia, PT Tanjung Alam Jaya, PT Jhonlin Baratama and PT Arutmin Indonesia for their help in sampling the coal seams.

References

Amijaya, H., Littke, R., 2005. Microfacies and depositional environment of Tertiary Tanjung Enim low rank coal, South Sumatra basin, Indonesia. Int. J. Coal Geol. 61, 197–221. https://doi.org/10.1016/j.coal.2004.07.004

Bechtel, A., Sachsenhofer, R.F., Zdravkov, A., Kostova, I., Gratzer, R., 2005. Influence of floral assemblage, facies and diagenesis on petrography and organic geochemistry of the Eocene Bourgas coal and the Miocene Maritza-East lignite (Bulgaria). Org. Geochem. 36 (11), 1498–1522. https://doi.org/10.1016/j.orggeochem.2005.07.003

Bojesen-Koefoed, J.A., Christiansen, F.G., Petersen, H.I., Piasecki, S., Stemmerik, L. & Nytoft, H.P., 1996. Resinite-rich coals of northeast Greenland - a hitherto unrecognized, highly oil-prone Jurassic source rock. Bull. Can. Pet. Geol. 44, 458–473. https://doi.org/10.35767/gscpgbull.44.3.458

Bray, E.E., Evans, E.D. 1961. Distribution of n-paraffins as a clue to recognition of source beds. Geochimica et Cosmochimica Acta, 22/1, 2-5. https://doi.org/10.1016/0016-7037(61)90069-2

Bustin, R.M., 1988. Sedimentology and characteristics of dispersed organic matter in Tertiary Niger Delta: Origin of source rocks in a deltaic environment. AAPG (Am. Assoc. Pet. Geol.) Bull., 72, 277–298. https://doi.org/10.1306/703C8C18-1707-11D7-8645000102C1865D

Calder, J., Gibling, M., Mukhopadhyay, P.K., 1991. Peat formation in a Westphalian B piedmont setting, Cumberland Basin, Nova Scotia: implications for the maceral-based interpretation of rheotrophic and raised paleomires. Bulletin Societe Geologique de France, 162/2, 283-298.

Clayton, J.L., Rice, D.D., Michael, G.E., 1991. Oil-generating coals of the San Juan Basin, New Mexico and Colorado, U.S.A. Org. Geochem. 17 (6), 735–742. https://doi.org/10.1016/0146-6380(91)90017-E

Daly, M.C., Cooper, M.A., Wilson, I., Smith, D.G., Hooper, B.G.D., 1991. Cenozoic plate tectonics and basin evolution in Indonesia. Mar. Pet. Geol. 81, 2–21. https://doi.org/10.1016/0264-8172(91)90041-X

Davis, R.C., Noon, S. W., Harrington, J., 2007. The petroleum potential of Tertiary coals from Western Indonesia: Relationship to mire type and sequence stratigraphic setting. Int. J. Coal Geol. 70, 35–52. https://doi.org/10.1016/j.coal.2006.02.008

Demaison, G., Huizinga, B.J., 1991. Genetic classification of petroleum systems. AAPG (Am. Assoc. Pet. Geol.) Bull. 75, 1626–1643. https://doi.org/10.1306/0C9B29BB-1710-11D7-8645000102C1865D

Demchuk, T., Moore, T.A., 1993. Palynofloral and organic characteristics of a Miocene bog-forest, Kalimantan, Indonesia. Organic Geochemistry, 20/2, 119–134. https://doi.org/10.1016/0146-6380(93)90032-7

Didyk, B.M., Simoneit, B.R.T., Brassell, S.T. and Eglinton, G., 1978. Organic geochemical indicators of palaeoenvironmental conditions of sedimentation. Nature, 272, 216-222. https://doi.org/10.1038/272216a0

Doust, H., Noble, R.A., 2008. Petroleum systems of Indonesia. Mar. Pet. Geol. 25, 103–109. https://doi.org/10.1016/j.marpetgeo.2007.05.007

Durand, B., Oudin, J.L., 1979. Exemple de migration des hydrocarbures dans une serie deltaique: le delta de la Mahakam, Kalimantan, Indonésie. Proceedings of the 10th World Petroleum Conference, 2, 3–11.

Durand, B., Paratte, M., 1983. Oil potential of coals: a geochemical approach. In: Brooks, J. (ed.): Petroleum geochemistry and exploration of Europe. Geol. Soc. Spec. Publ. 12, 255–264. https://doi.org/10.1144/GSL.SP.1983.012.01.26

Eglinton, T. I., Damsté, J. S. S., Kohnen, M. E., de Leeuw, J. W., 1990. Rapid estimation of the organic sulphur content of kerogens, coals and asphaltenes by pyrolysis-gas chromatography. Fuel 69, 1394–1404. https://doi.org/10.1016/0016-2361(90)90121-6

Espitalie, J., Madec, M., Tissot, B., Mennig, J.J., Leplat, P., 1977. Source Rock Characterization Method for Petroleum Exploration. Offshore Technology Conference. https://doi.org/10.4043/2935-MS

Ficken, K.J., Li, B., Swain, D., Eglinton, G., 2000. An n-alkane proxy for the sedimentary input of submerged/floating freshwater aquatic macrophytes. Organic Geochemistry, 31/7-8, 745-749. https://doi.org/10.1016/S0146-6380(00)00081-4

Fikri, H.N., Sachsenhofer, R.F., Bechtel, A., Gross, D., 2022a. Organic geochemistry and petrography in Miocene coals in the Barito Basin (Tutupan Mine, Indonesia): Evidence for astronomic forcing in kerapah type peats. Int. J. Coal Geol. 256, 103997. https://doi.org/10.1016/j.coal.2022.103997

Fikri, H.N., Sachsenhofer, R.F., Bechtel, A., Gross, D., 2022b. Coal deposition in the Barito Basin (Southeast Borneo): The Eocene Tanjung Formation compared to the Miocene Warukin Formation. Int. J. Coal Geol. 263, 104117. https://doi.org/10.1016/j.coal.2022.104117

Fikri, H.N., Sachsenhofer, R.F., Bechtel, A., Gross, D., submitted. Organic geochemistry and petrography of Miocene ombrotrophic coals in the tropical Asem-Asem Basin (Borneo, Indonesia): Comparison to coeval subtropical coals in the Eastern Alps. Austrian Journal Earth Sciences.

Friederich, M.C., Moore, T.A., Flores, R.M., 2016. A regional review and new insights into SE Asian Cenozoic coal-bearing sediments: why does Indonesia have such extensive coal deposits? Int. J. Coal Geol. 166, 2–35. https://doi.org/10.1016/j.coal.2016.06.013

García-González, M., Surdam, R. C., Lee, M. L., 1997. Generation and expulsion of petroleum and gas from Almond Formation coal, greater Green River basin, Wyoming. AAPG (Am. Assoc. Pet. Geol.) Bull. 81(1), 62–81.

Gordon, T.L., 1985. Talang Akar coals - Ardjuna Subbasin oil source. 14th Annu. Conv. Proc.: Indonesian Petroleum Association, 91–120.

Hall, R., Morley, C.K., 2004. Sundaland basins. In: Clift, P.,Wang, P., Kuhnt,W., Hayes, D.E. (Eds.), Continent-Ocean Interactions Within the East Asian Marginal Seas. vol. 149, Geophysical Monograph, American Geophysical Union, Geophysical Monograph, Washington, D.C., pp. 55–85. https://doi.org/10.1029/149GM04

Hendrix, M.S., Brassell, S.C., Carroll, A.R., Graham, A.A., 1995. Sedimentology, Organic Geochemistry, and Petroleum Potential of Jurassic Coal Measures: Tarim, Junggar, and Turpan Basins, Northwest China. AAPG (Am. Assoc. Pet. Geol.) Bull. 79, 929–959. https://doi.org/10.1306/8D2B2187-171E-11D7-8645000102C1865D

Horsfield, B., 1984. Pyrolysis studies and petroleum exploration. Advances in Petroleum Geochemistry 1, 247–298.

Horsfield, B., 1989. Practical criteria for classifying kerogens: some observations from pyrolysis-gas chromatography. Geochim. Cosmochim. Acta 53, 891–901. https://doi.org/10.1016/0016-7037(89)90033-1

Horsfield, B., 1990. Evaluating kerogen type according to source quality, compositional heterogeneity and thermal lability. Rev. Palaeobot. Palynol. 65, 357–365. https://doi.org/10.1016/0034-6667(90)90086-X

Horsfield, B., 1997. The bulk composition of first-formed petroleum in source rocks. In: Welte, D.H., Baker, D.R., Horsfield, B. (Eds.), Petroleum and Basin Evolution, pp. 337–402.

Horsfield, B., Yordy, K.L., Crelling, J.C., 1988. Determining the petroleum generating potential of coal using organic geochemistry and organic petrology. In: Matavelli, L., Novelli, L. (Eds.), Advances in Organic Geochemistry 1997. Pergamon Press, Oxford, pp. 121–131. https://doi.org/10.1016/B978-0-08-037236-5.50018-X

Huang, D., Zhang, D., Li, J. & Huang, X., 1991. Hydrocarbon genesis of Jurassic coal measures in the Turpan Basin, China. Org. Geochem. 17 (6), 827–837. https://doi.org/10.1016/0146-6380(91)90023-D

Hunt, J.M., 1991. Generation of gas and oil from coal and other terrestrial organic matter. Org. Geochem. 17 (6), 673–680. https://doi.org/10.1016/0146-6380(91)90011-8

IPA (Indonesian Petroleum Association), 1991. Indonesia, Oil and Gas Field Atlas, vol. 5: Kalimantan.

Isaksen, G.H., Curry, D.J., Yeakel, J.D., Jenssen, A.I., 1998. Controls on the oil and gas potential of coals. Org. Geochem. 29 (1–3), 23–44. https://doi.org/10.1016/S0146-6380(98)00042-4

Issler, D.R. & Snowdon, L.R., 1990. Hydrocarbon generation kinetics and thermal modelling, Beaufort-Mackenzie Basin. Bull. Can. Pet. Geol 38, 1–16. https://doi.org/10.35767/gscpgbull.38.1.001

Johnston, J. H., Collier, R. J., Maidment, A. I., 1991. Coals as source rocks for hydrocarbon generation in the Taranaki Basin, New Zealand: a geochemical biomarker study. J. Southeast Asian Earth Sci. 5, 283–289. https://doi.org/10.1016/0743-9547(91)90038-Y

Killops, S.D., Woolhouse, A.D., Weston, R.J., Cook, A.R., 1994. A geochemical appraisal of oil generation in the Taranaki basin, New Zealand. AAPG (Am. Assoc. Pet. Geol.) Bull. 78, 1560–1585. https://doi.org/10.1306/A25FF21F-171B-11D7-8645000102C1865D

Killops, S.D., Funnell, R.H., Suggate, R.P., Sykes, R., Peters, K.E., Walter, C., Woolhouse, A.D., Weston, R.J., Boudou, J.P., 1998. Predicting generation and expulsion of paraffinic oil from vitrinite-rich coals. Org. Geochem. 29 (1–3), 1–21. https://doi.org/10.1016/S0146-6380(98)00087-4

Khorasani, G.K. 1987. Oil-prone coals of the Walloon Coal Measures, Surat Basin, Australia. In: Scott, A.C. (ed.): Coal and coal-bearing strata: recent advances. Geol. Soc. Spec. Publ 32, 303–310. https://doi.org/10.1144/GSL.SP.1987.032.01.1

Kleibacker, D., Tasrianto, R., Saripudin, A., 2015. Long Distance Migration in Central Kalimantan: A Solution to the Barito Dilemma? 39th Annu. Conv. Proc.: Indonesian Petroleum Association IPA15-G-085

Kusuma, I., Darin, T., 1989. The hydrocarbon potential of the Lower Tanjung Formation, Barito Basin, SE Kalimantan. 18th Annual Conv. Proc.: Indonesian Petroleum Association IPA 89-11.09

Larter, S.R., 1984. Application of analytical pyrolysis techniques to kerogen characterization and fossil fuel exploration/ exploitation. In: Voorheers, K.T. (Ed.), Analytical Pyrolysis Techniques and Applications, pp. 212–275.

Levine, J.R., 1993. Coalification: the evolution of coal as source rock and reservoir rock for oil and gas. In: Law, B.E., Dudley, D.R. (Eds.), Hydrocarbons from Coal. AAPG Studies in Geology, vol. 38, pp. 39–77. https://doi.org/10.1306/St38577C3

Lutz, M., Kaaschieter, J.P.H., Van Wijke, D.H., 1975. Geological factors controlling Rotliegend gas accumulations in the Mid-European Basin. Proc. 9th World Pet. Congr. Toyko. Applied Science Publication, London, 22, pp. 93–103.

Misch, D., Riedl, F., Liu, B., Horsfield, B., Ziegs, V., Mendez-Martin, F., Vranjes-Wessely, S., Sachsenhofer, R.F., 2019. Petrographic and sorption-based characterization of bituminous organic matter in the Mandal Formation, Central Graben (Norway). Int. J. Coal Geol. 211, 103229. https://doi.org/10.1016/j.coal.2019.103229

Moore, T.A., Ferm, J.C., 1992. Composition and grain size of an eocene coal bed in southeastern Kalimantan, Indonesia. Int. J. Coal Geol. 21, 1–30. https://doi.org/10.1016/0166-5162(92)90033-S

Morley, R.J., 2012. A review of the Cenozoic climate history of Southeast Asia. In: D.J. Gower et al. (eds.) Biotic Evolution and Environmental Change in Southeast Asia. Cambridge University Press, 2012, 79-114. https://doi.org/10.1017/CBO9780511735882.006

Morley, R.J., 2013. Cenozoic ecological history of South East Asian peat mires based on the comparison of coals with present day and Late Quaternary peats. J. Limnol. 72, 36–59 . https://doi.org/10.4081/jlimnol.2013.s2.e3

Murchison, D.G., 1987. Recent advances in organic petrology and organic geochemistry: an overview with some reference to “oil from coal”. In: Scott, A.C. (ed.): Coal and coal-bearing strata: recent advances. Geol. Soc. Spec. Publ 32, 257–302. https://doi.org/10.1144/GSL.SP.1987.032.01.15

Newman, J., Price, L.C., Johnston, J.H., 1997. Hydrocarbon source potential and maturation in Eocene New Zealand vitrinite-rich coals: insights from traditional coal analysis, and Rock-Eval and biomarker studies. J. Pet. Geol 20, 137–163. https://doi.org/10.1111/j.1747-5457.1997.tb00770.x

Noble, R. A., Wu, C. H., Atkinson, C. D., 1991. Petroleum generation and migration from Talang Akar coals and shales offshore NW Java, Indonesia. Org. Geochem. 17 (3), 363–374. https://doi.org/10.1016/0146-6380(91)90100-X

Noble, R.A., Pratomo, K.H., Nugrahanto, K., Ibrahim, A.M.T., Praseetya, I., Mujahidin, N., Wu, C.H., Howes, J.V.C., 1997. Petroleum systems of Northwest Java, Indonesia. In: Howes, J.V.C., Noble, R.A. (Eds.), Proceedings of International Conference on Petroleum Systems of SE Asia and Australasia. Indonesian Petroleum Association, pp. 585–600.

Peters, K.E., Rohrback, B.G., Kaplan, I.R., 1981. Geochemistry of Artificially Heated Humic and Sapropelic Sediments—I: Protokerogen. AAPG (Am. Assoc. Pet. Geol.) Bull. 65, 688-705. https://doi.org/10.1306/2F9199AE-16CE-11D7-8645000102C1865D

Petersen, H.I., Andsbjerg, J., Bojesen-Koefoed, J.A., Nytoft, H.P., Rosenberg, P., 1998. Petroleum potential and depositional environments of Middle Jurassic coals and non-marine deposits, Danish Central Graben, with special reference to the Søgne Basin. Geol. Surv. Den 36, 1–80. https://doi.org/10.34194/dgub.v36.5022

Pubellier, M., Morley, C.K., 2014. The basins of Sundaland (SE Asia): Evolution and boundary conditions. Mar. Pet. Geol. 58/Part B, 555–578. https://doi.org/10.1016/j.marpetgeo.2013.11.019

Radke, M., Schaefer, R.G., Leythaeuser, D., Teichmüller, M., 1980. Composition of soluble organic matter in coals: relation to rank and liptinite fluorescence. Geochim. Cosmochim. Acta 44, 1787–1800. https://doi.org/10.1016/0016-7037(80)90228-8

Satyana, A.H., Nugroho, D., Surantoko, I., 1999. Tectonic controls on the hydrocarbon habitats of the Barito, Kutei, and Tarakan Basins, Eastern Kalimantan, Indonesia: major dissimilarities in adjoining basins. J. Asian Earth Sci. 17/1-2, 99–122. https://doi.org/10.1016/S0743-9547(98)00059-2

Schenk, H. J., Di Primio, R., Horsfield, B., 1997. The conversion of oil into gas in petroleum reservoirs. Part 1: Comparative kinetic investigation of gas generation from crude oils of lacustrine, marine and fluviodeltaic origin by programmed-temperature closed-system pyrolysis. Org. Geochem. 26 (7–8), 467–481. https://doi.org/10.1016/S0146-6380(97)00024-7

Shibaoka, M., Saxby, J. D., Taylor, G. H., 1978. Hydrocarbon generation in Gippsland basin, Australia—comparison with Cooper basin, Australia. AAPG (Am. Assoc. Pet. Geol.) Bull. 62, 1151–1158. https://doi.org/10.1306/C1EA4FC7-16C9-11D7-8645000102C1865D

Shanmugam, G., 1985. Significance of coniferous rain forests and related organic matter in generating commercial quantities of oil, Gippsland Basin, Australia1. AAPG (Am. Assoc. Pet. Geol.) Bull. 69, 1241–1254. https://doi.org/10.1306/AD462BC3-16F7-11D7-8645000102C1865D

Snowdon, L.R., 1980. Resinite — a potential source in the Upper Cretaceous/Tertiary of the Beaufort-Mackenzie Basin. In: Miall, A.D. (ed.): Facts and principles of world oil occurrence. Canadian Society of Petroleum Geologists Memoir 6, 421–446.

Snowdon, L.R., 1991. Oil from Type III organic matter: resinite revisited. Org. Geochem. 17 (6), 743–747. https://doi.org/10.1016/0146-6380(91)90018-F

Snowdon, L.R., Powell, T.G., 1982. Immature oil and condensate - modification of hydrocarbon generation model for terrestrial organic matter. AAPG (Am. Assoc. Pet. Geol.) Bull. 66, 775–788. https://doi.org/10.1306/03B5A313-16D1-11D7-8645000102C1865D

Stankiewicz, B.A., Kruge, M.A., Mastalerz, M., 1996. A geochemical study of macerals from a Miocene lignite and an Eocene bituminous coal, Indonesia. Org. Geochem. 24 (5), 531–545. https://doi.org/10.1016/0146-6380(96)00038-1

Sykes, R., Snowdon, L.R., 2002. Guidelines for assessing the petroleum potential of coaly source rocks using Rock-Eval pyrolysis. Org. Geochem. 33 (12), 1441–1455. https://doi.org/10.1016/S0146-6380(02)00183-3

Thomas, B. M., 1982. Land-plant source rocks for oil and their significance in Australian basins. The APPEA Journal 22, 164–178. https://doi.org/10.1071/AJ81012

van Aarssen, B.G.K., Cox, H., Hoogendoorn, N.P., de Leeuw, J.W., 1990. A cadinene biopolymer in fossil and extant dammar resins as a source for cadinanes and bicadinanes in crude oils from South East Asia. Geochim. Cosmochim. Acta 54, 3021–3031. https://doi.org/10.1016/0016-7037(90)90119-6

van Aarssen, B.G.K. de Leeuw, J.W., Collinson, M., Boon, J.J., Goth, K., 1994. Occurrence of polycadinene in fossil and recent resins. Geochimica et Cosmochimica Acta, 58/1, 223-229. https://doi.org/10.1016/0016-7037(94)90459-6

Vu, T.T.A., Horsfield, B., Sykes, R., 2008. Influence of in situ bitumen on the generation of gas and oil in New Zealand coals. Org. Geochem. 39 (11), 1606–1619. https://doi.org/10.1016/j.orggeochem.2008.07.005

Vu, T.T.A., Zink, K.G., Mangelsdorf, K., Sykes, R., Wilkes, H., Horsfield, B., 2009. Changes in bulk properties and molecular compositions within New Zealand Coal Band solvent extracts from early diagenetic to catagenetic maturity levels. Org. Geochem. 40 (9), 963–977. https://doi.org/10.1016/j.orggeochem.2009.06.002

Vu, T.T.A., Horsfield, B., Mahlstedt, N., Schenk, H.J., Kelemen, S.R., Walters, C.C., Kwiatek, P.J., Sykes, R., 2013. The structural evolution of organic matter during maturation of coals and its impact on petroleum potential and feedstock for the deep biosphere. Org. Geochem. 62, 17–27. http://dx.doi.org/10.1016/j.orggeochem.2013.06.011

Wibowo, R., Sutrisno, A.A., 2013. Soaking and formation squeeze method for paraffin control application to increase oil production at Tanjung oilfield. Forum Sharing Teknologi Hulu ke-2. Batam, 22-25. April. 2013.

Wilkins, R.W.T., George, S.C., 2002. Coal as a source rock for oil: a review. Int. J. Coal Geol. 50, 317–361. https://doi.org/10.1016/S0166-5162(02)00134-9

Witts, D., Davies, L., Morley, R., 2014. Uplift of the Meratus Complex: Sedimentology, biostratigraphy, provenance and structure. 38th Annu. Conv. Proc.: Indonesian Petroleum Association IPA14-G-082

Witts, D., Hall, R., Nichols, G., Morley, R., 2012. A new depositional and provenance model for the Tanjung Formation, Barito Basin, SE Kalimantan, Indonesia. J. Asian Earth Sci. 56, 77-104. https://doi.org/10.1016/j.jseaes.2012.04.022

Zahirovic, S., Seton, M. and Müller, R.D., 2014. The Cretaceous and Cenozoic tectonic evolution of Southeast Asia. Solid Earth 5, 227-273. https://doi.org/10.5194/se-5-227-2014

Ziegs, V., Horsfield, B., Skeie, J.E., Rinna, J., 2017. Petroleum retention in the Mandal Formation, Central Graben, Norway. Mar. Pet. Geol. 83, 195–214. https://doi.org/10.1016/j.marpetgeo.2017.03.005

Appendix list

1. *n*-Alkanes and aliphatic compound list of Tutupan coal
2. Aromatic compound list of Tutupan coal
3. Probabilistic approach of cyclicity Tutupan coal seam
4. *n*-Alkanes and aliphatic compound list of TAJ Pit-1D coal
5. Aromatic compound list of TAJ Pit-1D coal
6. *n*-Alkanes and aliphatic compound list of Jumbang coal
7. Aromatic compound list of Jumbang coal
8. Pyrolysis-GC results of five coal samples

1. *n*-Alkanes and aliphatic compound list of Tutupan coal

A. *n*-Alkanes

Name	RT
Farnesane	28.86
n-C14	30.13
i-C16	32.81
n-C15	34.23
n-C16	38.12
Norpristane	40.1
n-C17	41.83
Pristane	42.22
n-C18	45.37
Phytane	45.85
n-C19	48.73
n-C20	51.94
n-C21	55.02
n-C22	57.96
n-C23	60.77
n-C24	63.49
n-C25	66.1
n-C26	68.61
ISTD	70.19
n-C27	71.04
n-C28	73.42
n-C29	75.75
n-C30	77.21
n-C31	78.78
n-C32	80.08
n-C33	83.01
n-C34	86.08
n-C35	88.83
n-C36	92.01

B. Aliphatic Compound

Name	RT
Drimene	31.35
Drimane? + additional compound?	31.47
Drimane	31.70
Drimane	31.75
Eudesmane	33.17
Cadinene	33.44
Cadinane	33.85
Cadinane	33.93
Drimane	34.72
Homodrimane	35.05
Cadinane	35.22 or 35.19
Longipolene	35.40
Cadinene	36.41
Cadinene	36.59
Homodrimane	37.33
Sanderacopimarane?	48.70
Pimarane	49.32
b-phyllocladane?	50.94
des-A-Lupane	58.76
des-E-hopane	60.74
17a Trisnorhopane ('TM)	68.04
C27 b-Hop	68.71 or 68.65
Neohop-13(18)-ene	70.33 or 70.27
Olean-13(18)-ene	70.44 or 70.38
Olean-12-ene	70.54
Olean-18-ene	70.85 or 70.77
Urs-12-ene	71.24 or 71.22
C30 ab-Hop	71.79
C29 bb-hop	72.18 or 72.14
C30 ba-Hop	72.55
C31 ab-Hop(S)	73.71
C31 ab-hop(R)	74.11 or 74.02
C30 bbHop	74.89 or 74.78
C32 ab-Hop(S)	75.47
C32 ab-Hop('R)	75.90
C31 bb-Hop	77.76
C33 ab-Hop(S)	77.90
C33 ab-Hop(´R)	78.42
ISTD	60.67

2. Aromatic compound list of Tutupan coal

Name	RT
Dimethylnaphthalene	32-34
Dimethyl Naphthalenes (DMN)	33.14
Dihydrocurcumene	33.73
Acenaphthylene?	34.05
b-Cadinene	35.33
Cis-Calamene? Or Trans-Calamene?	35.47
Tetramethyl-tetrahydronaphtyl	36.20
Calamenene or Cis-Calamene?	36.33
6-(1-Ethylpropyl)-1,2,3,4-tetrahydronaphthalene	37.13
Tetrahydronaphthalene	37.80
Cadinatriene?	37.90
1-(1,1-Dimethylethyl naphthalene)	38.18
Curcumene/Dimethylethylnaphthalene	38.21
Tetramethylnaphla	39.6 - 42.6
Cadalene	40.81
Tetra-MN	42.40
Phenanthrene	43.76
Alkyl-benzene	46.06
Hexahydroretene	46.30
MP	46.75-47.53
Norabiete-triene	47.85
19-Norabieta-tetraene	48.56
18-Norabieta-tetraene	48.91
Dimethylphenanthrene	50.11
Dimethylphenanthrene	50.26
Dimethylphenanthrene	50.50
Dehydroabietane	50.68
Fluoranthene	50.88
Pyrene/Methylbenzene	52.16
Simonellite	52.42
diaromatic-totarane	53.27
Retene	53.66

Name	RT
Retene	54.36
Methylpenanthrene	54.63
Corannulene? Dicyclopento-(cd, mn)-pyrene?	55.08
?	56.20
?	56.39
des-A-arbora-triene or des-A-aboratriene?	58.16
Tetramethyl-octahydro-chrysene	59.27
des-E-D:C-frido-25-norhopa-5,7,9-triene?	59.55
Trimethyl-tetrahydro-chrysenes (?)	63.18
Monoaromatic 8,14 seco-oleanane	
Monoarom. Hopanoid (?)	64.34
Diaromatic 8,14 seco-oleanane	64.85
? Dinorlup a triene	66.82
?	67.54
Norarbora(ferna)-triene	67.75
Norarbora(ferna)-triene	67.93
Monoaromatic 8,14 fernane derivate (?)	68.40
dinorursa-1,3,5(10),7,9-tetraene	70.00
?	70.33
Dinoroleana-tetraene (?) ?? Maybe Norlanosta(eupha)hexaene	70.98
Dinorabora(ferna)tetraene or Tetranor-lupa-heptaene?	71.38
Tetramethyl-octahydropicene	72.78
Tetramethyl-octahydropicene	73.05
Tetramethyl-octahydropicene	73.27
Lanosta(eupha)hexaene	74.00
Lanosta(eupha)hexaene?	74.30
Dinorarbora(ferna)-pentaene	75.08
?	76.7-77.36
Benzohopane C32	81.20
Benzohopane C33	83.72
Benzohopane C34	85.97
ISTD	57.35

3. Probabilistic approach of cyclicity Tutupan coal seam

Probabilistic range of ages (x 1000) for peat accumulation (500,000 scenario runs/iterations)

Interval	Coal thickness (m)			Decompaction ratio			Accumulation rate (mm/yr)		
	Low	Best	High	Low	Best	High	Low	Best	High
Seam T110	46	46	46	3.3	3.5	11	0.5	1.3	4.5
Seam T210	24	24	24						
Seam T110_per_cycles	6	7	13						
Seam T210_per_cycles	6	7	8						
Seam T110	46	46	46	3.3	3.5	11	0.2	1.3	4.5
Seam T210	24	24	24						
Seam T110_per_cycles	6	7	13						
Seam T210_per_cycles	6	7	8						
Seam T110	46	46	46	3.3	3.5	11	0.2	1.3	6.25
Seam T210	24	24	24						
Seam Cycles	6	8.5	13						

Interval	Result					Deterministic Result
	P10	P50	P90	Max	Min	
Seam T110	73.5	132.2	259.9	841	35.5	115-125
Seam T210	38.3	69.0	135.6	439	19.4	60-65
Seam T110_per_cycles	13.5	24.8	49.4	192	5.9	15-35
Seam T210_per_cycles	11.1	20.1	39.7	146	5.1	15-35
Seam T110	72.5	136.2	319.3	1966	35.8	115-125
Seam T210	37.8	71.1	167.0	973	18.4	60-65
Seam T110_per_cycles	13.3	25.5	60.5	364	5.7	15-35
Seam T210_per_cycles	10.9	20.7	48.8	327	5.2	15-35
Seam T110	58.4	119.2	316.5	####	23.9	115-125
Seam T210	30.5	62.2	164.9	995	13.8	60-65
Seam Cycles	10.8	22.7	61.1	421	3.8	15-35

4. *n*-Alkanes and aliphatic compound list of TAJ Pit-1D coal

A. *n*-Alkanes

Name	RT
Farnesane	27.69
n-C14	29.53
i-C16	31.21
n-C15	32.62
n-C16	36.50
Norpristane	38.43
n-C17	40.18
Pristane	40.59
n-C18	43.70
Phytane	44.19
n-C19	47.04
n-C20	50.23
n-C21	53.29
n-C22	56.23
n-C23	59.04
n-C24	61.73
n-C25	64.35
n-C26	66.83
n-C27	69.24
n-C28	71.56
n-C29	73.89
n-C30	76.03
n-C31	78.18
n-C32	80.17
n-C33	82.11
n-C34	84.18
n-C35	86.55
n-C36	88.26
ISTD	68.39

B. Aliphatic Compound

Name	RT
Drimene	31.50
Drimene	32.36
Drimane	32.53
Longifolane	33.46
Eudesmane	34.11
Isopatchoulane	34.50
Cadinane	34.79
Cadinane	34.92
Homocadinane	36.09
Homodrimane	38.45
Pimarane	50.33
a-phyllocladane	51.46
des-E-hopane	61.56
ISTD	69.48
17a-Trisnorhopane(TM)	68.98
C27-b-Hopane	69.62
C29-Neohop-13(18)ene	71.10
C29-ab-Norhopane	71.20
?	71.35
?	71.58
Olean(18)-ene	72.06
C29-ba-Normoretane	72.16
C30-ab-Hopane	72.79
C30-ba-Moretane	73.65
C31-ab-Hop(S)	74.89
C31-ab-Hop(R)	75.15
C30-bb-Hop_or_Methylhopane?	76.04
C32-ab-Hop(S)	76.75
C32-ab-Hop(R)	77.16
C32-ba-Hop?	78.24
C32-ab-Hop(S)	64.34
C32-ab-Hop(R)	64.83
C33-ab-Hop(S)	67.26
C33-ab-Hop(R)	68.00
C34-ab-Hop(R)	69.82

5. Aromatic compound list of TAJ Pit-1D coal

Name	RT
a-cedrene	34.64
Cadinatriene	34.74
Curcumene	34.74
?	36.08
Tetramethyl-(1,1,5,6)-tetrahydronaphthalene??	37.00
Tetramethyl-tetrahydro-naphthalene Calamenene	37.15
? Dibenzofuran	37.20
Trimethylnaphthalenes	37.53
Trimethylnaphthalenes	37.97
Trimethylnaphthalenes	38.11
Trimethylnaphthalenes	38.43
Trimethylnaphthalenes	38.59
Eudalene	39.08
Trimethylnaphthalenes	39.25
Tetramethylnaphthalenes	40.11
Tetrahydrocadalene	40.40
Tetramethylnaphthalenes	40.76
Cadalene	41.65
Tetramethylnaphthalenes	42.02
Tetramethylnaphthalenes	42.13
Tetramethylnaphthalenes	42.62
Tetramethylnaphthalenes	43.39
Tetramethylnaphthalenes	43.63
Methyl-cadalene	44.89
Phenanthrene	45.00
1,4-dimethyl-7-(1-methylethyl)-Azulene	47.17
3-Methylphenanthrenes	47.81
9-Methylphenanthrenes	48.21
1-Methylphenanthrenes	48.42
Norabieta-triene (have 2nd compound) is Methyl-cadalene	48.70
2-Methylphenanthrene	49.99
Dimethylphenanthrenes	50.69
Dimethylphenanthrenes	50.79
Tetrahydro-selene	51.07
Dimethylphenanthrenes	51.26
Dimethylphenanthrenes	51.36
Dimethylphenanthrenes	51.42
Dimethylphenanthrenes	51.61
Fluoranthene	51.94

Name	RT
Dimethylphenanthrenes	52.04
Dimethylphenanthrenes	52.39
Pyrene+Benzo(b)naphthofuran	53.24
Trimethylphenanthrenes	55.65
ISTD	58.18
des-A-seco-noroleana-tetraene	58.89
?	59.71
?	60.03
des-E-D,C-frida-25-norhop-5,7,9-triene	60.39
Benzo(a)anthracene+?	60.57
?	61.31
?	61.36
5-methyl-chrysene	63.51
5-methyl-chrysene	63.71
Trimethyl-(3,3,7)-Tetrahydrochrysene	63.79
Monoaromatic hopanoid	64.90
?	68.59
?	68.88
?	69.44
Dinor(24,25)arbora(ferna)-5,7,9-triene	70.83
diarom.secobicadinane	71.18
? Norlanosta(eupha)hexaene	71.81
diarom.secobicadinane	71.93
Dinorarbora(ferna)tetraene	72.16
? 4,8-diethyl-1,5-dimethyl-dicyclopenta(a,d)benzene	72.25
?	72.41
Tetramethyl-octahydropicene	73.32
Tetramethyl-octahydropicene	73.72
Tetramethyl-octahydropicene	74.01
Dinorarbora(ferna)pentaene	75.27
lanosta(eupha)hexaene	76.10
Dinorarbora(ferna)pentaene	76.19
Nor(25)arbora(ferna)pentaene or Dinoroleanapentaene	76.96
? Trimethyl-(2,2,9)-tetrahydropicene	78.55
BenzohopanesC32	82.73
BenzohopanesC33	85.32
BenzohopanesC34	87.72
BenzohopanesC35	90.82

6. *n*-Alkanes and aliphatic compound list of Jumbang coal

A. *n*-Alkanes

Name	RT
farnesane	26.94
nC14	28.32
iC16	30.98
nC15	32.47
nC16	36.25
Norpristane	38.20
nC17	39.93
Pristane	40.30
nC18	43.43
Phytane	43.91
nC19	46.77
nC20	49.97
nC21	53.02
nC22	55.95
nC23	58.76
nC24	61.45
nC25	64.04
nC26	66.54
nC27	68.95
nC28	71.28
nC29	73.46
nC30	75.68
nC31	77.78
nC32	79.82
nC33	81.80
nC34	83.77
nC35	86.14
nC36	88.82
ISTD	68.11

B. Aliphatic Compound

Name	RT
Longifolene	29.88
Cadinane	30.03
Longifolane	30.36
Eudesmane	30.87
Longifolane	30.96
Elemane	31.32
Muurolane	32.69
Drimane	32.82
Drimane	32.95
Longifolane	33.14
Drimane	33.46
Longifolane	33.61
Longifolane	34.08
Cadinane	34.73
Pimarane	35.40
Pimarane	35.72
Drimane	38.75
Drimane	38.97
C20-diterpane	48.78
Pimarane	48.80
Cadinane	53.12
Cadinene	55.70
phyllocladane	56.04
phyllocladane	56.42
phyllocladane	56.74
des-E-hop	57.36
C27b-hop	59.38
Oleanene?	62.87
Olean-12(18)-ene?	69.40
Neohopane	69.70
urs-12-ene	69.83
Olea-13(18)-ene	69.93
?	70.38
Urs-12-ene	70.60
C32hop1	71.08
C32Hop2	71.92
C32Hop3	73.17
C32Hop4	73.38
C32Hop5	77.03
ISTD	60.20

7. Aromatic compound list of Jumbang coal

Name	RT
CIS-calamene	35.03
Calamene	35.86
xx-tetrahydro-naphthalene	36.65
tetrahydrocadalene	37.42
Curcumene	37.75
1-(1,1-Dimethylethyl-naphthalene)	38.76
Alkyl-benzene	39.20
Calamanene	39.83
Cadalene	40.36
Cadalene2	40.60
Isopropyl-dimethyl-azulene	42.43
Diisopropyl-naphthalene	42.57
Cadinatriene	43.45
Hexahydroretene	45.90
Norabiete-triene2	47.35
19-Norabiete-tetraene	48.09
?	48.32
18-Norabiete-tetraene	48.45
DMP	50.21
Alkyl-benzene3	53.21
?	54.89
des-A-arbora-triene	57.63
Tetramethyl-octahydro-chrysene	58.77
Tetramethyl-octahydro-chrysene	59.08
Monoaromatic8,14,seco-oleanane	62.64
Monoaromatic-hopanoids	63.80
?	65.19
?	65.35
?Dinorlupatriene	66.31
?Dinor-oleana(ursa)-triene	67.03
Norabora(ferna)-triene	67.18
Norabora(ferna)-treine2	67.39
Arbora(ferna)triene+??	67.86
Dinorursa-1,3,4,(10),7,9-tetraene	69.46
Dinoroleana-tetraene?	69.68
Dinoroleana-tetraene?	70.38
Dinorarbora(ferna)tetraene	70.78
Tetramethyl-octahydropicene	72.10
Tetramethyl-octahydropicene2	72.34
Tetramethyl-octahydropicene3	72.56
Dinoarbora(ferna)-pentaene	74.29
Benzohopanes	76.10
ISTD	56.83

8. Pyrolysis-GC results of five coal samples

Sample	T300-09	T300-22	T210-04	C-3	D-1
			µg/g sample		
C1	9030	11799	12542	18324	19399
C2-C5 Total	11799	15506	19156	30241	26211
C6-14 Total	23128	28947	37211	65758	61561
C15+ Total	32957	44636	92002	146819	121731
C1-5 Total	20829	27305	31697	48565	45610
C1-30+ Total	76914	100888	160910	261141	228902
GOR* Total	0,37	0,37	0,25	0,23	0,25
C6-C14 Resolved	16364	22545	28813	49430	47208
C15+ Resolved	14652	18572	38966	58155	45373
C1-30+ Resolved	51845	68422	99476	156151	138191
GOR* Resolved	0,67	0,66	0,47	0,45	0,49
Isoprenoids					
iC18	29	51	75	112	128
Prist-1-ene	29	75	324	0	87
Prist-2-ene	156	165	217	56	80
Aromatics					
Benzene	309	390	395	390	516
Toluene	711	950	1817	1143	1222
Et-Benzene	133	202	424	252	274
m+p Xylene	448	696	703	1179	1092
Sulfotyrosyl (Styr)	115	136	269	0	164
o-Xylene	193	281	348	400	324
Phenol	1749	2302	2041	2646	3387
o-Cresol	500	654	715	1541	2024
m+p Cresol	1038	1429	1364	2174	2705
Naphthalene	100	130	139	85	110
2-methylnaphthalene	118	144	200	261	232
1- methylnaphthalene	47	90	124	224	244
Sum dimethylnaphthalene	971	1701	3808	2718	1171
Tetra-methylnaphthalene	123	212	381	291	53
Sum monoaromatic hydrocarbon	1909	2655	3957	3363	3592
Sum diaromatic hydrocarbon	1360	2278	4652	3579	1811
Sum phenols	3287	4384	4120	6361	8116
Sulphur compounds					
Thiophenes	83	84	101	357	352
2-methylthiophene	0	0	0	0	0
3-methylthiophene	80	107	131	355	302
2,5-dimethylthiophene	0	0	713	0	0
2,3-dimethylthiophene	9	12	8	56	45
Σ alkylthiophenes	89	120	851	411	346
*GOR: C1 to C5/C6 to C30+					